



Terms and Conditions of Use of Digitised Theses from Trinity College Library Dublin

Copyright statement

All material supplied by Trinity College Library is protected by copyright (under the Copyright and Related Rights Act, 2000 as amended) and other relevant Intellectual Property Rights. By accessing and using a Digitised Thesis from Trinity College Library you acknowledge that all Intellectual Property Rights in any Works supplied are the sole and exclusive property of the copyright and/or other IPR holder. Specific copyright holders may not be explicitly identified. Use of materials from other sources within a thesis should not be construed as a claim over them.

A non-exclusive, non-transferable licence is hereby granted to those using or reproducing, in whole or in part, the material for valid purposes, providing the copyright owners are acknowledged using the normal conventions. Where specific permission to use material is required, this is identified and such permission must be sought from the copyright holder or agency cited.

Liability statement

By using a Digitised Thesis, I accept that Trinity College Dublin bears no legal responsibility for the accuracy, legality or comprehensiveness of materials contained within the thesis, and that Trinity College Dublin accepts no liability for indirect, consequential, or incidental, damages or losses arising from use of the thesis for whatever reason. Information located in a thesis may be subject to specific use constraints, details of which may not be explicitly described. It is the responsibility of potential and actual users to be aware of such constraints and to abide by them. By making use of material from a digitised thesis, you accept these copyright and disclaimer provisions. Where it is brought to the attention of Trinity College Library that there may be a breach of copyright or other restraint, it is the policy to withdraw or take down access to a thesis while the issue is being resolved.

Access Agreement

By using a Digitised Thesis from Trinity College Library you are bound by the following Terms & Conditions. Please read them carefully.

I have read and I understand the following statement: All material supplied via a Digitised Thesis from Trinity College Library is protected by copyright and other intellectual property rights, and duplication or sale of all or part of any of a thesis is not permitted, except that material may be duplicated by you for your research use or for educational purposes in electronic or print form providing the copyright owners are acknowledged using the normal conventions. You must obtain permission for any other use. Electronic or print copies may not be offered, whether for sale or otherwise to anyone. This copy has been supplied on the understanding that it is copyright material and that no quotation from the thesis may be published without proper acknowledgement.

**Design and development of a pre-clinical test for
cemented femoral hip replacements**

By

Suzanne Adele Maher, B.E. (N.U.I), M.Eng.Sc. (N.U.I).

A thesis submitted to the University of Dublin, in partial fulfillment
of the requirements for the degree of

Doctor in Philosophy

Trinity College Dublin

April 2000

Dr. Patrick J. Prendergast

Supervisor

Prof. John Monaghan

Internal examiner

Prof. Georges Van der Perre

External examiner

TRINITY COLLEGE
9 NOV 2000
LIBRARY DUBLIN

*Thesis
5892*

*This thesis is dedicated to my parents,
Maureen and Kieran.*

CONTENTS

List of Figures.....	i
List of Tables.....	viii
Declaration.....	x
Acknowledgments.....	xi
Abstract.....	xii
Chapter 1 Introduction.....	1
Deficiencies in current methods used to evaluate new implant technology are presented. The importance of developing a pre-clinical testing platform for the effective evaluation of new implant designs is argued.	
Chapter 2 Literature review.....	7
Cemented implant features and material properties are outlined. Modes of implant failure are discussed and the conclusion that implant loosening is the main mode of failure is arrived at. A critique of the <i>in vitro</i> quantification of implant loosening is performed and the improvements that could be made on the state-of-the-art methods used are outlined.	
Chapter 3 Design and development of experimental procedures.....	34
The two prostheses tested are described. The design and application of each step in the sample preparation, testing and analysis protocol are presented.	
Chapter 4 Results.....	77
The paths of migration of all prostheses tested are graphically illustrated. The average total migration at various different stages throughout testing and the steady-state rate of migration for the two prosthesis designs are compared. The inducible displacement as a function of migration is graphically plotted.	
Chapter 5 Discussion.....	120
The clinical relevance of the migrations measured and the failure modes quantified are discussed. Some limitations in the testing set-up are outlined. The ability of the pre-clinical test to differentiate between the prosthesis designs on the basis of absolute migration, steady-state rate of migration, and inducible displacement are presented.	
Chapter 6 Conclusions.....	141
The main results of this study are listed and recommendations for future work are given.	
References.....	144
Appendices.....	157

LIST OF FIGURES

- 1.1 An overview of the some important landmark developments in the evolution of implant technology over the past 100 years, compiled from LeVay (1990) McElfresh (1991) Charnley (1961), Bargar et al. (1998), Wiles (1958), Haboush (1953), and Thompson (1952). 2
- 1.2 Schematic of a cemented total hip joint replacement, after Hardinge, 1983. 2
- 1.3 The evolution of the Stanmore prosthesis from the early 1980s to the present, adapted from Dobbs (1980). Note the incremental nature of design modifications. 3
- 1.4 Survival curves from the Swedish Hip Register: performance of the Lubinus SPII (from Malchau and Herberts, 1998) and the Muller Curved prosthesis (from Malchau et al., 1993). The dark bands represent the 95% confidence interval. 4
- 1.5 The stepwise introduction of new implant technology from Malchau, 1995. 5
- 1.6 A preclinical testing platform, from Prendergast and Maher, 1999. 6
- 2.1 The effect of prosthesis cross sectional shape on the maximum compressive stresses (a) and maximum tensile stresses (b) seen in bone cement, from Crowninshield et al. (1980). 12
- 2.2 A typical polymerisation curve of PMMA. The steep rise in temperature occurs prior to setting, from Perry (1991). 14
- 2.3 The prosthesis used to measure the forces exerted on the hip joint during walking and stair climbing, from Rydell (1966). 17
- 2.4 The twin peaks of the reaction forces on the hip joint during gait, measured by Rydell (1966). 18
- 2.5 The co-ordinate system as used by Bergmann et al., 1993, from Gait98. The forces presented are in the x, y, z axes, and the moments discussed are relative to the x, y' and z' axes. The x, y' and z' axes are assumed to be rotated by five degrees about the x axis of the x, y, z system. 19
- 2.6 The migration of an implanted prosthesis when a sinusoidally varying load is applied to its head is schematically illustrated. Migration occurs between the first set of displacement curves and the second but no increase in inducible displacement is shown. In the last set of loading curves, an increase in inducible displacement, but no migration is illustrated. 24
- 2.7 (a) Schematic of the principle behind RSA techniques. The patient lies in the supine position, over the calibration cage, which defines the laboratory coordinate system (from Malchau, 1995) (b) By working out the intersection of the rays the three dimensional position of the markers can be worked out (from Huiskes and Verdonschot, 1997). 26
- 2.8 A displacement transducer one end of which is fixed to the femoral bone (not shown) the other end is in contact with the neck of the prosthesis. If the prosthesis translates in the direction shown by the black arrow, the transducer will measure the pure translation. If the prosthesis rotates as illustrated by the red arrow, the rotation will be measured as a translation by the transducer. 28

2.9	Four displacement transducers are needed to measure the rotation of the line AB about the z axis and the displacement in the x and y directions. To measure the rotation about the y axis and translation along the z axis, a further two transducers are needed, pointing out of the plane of the page. Using these six LVDTs, one degree of rotation θ_y is still not measurable.	30
2.10	Schematic of the test set-up used by Berzins et al., 1993 to measure the six degrees of freedom of motion of a cementless type implant (from Berzins et al., 1993)	30
3.1	The two prostheses that are tested using the protocol herein described: (a) the Müller Prosthesis and (b) the Lubinus prosthesis.	35
3.2	The concept of graphically animating the path of insertion of a prosthesis. A solid model of a prosthesis is incrementally moved into a solid model of a femur. The challenge is to reproduce this motion in space.	37
3.3	Two points (point A and point B) are fixed to the stem of the prosthesis during the animated insertion. During insertion, they graphically plot two trajectories that describe the path of insertion. The trajectories for the Müller prosthesis are illustrated.	38
3.4	Cam (a) was produced by joining the trajectories plotted by the Müller prosthesis. Cam (b) was produced by joining the trajectories plotted by the Lubinus prosthesis. The holes in both cams are for attachment to the insertion machine	38
3.5	Schematic of the two rollers, the carriage, the pneumatics and the composite femur.	39
3.6	The pneumatics which pushed the prosthesis into the femur.	40
3.7	The alignment plate used to position the composite femur in a reproducible orientation.	41
3.8	Set-up for drilling the composite femur.	42
3.9	The alignment plate bolted to the insertion machine, with the measurement brackets in place. The vertical position of the measurement brackets were defined in the animation software, and varied for different prosthesis designs.	44
3.10	A front view (a) and a side view (b) of the spherical joint and toolmakers clamp which give the insertion machine flexibility in gripping either a tapered prosthetic head or a spherical prosthetic head.	45
3.11	The x-y table and the threaded bars allowing for adjustment of the position of the clamped femur in the x, y and z directions are illustrated. The prosthesis head has been aligned, its head clamped and retracted to its start position along the cam profile.	46
3.12	A schematic of the assembled insertion machine. Note: engineering drawings of the insertion machine are presented in Appendix G, page 209.	47
3.13	The insertion machine as it was setup for the validation of the design concept. Replica prosthesis (shaded in the diagram) were inserted into aluminium box section.	48
3.14	The Perspex frame that was manufactured with dimensions identical to the femoral alignment plate (compare with Figure 3.7).	50

3.15	The measurements made from the radiographs in the frontal views. The dark solid lines are the first construction lines drawn on the magnified images. A mid line is drawn connecting the prosthesis cross section centres at the 10 mm and 80 mm level. All other lines along which measurements are made are drawn perpendicular to this line.	51
3.16	The implanted composite femur is mounted on a milling machine, and using a long series solid carbide drill, 3mm is machined from the bone underneath the collar.	52
3.17	A rotation of a body fixed coordinate system about the $z = Z$ axis through an angle θ . The space fixed axes are (x,y,z) , the body fixed axes are (X,Y,Z) .	53
3.18	Concept behind the design of the migration measurement device. The displacement transducers that measure the movement of the target device are illustrated. The local coordinate axes are labelled and each LVDT is assigned an identification number.	57
3.19	Press fitting of the migration target device.	60
3.20	Clamp for the Müller Prosthesis.	61
3.21	Clamp for the Lubinus prosthesis.	61
3.22	The LVDT cylinders as they were press fitted into the LVDT bracket.	62
3.23	A top view (a) and a side view (b) of the femoral ring used to rigidly lock the LVDT holder to the wall of the composite femur. Four pointed bolts act through holes in the ring. Once tightened into the femoral cortex, nuts lock them in place against the femoral ring.	63
3.24	The steps in using the aligner to reproducibly locate the LVDT bracket relative to the migrating device. The underside of the aligner has two pins protruding from its base and two tapped hole in its base to allow the LVDT holder to be pinned and bolted to it.	64
3.25	The gap between the LVDT bracket and the femoral ring must be spanned by some form of attachment.	65
3.26	Two side view of the couplings between the LVDT bracket and the femoral ring. The translational and rotational freedom of motion of the joints are illustrated by the black arrows. For clarity, neither the femur, target device nor the aligner are shown.	65
3.27	The assembled migration measurement device. Once the flexible attachments between the LVDT holder and the femoral ring are locked in place, the aligner is removed and the LVDTs are placed in the LVDT holder, zeroed and locked in place.	66
3.28	A Müller prosthesis that was implanted into a composite femur. The femur is still clamped on the alignment plate. The tapered cylinder of PTFE which was used to plug the pre-drilled hole in through the wall of the femoral cortex is visible. The rod for the attachment of the migration measurement device has been press fitted into place.	67
3.29	The frequency of data sampling in relation to the testing frequency.	69
3.30	Schematics comparing the local coordinate systems of the Lubinus prosthesis (i) and the Müller prosthesis (ii). The body fixed and space	70

	fixed coordinate systems are defined by the orientation of the target device. This is dependent on the orientation of the holes drilled in the prosthesis and the orientation of the prosthesis within the femoral bone.	
3.31	Test setup used to investigate whether the attachment between the target device and the prosthesis was rigid enough to withstand cyclic loading for two million loading cycles.	71
3.32	A Lubinus prosthesis, with migration measurement device attached. The femur is clamped in 9° of flexion and 10° of adduction following from the recommendations of the international standard ISO 7206-3 for the determination of the endurance properties of stemmed femoral components.	75
3.33	A schematic of the complete pre-clinical testing protocol.	76
4.1	The calibration curves for the six LVDTs as labelled in Figure 3.18.	81
4.2	The error in computed translations in the lateral direction (-ve x), in the anterior direction (-ve y) and in the distal direction (+ve z) for vertical movement over a distance of 0.45 mm. The measurements were repeated three times, the graphs present the average, and standard deviation for the three measurements.	82
4.3	The error in computed rotations for vertical movement over 0.45 mm. The measurements were repeated three times, the graphs present the average, and standard deviation for the three measurements. Directions defined as follows: head translates anteriorly and the tip posteriorly (-ve θ_x), the prosthesis tip translates laterally and the head translates medially, otherwise known as varus rotation (-ve θ_y) and the medial face translates anteriorly and the lateral face translates posteriorly (-ve θ_z).	83
4.4	Displacements measured for the six LVDTs (as labelled in Figure 3.18) that were used to measure the migration of a Müller prosthesis. Fluctuations in the data are visible. Note the different scales on the axes.	84
4.5	The sixth order polynomial that was fitted to the raw data of LVDT 4.	85
4.6	The translation of a Müller prosthesis in the x', y' and z' directions.	86
4.7	The rotation of a Müller prosthesis about the x, y and z axes.	86
4.8	The translation of the each Müller prosthesis head centre (n = 5) in the x' direction during cyclic loading.	87
4.9	The translation of each Müller prosthesis head centre (n = 5) in the y' direction during cyclic loading.	88
4.10	The translation of each Müller prosthesis head centre (n= 5) in the z' direction during cyclic loading.	88
4.11	The rotation of each Müller prosthesis about the x axis during cyclic loading.	89
4.12	The rotation of each Müller prosthesis about the y axis during cyclic loading.	89
4.13	The rotation of each Müller prosthesis about the z axis during cyclic loading.	90
4.14	The translation of each Lubinus prosthesis head centre in the x' direction during cyclic loading.	91
4.15	The translation of each Lubinus prosthesis head centre in the y' direction during cyclic loading.	91

4.16	The translation of each Lubinus prosthesis head centre in the z' direction during cyclic loading.	92
4.17	The rotation of each Lubinus prosthesis about the x axis during cyclic loading.	92
4.18	The rotation of each Lubinus prosthesis about the y axis during cyclic loading.	93
4.19	The rotation of each Lubinus prosthesis about the z axis during cyclic loading.	93
4.20	Translation of the Müller (n=5) and Lubinus (n=5) prosthesis head centres medially during cyclic loading.	94
4.21	Translation of the Müller (n=5) and Lubinus (n=5) prosthesis head centres posteriorly during cyclic loading.	94
4.22	Translation of the Müller (n=5) and Lubinus (n=5) prosthesis head centres in the distal direction during cyclic loading .	95
4.23	Rotation of the Müller (n=5) and Lubinus (n=5) prostheses so that the head translates posteriorly and the tip translates anteriorly during cyclic loading.	95
4.24	Rotation of the Müller (n=5) and Lubinus (n=5) prostheses into varus during cyclic loading .	96
4.25	Rotation of the Müller (n=5) and Lubinus (n=5) prostheses about the longitudinal axis so that the medial face rotates posteriorly and the lateral face rotates anteriorly, during cyclic loading.	96
4.26	The average translations of the Müller and Lubinus head centres after 0.2 million loading cycles.	97
4.27	The average rotations of the Müller and Lubinus head centres after 0.2 million loading cycles.	97
4.28	The average translations of the Müller and Lubinus head centres after 1 million loading cycles.	98
4.29	The average rotations of the Müller and Lubinus head centres after 1 million loading cycles.	98
4.30	The average and standard deviation of the migrations of the Müller and Lubinus head centres at the end of 2 million loading cycles.	99
4.31	The average and standard deviation of the rotations of the Müller and Lubinus head centres at the end of 2 million loading cycles.	99
4.32	The translation of the Müller and Lubinus head centres when migration over the first 0.2 million cycles was subtracted.	100
4.33	The rotation of the Müller and Lubinus head centres when migration over the first 0.2 million cycles was subtracted.	100
4.34	Translation of Müller 1 after 4 million loading cycles. For 0 - 2 million cycles, the cemented prosthesis was tested without resorption. For 2 - 4 million cycles, resorption was simulated.	102
4.35	Rotation of Müller 1 after 4 million loading cycles. For 0 - 2 million cycles, the cemented prosthesis was tested without resorption. For 2 - 4 million cycles, resorption was simulated.	103
4.36	Translation of Müller 3 after 4 million loading cycles. For 0 - 2 million cycles, the cemented prosthesis was tested without resorption. For 2 - 4 million cycles, resorption was simulated.	103

4.37	Rotation of Müller 3 after 4 million loading cycles. For 0 - 2 million cycles, the cemented prosthesis was tested without resorption. For 2 - 4 million cycles, resorption was simulated.	104
4.38	Translation of Lubinus 2 after 4 million loading cycles. For 0 - 2 million cycles, the cemented prosthesis was tested without resorption. For 2 - 4 million cycles, resorption was simulated	104
4.39	Rotation of Lubinus 2 after 4 million loading cycles. For 0 - 2 million cycles, the cemented prosthesis was tested without resorption. For 2 - 4 million cycles, resorption was simulated.	105
4.40	Translation of Lubinus 3 after 4 million loading cycles. For 0 - 2 million cycles, the cemented prosthesis was tested without resorption. For 2 - 4 million cycles, resorption was simulated.	105
4.41	Rotation of Lubinus 3 after 4 million loading cycles. For 0 - 2 million cycles, the cemented prosthesis was tested without resorption. For 2 - 4 million cycles, resorption was simulated.	106
4.42	Migration of Müller 1 with and without resorption at 2 million cycles.	107
4.43	Migration of Müller 3 with and without resorption at 2 million cycles.	107
4.44	Migration of Lubinus 2 with and without resorption at 2 million cycles.	108
4.45	Migration of Lubinus 3 with and without resorption at 2 million cycles.	108
4.46	Four sections of the Müller prosthesis where cracks were evident. The cracks are highlighted with dye penetrant which colours them red, and for clarity areas where cracks were seen are circled.	110
4.47	Two sections taken through Lubinus prostheses. No cracks in the cement mantle were evident.	111
4.48	The stress at failure during push out tests carried out on two sectioned Lubinus prostheses.	111
4.49	The migration and inducible rotation in θ_z of Müller 2 throughout its loading history is illustrated.	112
4.50	The average inducible rotation of the Müller and the Lubinus prostheses about the x, y and z axes.	113
4.51	The average inducible displacement of the point of contact between the migration measurement device and the prosthesis for the Müller and Lubinus prostheses along the x' , y' and z' axes	113
4.52	The inducible displacement at 0.02 million cycles versus migration at 2 million cycles. Note: circles filled in white = Müller prostheses, blackened circles = Lubinus prostheses.	115
4.53	The inducible displacement at 0.2 million cycles versus migration at 2 million cycles. Note: circles filled in white = Müller prostheses, blackened circles = Lubinus prostheses.	116
4.54	The inducible displacement at 1 million cycles versus migration at 2 million cycles. Note: circles filled in white = Müller prostheses, blackened circles = Lubinus prostheses.	117
4.55	The average inducible over 2 million cycles versus migration at 2 million cycles. Note: circles filled in white = Müller prostheses, blackened circles = Lubinus prostheses.	118
5.1	The non-linear damage accumulation in 5 bone cement samples (Murphy and Prendergast, 1999). As the stress increases, the non-linearity of	122

	damage accumulation decreases.	
5.2	The cement mantle for a Müller prosthesis at various stages along the path to failure. (a) Only two cracks are present in the mantle. The rest of the mantle is intact: prosthesis migration will not be much affected. (b) The cement mantle is fractured at numerous locations. Migration is more likely.	123
5.3	A cement creep curve for static compressive stress of 12.1 MPa tested at 37°C, from Chwirut (1984). Note: A - E indicate the different cements that were tested. The division between the primary and secondary phases of creep for cement B, which is closest to the cement used in the current study, is shown.	125
5.4	A typical dynamic creep curve for bone cement, from Verdonshot and Huiskes (1994).	126
5.5	Schematic of a transverse slice through a Müller prosthesis.	128
5.6	Proposal for the failure mechanism of the prostheses tested.	130
5.7	Graph illustrating the concept of the Monkman-Grant relationship, where the product of the steady-state creep rate and the time-to-failure are constant for a material. A high steady-state creep rate, indicates that the time to failure will be low.	135

LIST OF TABLES


2.1	Mechanical Properties of Materials Frequently Used for Femoral Hip Prostheses; after Kabo (1991).	13
2.2	Young's Modulus of composite femora compared with average mechanical properties of autopsied femora.	33
3.1	The percentage error in assuming the angles of rotation are small, from Selvik (1989).	55
4.1	The average and standard deviations of the cement mantle thickness around the cemented replica prostheses. The thickness was measured at three points along the 'posterior' face of the prosthesis (A, B and C) and at three points along the 'medial' face of the prosthesis (D, E and F).	78
4.2	Mean and standard deviation of the distance between the prosthesis surface and the outer cortical bone as measured from the radiographs (n = 6) of the coronal plane of the implanted femora, compared to measurements made from the animation.	79
4.3	Mean and standard deviation of the distance between the prosthesis surface and the outer cortical bone as measured from the radiographs (n = 6) of the sagittal plane of the implanted femora, compared to measurements made from the animation.	79
4.4	The (x, y, z) coordinates of the centre of spheres A, B and C as measured by a co-ordinate measuring machine in the global coordinate system, see Figure 3.18 in section 3.2.2 for location of the spheres. The diameter of each sphere is also given.	80
4.5	Distance between spheres as computed before and after testing.	80
4.6	The p values as computed by the Student's t test for the differences between the migration of the Müller and Lubinus prostheses as measured at different stages during the cyclic loading history.	101
4.7	The average steady state migration rate of the cement mantle around the Müller prostheses (n=5) and Lubinus prostheses (n=5), evaluated at 1 million cycles. The significance of the difference between the two data sets computed by the Student's t test are also presented.	101
4.8	The steady state migration at 1 million and 3 million loading cycles for the prostheses tested to 4 million cycles, 0 – 2 million was without resorption and 2 – 4 million was with resorption modelled. The units of the steady state migration rate are $\mu\text{m}/\text{cycle}$.	109
4.9	The Pearson's correlation coefficient for the variation in inducible rotation and translation for each prosthesis throughout its loading history. The samples with a correlation coefficient greater than 0.9 are highlighted.	114
4.10	The Percentage of total migration (translation of the head centre in the x', y' and z' directions and rotation of the prosthesis about the x, y and z axes) that is recovered up to ten hours after the removal of load. Note: - indicates that the measured translation was within the error of the system.	119

- 5.1 Comparison of the average migration of the centre of the head of the Lubinus prosthesis computed from the clinical measurements of Karrholm et al., 1994) and experimentally in five cyclic tests of this study. 134

DECLARATION

I declare that the present work has not previously been submitted for a degree at any University. It consists entirely of my own work, except where references indicate otherwise.

The library of Trinity College, Dublin may lend or copy this thesis on request.



Suzanne Maher

4th April, 2000.

ACKNOWLEDGMENTS

Heartfelt thanks to my supervisor Dr. Patrick Prendergast for being a constant source of inspiration and encouragement for the entire duration of this thesis (even when things weren't going as they should!). Thank you for your continual guidance, and a friendship which I cherish.

My sincere thanks to Senior Lecturer Garrett Lyons for his advice on the development of the migration measurement device. Thanks to Alan Reid, Senior Experimental Officer, for help with the design of the Insertion Machine and also to Victor Waide, for help with both the insertion machine and the migration measurement device designs. Many thanks to Gabriel Nicholson for his expert machining skills which made our design concepts a physical reality.

Having engaged in a practical oriented thesis, I have spent many enjoyable hours working in our departmental workshop and materials testing laboratories. I would like to thank Peter O'Reilly for his unfailing help with the practical side of things, particularly at the beginning of the project. Many thanks to Sean Doonan and Tom Haveron for their assistance and use of the workshop tools! Thanks to John Gaynor for his help with CNC programming and to Paul Normoyle for photographic assistance. Thanks also to Frank Mowlds, Ray Walsh, Gerry Byrne, and to Danny Boardmann.

I have been fortunate enough to work with Bioengineering researchers that are enthusiastic about their work, but enjoy a couple of pints too. To Damien, Linda, Bruce, Alex, Seosamh, Adrielle, Danny and John; it has been great *craic* working with you all! I hope we keep in touch regardless of where our research leads us.

I would also like to express my thanks to Professor John Monaghan, Joan Gillen and Virginia Coulter for their assistance whenever it was necessary.

Finally, I thank my parents without whose continual support, this thesis would never have been.

I acknowledge the funding of the Standards, Measurement and Testing programme of the European Commission, project number: SMT-CT96-2076. I thank W.Link, Hamburg, Germany for donation of the Lubinus prostheses, Tecres, Verona, Italy, for donation of cement and Mitab, Sjöbo, Sweden, for donation of the vacuum mixing system.

ABSTRACT

Current state of the art testing methods do not allow implant performance to be assessed relative to known failure modes, prior to clinical use. Even clinically, it can take up to 5 years before implant performance can be readily quantified. This situation is not desirable for either the surgeons who have to choose from amongst the wide array of implants on the market, or for the engineers who are effectively selling a device of un-proven performance.

Femoral hip implants loosen. The rate at which they loosen is determined by many factors, but dominated by implant design. Loosening has been correlated with the migration measured at 2 years post-operatively. This thesis presents a pre-clinical testing protocol which measures prosthesis migration, migration rates, and inducible displacement (*i.e.* amplitude of motion) in six degrees-of-freedom, for 2 million cycles. Using this protocol, the performance of two prostheses known to loosen at different rates clinically are assessed: the Müller Curved prosthesis, which has a high revision rate, and the Lubinus SPII prosthesis, which has a low revision rate.

The implants tested migrated at a relatively fast rate for the first 0.2 million cycles, then migrated at a lower rate thereafter. The Müller Curved prostheses subsided significantly more than the Lubinus SPII prosthesis at $p = 0.05$ level of significance, after 2 million loading cycles, and at $p = 0.04$ after 1 million loading cycles. Qualitatively, this mirrors the differences expected clinically. A three-fold increase in the steady state migration rate of the Müller prosthesis, evaluated at 1 million cycles, compared to the Lubinus prosthesis was quantified. Those prostheses with a tendency to migrate by a comparatively large amount in any direction were found to have a high inducible displacement in that direction.

This experimental test has been proven to differentiate between what may be termed a 'poor' prosthesis design that is prone to early loosening, and a 'good' design that is not. The testing protocol is therefore proposed as a suitable method for assessing between prosthesis performance *in vitro* before clinical trials are begun.

1: Introduction

1.1	HIP IMPLANTS: A HISTORY OF DEVELOPMENT	2
1.2	EVALUATION OF PROSTHESES	3
1.3	MALCHAU'S PROPOSAL FOR THE INTRODUCTION OF NEW IMPLANT TECHNOLOGY	5
1.4	CONCLUSION	6

1.1 HIP IMPLANTS: A HISTORY OF DEVELOPMENT

Total Hip Arthroplasty (THA) is the name given to the procedure whereby the femoral and acetabular sides of the hip joint are replaced with a prosthesis. From the first THA in the 1890s, many landmark developments have led to the implant designs of modern orthopaedic surgery, as shown in Figure 1.1 overleaf. A common problem facing the early innovator of orthopaedic implants was to find a reliable method of implant fixation. Sir John Charnley popularised the successful procedure of using a cold curing acrylic polymeric dental cement based (polymethyl methacrylate, PMMA) as a filler material between a prosthesis and bone. According to Charnley, its primary function was to

‘transfer the weight of the body from the metallic stem of the prosthesis uniformly to the cancellous bone of the interior of the neck and upper end of the femur’, (Charnley, 1961).

Addition of antibiotic compounds (for example gentamicin) to decrease the risk of infection, creates a material commonly referred to as *bone cement*. Cemented hip prostheses in use today are based on the concepts of Charnley, but with more advanced cementing techniques. Typically, a cemented THA has a metallic femoral component and an acetabular component made of ultra high molecular weight polyethylene (UHMWPE). The femoral stem has a semi spherical head which articulates within the acetabular component and a shaft that is fixated into the medullary cavity of the femur by a mantle of bone cement, see Figure 1.2.

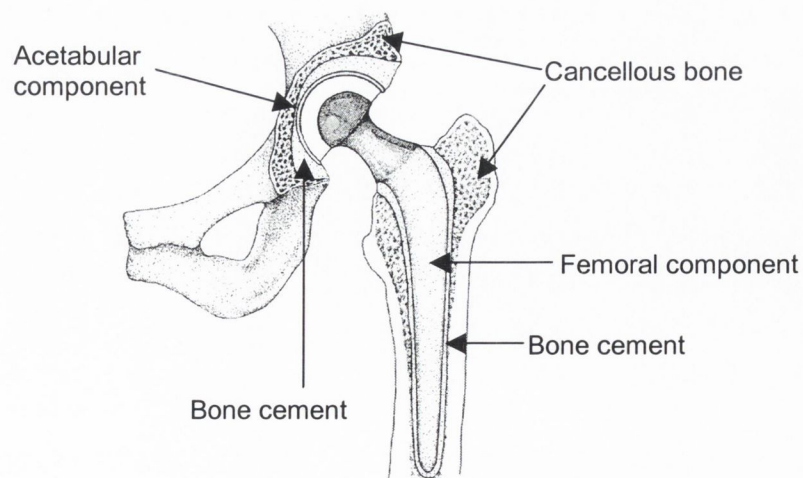


Figure 1.2: Schematic of a cemented total hip joint replacement, after Hardinge (1983).

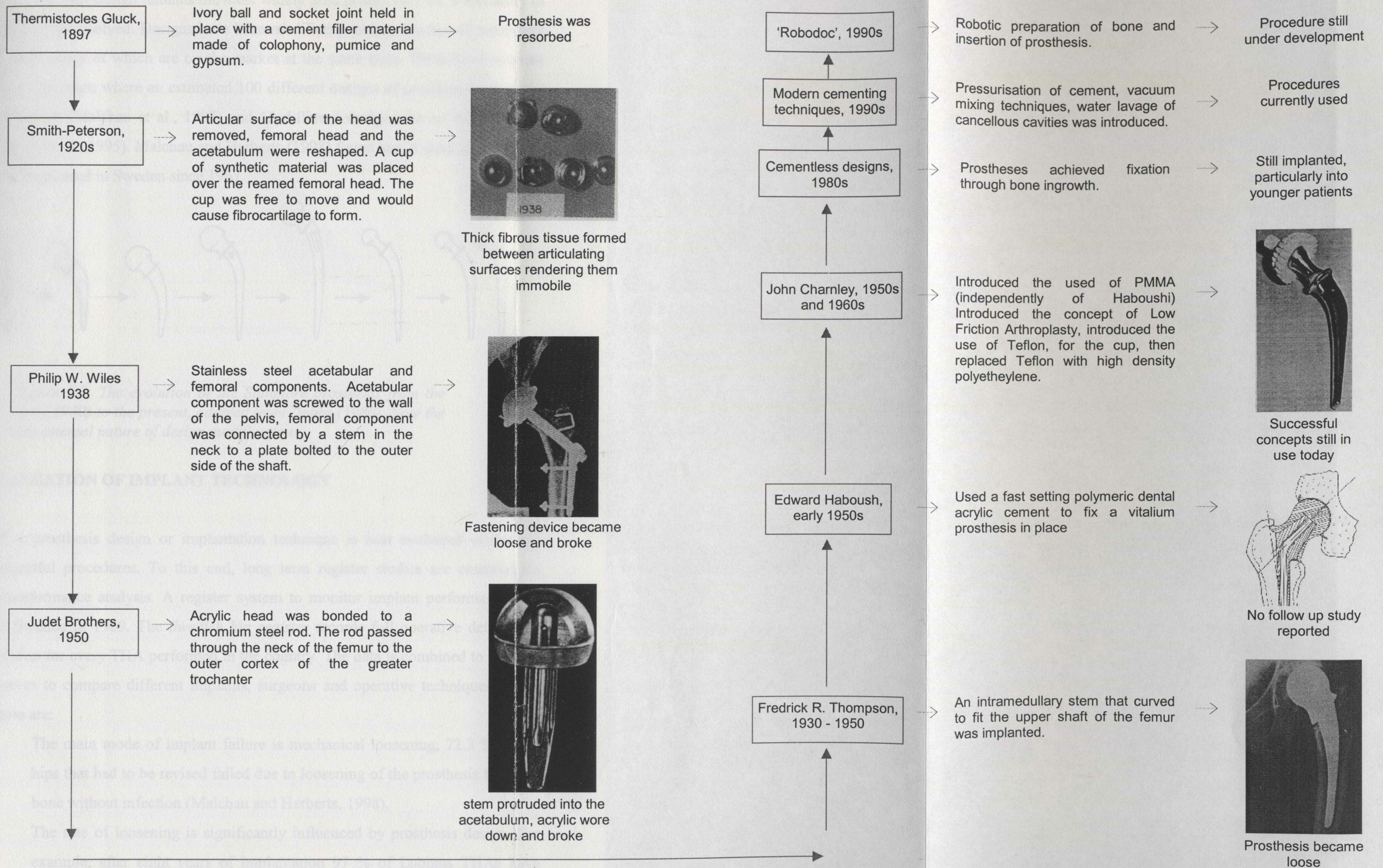


Figure 1.1: An overview of the some important landmark developments in the evolution of implant technology over the past 100 years compiled from LeVay (1990) McElfresh (1991) Charnley (1961), Bargar et al. (1998), Wiles (1958), Haboush (1953), and Thompson 1952.

Although the Charnley design remains the most widely used prosthesis type, a vast array of other prostheses has evolved. Designs have been modified to create families of prostheses (see Figure 1.3) many of which are on the market at the same time. These developments have created a situation where an estimated 100 different designs of prostheses are on the market in Sweden (Malchau et al., 1993) and 62 different designs are on the market in Britain (Murray et al., 1995). Malchau and Herberts (1998) found that at least 240 different designs have been used in Sweden since 1967.

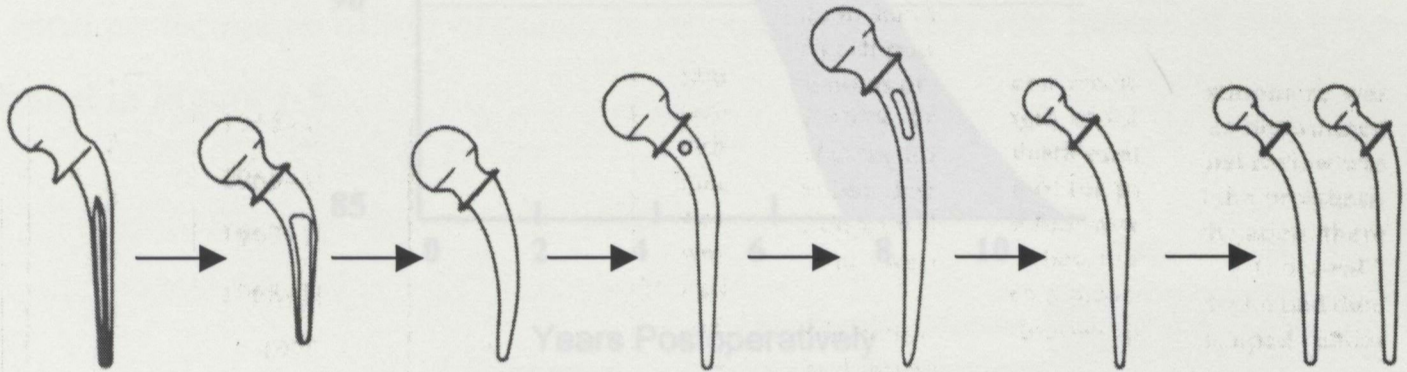


Figure 1.3: The evolution of the Stanmore prosthesis from the early 1980s to the present, adapted from Dobbs (1980). Note the incremental nature of design modifications.

1.2 EVALUATION OF IMPLANT TECHNOLOGY

Success of a prosthesis design or implantation technique is best evaluated relative to known successful procedures. To this end, long term register studies are essential for prosthesis performance analysis. A register system to monitor implant performance was initiated in Sweden in 1969. The *Swedish hip register* records full operative details and time-to-revision for every THA performed in the country. The data is combined to produce survival curves to compare different implants, surgeons and operative techniques. Three points of note are:

- i) The main mode of implant failure is mechanical loosening; 72.3 % of the hips that had to be revised failed due to loosening of the prosthesis from the bone without infection (Malchau and Herberts, 1998).
- ii) The rate of loosening is significantly influenced by prosthesis design. For example, after eight years of implantation 97 % of Lubinus THAs have survived, whereas only 85 % of Müller THAs have survived, see Figure 1.4.

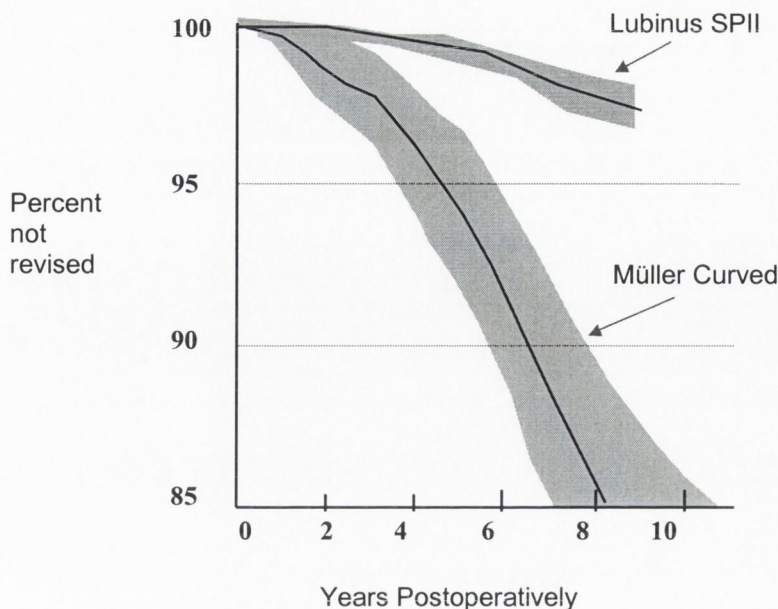


Figure 1.4: Survival curves from the Swedish Hip Register: performance of the Lubinus SPII (from Malchau and Herberts, 1998) and the Müller Curved prosthesis (from Malchau et al., 1993). The dark bands represent the 95% confidence interval.

- iii) There has been a decrease in the number of the designs used in Sweden since information from the register has been made public (Malchau and Herberts, 1998).

The Swedish hip register gives surgeons the opportunity to select prostheses on the basis of documented performance. Insofar as surgeons aim to implant the best prosthesis, this register effectively generates an environment where prostheses compete — or a survival-of-the-fittest environment as noted by Bassala (1996) for other technological artifacts. Such competition will ultimately determine which prosthesis designs are superseded and which are not. However, it can take many years to distinguish between prostheses in a register, by which time hundreds, possibly thousands, of potentially inferior designs will have been implanted. Although register studies are an essential final step in implant evaluation, they are not suitable as a procedure for testing new implants.

1.3 MALCHAU'S PROPOSAL FOR THE INTRODUCTION OF NEW IMPLANT TECHNOLOGY

A four steps procedure for the introduction of new implant technology has been suggested by Malchau (1995), as follows: *preclinical testing* which tests for the dominant mode of prosthesis failure, *prospective randomised studies* in a small patient population, *multi-centre studies* where global clinical outcomes are recorded and *register studies* where the long term performance of hip implants is recorded. The stepwise nature of this proposal is illustrated in Figure 1.5.

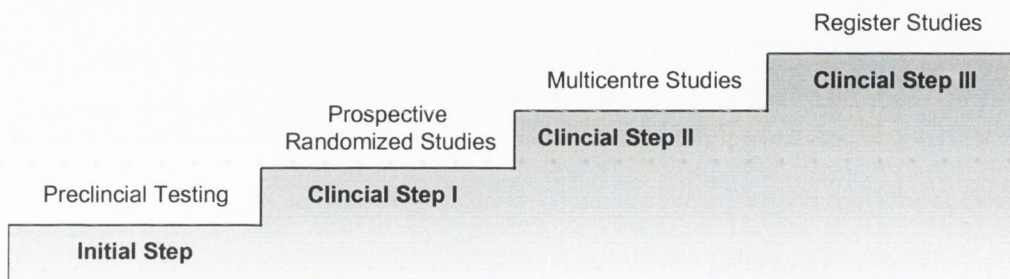


Figure 1.5: The stepwise introduction of new implant technology from Malchau (1995).

The success of this stepwise approach depends on a reliable preclinical testing platform. Preclinical testing aims to quantify prosthesis performance relative to the dominant failure modes and should screen out flawed designs before they are implanted into humans. Preclinical testing methods should:

- (i) Inspire confidence in the surgical community about the potential performance of new implant technology.
- (ii) Aid in the design and development process, by allowing the consequences of design changes to be thoroughly evaluated prior to large scale implantations.
- (iii) Encourage the development of new innovative technology, by providing a realistic bench test for its assessment.
- (iv) Involve computer models, experimental models, and animal trials (see Figure 1.6).

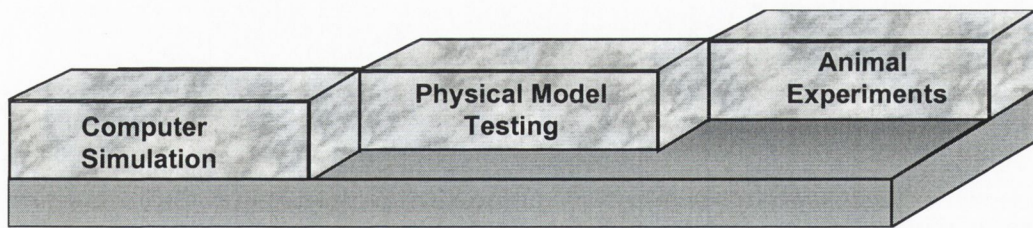


Figure 1.6: A preclinical testing platform, from Prendergast and Maher (1999).

1.4 CONCLUSION

There are a plethora of hip prosthesis of the market, and new designs are continually being introduced. Are patients well served by such a proliferation of designs? Due to the Swedish hip register, five cemented implants now constitute 78% of the market in Sweden, without any suggestion of reduced quality of care, indicating that the answer to this question is certainly 'no'. We may well ask what drives the technological evolution of hip implant designs.

THA is the most commonly carried out orthopaedic replacement operation performed worldwide (Huiskes and Verdonschot, 1997). It is estimated that about 800,000 THAs are carried out each year (Malchau et al., 1993). The revenue generated with the sale of so called 'new' designs is high, even if their marketed life is short (Huiskes, 1993). Since current pre-clinical testing methodologies cannot reliably predict the performance of new designs, the surgical community is at the mercy of the marketing from orthopaedic implant manufacturers. The wave of dissent rising amongst clinicians was voiced some years ago by the then president of the American Academy of Orthopaedic Surgeons, Augusto Sarmiento, who felt that,

'the difference between many of these widely advertised prostheses is non-existent, or minimal at best, when measured against clinical outcomes and benefits derived by patients', (Sarmiento, 1991).

It is no longer acceptable to depend solely on clinical studies to drive the implant innovation process. To stem the tide of the increasing number of alternative designs that are introduced without a solid scientific basis, an industry-standard preclinical testing protocol is essential. It is the contention of this thesis that it is possible to design an *in vitro* bench test for cemented femoral hip replacements which reliably correlates with their clinical performance.

2: Literature Review

2.1	IMPLANT TECHNOLOGY	8
2.1.1	Cemented versus cementless hip prostheses	8
2.1.2	Cemented fixation design concepts	8
2.1.3	Cemented stem design features	10
	2.1.3.1 <i>Collared versus collarless prostheses</i>	10
	2.1.3.2 <i>Prosthesis cross sectional profile</i>	11
	2.1.3.4 <i>Prosthesis material selection</i>	12
2.1.4	Bone cement and its interfaces	13
	2.1.4.1 <i>Polymerisation characteristics</i>	13
	2.1.4.2 <i>Preparation techniques</i>	14
	2.1.4.3 <i>Cement insertion techniques</i>	15
	2.1.4.4 <i>Cement/bone and cement/stem interfacial properties</i>	15
	2.1.4.5 <i>Bone cement mechanical properties and failure characteristics</i>	16
2.2	LOADING OF HIP JOINTS	17
2.3	MODES OF FAILURE OF FEMORAL HIP PROSTHESES	20
2.4	CLINICAL PERFORMANCE ANALYSIS	22
2.4.1	Prospective randomised studies	22
2.4.2	Multicentre studies	23
2.4.3	Register studies	23
2.5	PROSTHESIS LOOSENING	24
2.5.1	Radiographic analysis	25
2.5.2	Radiostereometric analysis	25
2.5.3	Migration and prosthesis loosening	27
2.6	MEASUREMENT OF MIGRATION RATES IN LABORATORY TESTS	28
2.6.1	Laboratory tests to measure prosthesis motion	28
2.6.2	Duration of laboratory tests	31
2.6.3	Presentation of test results	31
2.6.4	Variability in laboratory tests	31
2.7	SUMMARY	33

2.1 IMPLANT TECHNOLOGY

2.1.1 Cemented versus cementless hip prostheses

Femoral hip prosthesis designs can be separated into two categories depending on their mechanism of fixation to bone:

- (i) *Non-cemented designs* rely on bone growth into the surface of the prosthesis for fixation. To encourage good bone growth, cementless type prostheses can have a microtextured finish, which increases the surface area available for ingrowth, or a bead coated surface which may be plasma-sprayed with hydroxyapatite or titanium beads to induce osseointegration (Søballe et al., 1993).
- (ii) *Cemented designs* rely on a polymeric bone cement to fix the prosthesis to the host bone.

For cementless designs, immediate post-operative implant micromotion must be less than approximately 150 microns to ensure that long term fixation will occur (Pilliar et al., 1986). This requires a good initial fit between the prosthesis and bone and requires the bone in the medullary cavity to be reamed about 0.5 mm smaller than the implant (Otani et al., 1995). In contrast, cemented designs do not require such accurate reaming of the medullary cavity, because the cement acts as a grout to fill the gaps between the prosthesis and bone. The bone cavity can be reamed to between 0.5 mm and 5 mm wider than the prosthesis, although a 2 mm wide cement mantle appears to be the ideal (Star et al., 1994).

The average clinically recorded success rates of cementless prostheses are considered low at 87% at 9 years, compared with 96% at 9 years for cemented type implants (Malchau and Herberts, 1998). An advantage of cementless designs is that revision is easier which indicates their use for younger patients where a revision will likely be required. However, cemented prostheses remain the most widely used design worldwide (Malchau et al., 1995).

2.1.2 Cemented fixation design concepts

Cemented designs can be categorised based on the mechanism of prosthetic fixation at the cement/prosthesis interface (Huiskes et al., 1998) as follows:

- (i) Type I, or *shape closed fixation*. This type aims to provide immediate prosthetic stability by maintaining a bond between the metal prosthesis and

the bone cement. This prosthesis type usually has a matt finished surface, sometimes with grooves, dimples or indents on the surface.

- (ii) Type II, or *force closed fixation*. This type relies on bone cement to maintain an immediate bond with the cancellous bone, *but* allows slip to occur along the prosthesis/cement interface. This design type is typified by the Exeter prosthesis which has a polished femoral surface (Lee, 1994).

Whereas the Type I design would seem to create the most durable fixation, advocates of the Type II design concept propose that failure of the prosthesis/cement interface is inevitable, and that it is better to facilitate slippage along this interface, allowing the prosthesis to 'self tighten' within the cemented cavity (Lee, 1994). The Exeter stem is the only implant to follow these design concepts for which there are long term follow-up studies available. It was first implanted in 1970 in Exeter, UK, (Lee, 1994) and it is made of a high fatigue strength stainless steel, Orthinox™ (Rokkum et al., 1995). Twenty four percent of all cemented type prosthesis implanted in Sweden in the period 1987 –1996 were Exeter stems (Malchau and Herberts, 1998). Of those prosthesis implanted since 1987, a revision rate of 4%, due to aseptic loosening at 9 years has been documented (Malchau and Herberts, 1998). This is within recommended limits (National Institutes of Health, 1994). The characteristic double taper of the stem was designed to act as an extruder of cement into the femoral canal (Fowler et al., 1988) but was subsequently found to facilitate the self tightening process in the medio-lateral and antero-posterior planes. The polished stem also minimises wear between the cement and the prosthesis during the 'inevitable' distal subsidence.

Although many stems are polished (Charnley; Depuy J&J, Leeds, U.K.; T-28, Zimmer, Ohio, USA (Collis and Mohler, 1998); Fulong Straight Stem, JRI; London, UK; CPT, Zimmer, Ohio, USA; (Murray et al., 1995)) they are not necessarily designed with the 'force closed fixation' concept in mind. In these cases, the purpose of the smooth stem is to minimise wear debris created by relative motion at the cement/prosthesis interface if, or when, the cement/prosthesis bond breaks down (Crowninshield et al., 1998). One motivation for introducing matt stems was to increase the surface area for cement/bone bonding, thereby delaying the onset of failure of this interface (Middleton et al., 1998). Upon failure of the cement/metal bond however, the matt stem can act as a wear debris generator, as it abrades the bone cement mantle. The survival of the implant is therefore dependent on the ability to maintain a strong cement/bone bond for as long as possible. To

improve the cement/metal interfacial strength, prostheses are manufactured with grooves into which the cement can interlock (for example the Lubinus prosthesis, W. Link, Hamburg, Germany), with hollowed out shoulders (roundbacked Charnley, Depuy J&J, Leeds, U.K.) or the stems are precoated with PMMA (Sheehan, Zimmer; Murray et al., 1995).

2.1.3 Cemented stem design features

2.1.3.1 Collared versus collarless prostheses

Further design differences include the presence or absence of a protrusion on the femoral prosthesis at the transition between the neck and the stem - otherwise known as a *collar*.

Femoral prostheses transfer loads distally through the stem and bypass the proximal area. According to Wolff's Law (Roesler, 1987) as the maximum principal stress decreases below the physiological level, bone resorption occurs due to *stress shielding*. Because of the reduction in bone support, bone resorption can cause increased bending stresses in the cement mantle and accelerated failure (Chang et al., 1998). To prevent proximal/medial bone resorption hinged prostheses have been proposed (Vander Sloten, 1993). A collar was designed primarily to transfer stresses directly to the proximo-medial femur. The success of collared prostheses in achieving their intended function was found to be dependent on whether collar/calcar contact was achieved in surgery (Kelley et al., 1993). However, the mere possibility of collar functionality was disputed by (Ling 1992) who provided evidence of cases where direct bone/collar contact was obtained in surgery, but bone resorption still occurred in over half of the implants within two years. O'Hara and McMinn (1991) found that at two years postoperatively at least 2 mm bone resorption had occurred under the collars of half the Lubinus SPII prostheses (W. Link, Hamburg, Germany) that they had implanted. At four years, all stems had a similar prognosis. However, despite resorption there was no associated loosening, or radiographic signs of impending loosening in any of the stems. This suggests that the collar does little to decrease resorption rates. Other reasons cited for the introduction of a collar are that it would:

- (i) help to pressurise the cement during prosthesis insertion,
- (ii) encourage precision in the seating of the prosthesis
- (iii) reduce stem micromotion,
- (iv) reduce strain in the cement in the proximal medial region.

However, Ling 1992 dismisses these claimed benefits, and cites the following damaging factors associated with collars:

- (i) debris production caused by the micromotion of the femoral stem even in a well fixed state,
- (ii) calcar pivot; where the stem tilts into varus, with the collar as its fulcrum
- (iii) non physiological loading of the cut surface of the femoral neck.

The ongoing debate for and against the use of a collar is typical of the challenges that have faced prostheses designers in the past. Both sides can present convincing arguments as to why one design characteristic is better than another, and the confounding factors in follow-up studies combined with the absence of agreed testing procedures means that the issue cannot be resolved experimentally.

2.1.3.1 Prosthesis cross sectional profile

Prosthesis cross sectional profiles are very different from one cemented design to another.

This affects:

- (i) the second moment of area of the stem, which influences the magnitude of the stresses transmitted to the cement mantle, and
- (ii) the stress concentrations at the cement/metal interface.

In a three dimensional finite element model of a stem cemented into a tubular construct representing the femur, Crowninshield et al. (1980) compared the stresses induced in the cement mantle by prostheses with different cross sectional profiles. The interfaces were modelled as being fully bonded, and the maximum tensile and compressive stresses in the most proximal 10 mm of bone cement are presented. Assuming that a force of 3 kN of force acts through the hip, it was reported that prostheses with relatively small anteroposterior medial dimensions, and with a sharp medial surfaces created maximum cement compressive stresses of up to 9.6 MPa and maximum cement tensile stresses of up to 2.7 MPa, see Fig. 2.1a and Fig. 2.1b, respectively. Whereas, prostheses with blunt medial profiles induced lower compressive and tensile stresses of 6.0 MPa and 1.5 MPa, respectively. The authors do not indicate what the average or the range of cement stresses were and they do not specify in what percentage of the mantle the quoted maximum stresses were generated. However, the magnitude of the reported stresses are high considering that ideal conditions, such as fully bonded interfaces, were simulated.

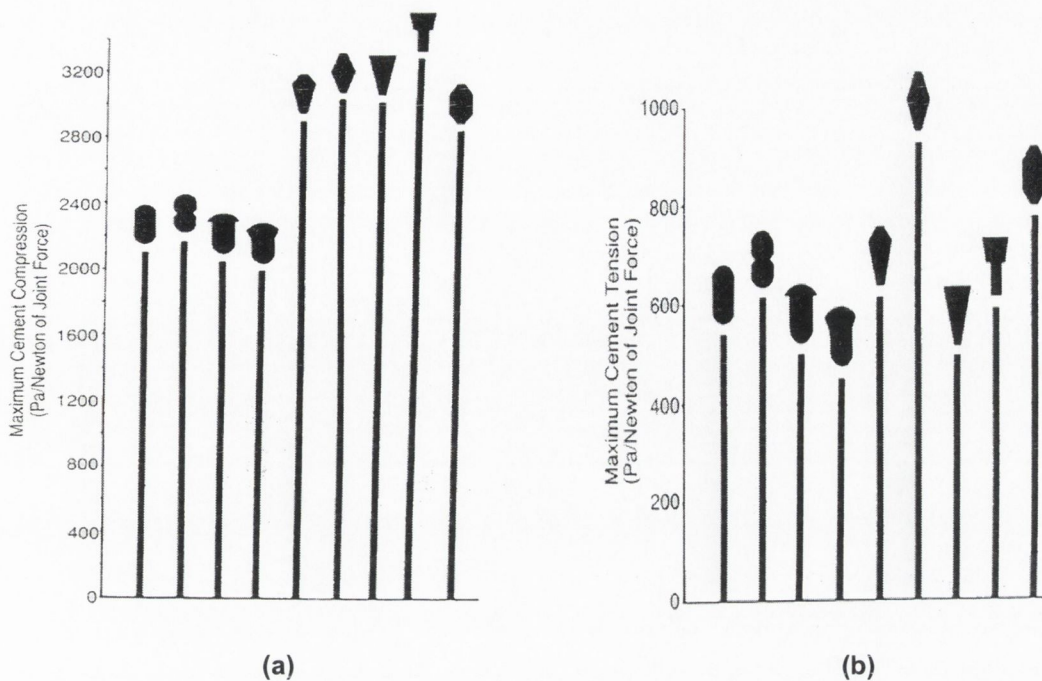


Figure 2.1: The effect of prosthesis cross sectional shape on the maximum compressive stresses (a) and maximum tensile stresses (b) seen in bone cement, from Crowninshield et al. (1980).

Despite the obvious limitations of the finite element model, the research indicates how much prosthetic stem profile can influence cement stresses, and therefore cement fatigue life.

2.1.3.4 Prosthesis material selection

A summary of the mechanical properties of some materials used for femoral prostheses is presented in Table 1. Prostheses are most commonly made of cobalt chrome molybdenum Co-Cr-Mo alloys (e.g. Austin Moore prostheses; McKellop et al., 1991), stainless steel (smooth flatback Charnley; Berry et al., 1998), steel alloys (Exeter, Rökkum et al., 1995), and titanium aluminium vanadium (Ti-Al-V) alloys (Harris-Galante; Callaghan et al., 1992). The high strength properties of cobalt chrome molybdenum allows the stem cross sectional area to be reduced without the risk of stem fracture, and its good wear resistant properties make the material suitable for use in an articular joint. Stem stiffness is reduced by using lower modulus alloys such as titanium rather than stainless steel or cobalt-chromium. However, although lower modulus materials can lead to a reduction in stem stresses and more physiological calcar bone stresses, these effects occur at the expense of higher cement stresses (Prendergast et al., 1989). Despite the reported high incidence of

wear of titanium implants (Witt and Swann, 1991), and an accompanying discoloration of the adjacent bone tissue due to the adverse reaction to the wear particles (Willert et al., 1996), prostheses made of Ti-Al-V alloys are still a popular choice (Murray et al., 1995).

Table 2.1: Mechanical Properties of Materials Frequently Used for Femoral Hip Prostheses; after Kabo (1991).

Material	Yield Strength (MPa)	Ultimate Strength (MPa)	Elastic Modulus (GPa)
Ti-Al6-V4	940	1000 - 1200	100 - 110
Co-Cr-Mo (forged)	450	1240	200 - 240
Co-Cr-Mo (Cast)	450	621	220 - 240
Stainless Steel (316L)	207	515	200 - 220

2.1.4 Bone cement and its interfaces

2.1.4.1 Polymerisation characteristics

The polymerisation characteristics of the many different bone cements available commercially differ little from the PMMA that was popularised by Charnley in 1960. Bone cement is prepared by mixing a monomer liquid component with a polymer powder component in the ratio of 2 g of powder to 1 ml of liquid (Meyer et al., 1973). Commercially available bone cement is typically sold in prepackaged compartments of 40 g powder and 20 ml liquid. The powder consists of 90% polymer, which can be either PMMA or a random co-polymer with a small amount of styrene, 10% radiopacifier and a small amount of polymerisation initiator named benzoyl peroxide (Brown, 1991). The liquid comprises 97% methyl methacrylate monomer, hydroquinone, and an activator, dimethyl-p-toluidine. The hydroquinone prevents polymerisation of the monomer during storage, and the dimethyl-p-toluidine causes the benzoyl peroxide to initiate polymerisation after mixing. When the two components are mixed, polymerisation commences. It is a cold curing material, but polymerisation is an exothermic reaction with most of the heat given out during the setting phase of polymerisation (Brown, 1991). A schematic of a typical polymerisation curve is illustrated in Figure 2.2. *Dough time* is the time that elapses between the first mixing of the powder and liquid and the time when the cement no longer sticks to a surgical glove. *Setting time* is the time between the start of mixing and the peak temperature is reached. *Working or handling time* is the time between the end of dough time and the end of setting time.

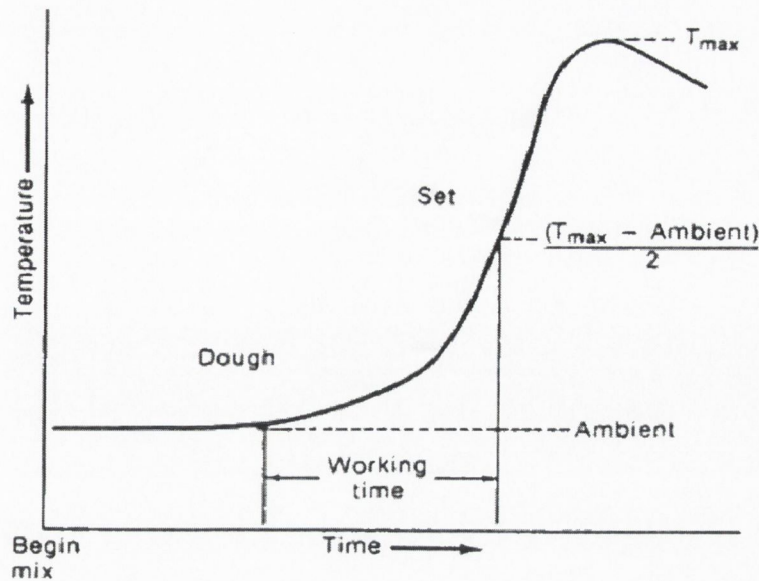


Figure 2.2: A typical polymerisation curve of PMMA. The steep rise in temperature occurs prior to setting, from Perry (1991).

2.1.4.2 Preparation techniques

There are two main methods of cement preparation currently used; the first where the mixture is mixed by hand in a container that is open to the environment and the second where the monomer and polymer are mixed in a chamber that is sealed from the environment and held under vacuum (Kindt-Larsen et al., 1995). Hand mixing is found to entrain and trap air bubbles in the mixture, which act as stress concentrators within the bulk material and decrease its fatigue life (Wixson 1992). Although vacuum mixing decreases the quantity of air bubbles throughout the material, it has a tendency to introduce large randomly distributed pores into the material (Murphy and Prendergast, 1999), both characteristics of which affect the fatigue life of the material. However, clinically it is generally accepted that vacuum mixing gives superior fatigue life to the mantle, thereby improving the longevity of the replacement (Oishi et al. 1994).

As polymerisation progresses the substance becomes more viscous. The rate of change of the viscosity and of the temperature of the cement during polymerisation depends on:

- (i) whether the materials contains barium sulphate (a radiopacifier),
- (ii) the ambient temperature,
- (iii) the storage methods used,
- (iv) the method of mixing employed,
- (v) the age of the cement.

2.1.4.3 Cement insertion techniques

Depending on the method of preparation, bone cement is introduced into the medullary cavity in different ways and at different stages during polymerisation. For example, hand mixed cement is stirred until it has a dough like constitution and can be manually moulded. It is rolled into an oblong shape and digitally packed into the canal. Typically, these cements require long handling times and short dough times. Vacuum mixed cement is usually injected into the canal at an earlier stage in the polymerisation process, when the cement is less viscous. Using a gun, the cement is injected into the canal in retrograde fashion — filling the canal in the inferior to superior direction. Longer dough times are required to allow enough time for the cement to be vacuum mixed and gun injected. These types of cements are called *low viscosity* cements.

Bone cement does not form a chemical bond with either the metallic stem or the cancellous bone, but relies on mechanical interlock to achieve fixation. The less viscous the cement is when injected into the cavity, the more likely it is to mechanically interlock with adjacent materials. Therefore the method of cement preparation and insertion determines, in part, the strength of the interlock achieved with the stem and the surrounding bone (Nobel and Swarts, 1983).

The viscosity of PMMA changes with shear rate (Brown, 1991). It becomes less viscous when it is injected using a gun into the medullary canal at a faster rate or higher pressure and can flow more easily into geometric features of the prosthesis. It has been found that the highest pressures generated along the cement/bone interface during the replacement procedure are developed during prosthesis insertion (Song et al., 1994). It follows that design of the prosthesis (Stone et al., 1991) and the path of insertion will influence the pressures generated along the interface (Turner et al., 1983), and hence affect the cement/bone interfacial strength (Askew et al., 1984). Some prosthesis designs have been developed to more evenly pressurise the cement mantle during prosthetic insertion (Fowler et al., 1988), and bone plugs are used to prevent distal cement flow and hence maintain pressure (Prendergast et al., 1999).

2.1.4.4 Cement/bone and cement/stem interfacial properties

Reported cement/bone shear strengths vary from 1–45 MPa, tensile strengths from 1–12 MPa and compressive strengths from 3–80 MPa (Maher and McCormack, 1999). The range of cement/bone interface mechanical properties are a function of bone canal

preparation techniques (Majkowski et al., 1993; Halawa et al., 1978), cement preparation and insertion techniques (Bannister and Miles 1988; Davies and Harris 1993), and cement type (Nobel and Swarts, 1983).

Variability also exists in the cement/prosthesis interface strength depending on the cement type, the stem profile and whether there is contamination of either interface (Stone et al., 1989). Stems with grooved surfaces, enable stronger mechanical interlock, whereas those with sharp corners along their profiles tend to encourage crack propagation due to stress concentration effects, particularly when loaded in torsion (McCormack et al., 1999). The metallurgical finish on the prosthesis also has a strong influence on the cement/bone interlock. The arithmetic mean (R_a) of different prosthesis surfaces ranges from 0.10 μm to 6.33 μm , for polished and rough stems respectively, with a corresponding five fold increase in push out strength (Crowninshield et al., 1998).

Prosthesis cemented type II (see section 2.1.2) with polished surfaces create an interface whose shear strength is negligible. Whereas cemented prosthesis type I, which aim to maintain a strong cement/bone interface can create a stronger bond of up to 12 MPa as measured in push out tests (Stone et al., 1989).

2.1.4.5 Bone cement mechanical properties and failure characteristics

Following polymerisation, residual stresses of up to 5 MPa have been measured within bone cement (Mann et al., 1991). These are high enough to cause cracking of the cement mantle. However, when the hip joint is loaded after polymerisation the cement creeps which helps to reduce peak cement stresses (Verdonschot and Huiskes, 1997). Lennon et al. (2000a), analysed the strains in a steel/cement/foam/PVC block using grating interferometry techniques and confirmed that, although residual stresses occurred in the immediate post-operative period, they relaxed over the following three week period.

Air entrapment (James et al., 1992), inclusions, different mixing processes (Barrack et al., 1992), residual monomer (Hailey et al., 1994), moisture and aging uptake (Hailey et al., 1994) contribute towards the variation in reported bone cement mechanical properties. In a review of literature, Kindt-Larsen et al. (1995) report tensile moduli ranging from 2.1 to 2.4 GPa, flexural modulus of 2.4 to 2.6 GPa, tensile strengths of 22 to 33 MPa, compressive strengths 84 to 99 MPa and shear strengths 32 to 37 MPa. Davies et al. (1988) recorded tensile strengths varying from 26 to 50 MPa and compressive strengths of between 76 to 131 MPa were reported by Haas et al., (1975). With numerous stress

concentrations at the cement/bone interface and voids within the cement, crack initiation is easily accomplished (Wright and Robinson, 1982). On the basis of fractography, Freitag and Cannon (1977) found that, at low stresses, many cracks grow through the bulk mantle and continue to grow as the cycling continues, until enough cracks are present that failure occurs through crack coalescence. The resulting fracture surface has a rough appearance. As the fatigue stress levels increase, crack propagation rates increase so that the fracture surface has a smoother appearance. More recently, failure of the bone cement mantle through an accumulation of cracks has been demonstrated experimentally in bending (McCormack and Prendergast, 1999) and in torsion (McCormack et al., 1999).

2.2 LOADING OF HIP JOINTS

One of the first attempts to experimentally measure the loads generated on the hip joint was carried out by Rydell (1966). A slightly larger version of the Moore prosthesis with strain gauges mounted on the neck was implanted into a patient (see Figure 2.3). It was found that, during gait, the reaction force on the hip consisted of two peaks. The first peak occurred just after heel strike and a second peak of higher magnitude occurred prior to toe off (see Figure 2.4).

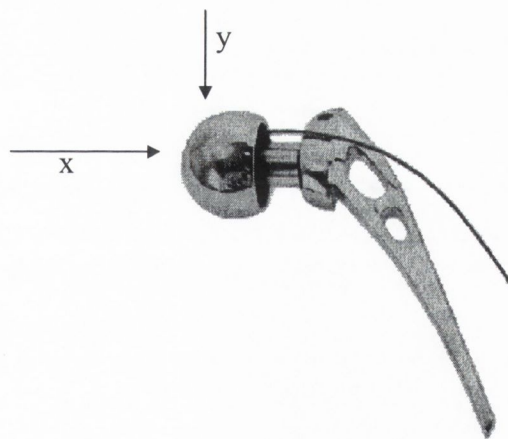


Figure 2.3: The prosthesis used to measure the forces exerted on the hip joint during walking and stair climbing, from Rydell (1966).

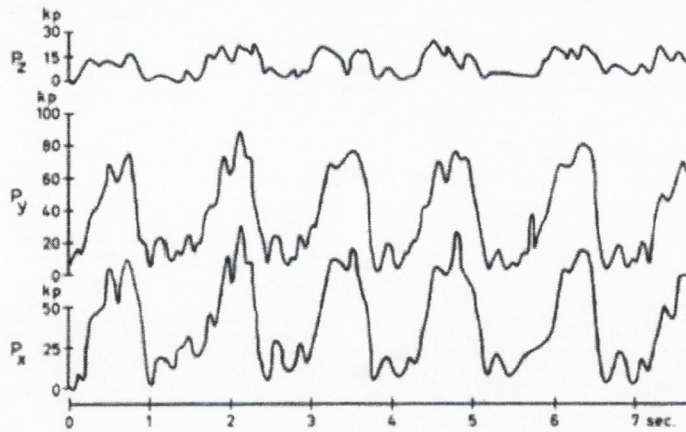


Figure 2.4: The twin peaks of the reaction forces on the hip joint during gait, measured by Rydell (1966).

More detailed analyses of forces and moments generated about the hip joint during daily activities have been gathered from telemetrised hip implants, for example by Kotzar et al. (1995), Bergmann et al. (1993) and Taylor et al. (1997). No consensus exists regarding a coordinate system for these studies; therefore correlations between results cannot be easily made. The coordinate system reported by Bergmann et al. (1993) is certainly comprehensive, and gives an indication of the complexity in trying to define a coordinate system for the irregularly shaped femur. The coordinate system is defined as follows:

- (i) A line is drawn connecting the mid point of the prosthetic neck and the centre of the prosthetic head (line A-A as illustrated in Figure 2.5).
- (ii) In the frontal plane a point is taken where the curved mid-line of the femoral shaft intersects the intercondylar notch and line A-A.
- (iii) A straight line is drawn connecting these two points, and this represents the z axis.
- (iv) The femur is viewed in saggital plane and the condyles are approximated as two semi circles. The centre points of the two semi-circles are joined.
- (v) The femur is viewed from the superior direction and is rotated about the z axis so that the x axis is horizontal.
- (vi) The line connecting the two points on the condyles represents the x-axis.
- (vii) The y axis is mutually perpendicular to the x and z axes.

- (viii) All three axes are translated to the centre of the prosthetic head which is taken as the origin of the x, y, z axes.
- (ix) Because of the natural curve in the femur, the implanted prosthesis is assumed to be angled at about 5 degrees relative to the z axis in the z - y plane. The x, y, z axes are rotated 5 degrees about the x axis to produce the x, y', z' axes. The forces quoted by Bergmann et al. (1995) are defined relative to the femoral axes (x, y, z) whereas the moments are defined relative to the prosthesis axes (x, y', z'), see Figure 2.5.

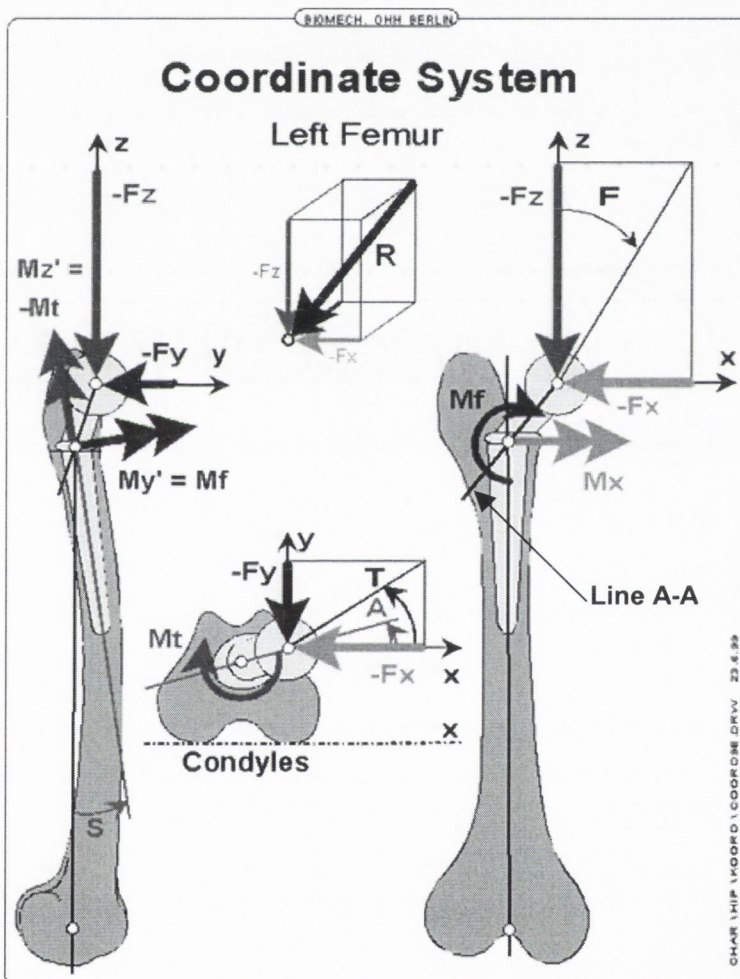


Figure 2.5: The co-ordinate system as used by Bergmann et al., 1993, from Gait98. The forces presented are in the x, y, z axes, and the moments discussed are relative to the x, y' and z' axes. The x, y' and z' axes are assumed to be rotated by five degrees about the x axis of the x, y, z system.

The author has found some problems with attempts to apply the axes as defined by Bergmann et al. (1993) to a physical model. For example:

- (i) It is difficult to physically align a femur according to the procedure.
- (ii) It is particularly difficult to choose the centre points of the idealised semi circular condyles.
- (iii) The axes will have a different origin depending on the position of the prosthetic head centre (*i.e.* will be different for different prosthesis designs).
- (iv) There will be variability in reported results according to how close the prosthesis is to the assumed 5 degree offset in the z and y axis.

These factors may explain the variability in results between patients found by Bergmann et al. (1995) and explain why their coordinate system has not been adopted by other research groups, as noted by Cristofolini et al. (1997).

Peak axial compressive forces have been found to vary from between two to three and a half times body weight, as the speed of walking increases from 0.9 m/s to 1.9 m/s by Kotzar et al. (1995). Bergmann et al. (1993) quantified higher force magnitudes varying from 2.8 to 4.8 times body weight as the speed of walking increased from 0.3 m/s to 1.4 m/s, in a patient with 'normal' gait patterns. Jogging and fast walking were found to raise the forces to 5.5 times body weight. The direction of the transverse resultant forces were found to vary from 15 degrees to -15 degrees during gait, and between 20 and 30 degrees in the frontal plane. Frontal bending moments of up to 32 Nm and torsional moments of up to 12 Nm have been reported by Bergmann et al. (1993). It has also been found by Kotzar et al. (1995), that the forces and moments that are measured during various activities do not support the widespread opinion that greater torques occur during stair climbing or rising from a chair compared with gait.

2.3 MODES OF FAILURE OF FEMORAL HIP PROSTHESES

Although prosthesis fracture was a common mode of failure in the 1970s (Paul, 1997; Pellicci et al., 1979), improved manufacturing techniques and material properties (Rokkum et al., 1995; Ritter and Albohm, 1997) have succeeded in virtually eliminating prosthesis fracture as a dominant mode of implant failure. Six failure scenarios which lead to implant failure were proposed by Huiskes (1993) as:

- (i) *Accumulated damage scenario*; based on the gradual accumulation of mechanical damage in materials and interfaces from repetitive dynamic loading. This eventually results in breakdown of the interfaces (Jasty et al., 1991; Gardiner et al., 1994), interface micromotion, bone resorption, fibrous tissue interposition (Hori and Lewis, 1982) and finally gross loosening.
- (ii) *Particulate-reaction scenario*; wear particles generated from articulating surfaces, debonded interfaces or modular-connections can migrate to interfaces and activate a macrophage cell response which results in bone resorption and eventual loosening.
- (iii) *Failed bonding scenario*; where ingrowth or osseous integration does not occur because of gaps and/or relative motion at the cement/bone interface (relevant for cementless prostheses).
- (iv) *Stress shielding scenario*; where bone, particularly in the proximo-medial cortex, is resorbed (Kelley et al., 1993). Bone resorption may lead to increased stresses in the implant materials and onset of the damage accumulation failure scenario.
- (v) *Stress bypass scenario*; when distal load transfer is favoured over to proximal load transfer. The proximal region is bypassed and bone resorption occurs. This can happen in cementless prosthesis, when failed osseointegration occurs proximally.
- (vi) *Destructive wear scenario*; where the articulating surfaces simply ‘wear out’, so that they no longer maintain mechanical integrity.

Certainly, more than one failure scenario may be active at any one time. The question is what failure scenario will dominate and lead to failure. The first two scenarios can eventually lead directly to gross prosthesis loosening. Although stress shielding is a problem, its link with prosthetic loosening is tenuous (O’Hara and McMinn, 1991). Destructive wear between the femoral head and the acetabular component has always been a problem associated with prosthesis design (Charnley, 1960). As the head wears into the cup, range of motion is decreased and the possibility of neck/cup impingement are increased. However, the particles generated by wear are more detrimental to the outcome of the replacement than the wearing process itself. As the wear particles migrate to the prosthesis/cement interface, third body wear mechanisms can break down the interfacial

bond, and can activate the particulate-reaction failure scenario, both of which can lead to implant loosening. Whatever the scenario that leads to failure of cemented femoral implants, implant loosening is the end result.

2.4 CLINICAL PERFORMANCE ANALYSIS

Because there is no accepted pre-clinical test to predict longevity of a prosthesis, longevity can only be measured in clinical trials. Sceptical surgeons are more likely to be convinced of the effectiveness of a prosthesis by follow-up studies. Follow-up studies may be categorised as:

- (i) prospective randomised studies,
- (ii) multicentre studies,
- (iii) register studies (see section 1.3).

2.4.1 Prospective randomised studies

The results from prospective studies indicate to a surgeon whether the new implant technology is likely to perform well in the long term. It is on the basis of these results that the prostheses are marketed and sold. To protect patients, preliminary studies are best performed in small patient populations. Some inherent difficulties with these studies are as follows:

- (i) **Randomisation:** There is a challenge in ensuring that there is no bias in the assignment of patient groups, especially if the surgeon feels that one design is better than another (Collis and Mohler, 1998), or a patient refuses to accept randomisation.
- (ii) **Defining an end point for survival of the prosthesis:** Variability exists in defining an end point for failure of a prosthesis. In some studies the end point is specified as when prosthesis loosening occurs (Mulroy and Harris, 1990; Koybayashi and Terayama, 1992). However, the identification of a loose prosthesis is a subjective procedure (Mjoberg et al., 1990). Other studies, take when the implant is revised as an end point for survival. Although time to revision more clearly defines an end point, different national health care systems mean that the time lag between prosthesis loosening and revision operation will be different.

- (iii) Specifying a reason for a failed design: due to the variety of prosthesis design features, (see section 2.1.3) it may be difficult to attribute failure to a particular feature of the implant.

2.4.2 Multicentre studies

After controlled prospective studies, multi centre clinical studies which include more patient and surgical variables are needed (Britton et al., 1996; Chang et al., 1998). However, many studies presented in literature are single centre (Kobayashi and Terayama., 1992; Mulroy and Harris, 1990), and records are kept for implantations carried out by a single surgeon (Browne and Sheehan, 1986; Kobayashi et al., 1997a), or by a number of surgeons from the same hospital (Sutherland et al., 1982). Often conclusions are based on the results of a small number of procedures (Rokkum et al., 1995), with no comparison made between the performance of different prosthesis designs (Rockborn and Ollson, 1993). Such studies, provide no comparative analyses, are surgeon or technique specific, and in general cannot reflect anything more than a local trend in implant performance. Murray et al. (1993) found that of 35 peer reviewed survivorship analyses, only one study reported full patient and operative data allowing a detailed interpretation of the results. In a further study Murray et al. (1995) found that there was an absence of peer reviewed published data on the clinical performance of 70% of 62 different primary THRs available on the British market.

2.4.3 Register studies

A hip register is a database which continually records the operative details, the patient details, and the clinical outcomes of *all* joint replacement operations performed in all clinics throughout a country. Registers provide a continuous analysis of the performance of new implant technology, and alert the surgical community to emerging problems. Also, factors other than implant technology such as patients weight or level of activity can be identified as risks associated with early implant failure.

Although registers, like the Swedish hip register (see section 1.2), have an important function to play in the long term analysis of prosthesis performance, they do not directly aid in the design of improved prostheses but rather screen-out unsatisfactory designs *after* they have been implanted in significant numbers of patients.

Problems include:

- (i) A substantial time passes before the diverging performances of different prostheses can be seen (see Figure 1.4).
- (ii) It is difficult to attribute failure to a particular design feature, because so many designs share similar features, and yet still have different survival rates.
- (iii) Variability due to surgical technique and patient factors masks variability due to prosthesis design.

2.5 PROSTHESIS LOOSENING

Prostheses can move relative to the host bone over time. Motion can have a *migrating* and a *inducible displacement* component. Migration is defined as any displacement that is not recovered upon removal of load (see Figure 2.6). Migration in the inferior ('downward') direction is frequently called *subsidence* (Speirs et al., 2000). *Inducible displacement* is the amplitude of motion of the prosthesis during one loading cycle. The inducible displacement could vary over time as the prosthesis loosens.

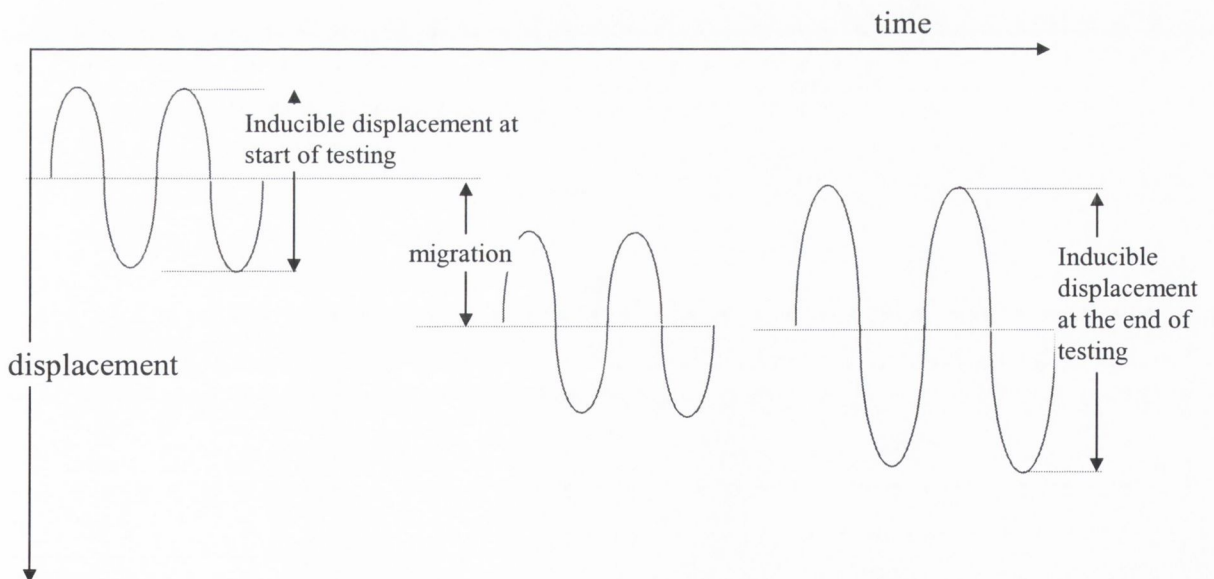


Figure 2.6: The migration of an implanted prosthesis when a sinusoidally varying load is applied to its head is schematically illustrated. Migration occurs between the first set of displacement curves and the second but no increase in inducible displacement is shown. In the last set of loading curves, an increase in inducible displacement, but no migration is illustrated.

2.5.1 Radiographic analysis

Loosening can be diagnosed from X-ray lucencies (or opaque lines) at the cement/bone interface (Olsson 1987), lucencies at the cement/metal interface (Jacobsson et al., 1995), damage in the bulk cement mantle (Brand et al., 1986, Harris et al., 1982) or as a physically quantifiable change in prosthesis position (Mjoberg et al., 1985, Ohlin and Önsten, 1990, Wirta et al., 1993). The visual assessment of radiographs is a subjective procedure and the conclusions reached depend on the accuracy and repeatability of the radiographic analysis technique. Brand et al. (1986) found that changes in position of less than 4 mm and 4°, and lucencies less than 2 mm as measured on anterior-posterior (AP) radiographs could not reliably identify a loose femoral component because measurements were within the experimental measurement error. Malchau (1995) found that a lower limit of 5 to 7 mm should be imposed on detectable motions of the prosthesis depending on the landmarks relative to which motion is quantified. Malchau (1995) also recommends that at least four radiographic exposures be taken for the optimum evaluation of a conventional radiographic examination. Many authors do not assess the accuracy of their measurement technique (Berry et al., 1998; Ohlin and Önsten, 1990, Harris et al., 1982), which limits the usefulness of some radiographic follow-up studies. Identification of a loose prosthesis can vary by as much as a factor of two as found by Brand et al. (1986) or from 14% to 22% as found by Olsson (1987) depending on the radiographic definition of a loose prosthesis that is adopted. It is acknowledged that there is no universally unambiguous criterion for identifying a loose prosthesis (Mjoberg et al., 1985). In fact, it is postulated by Mjoberg et al. (1990) that the clinical definition of 'late loosening' is a consequence of late detection rather than the late occurrence of loosening. Since, the threshold of detectable migration is limited by the accuracy of the radiographic technique, rather than identifying a prosthesis that is likely to become asymptotically loose, radiographic analysis allows only for a prosthesis which is already loose to be identified.

In summary, radiographic identification of loosening is problematic and a superior technique is required.

2.5.2 Radiostereometric analysis

One technique that has been developed to measure the six degree-of-freedom of motion of prostheses over an extended period of time is roentgenstereophotogrammetric analysis, otherwise known as *radiostereometry*, or RSA, originally developed by Selvik (1989).

The method is based on the principle that the three dimensional coordinates of an object can be reconstructed from two radiographic images.

In a radiostereometric procedure described by Malchau (1995), tantalum pellets are inserted into the proximal femoral bone, and into the prosthesis. Tantalum has a high density so that the markers appear radiopaque on radiographs. Postoperatively, the patient is radiographed using a biplanar exposure technique, where a calibration cage marked with tantalum markers which defines the laboratory co-ordinate system is placed below the radiographic table (see Figure 2.7a). To work out the three dimensional position of an object, a laboratory coordinate system is defined, the positions of the two X ray foci are calculated and the position of the two radiographic plates are recorded. The position of the object relative to the laboratory coordinate system can be calculated by computing the intersection of the X-ray beams, see Figure 2.7(b). Basing calculations on the assumption of rigid body motion of the prosthesis and of the femur (Chafetz et al., 1985), relative motion between the prosthesis and the tantalum spheres can be measured in exposures taken months or years apart. Reported rotational accuracies of this technique vary from 0.3° (Søballe et al., 1993) to 1.8° (Karrholm et al., 1994); and from 0.2 mm (Karrholm et al., 1994) to 1.3 mm (Søballe et al., 1993) in translation depending on technique used, the axis along which the motion is being measured, and the point along the prosthesis surface that is being analysed.

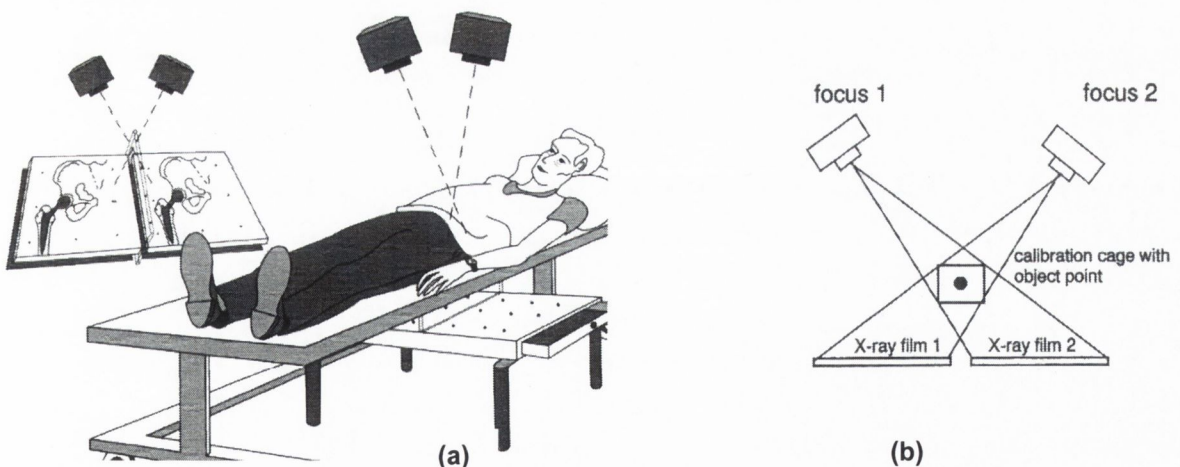


Figure 2.7: (a) Schematic of the principle behind RSA techniques. The patient lies in the supine position, over the calibration cage, which defines the laboratory coordinate system (from Malchau, 1995) (b) By working out the intersection of the rays the three dimensional position of the markers can be worked out (from Huiskes and Verdonchot, 1997).

2.5.3 Migration and prosthesis loosening

A correlation between the distal migration, or subsidence, of a prosthesis and its subsequent failure due to loosening has been found clinically. In an RSA follow-up study, Karrholm et al. (1994) found that, if a Lubinus SPII prosthesis migrated distally more than 1.2 mm in the first two years, the probability of revision was 50%. If the prosthesis migrated by more than 2.3 mm, the probability of failure increased to 99%. It was concluded that the subsidence after two years of implantation could be correlated with early failure. Some radiographic results correlate with Karrholm's findings. Walker et al. (1995) found that the migration of Charnley (n=51) and Stanmore (n=57) stems at two years post-operatively could be used as a predictor for the long term outcome. Using a radiographic analysis technique with an accuracy of 0.13 mm they found that 84% of the failed stems had migrated more than 2 mm and that 76% of the successful stems had migrated less than 2 mm. Using digitised radiographic techniques with accuracies of ± 0.5 mm, Freeman and Plante-Bordeneuve (1994), found that, for a custom designed prosthesis inserted using cementless and cemented techniques, subsidence of greater than 1.2 mm per year in the first two years after implantation could be correlated with late aseptic loosening for both types of fixation. Radiographically, Kobayashi et al. (b) found in a follow-up study of 527 Freeman hip replacements of cemented and cementless type, that subsidence of greater than 2 mm and radiolucencies greater than 2 mm in one third of any zone two years post-operatively, were good predictors of long term clinical outcome. A threshold migration of 2 mm per year appears to be applicable to a variety of cemented type I prostheses. However for cemented type II stems, as defined in section 2.1.2, it is found clinically that stem migration is not necessarily associated with stem loosening (Howie et al., 1998; Middleton et al., 1998).

There are two clinical consequences of using a more accurate radiographic analysis technique:

- (i) RSA has the potential to diagnose an asymptotically loose prosthesis. If required, the prosthesis can be replaced before irreparable damage is done to the host bone.
- (ii) This will reduce the time taken to clinically analyse the performance of new implants. No longer will studies have to wait for failure of the implant to assess implant longevity. Longevity can be extrapolated on the basis of the RSA results at two years.

2.6 MEASUREMENT OF MIGRATION RATES IN LABORATORY TESTS

2.6.1 Laboratory tests to measure prosthesis motion

Measuring the migration of a prosthesis relative to bone during a fatigue test is a challenging task. When a testing machine is running in load control mode, the actuator applying the force to the sample continually adjusts its position so that the predetermined loads are applied throughout testing. Therefore, if the prosthesis migrates distally, the actuator will also move distally to compensate for any change in sample position. It is possible to record the position of the actuator throughout testing. This measures the combined displacement of the prosthesis, cement and bone, but does not provide a measure of the prosthesis motion relative to the femoral bone.

To measure relative motions, displacement transducers are used. Prosthesis motion during mechanical testing has been measured; using linear variable displacement transducers (Berzins et al., 1993), strain gauge based extensometers (Schneider et al., 1989), dial gauges (Whiteside and Easley, 1989; Charnley and Kettlewell, 1965) and in some cases custom designed transducers (Buhler et al., 1997a). Typically, one end of the transducer is mounted on the femoral bone, the other is usually spring loaded and in contact with the surface of the prosthesis. The transducers allow linear movement to be measured. It is therefore important that the line of action of the transducer is aligned with the axis of displacement, otherwise what is measured as a translation is actually the result of a combined translation and rotation (see Figure 2.8).

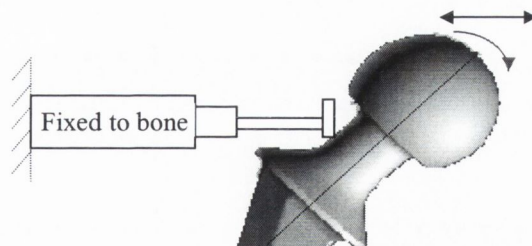


Figure 2.8: A displacement transducer one end of which is fixed to the femoral bone (not shown) the other end is in contact with the neck of the prosthesis. If the prosthesis translates in the direction shown by the black arrow, the transducer will measure the pure translation. If the prosthesis rotates as illustrated by the red arrow, the rotation will be measured as a translation by the transducer.

Despite this obvious limitation, some studies use a single transducer placed either resting on the neck of the prosthesis (Manley et al., 1987; Nunn et al., 1989), on the head of the prosthesis (Weightman et al., 1987; Phillips et al., 1991) or at the tip of the prosthesis (Charnley and Kettlewell, 1965) and measure the overall non recoverable motion of the prosthesis during testing. Even if a measurement of the neck displacement is deemed satisfactory, to fully describe neck translation more than one transducer is needed. However, a combination of more than one transducer at the site of the neck is difficult to achieve due to the lack of space for contact with the prostheses. As a result, many studies measure the motion of a point on the prosthesis at some distance from the prosthetic head (Harman et al, 1995). In other studies one transducer is used and its orientation is altered at different stages throughout testing (Callaghan et al., 1992; McKellop et al., 1991; Engh et al., 1992). Although this allows the motion of the prosthesis along various axes to be measured at different times, the six degrees-of-freedom of motion of the prosthesis is still unmeasurable. Some studies also limit their testing to analysis of prosthesis motion under static loads (Vanderby et al., 1992; Walker et al., 1987), which although gives a measure of the elastic movement of the prosthesis, does not provide a measure of the permanent displacement of the prosthesis under a number of cyclic loads.

The most advanced three dimensional analyses of prosthesis motion have been applied to *cementless* prostheses. Typically three (Buhler et al., 1997b) or more (Gilbert et al., 1992) transducers are used to quantify motion of the prosthesis relative to the surrounding bone. Some studies use a number of transducers that are located randomly along the surface of the prosthesis (Schneider et al., 1989) that measure the combined rotation and translation of the stem (Spiers et al., 2000). In a study by Walker et al. (1987) despite using six LVDTs, distributed between two points on the stem, rotation about the longitudinal axis was still not measurable. In separating the locations of the measurement transducers to two points, seven transducers are needed to fully describe prosthesis motion, as illustrated in Figure 2.9.

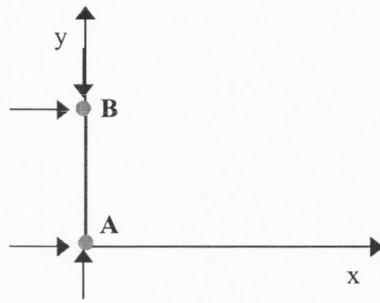


Figure 2.9: Four displacement transducers are needed to measure the rotation of the line AB about the z axis and the displacement in the x and y directions. To measure the rotation about the y axis and translation along the z axis, a further two transducers are needed, pointing out of the plane of the page. Using these six LVDTs, one degree of rotation θ_y is still not measurable.

In a study by Berzins et al. (1993) six LVDTs, were used to measure the six degrees-of-freedom of motion of a cementless prosthesis proximally and distally at different times during the loading history (see Figure 2.10). This is the most sophisticated approach published in literature and is capable of measuring the three-dimensional motion of the prosthesis relative to the bone. However, it is not clear that accurate and reliable methods were used to attach the transducers to the bone and to align the LVDTs relative to the target device. Furthermore, results are only reported for periodic static loads.

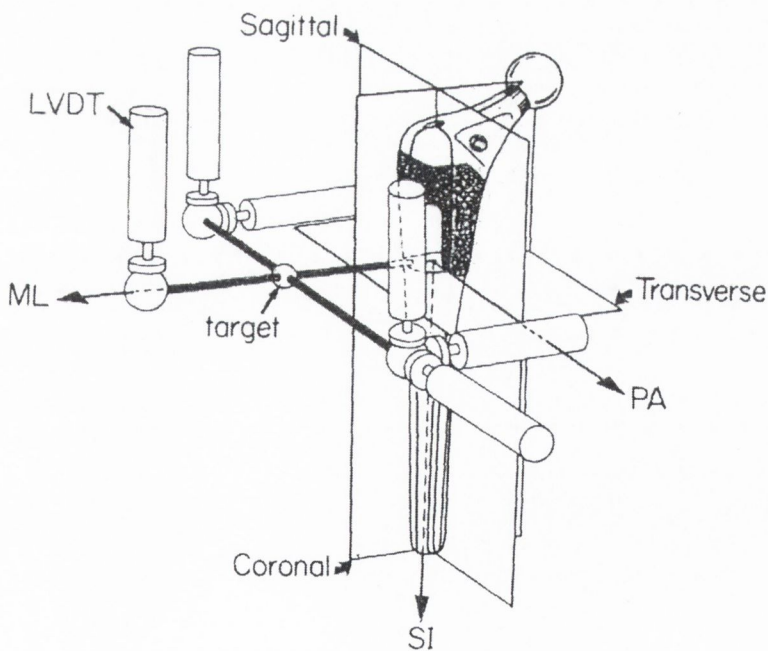


Figure 2.10: Schematic of the test set-up used by Berzins et al., 1993 to measure the six degrees of freedom of motion of a cementless type implant (from Berzins et al., 1993).

2.6.2 Duration of laboratory tests

Many studies report the motion of the prosthesis under a low number of loading cycles (Gilbert et al., 1992; Buhler et al., 1997a; Hua and Walker, 1994). This is of most interest for cementless prostheses where the initial micromotion of the prosthesis determines the extent of bone ingrowth (McKellop et al., 1991; Phillips et al., 1991; Schneider et al., 1989). This is in contrast to cemented prostheses where the initial fixation is generally good, but long term fixation is a problem. Despite this, many tests on cemented replacements have durations of 3000 cycles (Spiers et al., 2000) and 5,000 cycles (McKellop et al., 1991). This is clearly insufficient for an analysis of long term loosening rates. A test which quantifies prosthesis loosening rates for cemented prostheses has not yet been presented.

2.6.3 Presentation of test results

Although measurements of the motion of a point are presented in the above studies, quantification of the overall motion of a prosthesis in an *in vitro* study has never been presented. Even in the most advanced study by Berzins et al. (1993), motion of a point of interest, for example the centre of the prosthesis head, is not presented. It is difficult for the reader to compute the motion of any point along the prosthesis other than that at the measurement site. This is partially due to incomplete description of axes of motion, of the test set-up and due to the complexity of combining the numerous transducer outputs into overall prosthetic motion. An exception to this is the work of Buhler et al. (1997b) where a visual plot of the magnitude and direction of motion of a cementless type prosthesis is presented. Gilbert et al. (1992) also illustrate how the motion of a cementless prosthesis can be animated to plot its movement; however the plot has no scale and it is not easy to interpret the actual motion.

In conclusion, the author has found that presentation of prosthesis migration results in published studies is difficult to interpret; particular attention to presentation of results will have to be considered in this thesis.

2.6.4 Variability in laboratory tests

Where statistical comparison of different prosthesis designs is envisaged, inter sample variation should be kept to a minimum in a laboratory setting. In this way, stem related variables can be distinguished from experimental error (Harman et al., 1995). Ideally, a

protocol which minimises experimental variables is needed which will describe a method to prepare the samples in a standardised way, to locate motion transducers reproducibly, and to compare the overall motion of a point common to the prosthetic designs being tested, for example the centre of the femoral head. In the case of cemented femoral hip replacements, experimental variability can take the following forms:

- (i) *Prosthesis orientation and path of insertion:* The final seated position of the femoral hip stem influences the stress gradients throughout the reconstruction (Andriacchi et al., 1976) and therefore has a significant affect longevity of the femoral hip replacement (Wirta et al., 1993; Ebramzadeh et al., 1994; Star et al., 1994). To minimise this variability in laboratory tests, some researchers have explored the use of milling machines (Schmidt et al., 1994) or materials testing machines (Markolf and Amstutz, 1976) to perform insertions. However, both methods produce linear insertion paths that are not observed clinically and they require excessive reaming of the proximal cavity. Other studies rely on surgeons to insert the prosthesis along a clinically acceptable path (Berzins et al., 1993; Burke et al., 1991, Schnedier et al., 1989). However, variability in the insertion paths and hence in cement pressures generated at the cement/bone interface can be expected. As a result, cement/bone interfacial strengths will differ and the experimental result is surgeon specific. Robots have been used to insert cementless prostheses in a clinical setting and the methodology is continually advancing (Paul et al., 1992; Bargar et al., 1998). However, the cost of multi-axial robotic arms is a distinct disadvantage.
- (ii) *Cementing techniques and canal preparation techniques:* The technique used to prepare bone cement for insertion into the medullary cavity of the femur influences the mechanical properties of the polymerised cement mantle (Brown, 1991). For example, vacuum mixing decrease porosity. The method used to prepare the cancellous bed influences the cement/bone interfacial mechanical properties. Both features influence the longevity of the replacement and therefore must be controlled to eliminate them as variables in an experimental test.
- (iii) *Bone material properties:* Cadaveric bone varies widely in both shape and mechanical properties (Rho et al., 1993; Gibson 1985). To avoid this

variability, composite synthetic femoral bone replicas have been designed with mechanical properties similar to that of bone, but with less variability in mechanical strength and in dimensions (Szivek et al., 1990). Synthetic femora have been used in a variety of experimental tests (Niederer et al., 1978; Szivek and Gealer, 1991) and a summary of the reported mechanical properties of a commercially available synthetic femur are presented in Table 2.2.

Table 2.2: Young's Modulus of composite femora compared with average mechanical properties of autopsied femora.

	Composite Femur	Cadaveric Femur
Cortical Bone	14.2 GPa	17 GPa
Cancellous Bone	0.41 GPa	1.5 GPa

2.7 SUMMARY

The dominant mode of implant failure is loosening relative to the host bone. It has been argued that with existing hip implant technology, prosthesis loosening is inevitable. Implant design clearly has a pivotal role to play in delaying the onset of loosening.

Design innovations are motivated by intuition and new design concepts are frequently implemented by the surgical community without a scientific basis. As a result, there appears to have been an almost frenzied attempt to include all possible design variations in the vast array of prostheses put on the market. In the words of Huiskes (1993),

‘the number of alternative designs, materials, fixation methods and surgical instruments for THR in use, many of which are of uncertain benefit, is staggering’.

It is obvious that there is need for a more controlled approach to the introduction of new implant technology. Such a controlled approach requires a reliable experimental pre-clinical test. Even though there are several attempts in this direction reported in literature, none have yet succeeded in developing a test that can screen-out inferior prostheses in advance of clinical trials.

3: Design and Development of Experimental Procedures

3.1	INTRODUCTION	35
3.2	THE FEMORAL INSERTION MACHINE	36
3.2.1	Conceptual design	36
3.2.2	Design embodiment	36
3.2.2.1	<i>The femur</i>	36
3.2.2.2	<i>The prosthesis</i>	37
3.2.2.3	<i>The cam</i>	37
3.2.2.4	<i>The alignment plate</i>	41
3.2.2.5	<i>Accounting for manufacturing tolerances</i>	43
3.2.2.6	<i>The assembled insertion machine</i>	46
3.2.3	Protocol for the use of the insertion machine	48
3.2.4	Validation of the insertion machine	48
3.2.4.1	<i>Validity of the concept</i>	48
3.2.4.2	<i>Accuracy and repeatability of the preparation and insertion protocol</i>	49
3.2.4.3	<i>Simulating calcar resorption</i>	51
3.3	THE MIGRATION MEASUREMENT DEVICE	52
3.3.1	Theoretical background	52
3.3.2	Conceptual design	56
3.3.3	Design embodiment	59
3.3.3.1	<i>Attachment of the migration measurement device to the prosthesis</i>	59
3.3.3.2	<i>Holder for displacement transducers</i>	61
3.3.3.3	<i>Attachment to the femur</i>	62
3.3.3.4	<i>Alignment of the LVDTs</i>	63
3.3.4	Data acquisition	68
3.3.5	Testing of the migration measurement device	71
3.3.5.1	<i>Testing the attachment between the target device and the prosthesis</i>	71
3.3.5.2	<i>Confirmation that the migrations calculated are the migrations that are occurring</i>	72
3.4	CYCLIC TESTING	73
3.4.1	Preliminary investigations	73
3.4.2	Set-up for cyclic loading for migration measurement	73
3.4.3	Post test analysis	74
3.5	SUMMARY	76

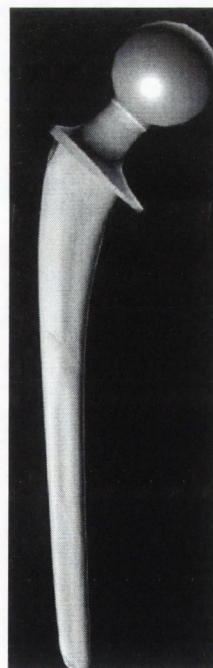
3.1 INTRODCUTION

In this chapter the design of an experimental preclinical testing protocol is presented. The technical challenges of each step in the protocol, the methods used to solve these challenges, the validation methods used, and the final protocol details are explained. The two prosthesis designs that are tested in this research are the Müller Curved Prosthesis, hereafter called the Müller prosthesis: Sulzer Medica, Winterthur, Switzerland (Figure 3.1a), and the Lubinus SPII prosthesis: W.Link, Hamburg, Germany (Figure 3.1b), hereafter called the Lubinus prosthesis. The prostheses are chosen because of the differences in their loosening rates, when implanted using similar cementing techniques:

- i) The Lubinus prosthesis has a radiographic loosening rate of 10% at ten years (Ohlin and Önsten, 1990).
- ii) The Müller prosthesis has a radiographic loosening rate of between 20% at six years (Krismer et al., 1991) and 40% at ten years (Sutherland et al., 1982).



(a)



(b)

Figure 3.1: The two prostheses that are tested using the protocol herein described: (a) the Müller Prosthesis and (b) the Lubinus prosthesis.

3.2 THE FEMORAL INSERTION MACHINE¹

Repeatability in sample preparation was achieved through the design of a custom built machine to insert cemented prostheses into synthetic femora of controlled dimensions.

3.2.1 Conceptual design

In order of importance, the design requirements for the insertion machine were that it should be able to:

- (i) Insert a femoral hip prosthesis along a pre-determined, reproducible insertion path.
- (ii) Insert it into a pre-determined, reproducible final position to achieve reproducibility in the cement mantle thickness.
- (iii) Implant all prostheses geometries.
- (iv) It should be possible to fabricate the machine in a standard workshop.

Many design concepts were initially proposed. The first was to use stepper motors to incrementally move a prosthesis into a femur via lead screws. The second approach was to use a telescopic arm which would pivot about one end and clamp the prosthesis at the other end. The third was to graphically animate a path of prosthesis insertion that could be reproduced in space. A design concept based on a graphical animation was selected. This approach offered the greatest flexibility for inserting different prostheses designs along user-specified insertion paths. Furthermore, the user could visualise the required insertion path and final seated position of the prosthesis in advance of the insertion.

3.2.2 Design embodiment

3.2.2.1 *The femur*

To decrease the variability in sample preparation, synthetic composite femora (Pacific Research Laboratories Inc., Vashon Island, Washington, USA) were used. The consistency in femoral dimensions aided in designing clamps and fixtures to hold the synthetic femora in specified orientations. A profile of a composite femur was obtained from the Standardised Femur Program (Prometeo Project, Rizzoli, Italy; Viceconti et al., 1996) where a composite femur was digitised and the slices assembled to produce a solid model.

¹ This has been published in Maher et al. (2000)

3.2.2.2 *The prosthesis*

Surface models of the Lubinus and Müller prostheses were created from data generated from a coordinate measurement machine (courtesy of M. Morlock, Technical University Hamburg, Germany).

3.2.2.3 *The cam*

A specific cam for a predetermined seated position and insertion path for each prosthesis was produced by graphically simulating the insertion of a prosthesis into a composite femur in the frontal plane (Figure 3.2). The animation was performed using 3D Studio software (Kinetix, California, USA).

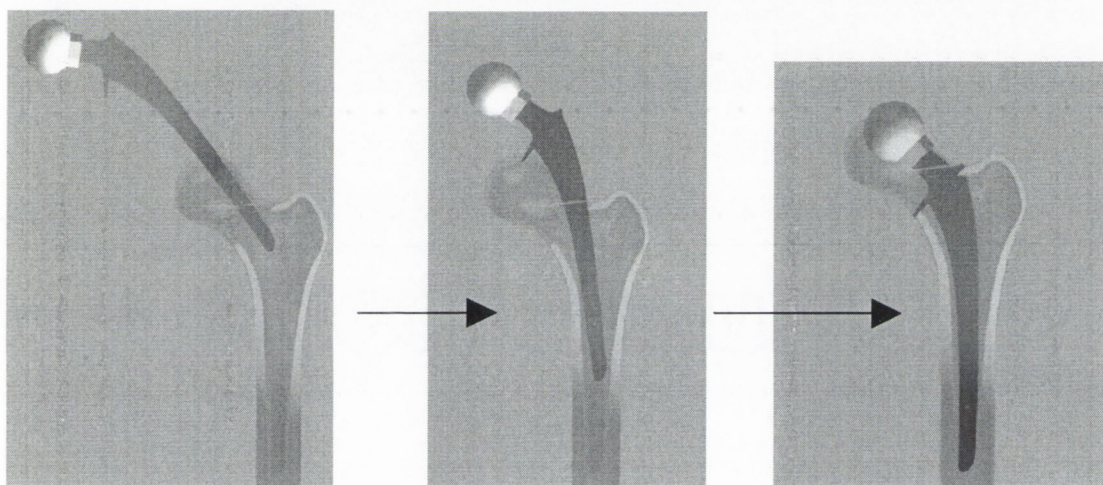


Figure 3.2: The concept of graphically animating the path of insertion of a prosthesis. A solid model of a prosthesis is incrementally moved into a solid model of a femur. The challenge is to reproduce this motion in space.

The final seated position in the frontal and the sagittal planes were defined by an experienced orthopaedic surgeon (Dr. Aldo Toni, Istituti Ortopedici Rizzoli, Bologna, Italy). The insertion path was typically designed to produce a smooth path of insertion, similar to that which might be attempted clinically. Prosthesis/bone contact during insertion was avoided. The motion of two points which were linked to the prosthesis (whose position was known relative to the prosthesis) were taken to describe the insertion path, see Figure 3.3. The motion of these two points during the simulated insertion are called *trajectories*.

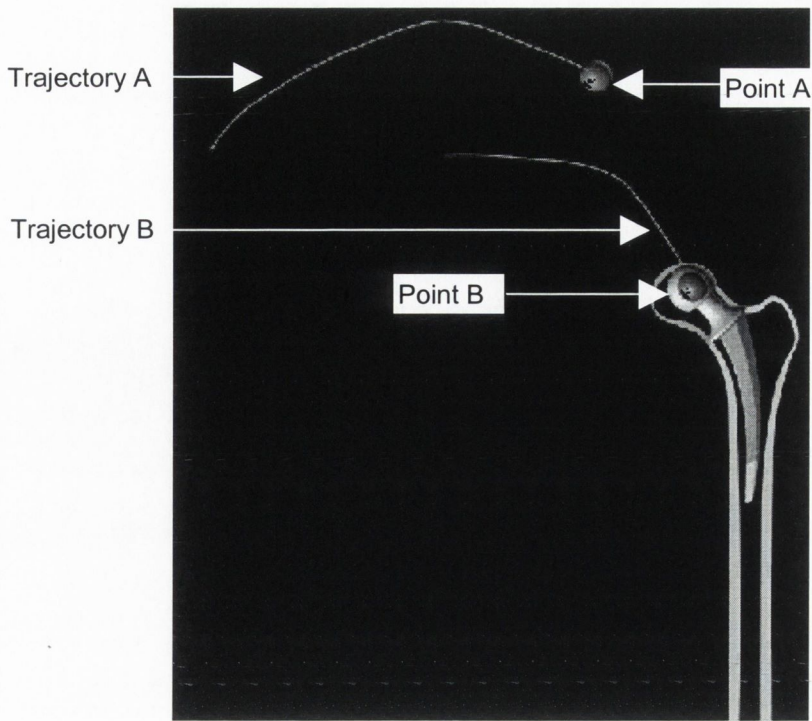


Figure 3.3: Two points (point A and point B) are fixed to the stem of the prosthesis during the animated insertion. During insertion, they graphically plot two trajectories that describe the path of insertion. The trajectories for the Müller prosthesis are illustrated.

The two trajectories for each prosthesis were exported to drawing software (in this case AutoCad v.13), offset to allow for the radii of the rollers would eventually produce the insertion movement, and joined to form a closed profile, see Figure 3.4. The profiles created were machined, using computer numerically controlled techniques, from mild steel plate to produce a *cam*.

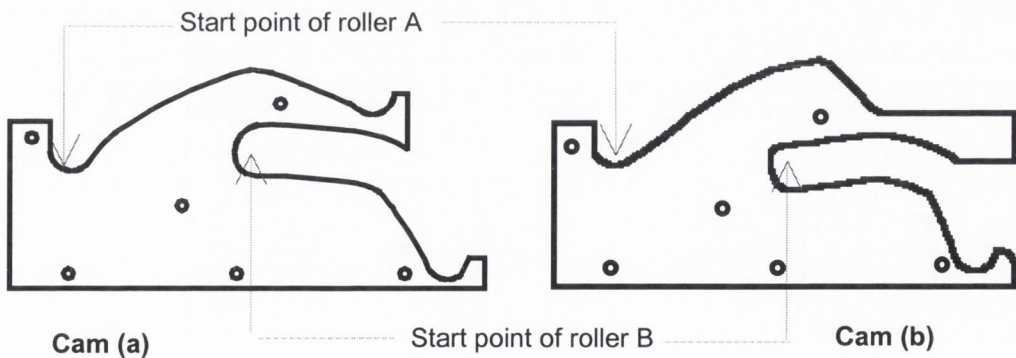


Figure 3.4: Cam (a) was produced by joining the trajectories plotted by the Müller prosthesis. Cam (b) was produced by joining the trajectories plotted by the Lubinus prosthesis. The holes in both cams are for attachment to the insertion machine.

A detailed breakdown of the steps followed in animating and designing the cam profile are listed in Appendix A, page 158.

Since the machine was intended to insert many different prosthesis profiles, the cam was designed to be a detachable fixture on the insertion machine. The cam was bolted to the back-plate of the insertion machine via six rigid pillars. The location of the pillars could vary depending on the shape of the cam. As illustrated in Figure 3.5, two rollers were seated on the cam (in this case the Müller cam is shown) and were connected via front and back cheek plates to produce a *carriage*, onto which the prosthesis was clamped.

Two pneumatic cylinders moved the carriage along the cam. The horizontal force component pushed the rollers along the cam, hence pushing the prosthesis into the femur. The line of action of the vertical cylinder acted between the two rollers of the carriage throughout the movement of the prosthesis along the cam, to keep the rollers in constant contact with the cam. The two pneumatic cylinders acted through perpendicular guide rails. The guide rails ensured that no out-of-plane motion of the arm connecting the pneumatics to the carriage occurred during insertion (see Figure 3.6).

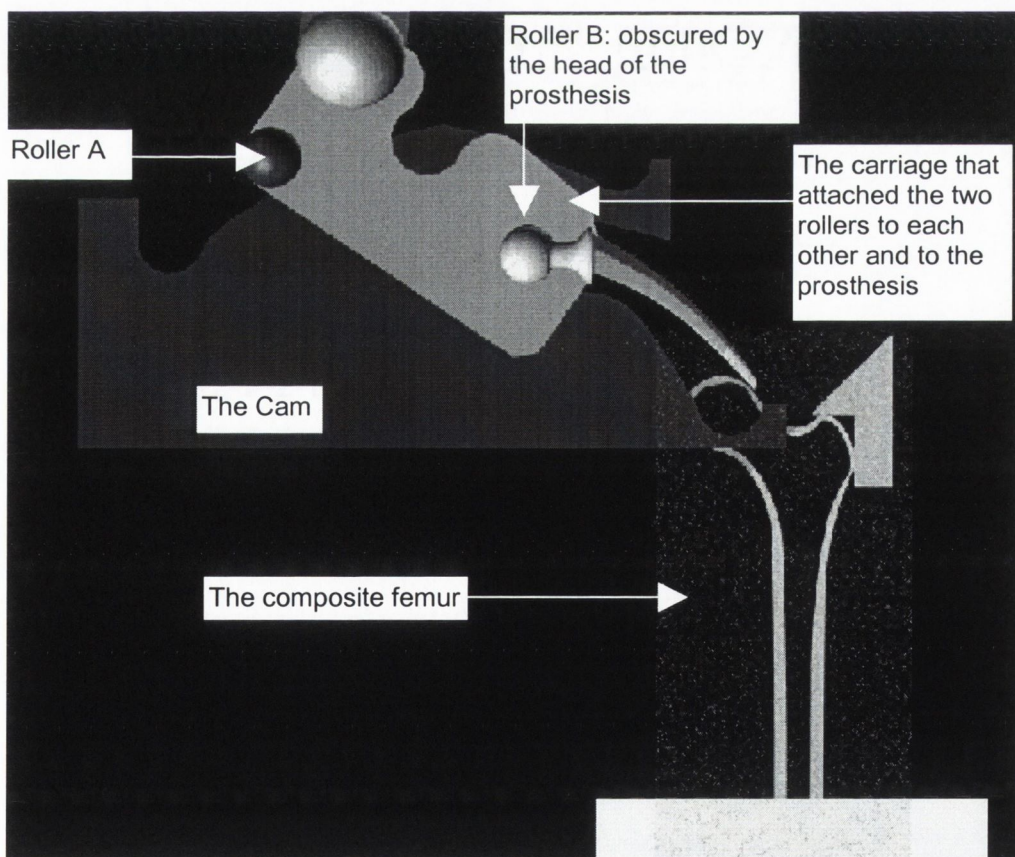


Figure 3.5: Schematic of the two rollers, the carriage, the pneumatics and the composite femur.

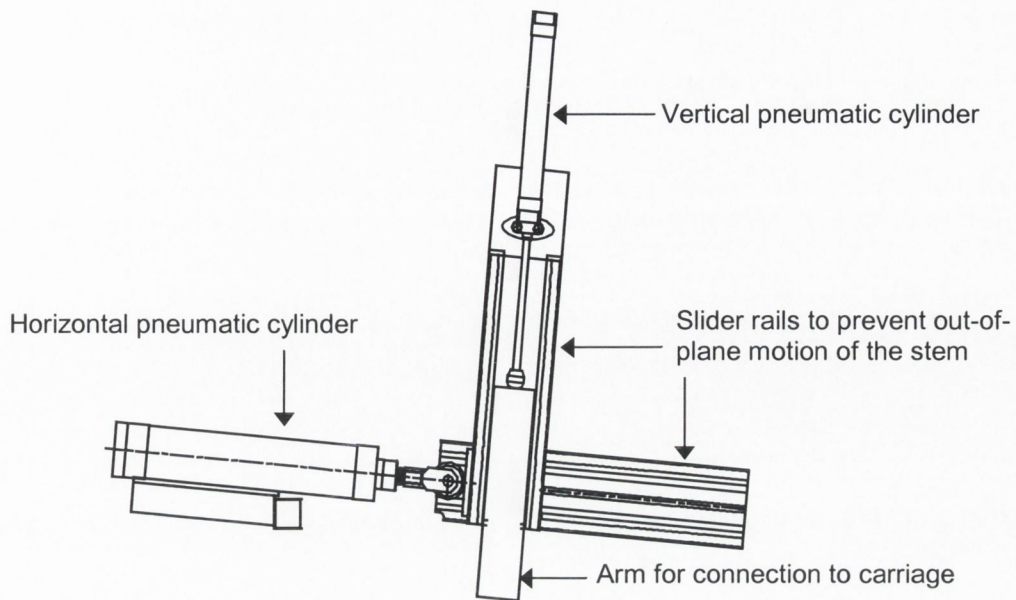


Figure 3.6: The pneumatics which pushed the prosthesis into the femur.

When designing the cam profile the following points were considered:

- (i) Any two points, A and B, could be chosen to represent the path of insertion of the femoral stem (see Figure 3.5). However to avoid changing the design of the carriage, after the first carriage had been manufactured, the two points were positioned on the centres of the original rollers.
- (ii) Any path could be chosen to join up the two trajectories to form a closed profile. However, the design was constrained to a cam profile that would not result in the rollers impacting off the underside of the cam — particularly the roller centered on point B, at the start of the cam.
- (iii) Before manufacturing the cam, an animation of all moving parts was made. If collision of moving parts happened, the starting point of roller A was moved to a different position along the circumference of a circle drawn centered on roller B, with a radius equal to the distance $|AB|$. This created a different trajectory for roller A, but the carriage design was not changed, because the distances between the rollers remained unchanged.
- (iv) The success of the implantation using the cam profile was dependent on how closely the femur and the prosthesis could be clamped relative to the intended orientation as specified in the animation software.

3.2.2.4 The alignment plate

An alignment plate was designed to orient the femur as specified in the animation, to provide a method to reproducibly rasp the medullary cavity, and to hold the femur in place during prosthesis insertion

As illustrated in Figure 3.7, the alignment plate had two blocks against which the femoral head and greater trochanter were located. The distal end of the femur rested on a third block. Two pockets were milled out of the base of the alignment plate and a third was milled out of the distal block. This allowed the femoral head, the greater trochanter and the distal end of the proximal femur to be supported at different heights relative to the base of the alignment plate which ensured that prosthesis insertion occurred in the plane specified in the animation. Once aligned, the femur was locked down to prevent further movement. The femoral head was resected at an angle which was guided by an angled block at the level of the greater trochanter (see dotted line in Figure 3.7).

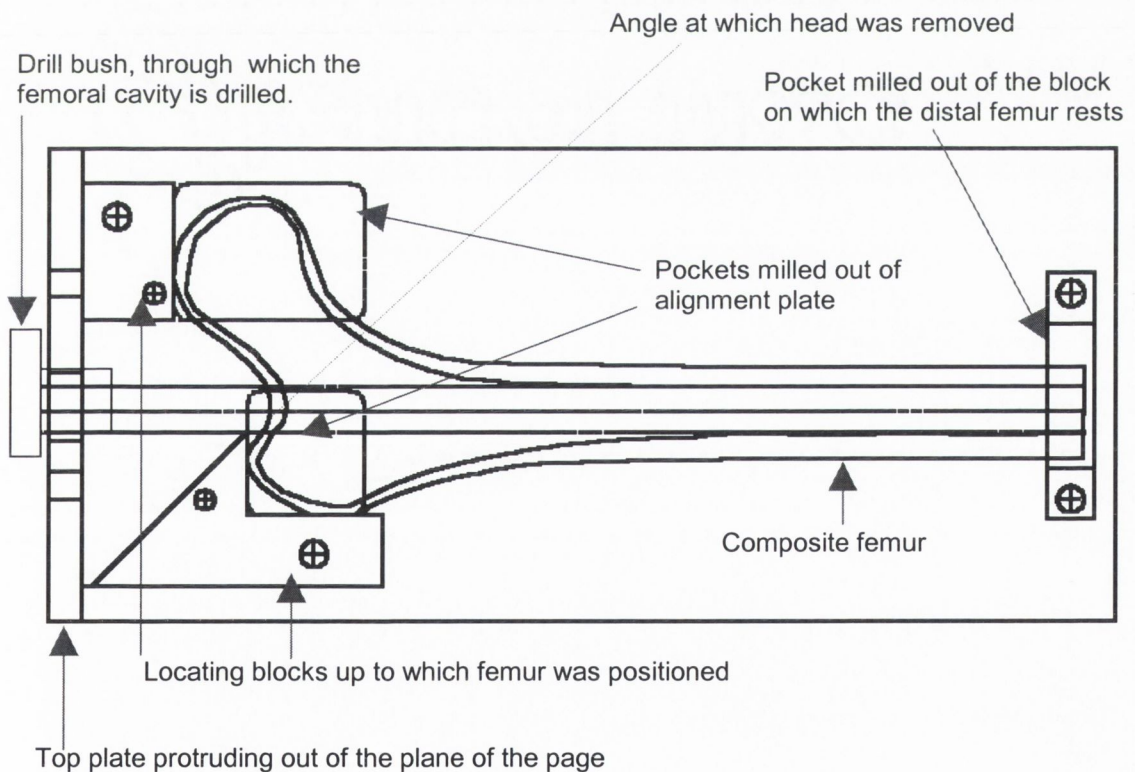


Figure 3.7: The alignment plate used to position the composite femur in a reproducible orientation.

A *top plate* was pinned and bolted to the top of the alignment plate, (see Figure 3.7). The plate had a drill bush press-fit into a reamed hole through the plate. The drill bush acted as a locator for rasping the mid and distal femoral cortex. The procedure used to rasp the medullary cavity was as follows:

- (i) The alignment plate was mounted on the base of a radial drill.
- (ii) Its verticality was checked using a dial gauge (see Figure 3.8).
- (iii) A 12 mm long series solid carbide centre drill was centered within the drill bush, and used to drill through the cortex of the proximal femur.
- (iv) A 12 mm slot drill was centered within the drill bush, and used to flatten the cone shaped cavity that remained after the centre drill.
- (v) A long series twist drill of diameter 13 mm drilled through the drill bush to a depth that would produce a mantle of cement at least 2 cm below the distal tip of each prosthesis.
- (vi) The alignment plate was removed from the base of the radial drill.
- (vii) The femoral head was resected by aligning a hacksaw with the angled plate as illustrated in Figure 3.7.
- (viii) The proximal femur was rasped using the implant manufacturer's rasp specific to the prosthesis that was being inserted.

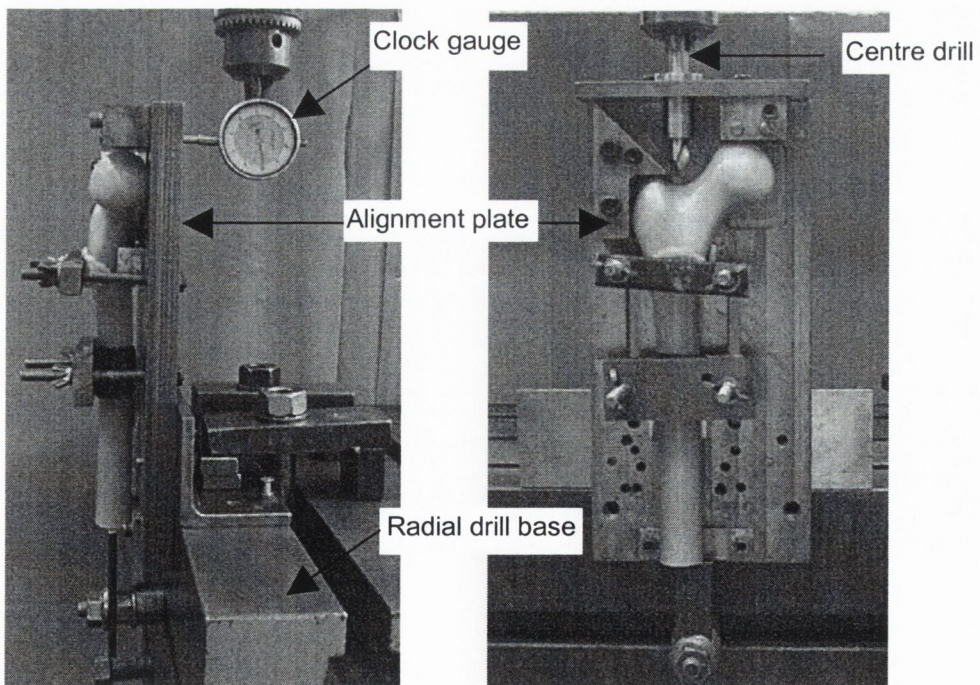


Figure 3.8: Set-up for drilling the composite femur.

3.2.2.5 Accounting for manufacturing tolerances

The exterior tolerance of the composite femora was ± 1.0 mm and the interior dimensional tolerance was ± 1.5 mm (personal communication, F. Millar, Sawbones, Pacific Research Labs, 1997). With such tolerances, it was expected that, by locating the femora using the alignment plate described in section 3.2.2.4, variations in the position of the femora would result. However, the drilled femoral medullary cavity would remain precisely located relative to the alignment plate. Therefore the prosthesis was reproducibly positioned relative to the rasped medullary cavity.

Depending on the manufacturing technique, tolerances of the femoral prostheses could also be wide, where significant variations between the neck-stem angle (up to 2°) and in the length of the prosthesis (by as much as 3 mm) were possible. These variations were noted by others (Kiss et al., 1995) and compensated for prior to insertion (Paul et al., 1992). With these high tolerances, it was impossible to simultaneously ensure both reproducible cement thickness around the entire stem profile and reproducible positioning of the prosthetic head. It was decided to create reproducible cement mantle thickness.

To control cement mantle thickness, certain pre-insertion tasks were necessary to align the prosthesis relative to a fixed frame. A femur was resected and rasped in a standard way and had *alignment slots* milled longitudinally on the medial, lateral, anterior and posterior sides. This femur was named an *alignment femur* and was used as a reference relative to which each prosthesis could be located prior to insertion. The concept of aligning the prosthesis was that the final seated position of the prosthesis, as measured at two predefined vertical heights in the animation software, could be recreated in the physical model. This could be achieved by pushing the prosthesis into its predefined position at a distal point, locking that point in place, and then pushing the proximal point into its required orientation, causing the prosthesis to rotate about its distal locked position.

The concept was embodied in the design illustrated in Figure 3.9, where micrometer heads were used to push the prosthesis into its predefined position. The micrometer heads were held in position in measurement brackets, which maintained the orthogonality of the micrometer heads, and allowed their vertical position along the alignment plate to be varied. This allowed for short stemmed prostheses, like the Müller prosthesis, to be aligned using the protocol developed. A detailed description of the alignment procedure is provided in Appendix A, Table A2 and Table A3, page 160.

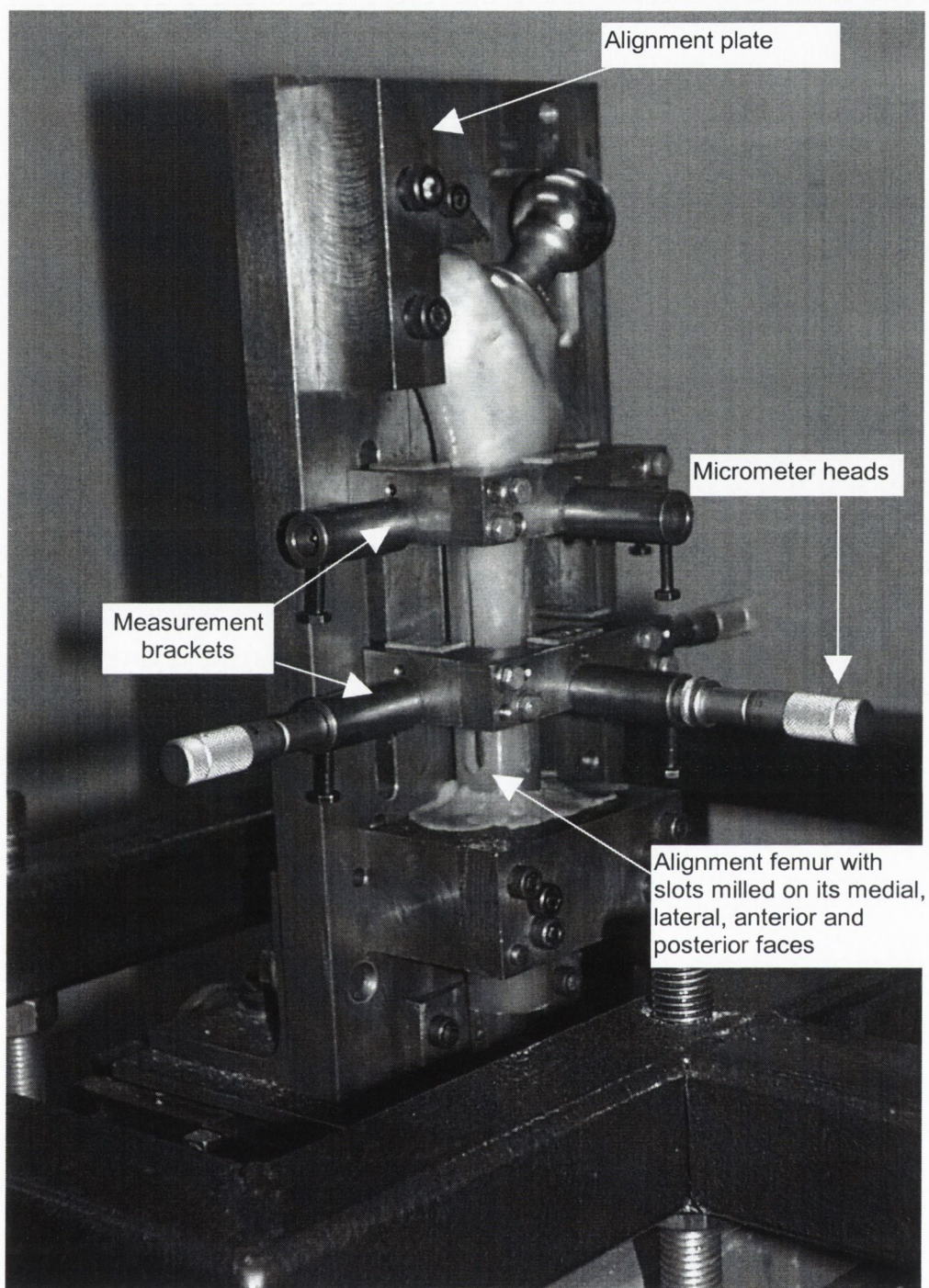


Figure 3.9: The alignment plate bolted to the insertion machine, with the measurement brackets in place. The vertical position of the measurement brackets were defined in the animation software, and varied for different prosthesis designs.

To facilitate this method of pre-insertion alignment, the mechanism to grip the prosthesis during the insertion procedure needed the ability to:

- i) Rigidly grip both tapered shafts (for modular prostheses) and spherical heads of prostheses: this was achieved using a toolmaker's clamp.
- ii) Allow for a prosthesis head to be gripped regardless of its final orientation: this was achieved using a *spherical joint* that could be locked in any rotational position, see Figure 3.10.

The alignment plate was bolted to an x-y table, which allowed movement in the medial/lateral (x) direction and in the anterior/posterior (y) direction. The xy table was mounted on threaded bars which allowed for adjustments of the clamp in the vertical (z) direction (see Figure 3.11). This feature allowed space for the user to access the prosthesis for the alignment procedure. Once the prosthesis was located within the alignment femur, as specified in the animation of the insertion, the spherical joint and the z position of the x-y table were adjusted to allow the head of the prosthesis to be clamped rigidly in the toolmaker's clamp¹. The x-y-z table also added additional flexibility to the insertion machine, so that if a longer insertion path for a prosthesis was required, the femur could be moved to accommodate a longer cam profile.

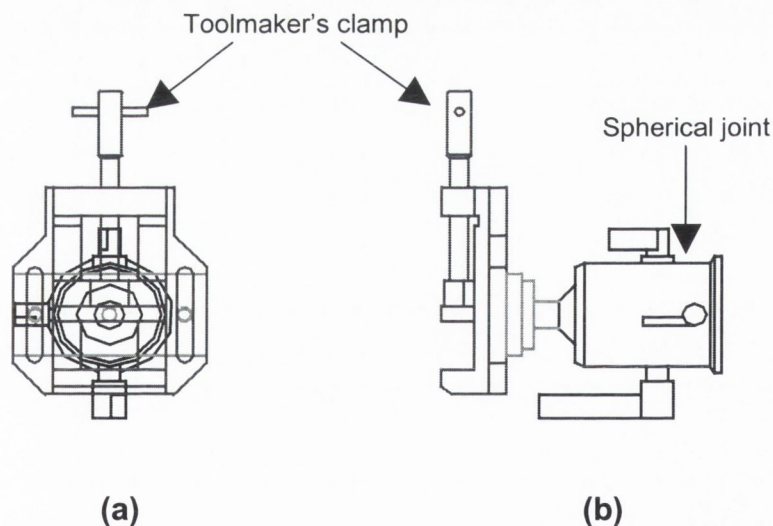


Figure 3.10: A front view (a) and a side view (b) of the spherical joint and toolmakers clamp which give the insertion machine flexibility in gripping either a tapered prosthetic head or a spherical prosthetic head.

¹A detailed description of the steps involved in aligning the prosthesis and femur for insertion are presented in Appendix A, Table A3, page 160.

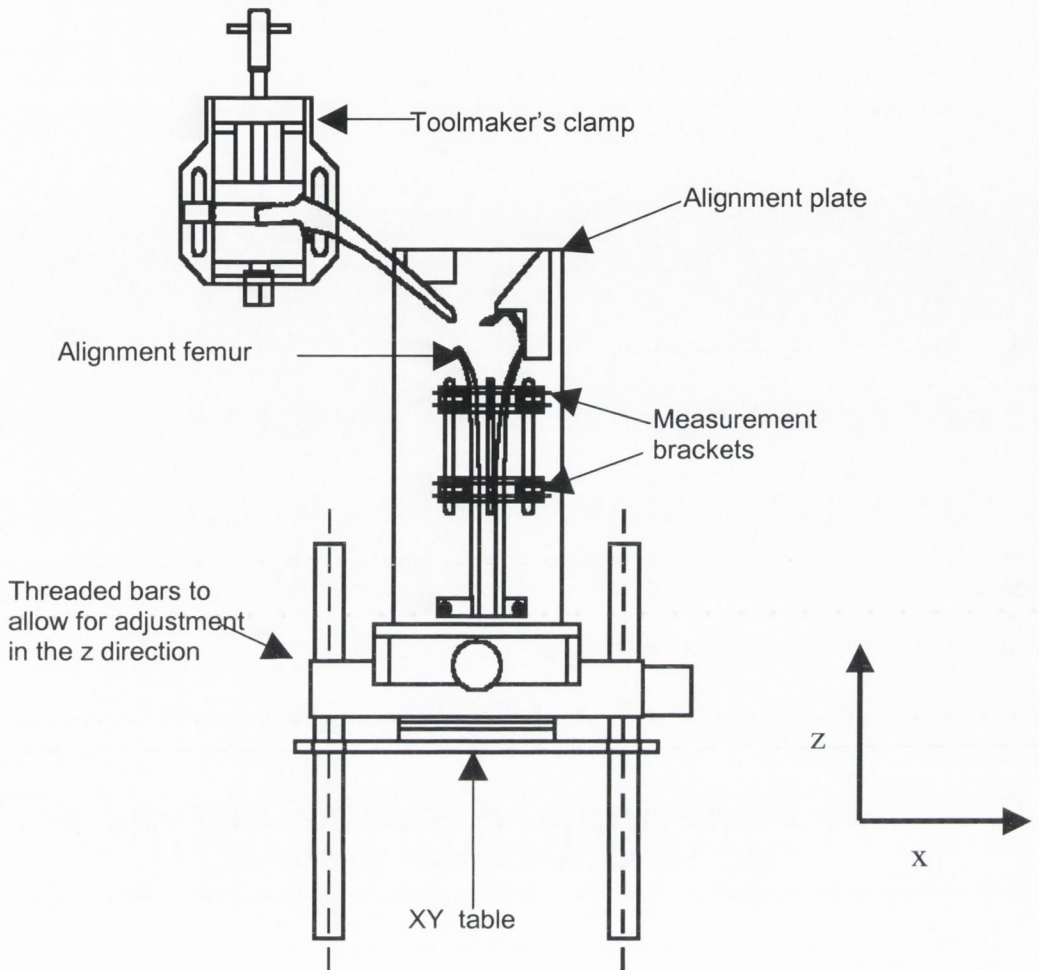


Figure 3.11: The x-y table and the threaded bars allowing for adjustment of the position of the clamped femur in the x, y and z directions are illustrated. The prosthesis head has been aligned, its head clamped and retracted to its start position along the cam profile.

3.2.2.6 The assembled insertion machine

The assembled insertion machine is illustrated in Figure 3.12. The frame is of mild steel box section construct, forming a rigid light-weight structure. It has wide base which provided good stability. The pneumatics, guide rails, and cam are mounted on a backplate, and their relative positions can be varied, if necessary to accommodate specific cam profiles.

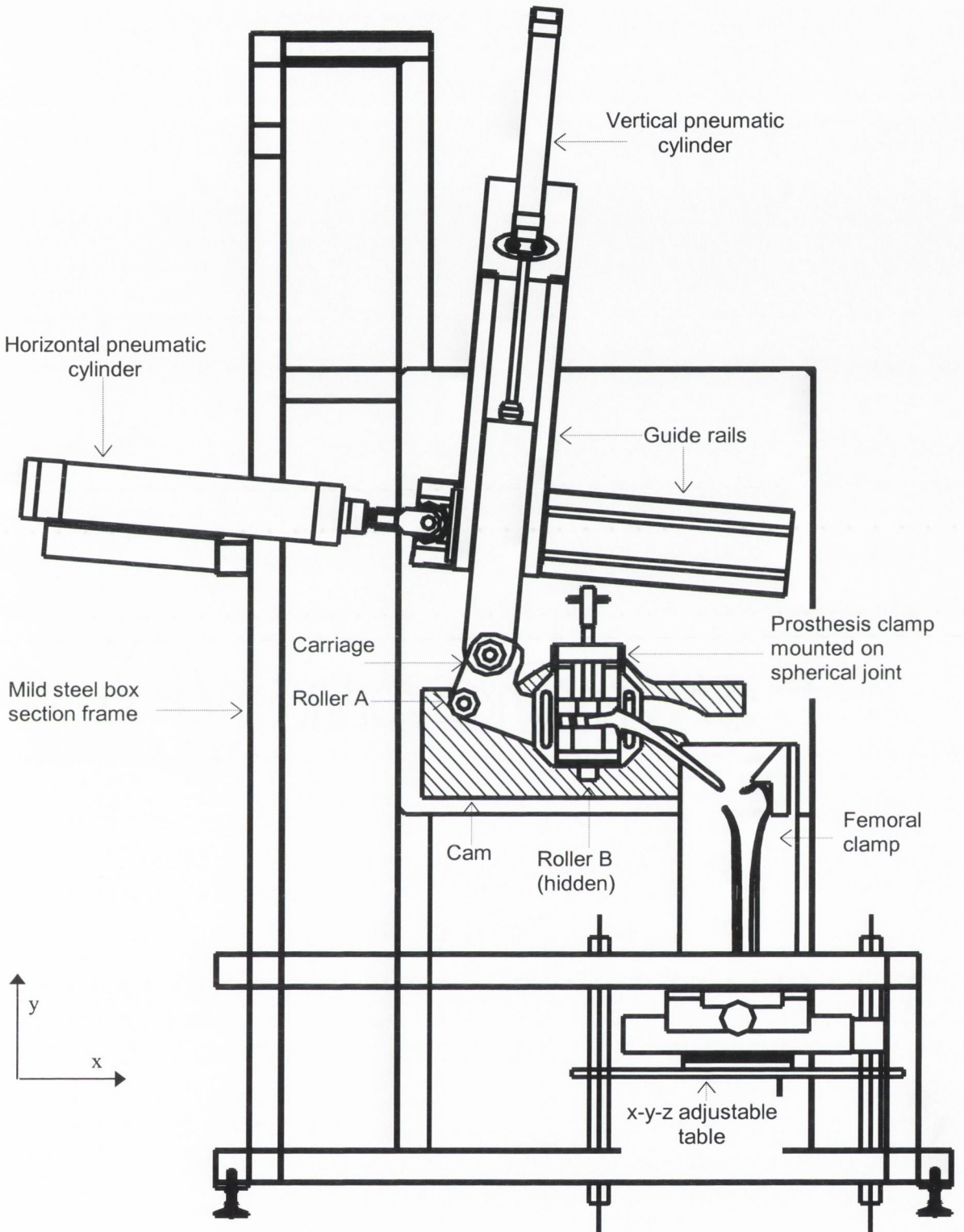


Figure 3.12: A schematic of the assembled insertion machine. Note: engineering drawings of the insertion machine are presented in Appendix G, page 209.

3.2.3 Protocol for the use of the insertion machine

The protocol for use of the insertion machine is given in detail in Appendix A, Table A3, page 160. In brief, the procedure involved is:

- (i) The prosthesis is aligned relative to the alignment femur and its head locked.
- (ii) The prosthesis is retracted it to its start position along the cam profile.
- (iii) The femur into which the prosthesis will be inserted — otherwise known as the *test femur* — is prepared and mounted on the insertion machine.
- (iv) Cemex Rx Low Viscosity cement (Tecres, Verona, Italy) is prepared using a vacuum mixing system named Optivac (Mitab, Sjöbo, Sweden).
- (v) The medullary canal is filled with cement in retrograde using a cement gun.
- (vi) Activating the pneumatics to push the prosthesis along the insertion path into the cemented cavity of the test femur.

3.2.4 Validation of the insertion machine

3.2.4.1 Validity of the concept

To explore the validity of the concept behind the insertion machine, a path of insertion for a simple curved stem fabricated in-house was determined. Six replica prostheses were made from aluminium plate. To explore the reproducibility of the insertion machine, the replica prostheses were inserted into cemented aluminium box section, see Figure 3.13.

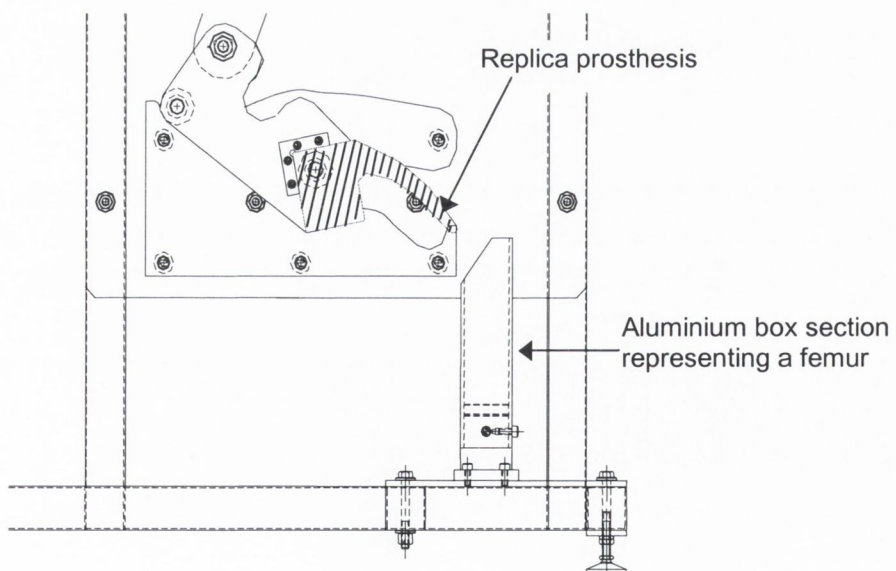


Figure 3.13: The insertion machine as it was setup for the validation of the design concept. Replica prosthesis (shaded in the diagram) were inserted into aluminium box section.

After polymerisation, the cemented box sections were sectioned transversely at 10 mm intervals using a Metaserv cut off machine, with abrasive cutting wheels (MetPrep Ltd., UK, Ref 10 99 24) and an oil based cutting fluid. This resulted in 12 slices for each box section. The distal side of the slices were scanned at 200% magnification into DeskScan II Software© via a Hewlett Packard ScanJet 4C. The images were imported into Paint Shop Pro 4©, and the cement thickness along medial and anterior sides were measured. The mean and standard deviation of the cement thickness for 12 corresponding slices of the five sectioned femora were evaluated. The Results are presented in Section 4.1.2.

3.2.4.2 Accuracy and repeatability of the preparation and insertion protocol

The *accuracy* of insertion was defined as how closely the final seated position of the prosthesis (as specified in the animation software) could be produced using the insertion machine. This was dependent on:

- (i) The dimensional accuracy of the profiles of the femoral stem and the composite femur that were imported into the animation software.
- (ii) The tolerances to which the cam profile was machined. This would, in turn, be influenced by the way in which the cam was clamped during machining, whether the cam deflected during machining, the speed of cutting, and whether the cam was machined in one or more passes of the cutting tool.
- (iii) The accuracy with which the vertical position of the *measurement brackets* was determined compared to the vertical position defined in the computer animation.

To quantify both accuracy and repeatability of cement mantle thickness, six Lubinus prostheses were inserted into composite femora along the cam shown in Figure 3.4(b). The position of the prostheses was quantified as follows:

- (i) The implanted femora were placed in a Perspex frame, designed so that each femur was positioned in the same orientation as achieved using the alignment plate, see Figure 3.14.

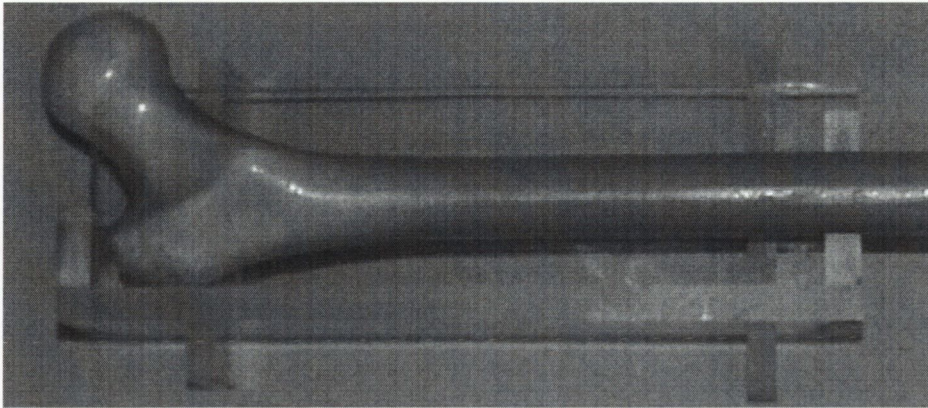


Figure 3.14: The Perspex frame that was manufactured with dimensions identical to the femoral alignment plate (compare with Figure 3.7).

- (ii) A metallic ruler was positioned adjacent to the Perspex box, to allow magnification factors to be calculated
- (iii) The implanted femora were radiographed in the frontal and sagittal planes.
- (iv) The radiographs were placed on an overhead projector which magnified the images.
- (v) The magnification factor was computed.
- (vi) In the frontal view on the magnified image, two levels were marked: one 10 mm from the prosthesis distal tip and one 80 mm from the distal tip.
- (vii) The stem thickness at these two levels were measured and a line called the *mid line* was drawn connecting the mid point of the stem at the two levels.
- (viii) At 20 mm intervals from the prosthesis tip, lines were drawn perpendicular to the mid line.
- (ix) The distance between the surface of the prosthesis and the outer cortex wall, and the between the surface of the prosthesis and the outer cortex wall were measured, at each horizontal line (see Figure 3.15).
- (x) Steps (v) to (ix) were repeated for measurements in the sagittal view.

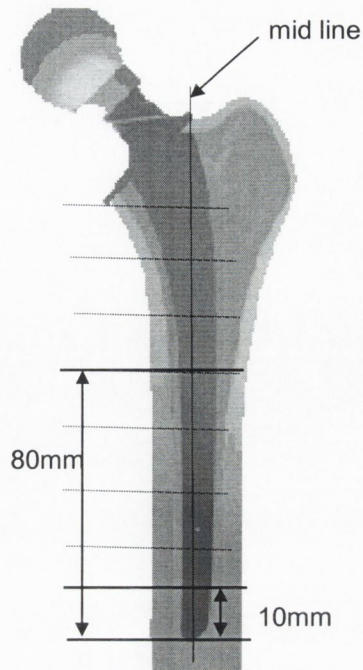


Figure 3.15: The measurements made from the radiographs in the frontal views. The dark solid lines are the first construction lines drawn on the magnified images. A mid line is drawn connecting the prosthesis cross section centres at the 10 mm and 80 mm level. All other lines along which measurements are made are drawn perpendicular to this line.

Due to difficulties in visualising the bone cement in the radiographs, the cement mantle thickness around the prosthesis was not quantified. The standard deviations between the measurements taken from the six implanted femora were computed to quantify the repeatability of the final seated position. A comparison between the animated seated position of the prosthesis and the actual seated position (as measured on the radiographs of the inserted femora) allowed the accuracy of the insertions to be quantified. The results are presented in Section 4.1.3.

Note: In all insertions it was necessary to keep the collar of the prosthesis slightly above the resected femoral head of the alignment femur during the alignment procedure. This was to prevent the collar from impacting on the neck of the resected test femur during insertion. This would cause the prosthesis to rotate about the point of contact into a different position than that specified during the alignment procedure.

3.2.4.3 Simulating calcar resorption

To simulate resorption under the collar of the prosthesis, 3 mm of cortical bone was machined from two implanted Müller and two implanted Lubinus stems (see figure 3.16).

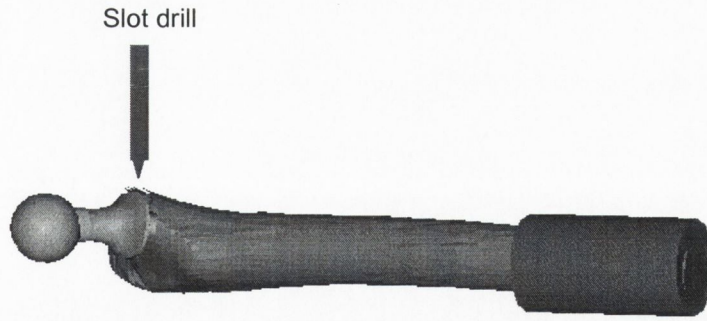


Figure 3.16: The implanted composite femur is mounted on a milling machine, and using a long series solid carbide drill, 3mm is machined from the bone underneath the collar.

3.3 THE MIGRATION MEASUREMENT DEVICE

3.3.1 Theoretical background

A rigid body can be defined as a set of particles subject to the constraint that the distances between all particles remain constant during motion. According to Selvik (1989), Euler (1776) proved that the displacement of a rigid body with one fixed point is a rotation about an axis through this point. A corollary to this theorem is that the general displacement of a rigid body is the sum of the translation of a base point and a rotation about this base point (Selvik, 1989). The concept behind the design of the migration measurement device was that prosthesis motion could be described as rigid body motion. The concepts presented in this section are largely based on the mathematical principles used by Selvik (1989) in describing how RSA techniques (see section 2.5.2, page 26) were used to quantify the rigid body dynamics of the skeletal system.

A cartesian coordinate system (x,y,z) is fixed in space — *space fixed system* — with its origin at O . Consider a rigid body, the extremities of which are joined to form the vector PO . A cartesian coordinate system (X,Y,Z) is fixed to PO — *body fixed system* — with its origin at O . Initially, the origins and orientations of the space fixed system and body fixed system coincide. Point P initially has known coordinates (x_0, y_0, z_0) relative to the body fixed axes and the space fixed axes. If PO , as illustrated in Figure 3.17, is rotated about O through θ_z . The new co-ordinates of P relative to the space fixed system become:

$$\begin{aligned} x_\theta &= x_0 \cos\theta - y_0 \sin\theta \\ y_\theta &= x_0 \sin\theta + y_0 \cos\theta \\ z_\theta &= z_0 \end{aligned} \quad (3.1)$$

where $x_\theta, y_\theta, z_\theta$ are the coordinates of the vector in the space-fixed system.

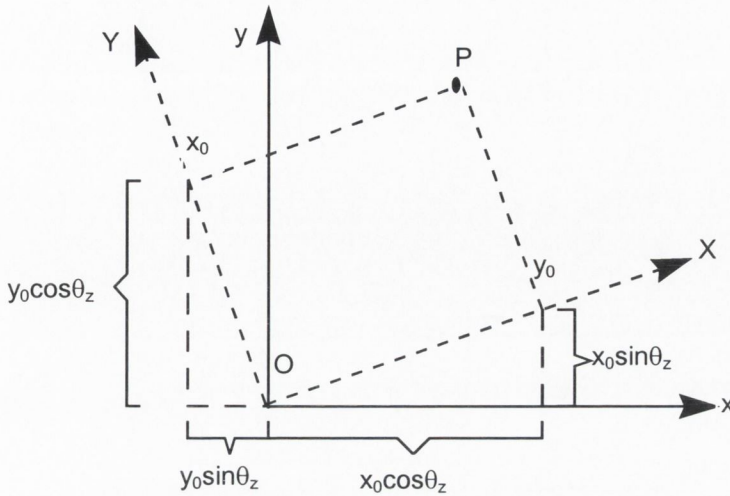


Figure 3.17: A rotation of a body fixed coordinate system about the $z = Z$ axis through an angle θ . The space fixed axes are (x,y,z) , the body fixed axes are (X,Y,Z) .

In matrix notation, this can be written as:

$$\begin{Bmatrix} x_\theta \\ y_\theta \\ z_\theta \end{Bmatrix} = \begin{bmatrix} \cos\theta_z & -\sin\theta_z & 0 \\ \sin\theta_z & \cos\theta_z & 0 \\ 0 & 0 & 1 \end{bmatrix} \begin{Bmatrix} x_0 \\ y_0 \\ z_0 \end{Bmatrix} \quad (3.2)$$

To quantify θ_z two displacement transducers can be placed in the x - y plane. These will measure x_θ and y_θ . The transducer along the x axis will measure $x_0 \cos\theta_z - y_0 \sin\theta_z$ and the transducer along the y axis will measure $x_0 \sin\theta_z + y_0 \cos\theta_z$. Knowing the start coordinates of P , (x_0, y_0, z_0) and the end coordinates of P , $(x_\theta, y_\theta, z_\theta)$, θ_z can be computed through solving the simultaneous equations from (3.2).

If rotation occurs, with O fixed, about the $y = Y$ axis, then about the $x = X$ axis, (3.2) becomes:

$$\begin{Bmatrix} x_\theta \\ y_\theta \\ z_\theta \end{Bmatrix} = \begin{bmatrix} 1 & 0 & 0 \\ 0 & \cos\theta_x & -\sin\theta_x \\ 0 & \sin\theta_x & \cos\theta_x \end{bmatrix} \begin{bmatrix} \cos\theta_y & 0 & \sin\theta_y \\ 0 & 1 & 0 \\ -\sin\theta_y & 0 & \cos\theta_y \end{bmatrix} \begin{bmatrix} \cos\theta_z & -\sin\theta_z & 0 \\ \sin\theta_z & \cos\theta_z & 0 \\ 0 & 0 & 1 \end{bmatrix} \begin{Bmatrix} x_0 \\ y_0 \\ z_0 \end{Bmatrix} \quad (3.3)$$

This is the complete formula for composite rotations about space fixed axes. Multiplying the three rotation matrices results in:

$$\begin{Bmatrix} x_\theta \\ y_\theta \\ z_\theta \end{Bmatrix} = [R] \begin{Bmatrix} x_0 \\ y_0 \\ z_0 \end{Bmatrix} \quad (3.4)$$

where,

$$[R] = \begin{bmatrix} \cos\theta_y \cos\theta_z & -\cos\theta_y \sin\theta_z & \sin\theta_y \\ \sin\theta_x \sin\theta_y \cos\theta_z + \cos\theta_x \sin\theta_z & -\sin\theta_x \sin\theta_y \sin\theta_z + \cos\theta_x \cos\theta_z & -\sin\theta_x \cos\theta_y \\ -\cos\theta_x \sin\theta_y \cos\theta_z + \sin\theta_x \sin\theta_z & \cos\theta_x \sin\theta_y \sin\theta_z + \sin\theta_x \cos\theta_z & \cos\theta_x \cos\theta_y \end{bmatrix} \quad (3.5)$$

To quantify θ_x , θ_y and θ_z , three displacement transducers are needed: one along the x axis, one along the y axis, and one along the z axis, which will measure x_θ , y_θ and z_θ . Knowing (x_0, y_0, z_0) and $(x_\theta, y_\theta, z_\theta)$ and by inverting equation (3.4), the three angles of rotation can be computed. However, there are problems associated with this method:

- (i) The multiplication of matrices is non commutative, so that the order in which the matrices are multiplied determines the result. There are six different possibilities of describing the rotation about the three body-fixed axes. Any statement that quantifies rotations according to equation (3.4) must state the order in which it was assumed that rotations took place.
- (ii) In solving for the angles, if the start and end position of the vector are known, the sign of the inverse angle as worked out is ambiguous because $\sin(\theta) = \sin(-\theta)$.

It has been observed by Selvik (1989) that if one makes the assumption that the angles through which the rotations occur are small, so that the sine and the cosine of the angle can be approximated as the first term in their series expansion, equation (3.4) reduces to:

$$\begin{Bmatrix} x_\theta \\ y_\theta \\ z_\theta \end{Bmatrix} = [R'] \begin{Bmatrix} x_0 \\ y_0 \\ z_0 \end{Bmatrix} \quad (3.6)$$

where $[R]$ is defined as:

$$[R'] = \begin{bmatrix} 1 & -\delta\theta_z & \delta\theta_y \\ \delta\theta_z & 1 & -\delta\theta_x \\ -\delta\theta_y & \delta\theta_x & 1 \end{bmatrix} \quad (3.7)$$

It can be shown through direct multiplication that this matrix is independent of the order in which it is assumed that the rotation takes place. The errors associated with this small angle approximation are determined by Selvik (1989) as shown in Table 3.1.

Table 3.1: The percentage error in assuming the angles of rotation are small, from Selvik (1989).

	10°	20°	30°
Sinθ : θ	99.5	98.0	95.5
Cosθ : θ	98.5	94.0	86.6

If PO (Figure 3.17) is not constrained to pure rotation about the origin, but can also translate by an amount u in the x direction, v in the y direction and w in the z direction, equation (3.6) becomes:

$$\begin{Bmatrix} x \\ y \\ z \end{Bmatrix} = [R'] \begin{Bmatrix} x_0 \\ y_0 \\ z_0 \end{Bmatrix} + \begin{Bmatrix} u \\ v \\ w \end{Bmatrix} \quad (3.8)$$

If x , y , and z are taken as the change in position of P , as opposed to the absolute position, equation (3.8) becomes:

$$\begin{Bmatrix} x \\ y \\ z \end{Bmatrix} = [R'] \begin{Bmatrix} x_0 \\ y_0 \\ z_0 \end{Bmatrix} + \begin{Bmatrix} u \\ v \\ w \end{Bmatrix} - \begin{Bmatrix} x_0 \\ y_0 \\ z_0 \end{Bmatrix} \quad (3.9)$$

Equation (3.9) is the theoretical basis upon which the migration measurement device is based.

3.3.2 Conceptual design

The *migration measurement device mechanism* is required to allow the six-degrees-of-motion of the prosthesis to be measured. The concept was based on a device used by Berzins et al. (1991) to measure the migration patterns of cementless type prostheses over a small number of loading cycles (see Figure 2.10 in Chapter 2). The device comprised three spheres, A, B and C, press-fitted onto the end of a cruciform structure: this was called the *target device*. The target device was attached to the prosthesis stem (see Figure 3.18). Displacement transducers were attached to the femur and rested on the surfaces of the spheres. During a cyclic loading test, if the prosthesis migrated, the spheres would also migrate. The relative movement between the migration device and the femur could be measured by the displacement transducers.

The displacement transducers in Figure 3.18, allow motion of the target device along the x, y and z space fixed axes to be measured. The body fixed coordinate axis x is aligned with the line joining the centres of spheres A and C. The body fixed coordinate axis y is aligned with the line joining the centre of sphere B and centre of the back of the attachment between the migration device and the prosthesis, and the body fixed coordinate axis z, is mutually perpendicular to x and y. Initially the body fixed coordinate axis and the space fixed coordinate axis are the same. A matrix representing the (x,y,z) coordinates of the centres of each of the spheres A,B and C is constructed, where $(A_x, A_y, 0)$ is the centre of sphere A, $(0, B_y, 0)$ is the centre of sphere B and $(C_x, C_y, 0)$ is the centre of sphere C. The matrix is as follows:

$$\begin{bmatrix} A_x & 0 & C_x \\ A_y & B_y & C_y \\ 0 & 0 & 0 \end{bmatrix} \quad (3.10)$$

Substituting (3.10) into (3.9) results in:

$$\begin{bmatrix} u_A & u_B & u_C \\ v_A & v_B & v_C \\ w_A & w_B & w_C \end{bmatrix} = [R'] \begin{bmatrix} A_x & 0 & C_x \\ A_y & B_y & C_y \\ 0 & 0 & 0 \end{bmatrix} + \begin{bmatrix} u & u & u \\ v & v & v \\ w & w & w \end{bmatrix} - \begin{bmatrix} A_x & 0 & C_x \\ A_y & B_y & C_y \\ 0 & 0 & 0 \end{bmatrix} \quad (3.11)$$

where B_x, B_y, C_y, D_x, D_y are known and the three rotations $(\theta_x, \theta_y, \theta_z)$ and the three translation (u, v, w) are unknown.

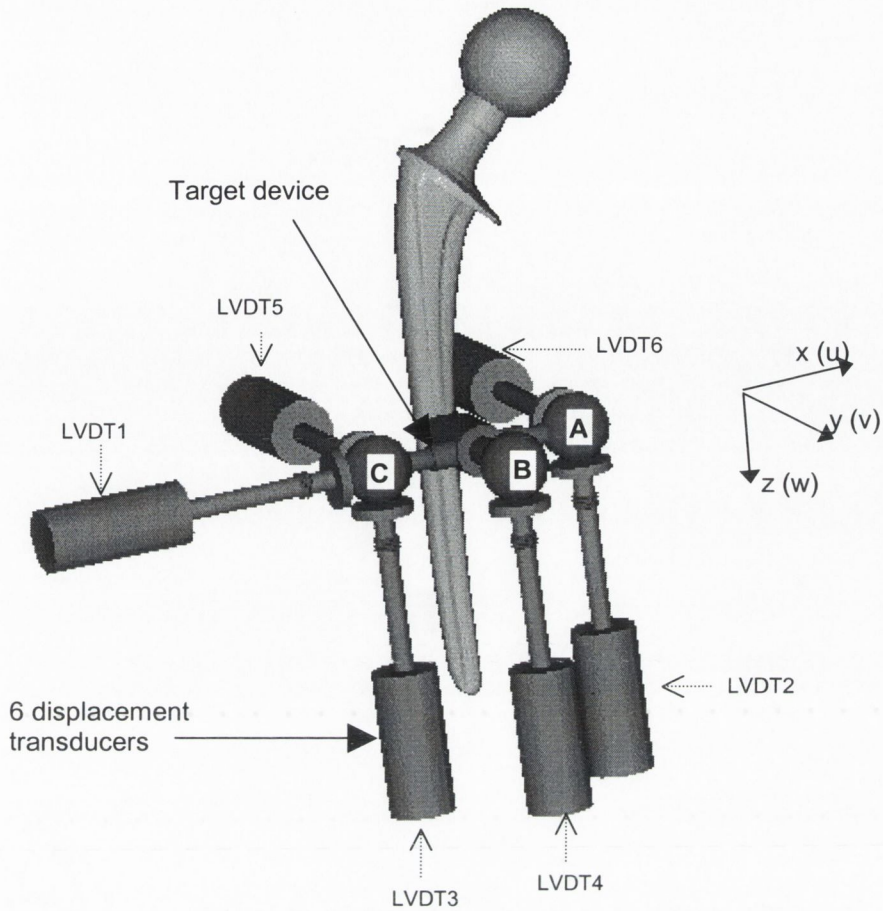


Figure 3.18: Concept behind the design of the migration measurement device. The displacement transducers that measure the movement of the target device are illustrated. The local coordinate axes are labelled and each LVDT is assigned an identification number.

Solving results in:

$$\begin{aligned}
 u &= u_C + \delta\theta_z C_Y \\
 v &= v_C - \delta\theta_z C_X \\
 w &= w_B - \delta\theta_x B_y \\
 \delta\theta_x &= \frac{C_X(w_B - w_A) + A_X(w_C - w_B)}{C_X(B_Y - A_Y) + A_X(C_Y - B_Y)} \\
 \delta\theta_y &= \frac{w + \delta\theta_x A_Y - w_A}{A_X} \\
 \delta\theta_z &= \frac{v_A - v_C}{A_X - C_X}
 \end{aligned} \tag{3.12}$$

Measurement of the centres of the spheres of the target device, allows equation (3.10) to be written as:

$$\begin{bmatrix} 29.845 & 0 & -30.165 \\ 32.235 & 62 & 32.195 \\ 0 & 0 & 0 \end{bmatrix} \quad (3.13)$$

By referring to Figures 3.18, it can be seen that LVDT1 measures u_C , LVDT2 measures w_A , LVDT3 measures w_C , LVDT4 measures w_B , LVDT5 measures v_C , and LVDT6 measures v_A . Equations (3.12) become:

$$\begin{aligned} u &= \text{lvd}t1 + (32.195)\delta z \\ v &= \text{lvd}t5 + (30.165)\delta z \\ w &= \text{lvd}t3 - \delta\theta_x(62) \\ \delta\theta_x &= \frac{(-30.165)(\text{lvd}t3 - \text{lvd}t2) + (29.845)(\text{lvd}t4 - \text{lvd}t3)}{(-30.165)(62 - 32.235) + (29.845)(32.195 - 62)} \\ \delta\theta_y &= \frac{w + (32.235)\delta z - \text{lvd}t2}{29.845} \\ \delta\theta_z &= \frac{\text{lvd}6 - \text{lvd}t5}{29.845 + 30.165} \end{aligned} \quad (3.14)$$

Equations (3.14) are used to compute the three translations and three rotations of the migration measurement device relative to the femur. Motion of the prosthesis is defined by quantifying the translation and rotation at the point of contact between the migration device and the prosthesis. However, depending on the point of contact between the device and the prosthesis, the translations that are quantified will vary. There is a need to combine the measured translations and rotations to evaluate the resulting translation of a point that is common to both prosthesis designs. This point is chosen as the centre of the prosthesis head. By knowing the co-ordinates of the centre of the head of the prosthesis relative to the origin in the local co-ordinate system (a, b, c), the translation of the centre of the head of the prosthesis (a', b', c') that results from the combined translation and rotation of the prosthesis can be computed as follows:

$$\begin{Bmatrix} a' \\ b' \\ c' \end{Bmatrix} = [R'] \begin{Bmatrix} a \\ b \\ c \end{Bmatrix} + \begin{Bmatrix} u \\ v \\ w \end{Bmatrix} \quad (3.15)$$

where $[R']$ is defined in equation (3.7)

3.3.3 Design embodiment

The Berzins et al. (1993) device (see Figure 2.10) was used to measure the migration of cementless type prostheses after a small number of loading cycles. To embody the design concepts into a migration measurement device for long term cyclic loading tests the following design questions were posed:

- i) How could the measurement device be attached to the prosthesis so that the connection could withstand two million loading cycles?
- ii) How could the displacement transducers be aligned so that they were mutually orthogonal and aligned with the centre of the spheres of the measurement device?
- iii) How could the displacement transducers be rigidly fixed to the bone so that measurement of the motion of the prosthesis relative to the femur could be made?
- iv) How would the protocol for use of the subsidence device complement the protocol for use of the insertion machine?

3.3.3.1 Attachment of the migration measurement device to the prosthesis

Attachment between the target device and the prosthesis was designed on the basis of press fitting connections using the following procedure:

- (i) A flat was machined on the posterior side of the clamped prosthesis.
- (ii) Two 2 mm diameter holes were machined through the prosthesis.
- (iii) A solid cylinder of mild steel was machined so that it had a flattened face.
- (iv) Two holes of 2 mm diameter were machined into the face of the cylinder.
- (v) Two 2 mm diameter silver steel pins were turned down so that they achieved a press fitting with the holes in the prosthesis and in the cylinder.
- (vi) The two pins were press fitted into the cylinder.

- (vii) After prosthesis insertion, the two pins of the cylinder were press fitted into the holes in the prosthesis (see Figure 3.19).
- (viii) The migration device was locked onto the cylinder using 3 mm grub screws. The flattened face on the cylinder, ensured that the subsidence device self aligned with the cylinder.
- (ix) After each test, the migration measurement device was removed, the cylinder remained fixed to the prosthesis. It proved necessary to make a new cylinder for the each test.

To ensure reproducible orientation of the target device, two clamps were designed — one for the Müller prosthesis and one for the Lubinus prosthesis — to hold both designs in a predefined orientation for drilling of the attachment holes. Each prosthesis was clamped so that its collar was held at 45 degrees to the vertical and the underside of the collar was held in a vertical plane perpendicular to the front face of the clamp (see Figure 3.20 and Figure 3.21). This defined the local axes according to which the rotations and translations as defined in equation (3.14) were computed.

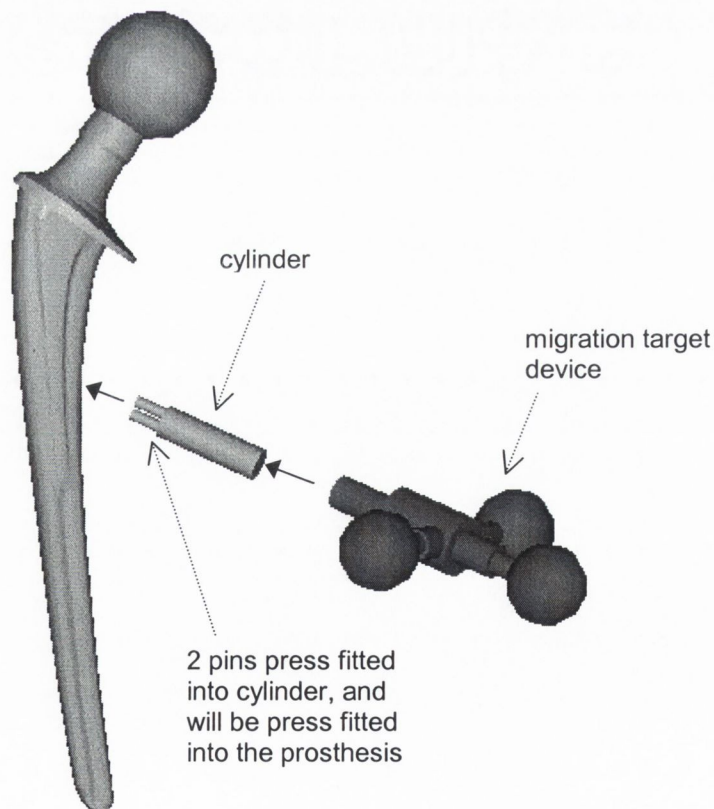


Figure 3.19: Press fitting of the migration target device.

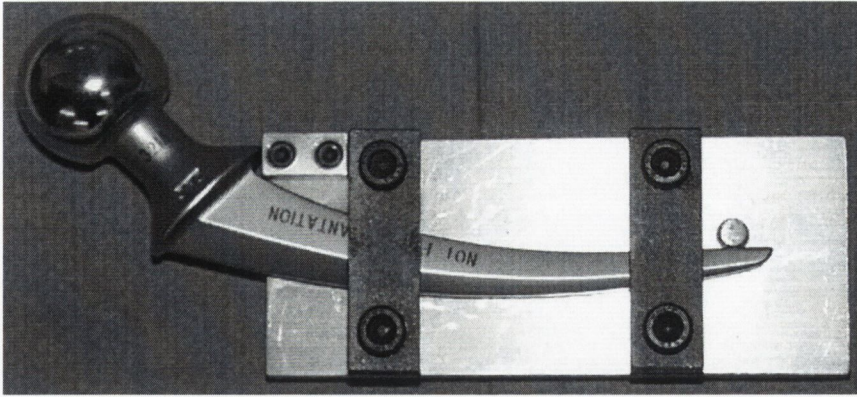


Figure 3.20: Clamp for the Müller Prosthesis.

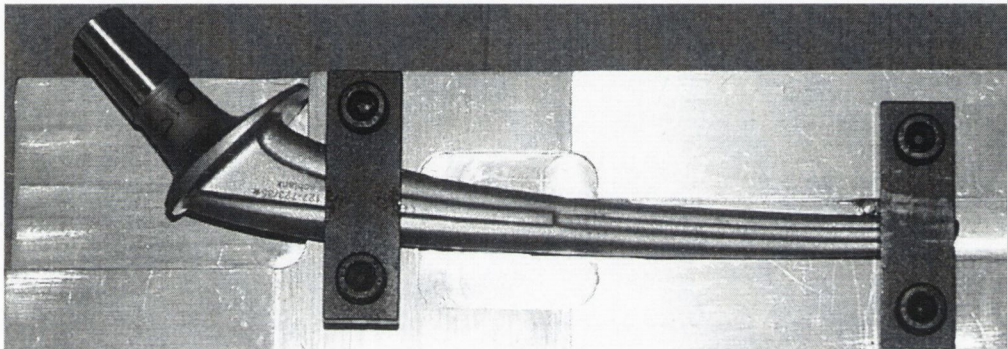


Figure 3.21: Clamp for the Lubinus prosthesis.

3.3.3.2 Holder for displacement transducers

The holder for the displacement transducers, otherwise known as the *LVDT bracket* was designed so that:

- (i) The LVDTs were held in mutually orthogonal planes and in line with the centres of the spheres of the target device.
- (ii) It was a light weight structure.
- (iii) The LVDTs could be translated within their holders to allow their positions to be set at the mean of their range of motion.
- (iv) No LVDT was held on a projection that was likely to vibrate during testing.
- (v) The structure had sufficient rigidity during machining and for testing.

The bracket was manufactured from aluminium to minimise weight. Six holes were drilled through the wall of the LVDT holder, in positions that aligned with the centres of the *migration measurement device*, see Figure 3.22. Six *LVDT Cylinders* were machined and press fitted into these holes. The cylinders allowed the LVDTs to slide freely through them, so that the LVDTs could be fixed in any position, and zeroed. Once positioned they were locked in place using two M3 grub screws for each LVDT.

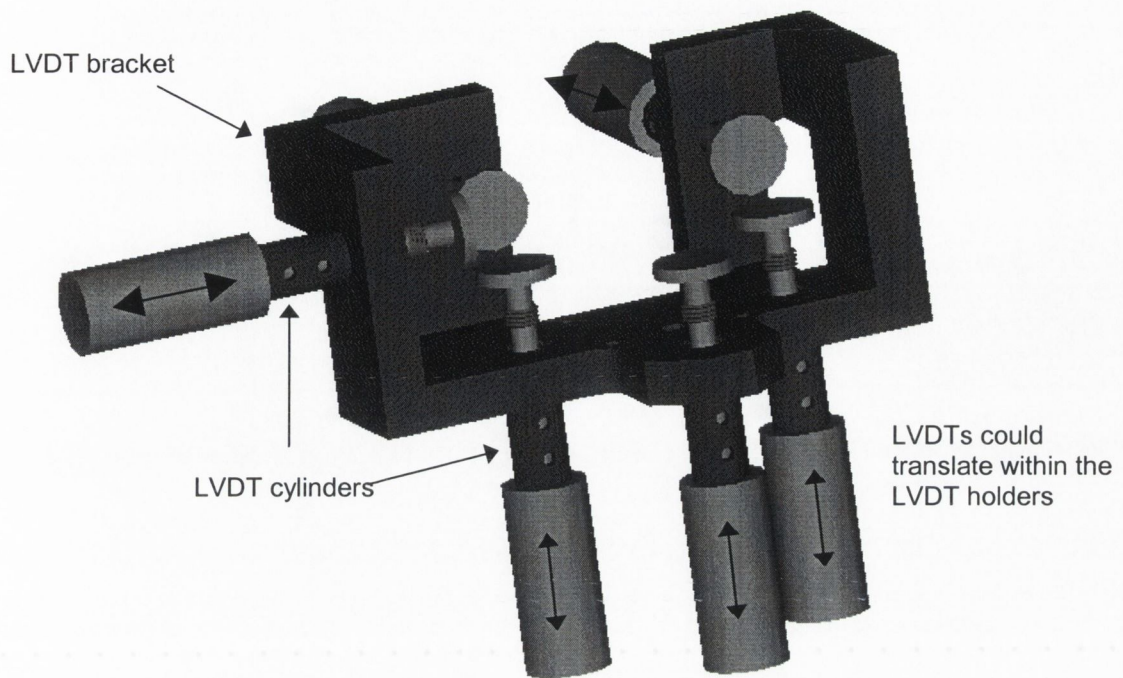


Figure 3.22: The LVDT cylinders as they were press fitted into the LVDT bracket.

3.3.3.3 Attachment to the femur

The method of attaching the LVDT holder to the wall of the femoral cortex had the following requirements:

- (i) That it would not interfere unduly with the tendency of the prosthesis to subside — for example by applying a compressive hoop stress to the implanted femur.
- (ii) That it would provide a rigid enough connection for two million loading cycles.
- (iii) That it could act as the attachment site for the LVDT holder.

It was decided to use pointed M6 bolts to tighten in through the wall of the femoral cortex, based on a method used and validated by others (Gilbert et al., 1992; McKellop et al., 1991). The M6 bolts protruded through a ring of aluminium that surrounded the femur: called a *femoral ring*, see Figure 3.23.

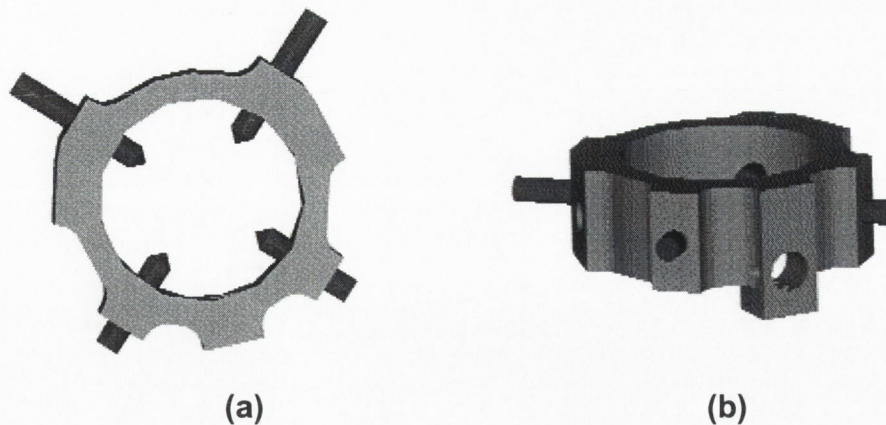


Figure 3.23: A top view (a) and a side view (b) of the femoral ring used to rigidly lock the LVDT holder to the wall of the composite femur. Four pointed bolts act through holes in the ring. Once tightened into the femoral cortex, nuts lock them in place against the femoral ring.

The internal diameter of the femoral ring was designed to allow enough room for locating the composite femur within its boundary. The outer ring profile was machined flat at the bolt attachment sites, to allow bolts to be tightened flush with the femoral ring, thereby increasing the stability of locking.

3.3.3.4 Alignment of the LVDTs

Each of the six LVDTs needed to be oriented so that:

- (i) They were aligned with the centres of the three spheres.
- (ii) They were mutually orthogonal.
- (iii) They were not pulled out of alignment when the femoral ring was being tightened to the wall of the composite femur.

These functions were achieved through the accurate machining of the LVDT holder, the repeatable positioning of the LVDT holder relative to the migration measurement device and the design of flexible linkages between the LVDT holder and the femur ring.

The concept behind the aligner (in orange in Figure 3.24) was that when fully seated, it would locate reproducibly against three of the ‘arms’ of the target device, (in green in Figure 3.24). Once seated, the LVDT holder (in blue in Figure 3.24) was pinned and bolted to it: thereby reproducibly aligning the LVDT bracket to the subsidence measurement device.

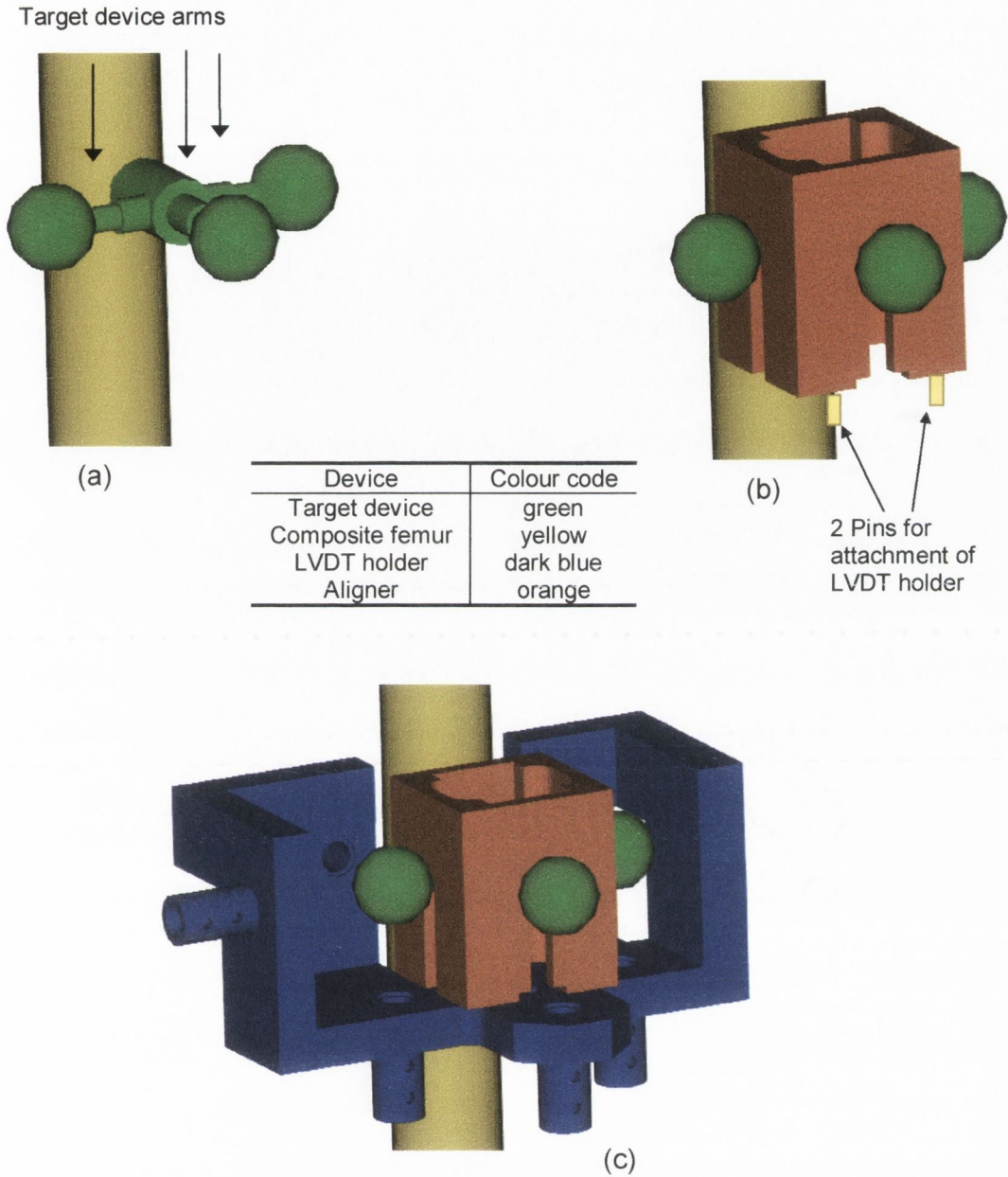
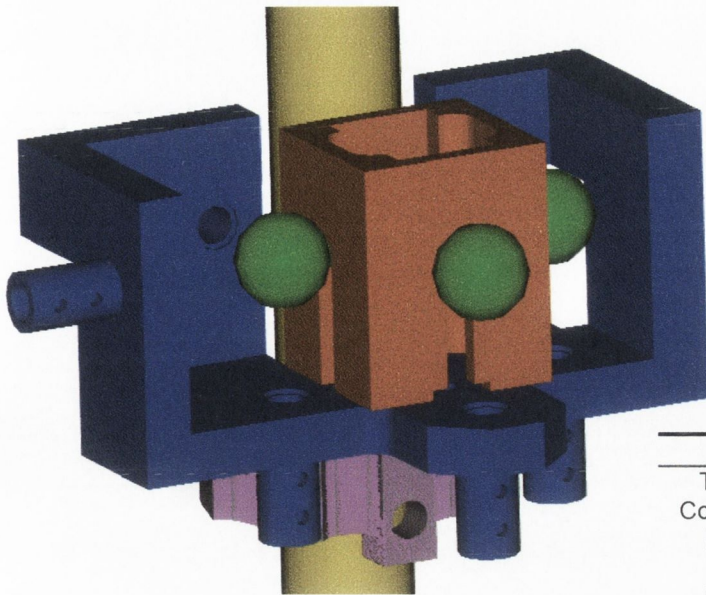


Figure 3.24: The steps in using the aligner to reproducibly locate the LVDT bracket relative to the migrating device. The underside of the aligner has two pins protruding from its base and two tapped hole in its base to allow the LVDT holder to be pinned and bolted to it.

To maintain the LVDTs in the correct orientation *during tightening* of the femoral ring (see purple component in Figure 3.25) to the wall of the femur, the connections between the LVDT bracket and the femoral ring needed to be flexible.



Device	Colour code
Target device	green
Composite femur	yellow
LVDT holder	dark blue
Aligner	orange
Femoral ring	purple

Figure 3.25: The gap between the LVDT bracket and the femoral ring must be spanned by some form of attachment.

Flexibility was achieved in rotation using *ball and socket couplings*, and in translation using *side ties* and *side linkers* (see Figure 3.26). These couplings remained flexible when the femoral ring was being locked to the wall of the femur, which allowed the femoral ring to move relative to the LVDT bracket and aligner, without causing distortion.

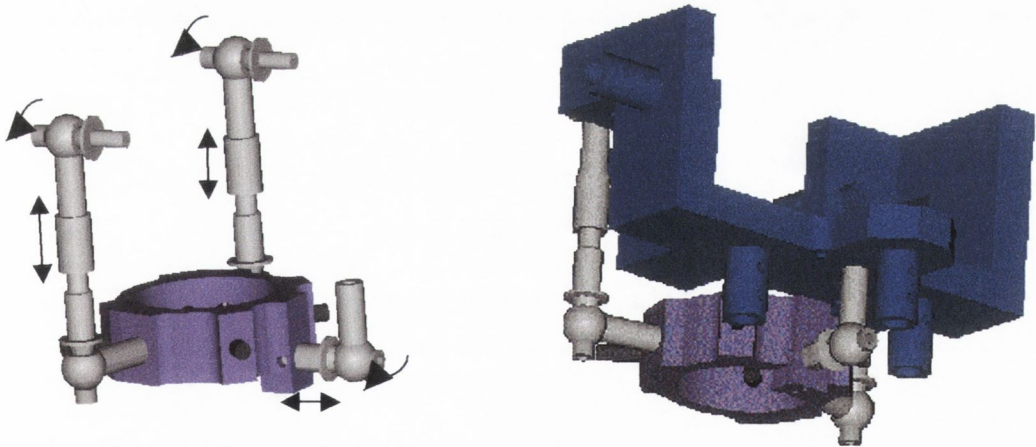


Figure 3.26: Two side view of the couplings between the LVDT bracket and the femoral ring. The translational and rotational freedom of motion of the joints are illustrated by the black arrows. For clarity, neither the femur, target device nor the aligner are shown.

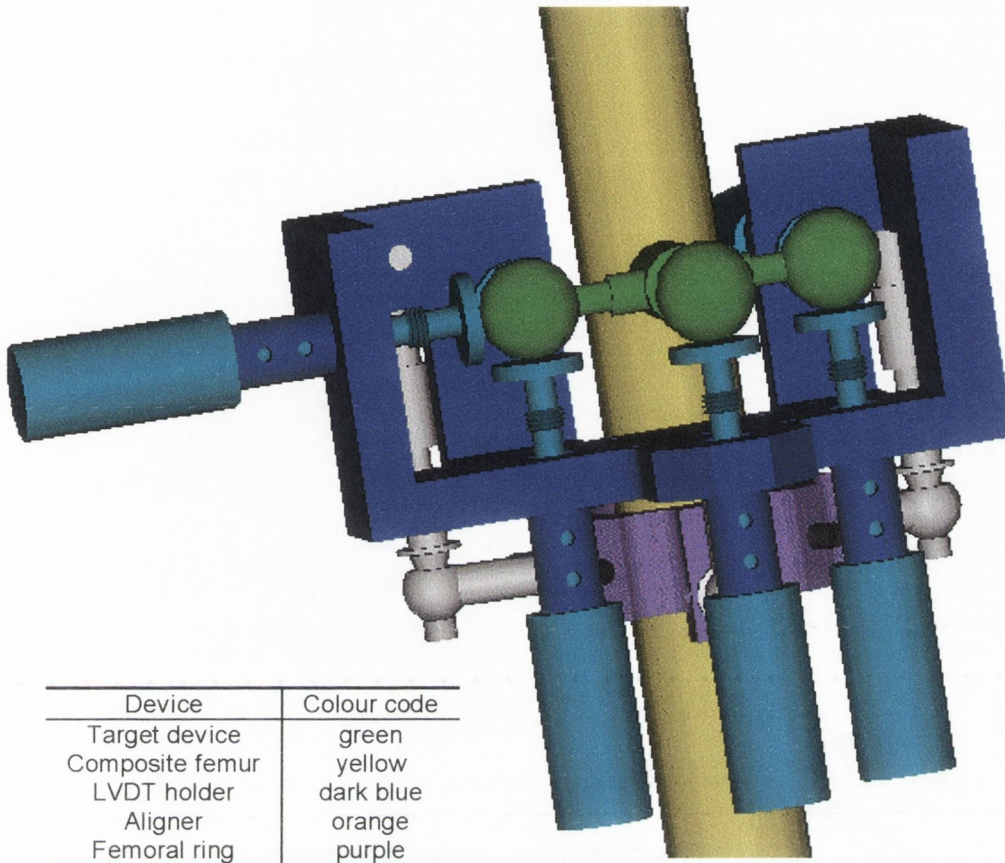


Figure 3.27: The assembled migration measurement device. Once the flexible attachments between the LVDT holder and the femoral ring are locked in place, the aligner is removed and the LVDTs are placed in the LVDT holder, zeroed and locked in place.

Once the femoral ring was locked to the wall of the femur, the couplings were locked in place. The aligner could now be removed and the LVDTs put in place. The assembled migration measurement device is illustrated in Figure 3.27. The protocol for use of the migration measurement device is described in Appendix B, page 163, and engineering drawings are presented in Appendix H, page 209.

To allow the migration measurement device to be used in conjunction with the insertion machine some additional steps were included in the protocol for use of the insertion machine. These steps were:

- (i) The two holes drilled in the prosthesis (see Figure 3.19) were filled with silicone gel.

- (ii) After the prosthesis was aligned in the alignment femur on the insertion machine, the position of the drilled holes in the femur were measured relative to known features on the alignment plate.
- (iii) When the test femur was clamped to the alignment plate, prior to resection of the femoral head, a 12 mm diameter hole was drilled through it, at the measured coordinates.
- (iv) Prior to insertion the hole in the femur was plugged with a cylinder of PTFE.
- (v) After insertion, the PTFE was removed, any cement covering the holes in the prosthesis was milled away.
- (vi) The cylinder for attachment of the target device was press fitted in place (see Figure 3.28).

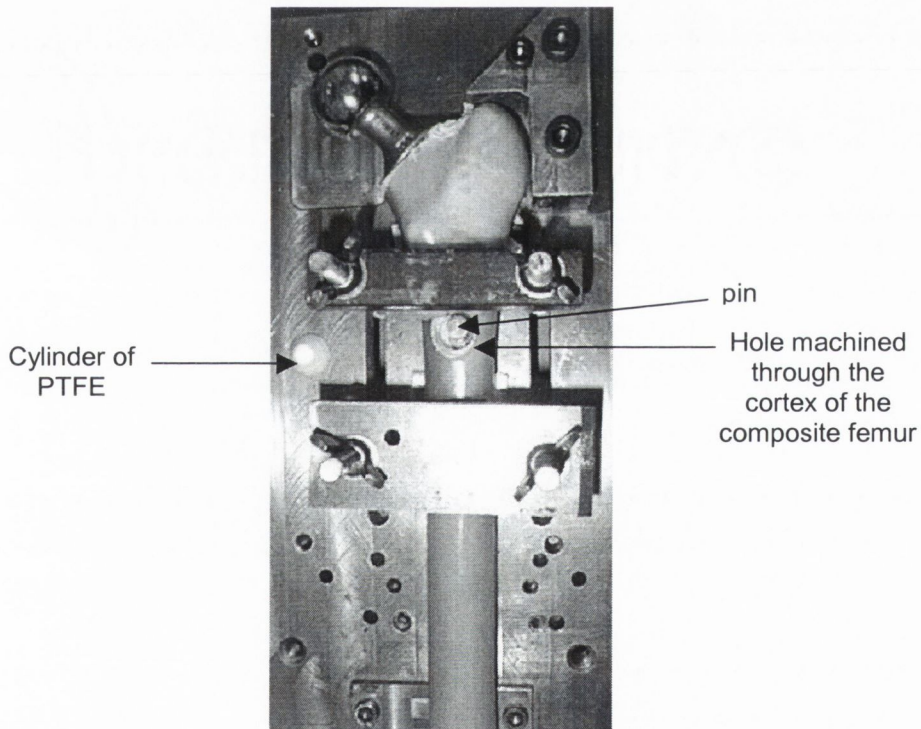


Figure 3.28: A Müller prosthesis that was implanted into a composite femur. The femur is still clamped on the alignment plate. The tapered cylinder of PTFE which was used to plug the pre-drilled hole in through the wall of the femoral cortex is visible. The rod for the attachment of the migration measurement device has been press fitted into place.

3.3.4 Data acquisition

Voltage output from the LVDTs and the materials testing machine were recorded using an analogue to digital data acquisition card AT-MIO-16XE-50 (National Instruments, Texas, USA). Prior to the first fatigue test, the six LVDTs were calibrated. Each LVDT was mounted via an aluminium clamp onto a rotating drum micrometer. The face of each LVDT was incrementally compressed by an amount read from the drum micrometer, and the voltage output at each position was recorded.

Programs were written through LabView v.5.0 software (National Instruments, Texas, USA) to record the voltages being generated in the LVDTs and in the materials testing machine at specified intervals, for specified time periods. The program written to acquire the data from the LVDTs required that the following information be input by the user:

- (i) The file name which would be used to store the data.
- (ii) The number of channels to be logged during testing (in this case, one for each LVDT plus one for channel to monitor the loads being applied: *i.e.* seven channels altogether).
- (iii) The number of data points to be sampled from each channel. In this case, 300 data points are taken from each channel.
- (iv) The frequency with which the data is sampled. In this case the sampling frequency was set at 100 Hz.
- (v) The duration between sampling, in tens of seconds. In this case, the value was set at 360: *i.e.* 3600 seconds or 1 hour between each sampling batch.

In summary, once every 18,000 loading cycles, 100 samples were recorded from each channel on the data acquisition board for a period of three seconds. Cyclic testing was done at a frequency of 5Hz, thus for each loading cycle applied, 20 data points were recorded from each channel, see Figure 3.29.

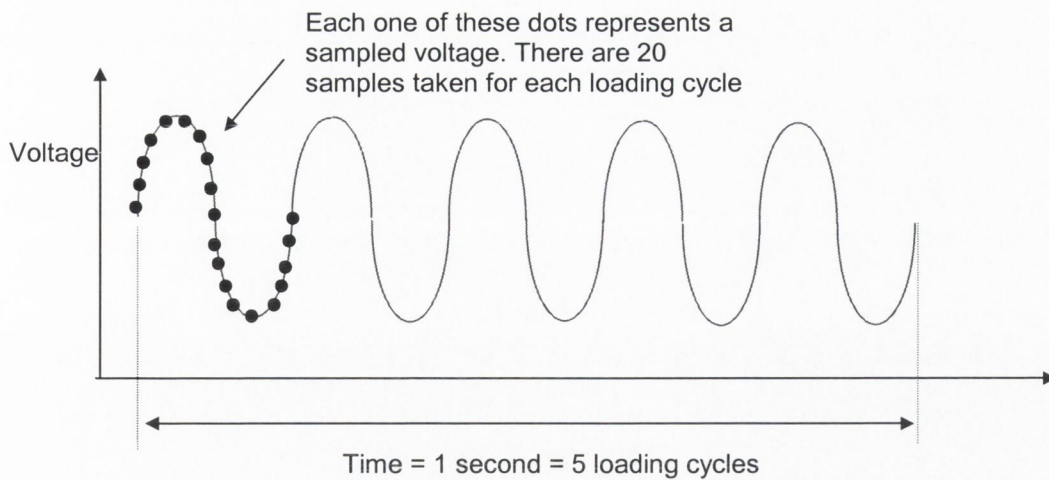


Figure 3.29: The frequency of data sampling in relation to the testing frequency.

After testing, the data files were imported into an Excel spreadsheet. The following operations are carried out on the raw data:

- (i) The voltage representing the load data and the LVDT voltage outputs were graphed for the first 70 data points.
- (ii) In one load cycle, the position representing the minimum load applied (*i.e.* 0.23 kN) was noted.
- (iii) Whether the voltage output from the LVDTs at the time when the load reached its minimum were at a maximum or minimum were recorded for each LVDT.
- (iv) For each set of 100 data points (*i.e.* 5 cycles), the voltage from each LVDT corresponding to the minimum load and the average voltage was computed.
- (v) The average of the maximum or minimum, and the average voltage for each LVDT readout over three data sets (*i.e.* 15 cycles) were computed: this represented the average maximum / minimum voltage corresponding to the minimum load.
- (vi) The LVDT voltages were converted to millimeters, using the calibration data.
- (vii) The LVDT displacements for the minimum load were zeroed, taking the first reading as the zeroing value.

- (viii) The signs of the LVDT outputs were changed so that their direction of measurement aligned with the right handed coordinate system of the migration measurement device.
- (ix) The three degrees of translation and three degrees of rotation of the prosthesis were computed using equation (3.14).
- (x) The resulting translation of the centre of the head of the prosthesis in the local coordinate system was computed using (3.15).
- (xi) The three dimensional solid models of the final seated positions of the Müller and Lubinus stems were used to measure the angle of the stem defined coordinate axes relative to the femoral shaft (see figure 3.31a and 3.31b).
- (xii) To allow the migration patterns of the two prosthesis designs to be compared, the coordinate axes were rotated so that they aligned with the shaft of the femur in both the frontal and sagittal planes.
- (xiii) The translations of the head centres relative to the femoral axis were computed.

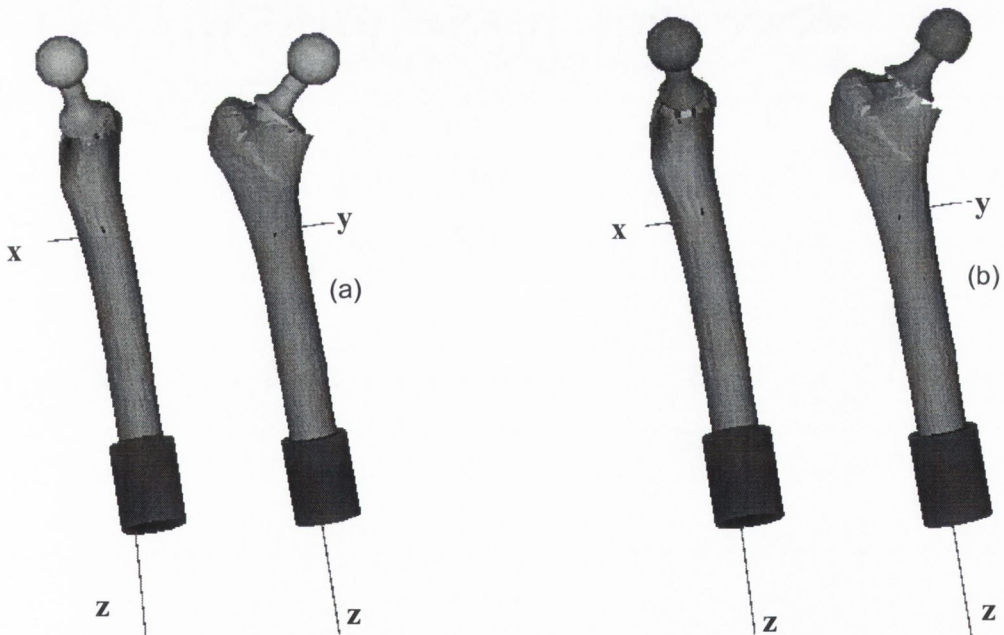


Figure 3.30: Schematics comparing the local coordinate systems of the Lubinus prosthesis (i) and the Müller prosthesis (ii). The body fixed and space fixed coordinate systems are defined by the orientation of the target device. This is dependent on the orientation of the holes drilled in the prosthesis and the orientation of the prosthesis within the femoral bone.

3.3.5 Testing of the migration measurement device

3.3.5.1 Testing of the attachment between the target device and the prosthesis

To confirm that the press fittings of the *migration measuring target device* would not become loose during fatigue testing, the device was press fit into a Müller prosthesis (see figure 3.31). The distal third of the femoral stem was cemented into a femoral clamp. The clamp was angled at 20° degrees to the vertical in the frontal plane. The position of the centre of the three spheres and the prosthesis head were recorded using a co-ordinate measuring machine (CMM). Cyclic loads ranging from -0.2 to -1.8 kN were applied at a frequency of 10Hz for 4×10^6 cycles. After testing, the relative positions of the spheres were recorded using the CMM.

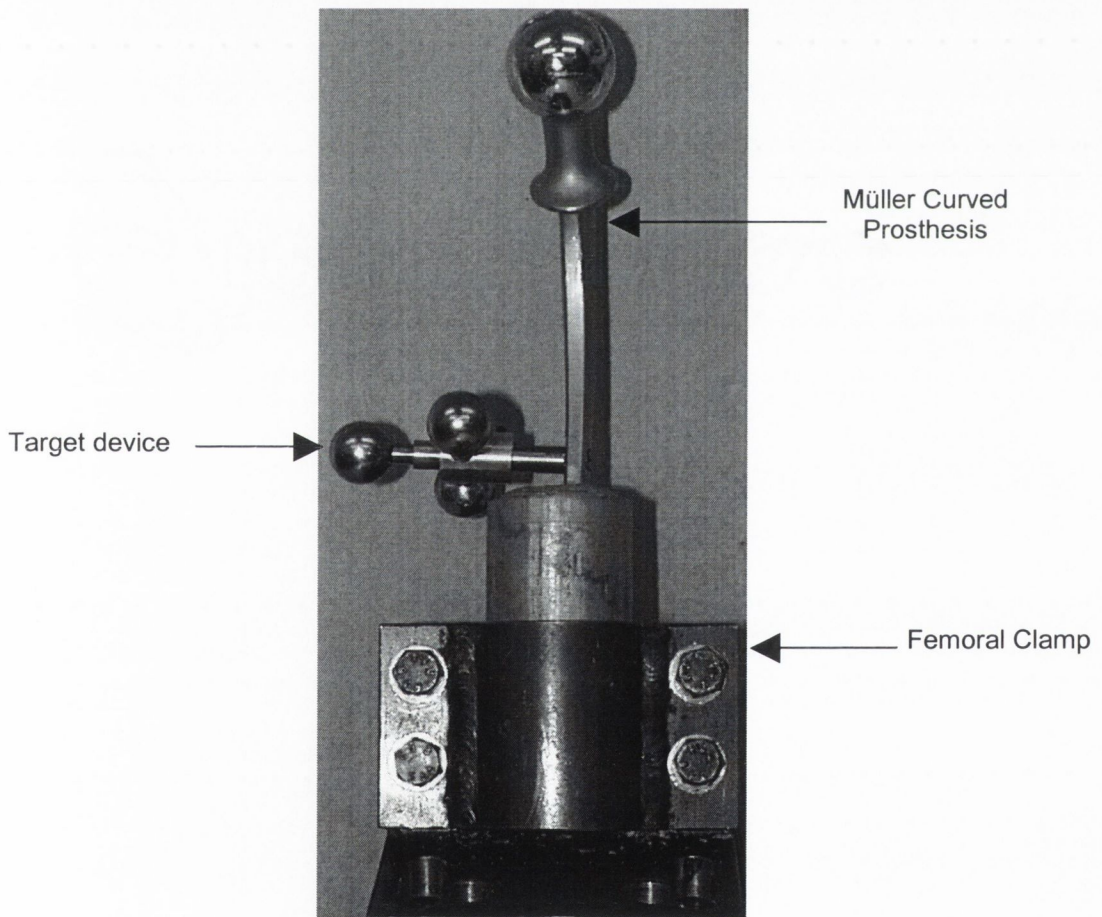


Figure 3.31: Test setup used to investigate whether the attachment between the target device and the prosthesis was rigid enough to withstand cyclic loading for two million loading cycles.

3.3.5.2 Confirmation that the migrations calculated are the migrations that are occurring.

A materials testing machine was used to move the prosthesis by a known amount to ensure the migration measurement device and analysis were correct. The following procedure was used:

- (i) A test femur was prepared by resecting the head, drilling the interior cavity, and rasping the proximal cavity.
- (ii) A Müller prosthesis was prepared for the attachment of the migration measurement device (as described in section 3.3.3.3).
- (iii) The distal end of the test femur was cemented into a mild steel cylinder which was clamped to the base of an Instron materials testing machine at 20° in the frontal plane.
- (iv) The prosthesis was placed resting in the test femur.
- (v) The attachment cylinder for the target device was press fitted to the prosthesis and the target device was attached. The prosthesis is not cemented inside the femur, rather it is free to translate and rotate within the shaft.
- (vi) The prosthesis head was rigidly clamped to the actuator of the materials testing machine.
- (vii) The migration measurement device, LVDT holder etc., were attached to the composite femur following the procedure outlined in Appendix B, page 164.
- (viii) The LVDTs were zeroed.
- (ix) The actuator of the materials testing machine was moved in 0.2 mm increments through a range of 1.5 mm.
- (x) The outputs from the LVDTs and the position of the actuator were recorded after each incremental move of the actuator.
- (xi) The data was imported into Excel and operated on according to the techniques described in section 3.3.4.
- (xii) The displacements of the centre of the head of the Müller that were computed were transformed to the world coordinate system, and a comparison between the known displacement of the actuator and the computed displacement of the centre of the head of the prosthesis was made.

3.4 CYCLIC TESTING

3.4.1 Preliminary investigations

The ability of synthetic femora to withstand physiological cyclic loads has not been reported in literature. A preliminary investigation was carried out to decide whether the composite femora were suitable for use throughout the project. Prostheses cemented into Sawbones composite femora (Pacific Labs, USA) were mechanically tested in fatigue to investigate the following:

- (i) Does splitting of the cortical wall occur as the prosthesis subsides?
- (ii) Does separation between the cortical bone replica and the cancellous bone replica occur?
- (iii) Does the stem break at the distal clamped position?

Six cyclic load tests were performed on four stem designs. A Sheehan stem (n=2), a Charnley stem (n=2), a cementless prosthesis (n=1) and a small Müller Curved stem (n=1) were cemented into composite femora, clamped at 20 degrees to the vertical in the frontal plane, and fatigued for up to five million cycles to maximum forces of up to 4 kN. These stems were chosen because they covered a range of stem profile designs. After testing, the femora were visually inspected for signs of cortical splitting and breakage around the distal support. The prostheses were removed from within the femora and the cemented femora were sectioned transversely into 5 mm thick slices using a band saw. The slices were inspected macroscopically for cancellous / cortical separation.

3.4.2 Set-up for cyclic loading for migration measurement

Once the cemented composite femur was prepared for testing, it was clamped to the base of an Instron 1341 materials testing machine (Instron, UK), at an angle of 10° adduction and 9° flexion, following from the International standard ISO 7206-3. The head of the prosthesis was placed resting in a nylon cup, the back of which was flat and free to translate across a PTFE sheet which is mounted on the actuator of the test machine. The PTFE sheet and the back of the nylon cup were lubricated with a molybdenum based lubricant. The test setup is illustrated in Figure 3.41. A compressive sinusoidally varying loading wave with a frequency of 5 Hz was applied to the head of the prosthesis with loads ranging from 0.23 kN to 2.3 kN. The data acquisition process was initiated.

This fatigue testing protocol was applied to fourteen cemented femora: five Müller prostheses without resorption simulated, two Müller prosthesis with resorption simulated, five Lubinus prosthesis without resorption and two with resorption simulated.

3.4.3 Post test analysis.

Four of the femora, two Müller prostheses and two Lubinus prostheses were sectioned using a Buhler abrasive cutting machine and diamond coated cutting wheels (Buhler, U.K.). After sectioning the slices were dyed with Dye Penetrant, left to soak for 24 hours and cleaned. The cement/metal interfaces in all of the sections were visually inspected for defects. Push out tests were performed on all samples.

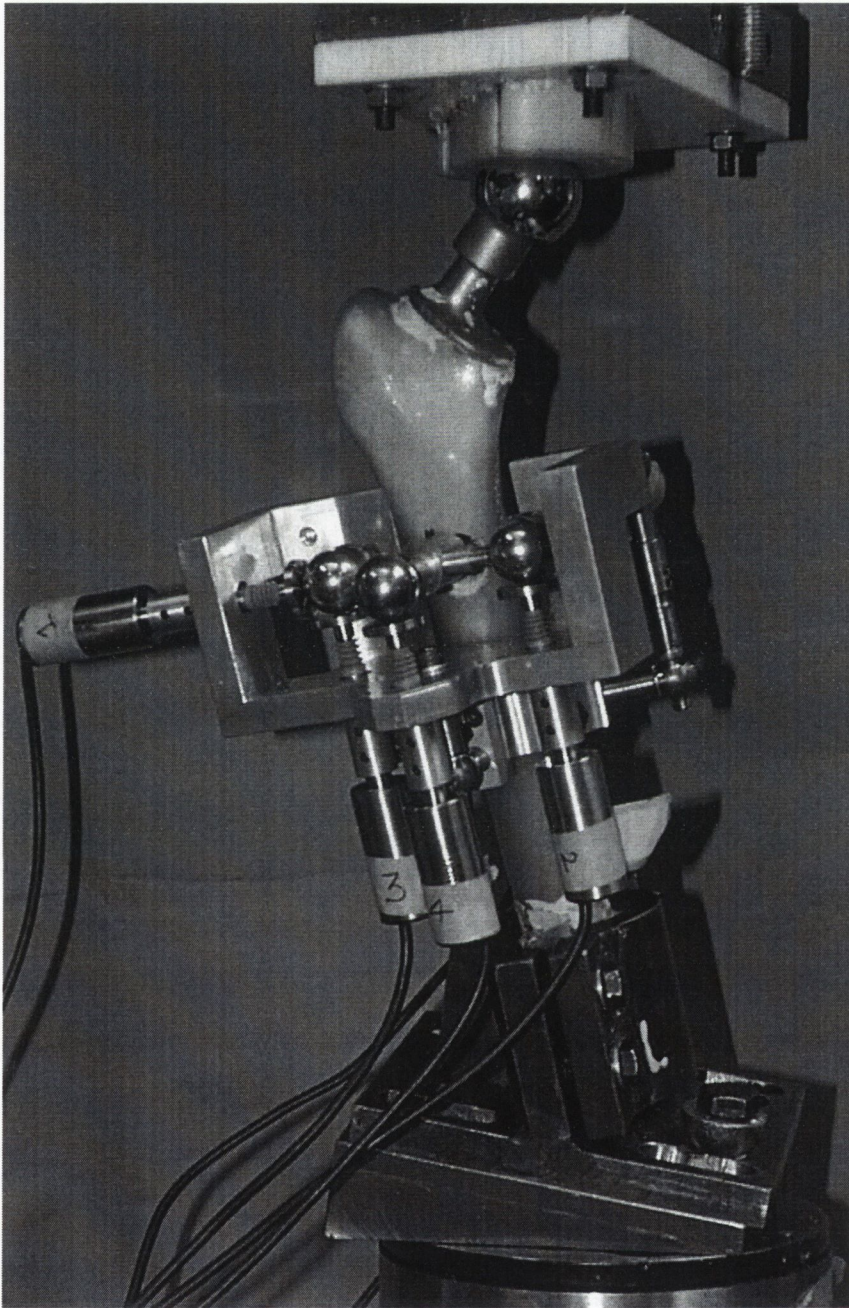


Figure 3.32: A Lubinus prosthesis, with migration measurement device attached. The femur is clamped in 9° of flexion and 10° of adduction following from the recommendations of the international standard ISO 7206-3 for the determination of the endurance properties of stemmed femoral components.

3.5 SUMMARY

In summary a protocol for the sample preparation, and migration measurement of cemented femoral hip implants subjected to fatigue loading for two million cycles has been presented. A schematic summary of some of the steps involved in the protocol is illustrated in Figure 3.33.

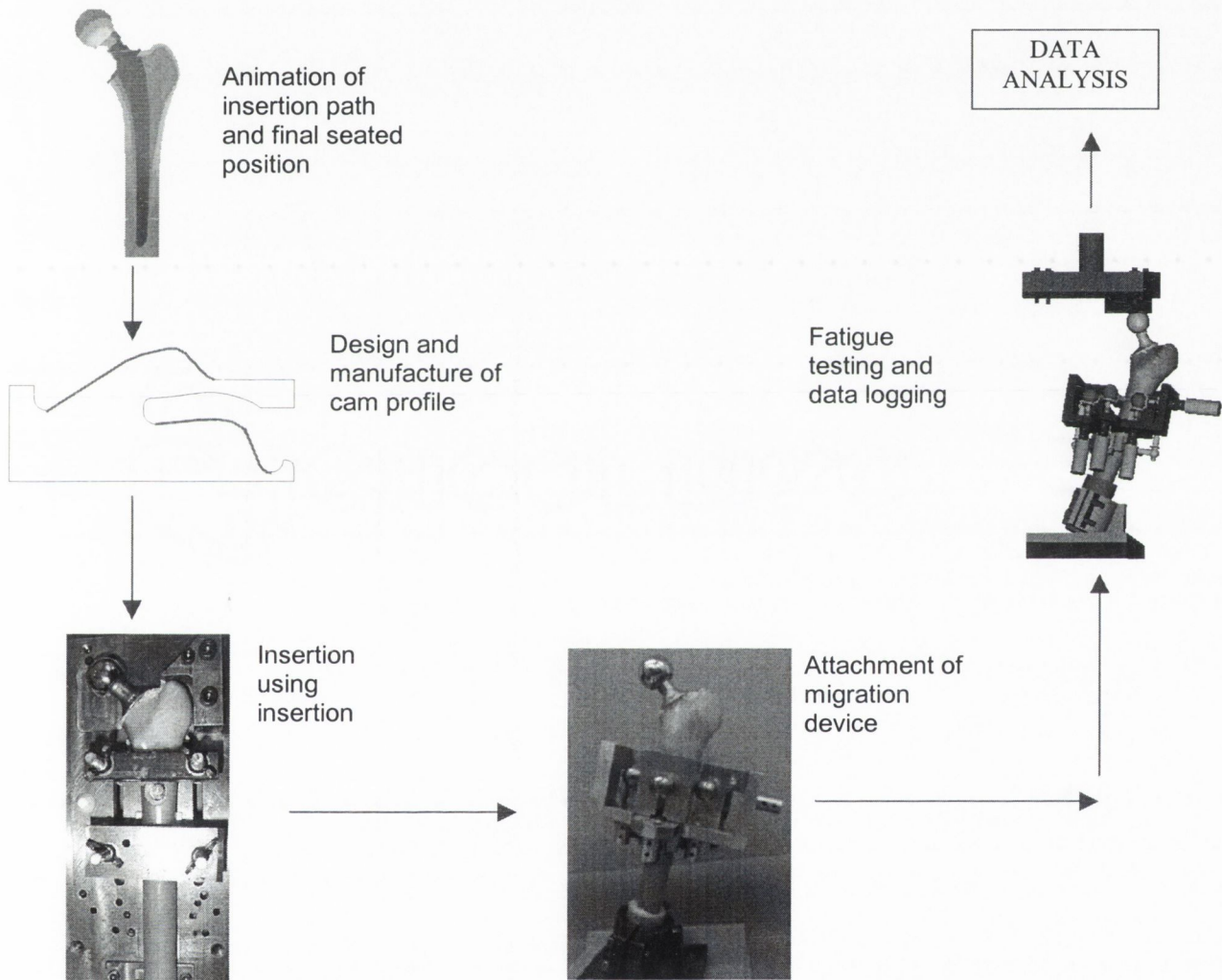


Figure 3.33: A schematic of the complete pre-clinical testing protocol.

4: Results

4.1.	CALIBRATION AND VALIDATION STUDIES	78
4.1.1	Validation of the suitability of synthetic femora for cyclic loading	78
4.1.2	Validation of the concept of the insertion machine	78
4.1.3	Accuracy and repeatability of the Insertion Machine	79
4.1.4	Accuracy of the migration measurement device	80
	<i>4.1.4.1 Rigidity of the attachment between the prosthesis and the migration measurement device</i>	<i>80</i>
	<i>4.1.4.2 Data acquisition card accuracy</i>	<i>81</i>
	<i>4.1.4.3 Results of the confirmation test described in Section 3.3.5.2</i>	<i>82</i>
4.2	MIGRATION OF THE MÜLLER AND LUBINUS PROSTHESES	83
4.2.1	Description of data processing: an example using migration of a Müller prosthesis	83
4.2.2	Müller migration histories	87
4.2.3	Lubinus migration histories	90
4.3	COMPARISON OF THE MÜLLER AND LUBINUS MIGRATION FEATURES	94
4.3.1	Comparison of the migration curves	94
4.3.2	Total migration at 0.2 million cycles	97
4.3.3	Total migration at 1 million cycles	98
4.3.4	Total migration at 2 million cycles	99
4.3.5	Total migration of the Müller and Lubinus prostheses with migration over the first 0.2 million loading cycles discounted	100
4.3.6	Rate of migration at 1 million cycles (steady state migration rate)	101
4.4	COMPARISON OF THE MIGRATION OF THE LUBINUS AND MÜLLER PROSTHESES WITH AND WITHOUT RESORPTION	102
4.4.1	Comparison of the migration curves	102
4.4.2	Comparison of Total Migration	106
4.4.3	Comparison of the steady state migration	109
4.5	THE CEMENT/METAL INTERFACE OF SECTIONED SAMPLES	110
4.6	INDUCIBLE DISPLACEMENT	112
4.6.1	Comparison between the average inducible displacement of the Müller prostheses and the Lubinus prostheses	112
4.6.2	Correlation between the inducible displacement at different stages throughout the loading history and the migration at 2 million cycles	114
4.7	THE COOLDOWN AFFECT	119

4.1. CALIBRATION AND VALIDATION STUDIES

4.1.1 Validation of the suitability of synthetic femora for cyclic loading

No evidence of cortical wall splitting was found in any of the six cemented femora tested. Similarly, in five of the prostheses tested, no evidence of cortical/cancellous bone separation was seen macroscopically. However, one stem, the small Müller Curved stem, fractured along its distal third. At the point of fracture, the cancellous bone replica was fully separated from the cortical bone replica. Since stem fracture was not expected in the subsequent tests, the composite femora were deemed suitable for use in cyclic loading tests.

4.1.2 Validation of the concept of the insertion machine

The standard deviations in the cement mantle thickness around the replica prostheses ranged from 0.1 to 0.6 mm, see Table 4.1 and 4.2. The variations can be partially accounted for by misalignment of the aluminium box section during transverse sectioning, distortion due to scanning of the cut surfaces, heat of polymerisation which may have caused the aluminium to expand, and the effect of tightening the aluminium box section against the base of the insertion machine, which may have caused the section to deflect (see Figure 3.13).

Table 4.1: The average and standard deviations of the cement mantle thickness around the cemented replica prostheses. The thickness was measured at three points along the 'posterior' face of the prosthesis (A, B and C) and at three points along the 'medial' face of the prosthesis (D, E and F).

	Cement thickness A (mm)	Cement thickness B (mm)	Cement thickness C (mm)	Cement thickness D (mm)	Cement thickness E (mm)	Cement thickness F (mm)
Proximal	4.8 ± 0.5	4.6 ± 0.5	4.4 ± 0.1	18.8 ± 0.6	18.7 ± 0.6	18.8 ± 0.7
	4.8 ± 0.5	4.6 ± 0.5	4.6 ± 0.4	14.7 ± 0.5	14.6 ± 0.5	14.7 ± 0.6
	5.0 ± 0.5	4.8 ± 0.3	4.8 ± 0.4	11.4 ± 0.2	11.3 ± 0.2	11.4 ± 0.5
	5.1 ± 0.4	5.0 ± 0.4	4.9 ± 0.3	8.8 ± 0.3	8.8 ± 0.2	8.7 ± 0.3
	5.2 ± 0.3	5.0 ± 0.5	5.1 ± 0.3	7.1 ± 0.1	7.2 ± 0.2	7.1 ± 0.2
Mid	5.4 ± 0.4	5.1 ± 0.5	5.1 ± 0.3	6.4 ± 0.2	6.2 ± 0.2	6.3 ± 0.1
	5.3 ± 0.3	5.2 ± 0.3	5.3 ± 0.2	6.2 ± 0.2	6.1 ± 0.2	6.2 ± 0.1
	5.5 ± 0.5	5.3 ± 0.4	5.3 ± 0.3	6.6 ± 0.2	6.5 ± 0.1	6.7 ± 0.2
	5.5 ± 0.3	5.2 ± 0.4	5.3 ± 0.4	7.6 ± 0.2	7.6 ± 0.1	7.3 ± 0.3
Distal	5.5 ± 0.4	5.4 ± 0.5	5.5 ± 0.4	8.9 ± 0.1	9.0 ± 0.2	9.0 ± 0.2
	5.5 ± 0.5	5.4 ± 0.5	5.4 ± 0.4	10.8 ± 0.1	10.8 ± 0.1	10.8 ± 0.1
	5.5 ± 0.6	5.4 ± 0.6	5.5 ± 0.5	15.7 ± 0.1	15.6 ± 0.1	15.6 ± 0.1

4.1.3 Accuracy and repeatability of the Insertion Machine

The results of the procedure described in section 3.2.4.2 are described in this section. The standard deviations of the distances between the Lubinus prosthesis surface and the outer cortical surface are reported in Table 4.2 and 4.3. These were averaged to get deviations of ± 0.5 mm medially, and ± 0.7 mm laterally. On the sagittal radiographs, standard deviations were averaged at ± 0.6 mm medially and ± 0.7 mm laterally. These ranges are within the exterior tolerances to which the composite femora are manufactured (± 1.0 mm).

The simulated position was achieved to within 0.9 mm, on average, of that specified in the animation software, in the coronal plane (range from 0.4 mm to 1.9 mm) and to within 1.1 mm, on average, in the sagittal plane (range 0.2 mm to 2.3 mm).

Table 4.2: Mean and standard deviation of the distance between the prosthesis surface and the outer cortical bone as measured from the radiographs ($n = 6$) of the coronal plane of the implanted femora, compared to measurements made from the animation.

	Radiographs (mm)		Animation (mm)		Difference (mm)	
	medial	lateral	medial	lateral	medial	lateral
Distal	8.2 ± 0.7	8.4 ± 0.9	8.7	9.6	-0.5	-1.2
	8.1 ± 0.4	8.0 ± 0.8	9.0	9.2	-0.9	-1.2
Mid	7.2 ± 0.7	8.6 ± 0.7	8.9	9.1	-1.7	-0.5
	6.8 ± 0.4	10.4 ± 0.7	8.7	9.7	-1.9	0.7
Proximal	6.9 ± 0.2	13.2 ± 0.6	7.4	12.5	-0.5	0.7
	8.5 ± 0.8	17.6 ± 0.4	7.7	18.0	-0.8	-0.4

Table 4.3: Mean and standard deviation of the distance between the prosthesis surface and the outer cortical bone as measured from the radiographs ($n = 6$) of the sagittal plane of the implanted femora, compared to measurements made from the animation.

	Radiographs (mm)		Animation (mm)		Difference (mm)	
	anterior	posterior	anterior	posterior	anterior	posterior
Distal	10.6 ± 0.7	7.8 ± 0.9	11.3	8.1	-0.7	-0.3
	9.3 ± 0.6	8.5 ± 1.1	11.4	7.5	-2.1	1.0
Mid	8.1 ± 0.5	9.8 ± 0.6	10.4	8.1	-2.3	1.7
	7.6 ± 0.7	10.6 ± 0.5	8.8	9.8	-1.2	0.8
Proximal	6.2 ± 0.7	12.4 ± 0.5	6.9	12.1	-0.7	0.3
	5.8 ± 0.5	15.6 ± 0.5	7.2	14.6	-1.4	1.0

4.1.4 Accuracy of the migration measurement device

4.1.4.1 Rigidity of the Attachment between the prosthesis and the migration measurement device

The coordinates of the centres of the three spheres of the migration measurement device, as recorded before and after two million loading cycles, are presented in Table 4.4. The coordinate measurement machine probe was programmed to touch off a number of points on each sphere, from which it computed the centre and diameter of each sphere. The small differences between the diameters of the spheres before and after testing indicates the accuracy of the measuring machine.

Table 4.4: The (x, y, z) coordinates of the centre of spheres A, B and C as measured by a co-ordinate measuring machine in the global coordinate system, see Figure 3.18 in section 3.3.2 for location of the spheres. The diameter of each sphere is also given.

		x coord (mm)	y coord (mm)	z coord (mm)	diameter (mm)
Sphere A	Before	-53.565	-29.134	-119.195	19.045
	After	-56.251	-32.097	-117.219	19.036
Sphere B	Before	-21.689	-55.783	-112.409	19.045
	After	-26.136	-60.379	-109.076	19.040
Sphere C	Before	4.739	-23.177	-106.071	19.048
	After	2.437	-29.283	-104.701	19.040

The distance between the centre of each of the three spheres, and the change in these distances computed using the data in Table 4.4, are presented in Table 4.5. These differences are within the error of the coordinate measuring machine. Therefore it was concluded that the migration measurement device remained rigidly fixed to the prosthesis for two million cycles of loading.

Table 4.5: Distance between spheres as computed before and after testing

spheres	distance before (mm)	distance after (mm)	change in position (mm)
AB	42.099	42.108	-0.009
AC	60.059	60.074	-0.015
BC	42.447	42.456	-0.009

4.1.4.2 Data acquisition card accuracy

The data acquisition card was a 16 bit card, theoretically capable of detecting changes in voltage of greater than 0.015 mV. Calibration curves, for each of the six linear variable displacement transducers (LVDTs) are presented in figure 4.1.

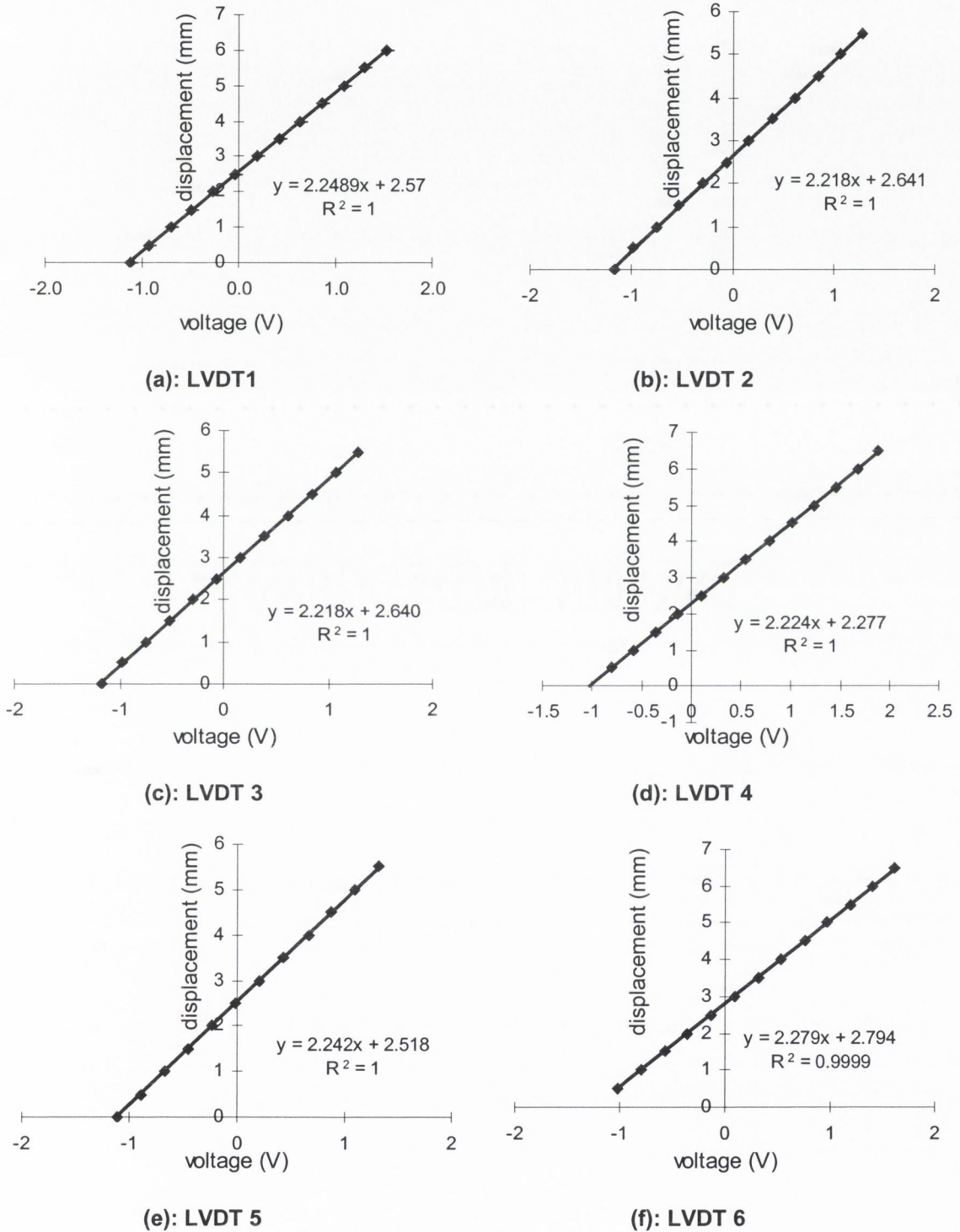


Figure 4.1: The calibration curves for the six LVDTs as labelled in Figure 3.18.

4.1.4.3 Results of the confirmation test described in Section 3.3.5.2

An analysis of the translation of the prosthesis head centre computed from the LVDT outputs using equations (3.14) and (3.15) (see section 3.3.2) was validated in a materials testing machine. Small differences between the actual displacement of the prosthesis and the computed displacement were revealed: 36 microns laterally; 23 microns anteriorly and 19 microns distally, for a travel of 1.4 mm. In the rotational sense, where θ_x , θ_y , and θ_z were held at zero, errors of 0.017° in θ_x , 0.037° in θ_y , and -0.011° in θ_z were found. The errors quantified are a function of the z displacement. Since it is not expected that 1.4 mm of distal migration will occur, errors in computed motion are presented for a migration of up to 0.45 mm. The errors were 21 microns laterally, 16 microns anteriorly, 15 microns distally, 0° in θ_x , -0.014° in θ_y and 0.007° in θ_z , see Figure 4.2 and 4.3

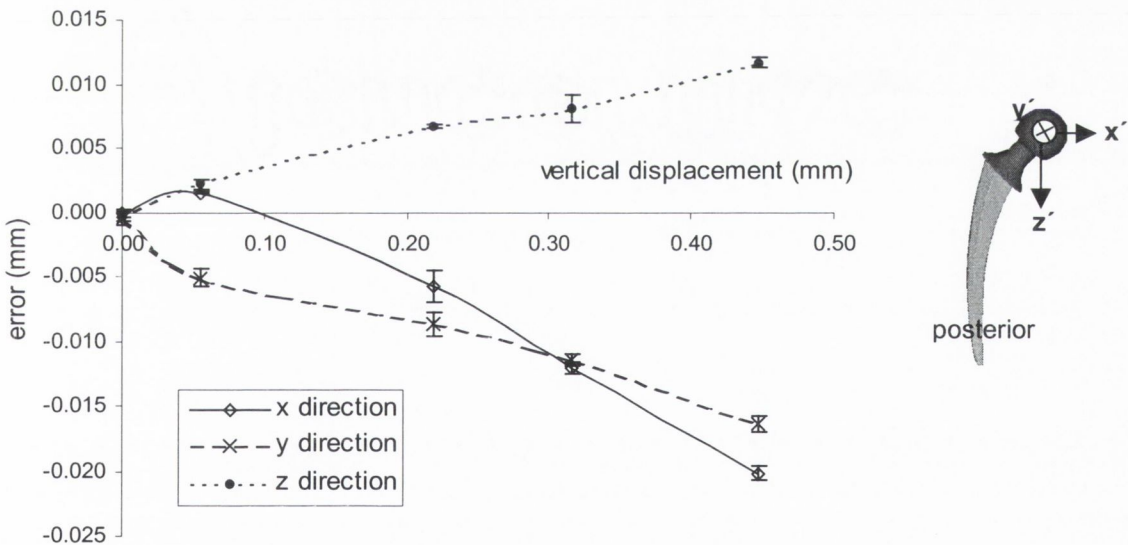


Figure 4.2: The error in computed translations in the lateral direction (-ve x), in the anterior direction (-ve y) and in the distal direction (+ve z) for vertical movement over a distance of 0.45 mm. The measurements were repeated three times, the graphs present the average, and standard deviation for the three measurements.

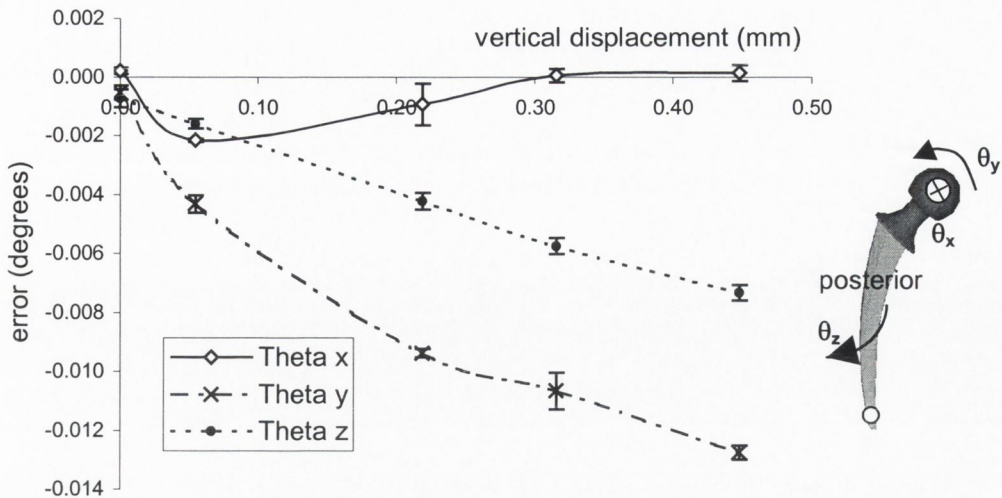


Figure 4.3: The error in computed rotations for vertical movement over 0.45 mm. The measurements were repeated three times, the graphs present the average, and standard deviation for the three measurements. Directions defined as follows: head translates anteriorly and the tip posteriorly (-ve θ_x), the prosthesis tip translates laterally and the head translates medially, otherwise known as varus rotation (-ve θ_y) and the medial face translates anteriorly and the lateral face translates posteriorly (-ve θ_z).

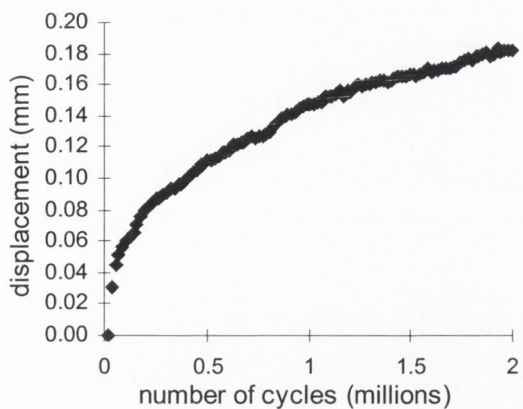
4.2 MIGRATION OF THE MÜLLER AND LUBINUS SPII PROSTHESES

Two sets of migration data are presented: the *rotation* and the *translation* of the prosthesis. The translation of the prosthesis head is computed from the combined translation and rotation measured at the point of contact between the migration measurement device and the prosthesis.

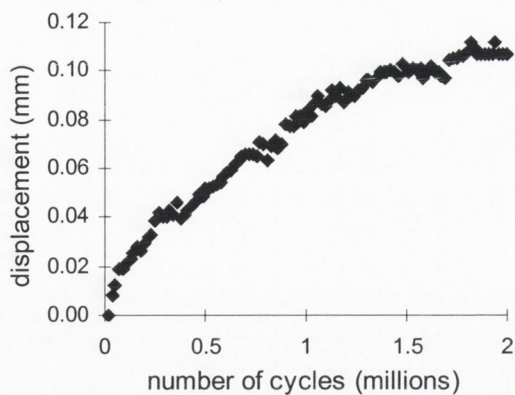
Results are presented for fourteen tests. The prostheses tested were: Lubinus prosthesis without calcar resorption (n=5) and with calcar resorption (n=2); and the Müller prosthesis without calcar resorption (n=5), and with calcar resorption (n=2).

4.2.1 Description of data processing: an example using migration of a Müller prosthesis

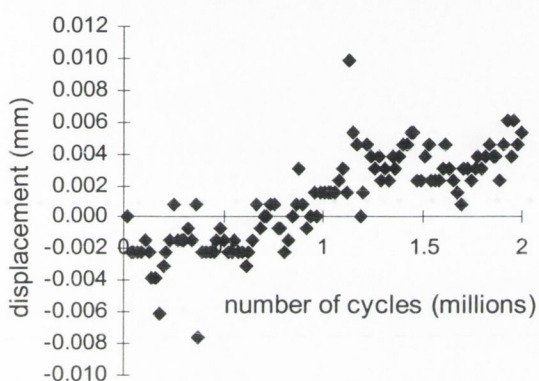
An example of the LVDT data recorded following the procedure described in section 3.3.4 is shown in Figure 4.4. Fluctuations in the data are seen due to noise.



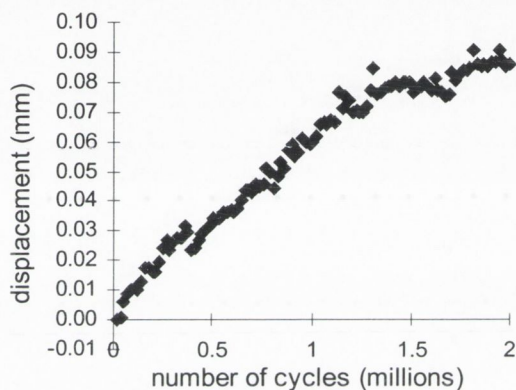
(a): LVDT 1



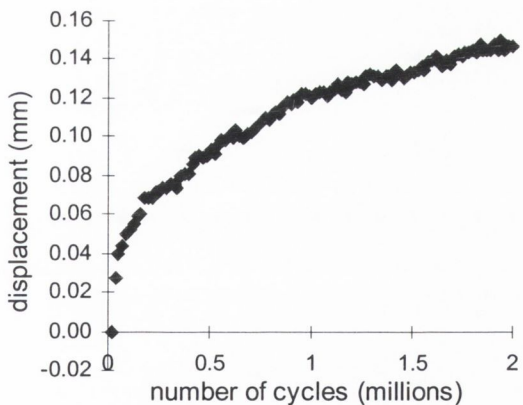
(b): LVDT 2



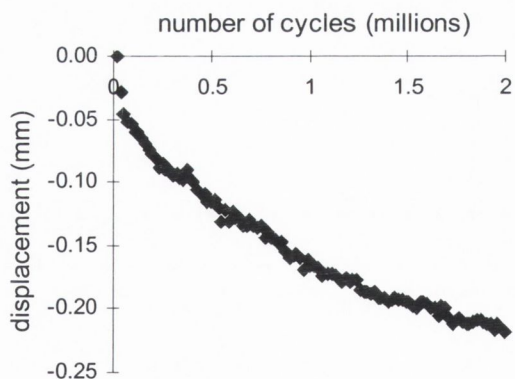
(c): LVDT 3



(d): LVDT 4



(e): LVDT 5



(f): LVDT 6

Figure 4.4: Displacements measured for the six LVDTs (as labelled in Figure 3.18) that were used to measure the migration of a Müller prosthesis. Fluctuations in the data are visible. Note the different scales on the axes.

To prevent these fluctuations leading to spurious results when the LVDT data is entered into the computational procedure, it was necessary to fit a polynomial to the data as shown in Figure 4.5. The raw data for all the LVDT measurements and the polynomials that were fitted to the data are shown in Appendix C.

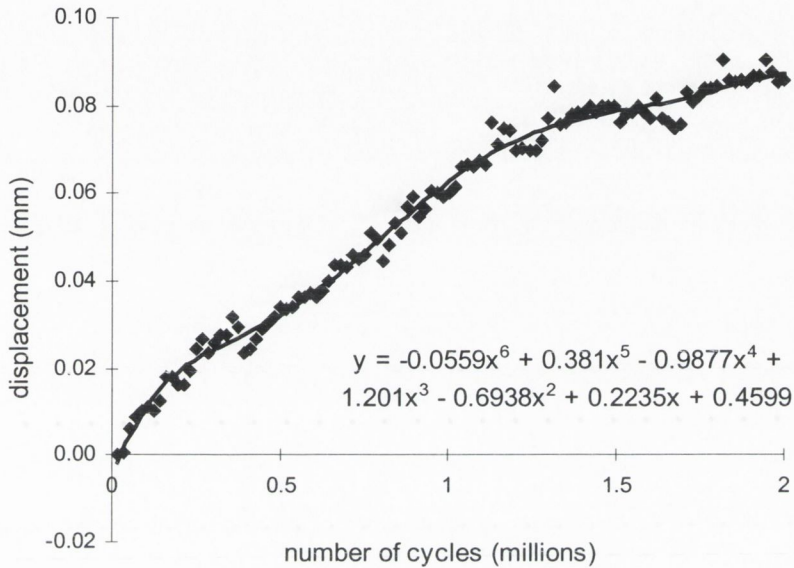


Figure 4.5: The sixth order polynomial that was fitted to the raw data of LVDT 4.

An example of the migration history of a Müller prosthesis where the prosthesis head centre migrated medially (+ve x direction) by 0.195 mm, posteriorly (+ve y direction) by 0.343 mm and distally by 0.086 mm, is illustrated in Figure 4.6. For this prosthesis, the highest rate of migration occurred in the first 0.2 million cycles, and migration appeared to approach a steady-state as 2 million cycles was approached, particularly in the x and z directions.

The prosthesis rotated so that its medial face turned posteriorly, and its lateral face turned anteriorly about the stem's longitudinal axis (+ve θ_z) by 0.307° (see Figure 4.7). The prosthesis rotated into varus by 0.0093° (-ve θ_y), and rotated so that the head moved posteriorly and the tip moved anteriorly (+ve θ_x) by 0.063° .

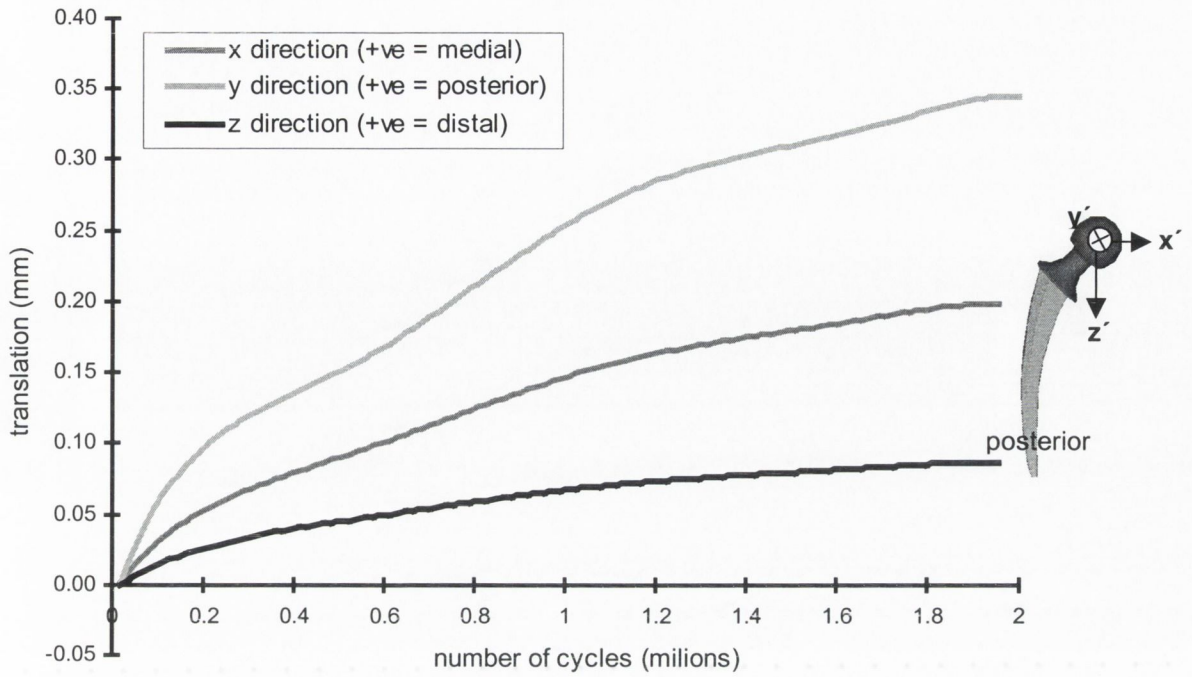


Figure 4.6: The translation of a Müller prosthesis in the x' , y' and z' directions.

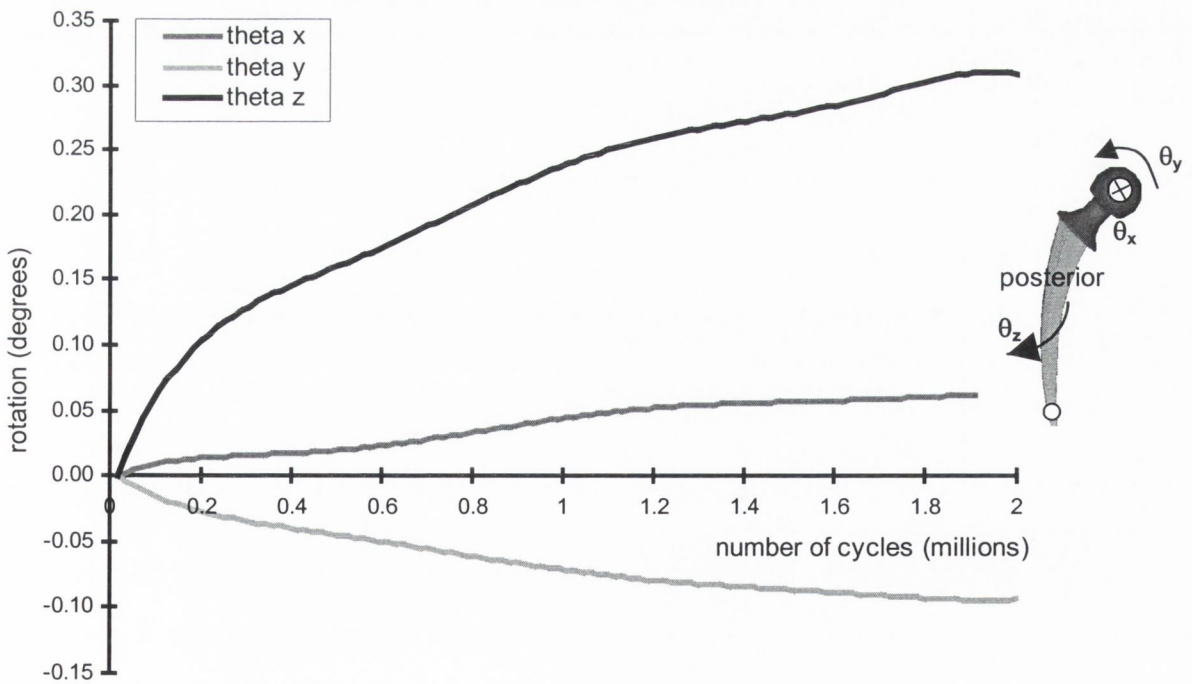


Figure 4.7: The rotation of a Müller prosthesis about the x , y and z axes.

4.2.2 Müller migration histories

The migration curves for each of the five Müller prostheses tested show that there are considerable differences in migration behaviour, despite the precautions taken to minimize variability (Figures 4.8 - Figure 4.13). However, the head of all Müller prostheses tested had a tendency to translate medially (Figure 4.8), posteriorly (Figure 4.9) and distally (Figure 4.10). All Müller prostheses had a tendency to rotate so that the head turned posteriorly and the tip anteriorly (Figure 4.11), to rotate into varus (Figure 4.12), and to rotate so that medial face turned posteriorly and the lateral face turned anteriorly (Figure 4.13).

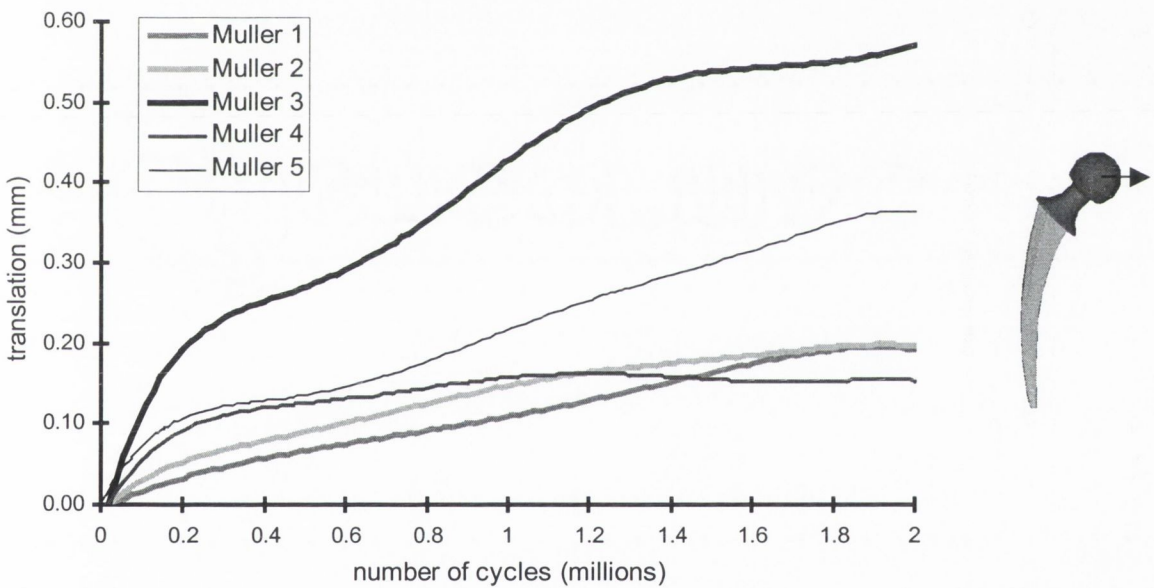


Figure 4.8: The translation of the each Müller prosthesis head centre ($n = 5$) in the x' direction during cyclic loading.

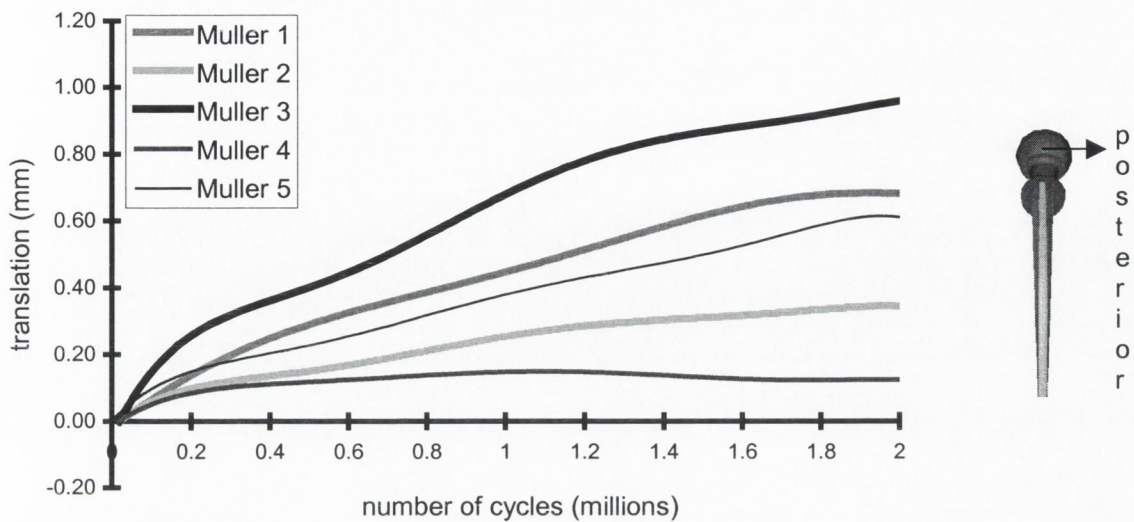


Figure 4.9: The translation of each Müller prosthesis head centre ($n = 5$) in the y' direction during cyclic loading.

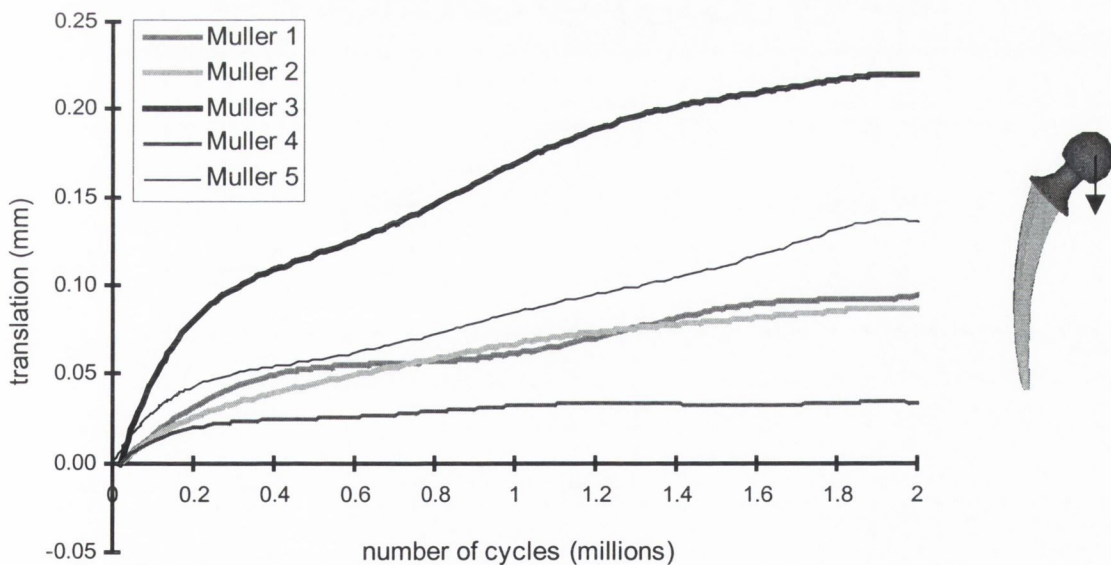


Figure 4.10: The translation of each Müller prosthesis head centre ($n = 5$) in the z' direction during cyclic loading.

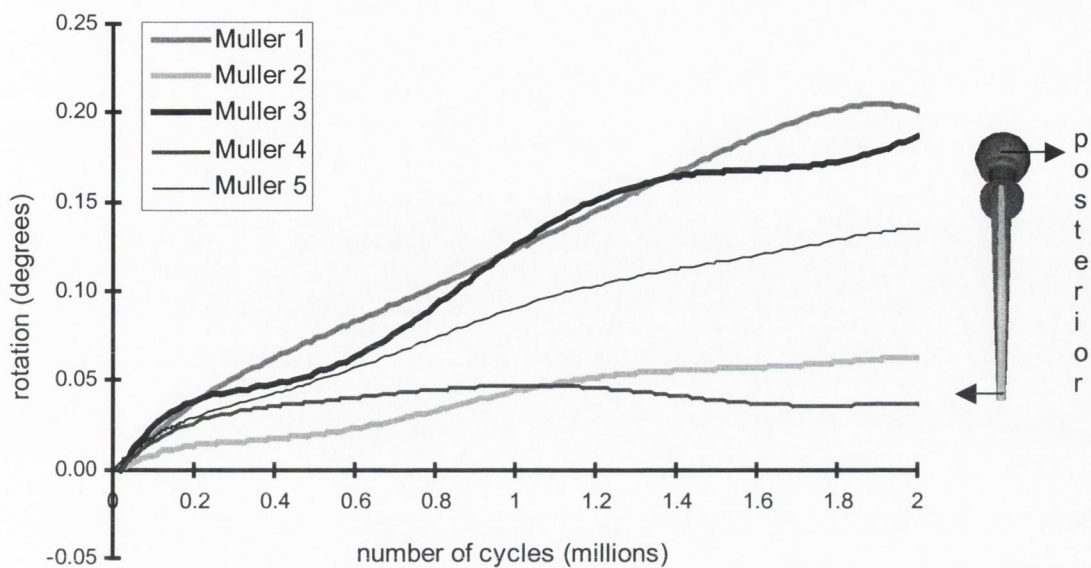


Figure 4.11: The rotation of each Müller prosthesis about the x axis during cyclic loading.

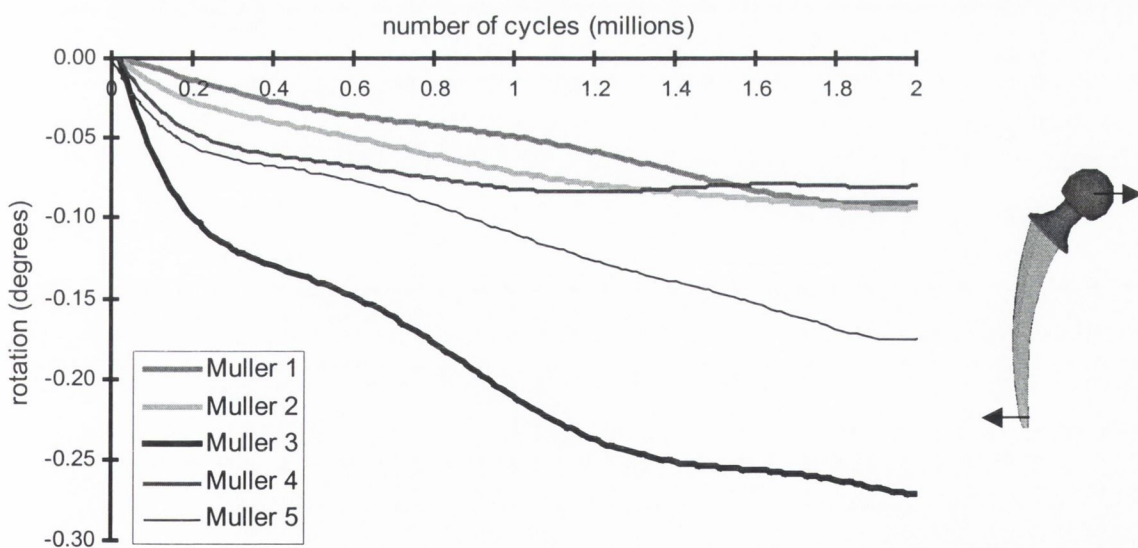


Figure 4.12: The rotation of each Müller prosthesis about the y axis during cyclic loading.

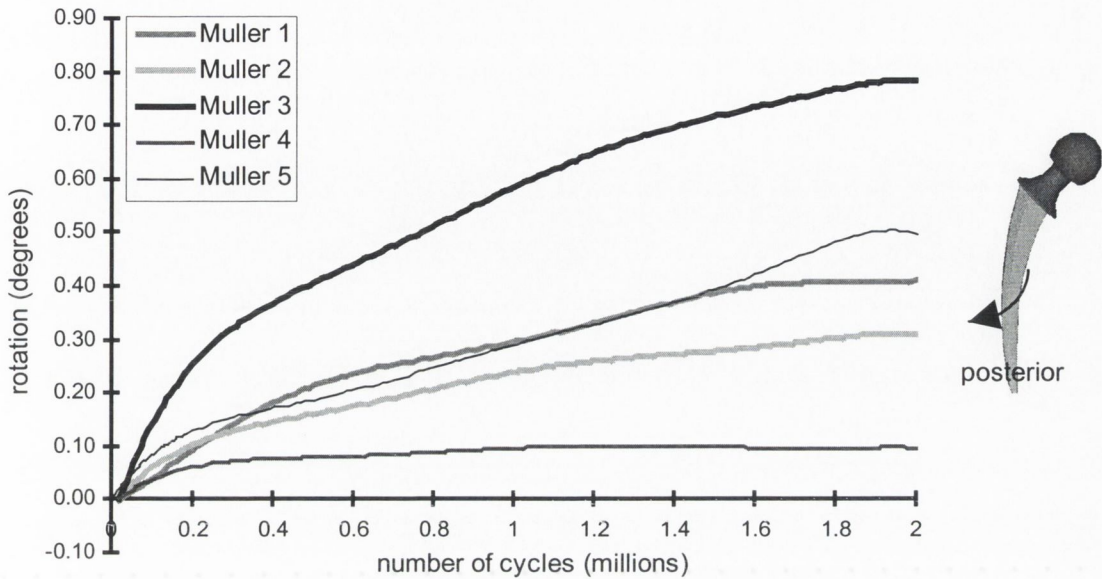


Figure 4.13: The rotation of each Müller prosthesis about the z axis during cyclic loading.

4.2.3 Lubinus migration histories

The migration curves for the five Lubinus prostheses tested, see Figures 4.14 - Figure 4.19, showed a similar degree of variability to the Müller prostheses. All Lubinus prostheses tested had a tendency to translate medially (Figure 4.14), and distally (Figure 4.16). One prosthesis translated anteriorly by 109 microns (Lubinus 3, see Figure 4.15), whereas the other four prostheses translated posteriorly. All Lubinus prostheses rotated into varus, and rotated so that the medial face turned posteriorly and the lateral face turned anteriorly. One Lubinus prosthesis rotated so that the head turned anteriorly and the tip turned posteriorly by 0.04° (Lubinus 3, see Figure 4.17), however the remaining four prostheses rotated in the opposite direction about the x axis.

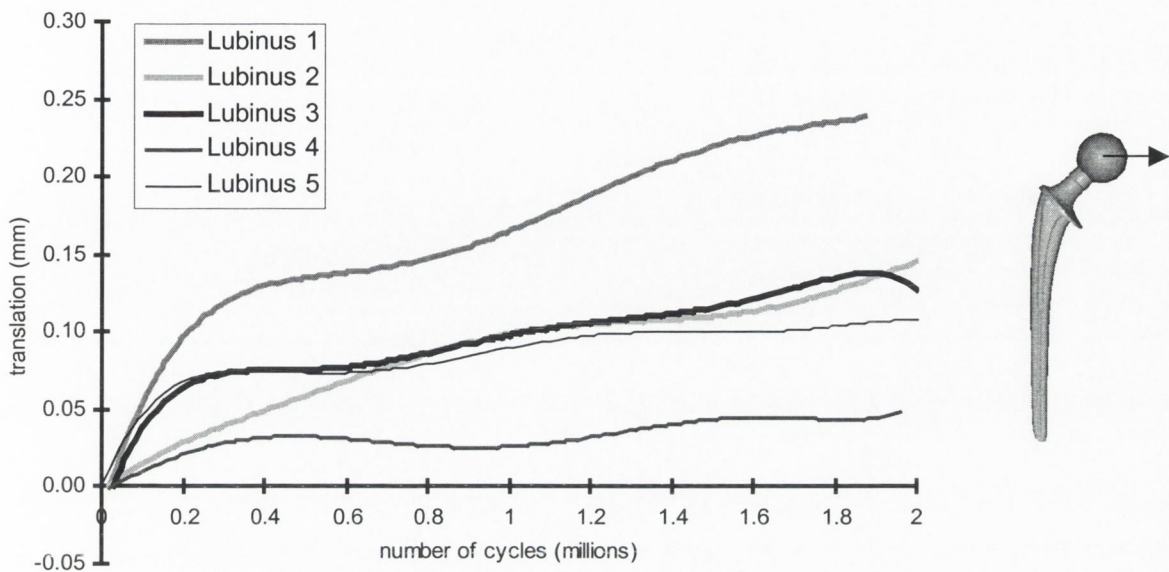


Figure 4.14: The translation of each Lubinus prosthesis head centre in the x' direction during cyclic loading.

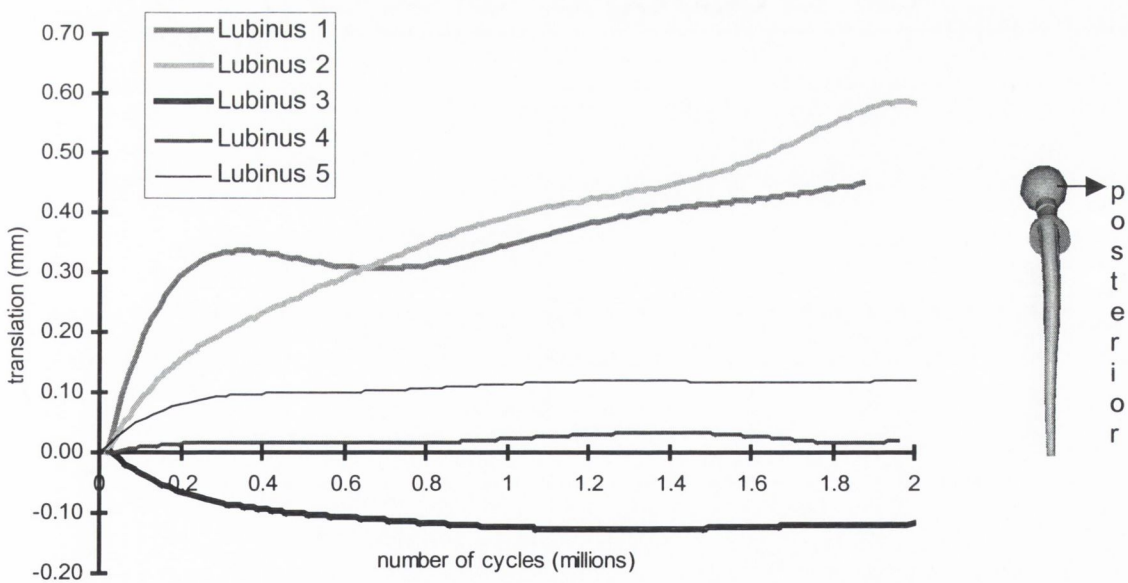


Figure 4.15: The translation of each Lubinus prosthesis head centre in the y' direction during cyclic loading.

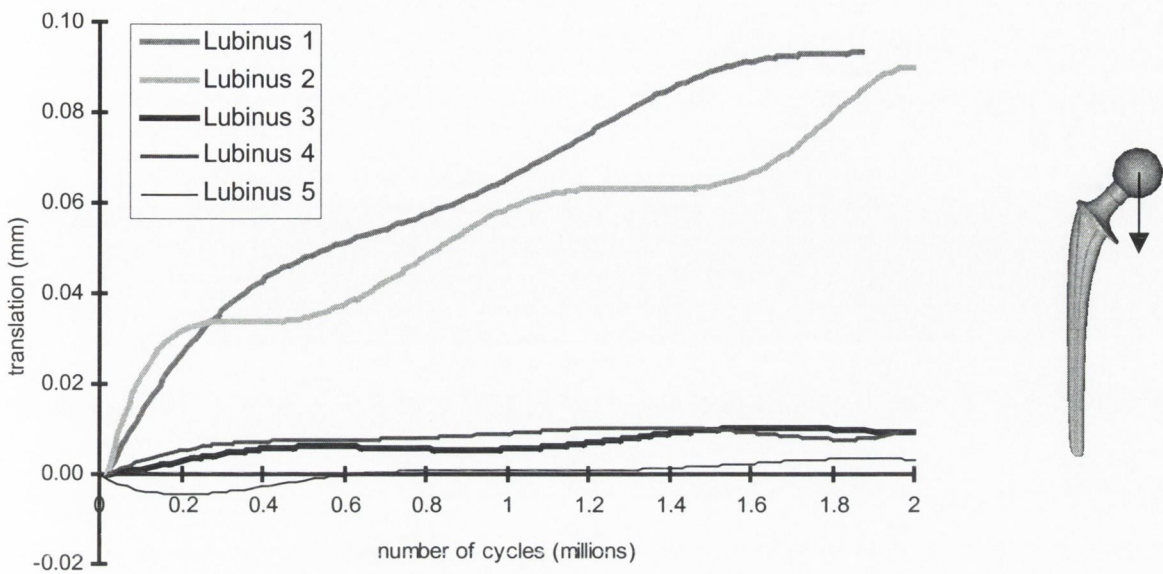


Figure 4.16: The translation of each Lubinus prosthesis head centre in the z' direction during cyclic loading.

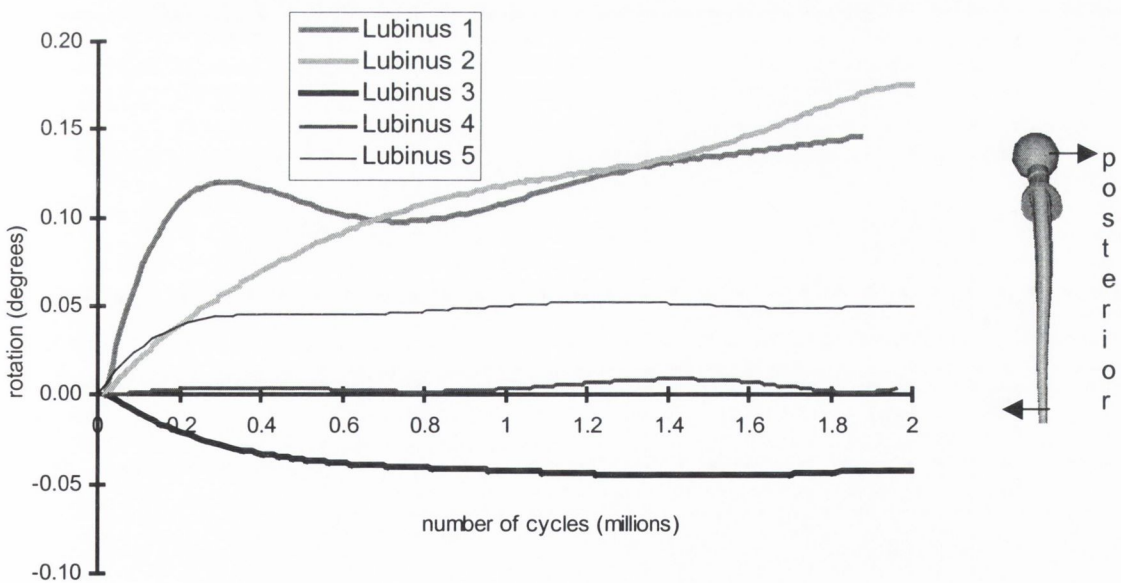


Figure 4.17: The rotation of each Lubinus prosthesis about the x axis during cyclic loading.

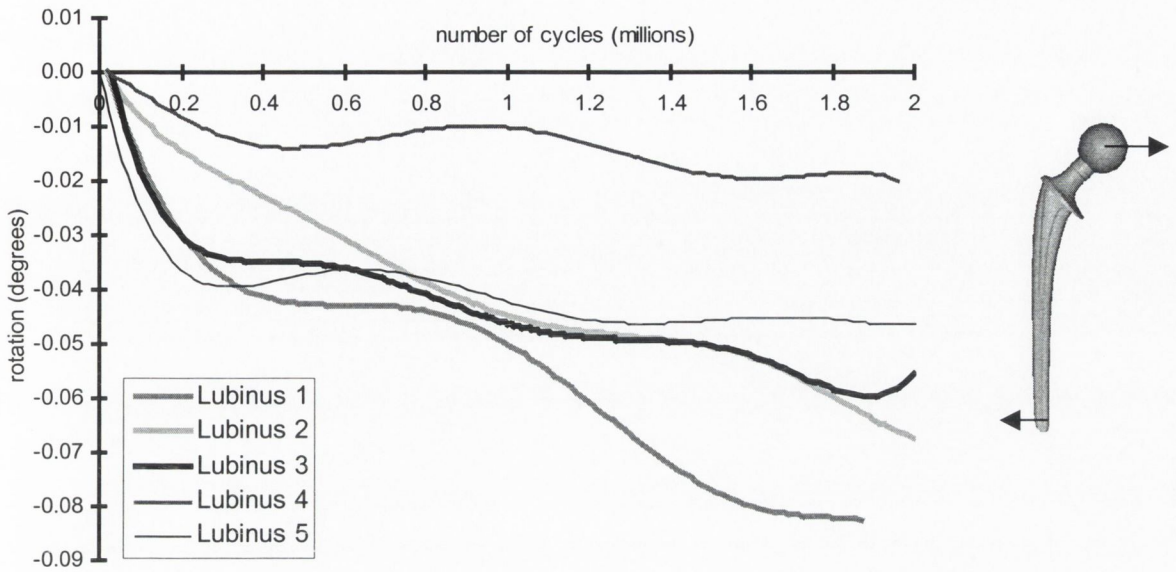


Figure 4.18: The rotation of each Lubinus prosthesis about the y axis during cyclic loading.

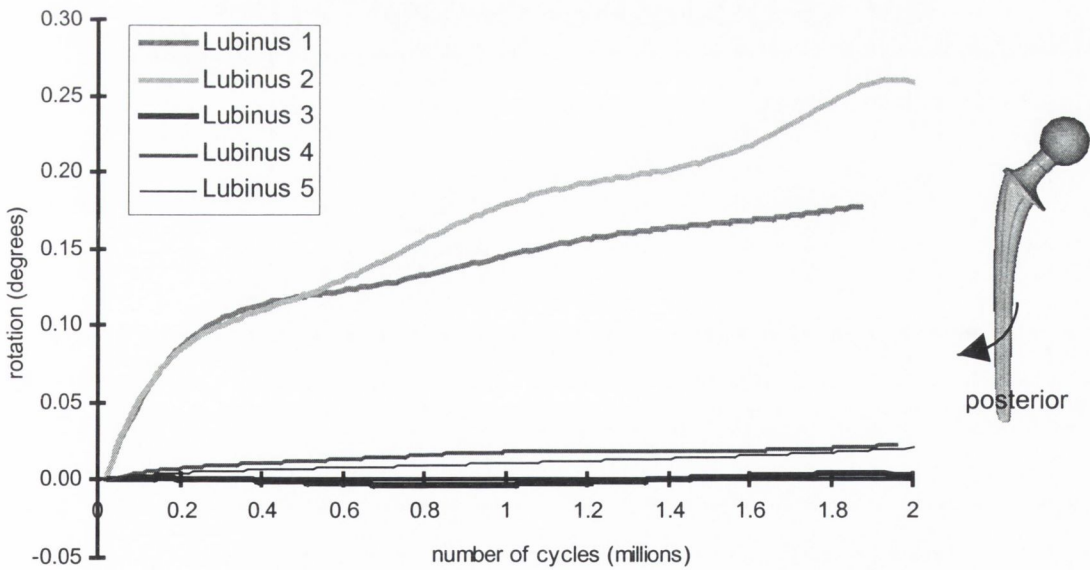


Figure 4.19: The rotation of each Lubinus prosthesis about the z axis during cyclic loading.

4.3 COMPARISON OF MÜLLER AND LUBINUS MIGRATION RATES

4.3.1 Comparison of Migration Curves

Despite significant variation in the recorded migration of the Lubinus and Müller prostheses, when the migrations are plotted together, visual assessment suggests that there may be significantly different migration patterns for the two designs, see Figure 4.20 through to Figure 4.25.

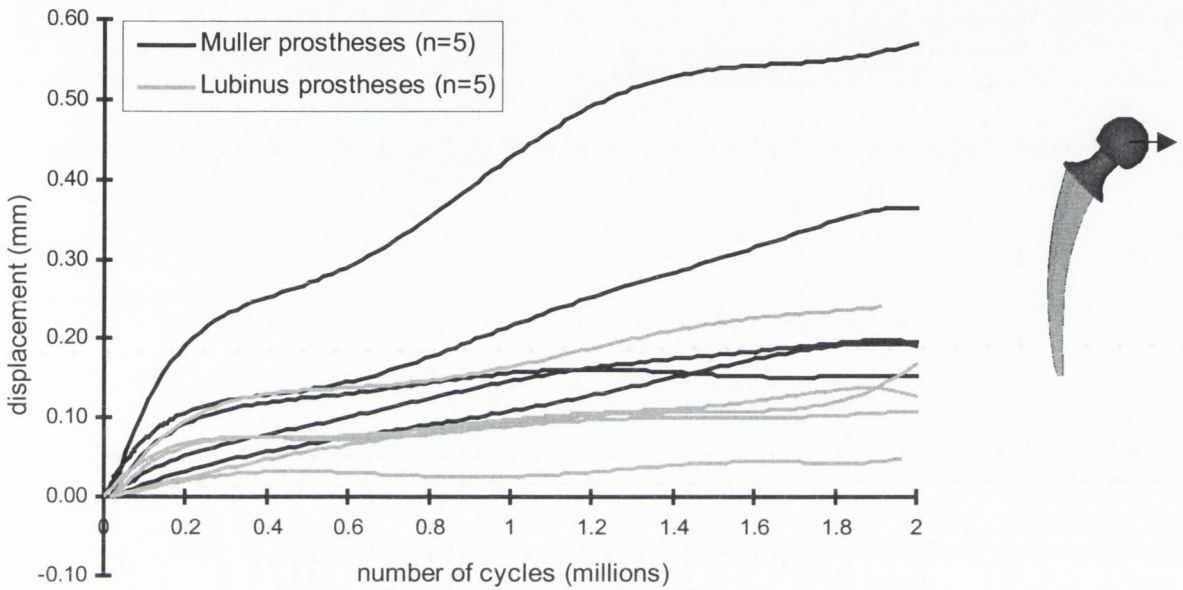


Figure 4.20: Translation of the Müller (n=5) and Lubinus (n=5) prosthesis head centres medially during cyclic loading.

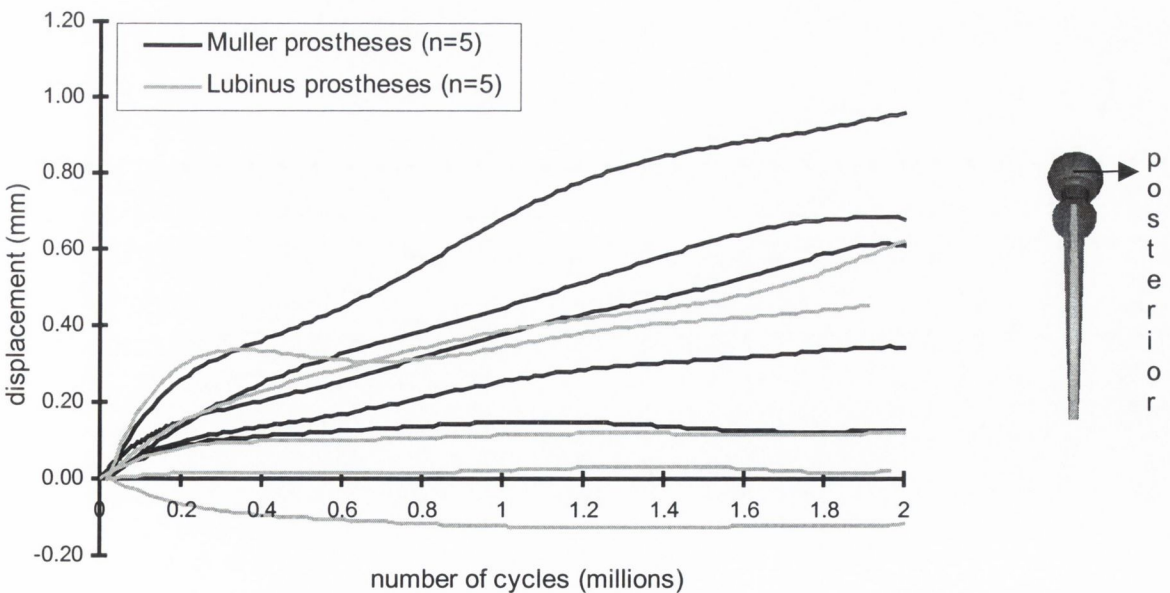


Figure 4.21: Translation of the Müller (n=5) and Lubinus (n=5) prosthesis head centres posteriorly during cyclic loading.

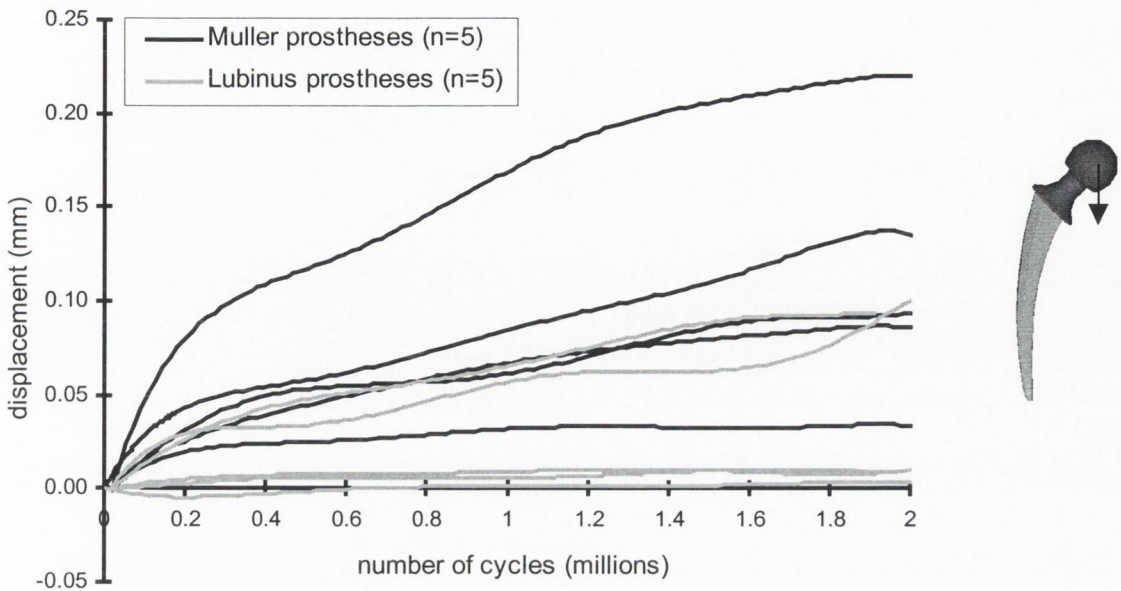


Figure 4.22: Translation of the Müller (n=5) and Lubinus (n=5) prosthesis head centres in the distal direction during cyclic loading .

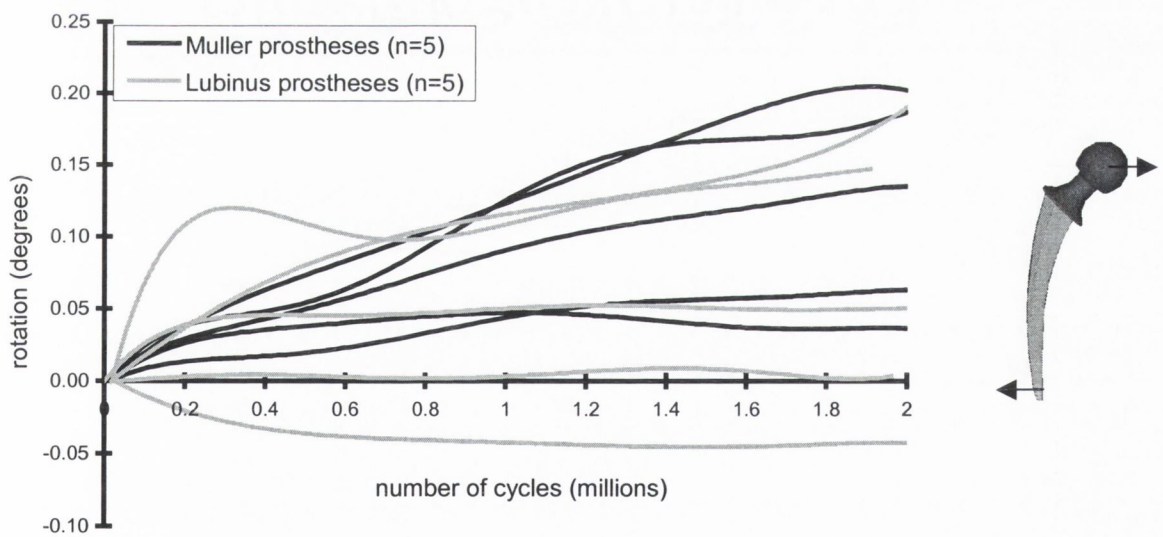


Figure 4.23: Rotation of the Müller (n=5) and Lubinus (n=5) prostheses so that the head translates posteriorly and the tip translates anteriorly during cyclic loading.

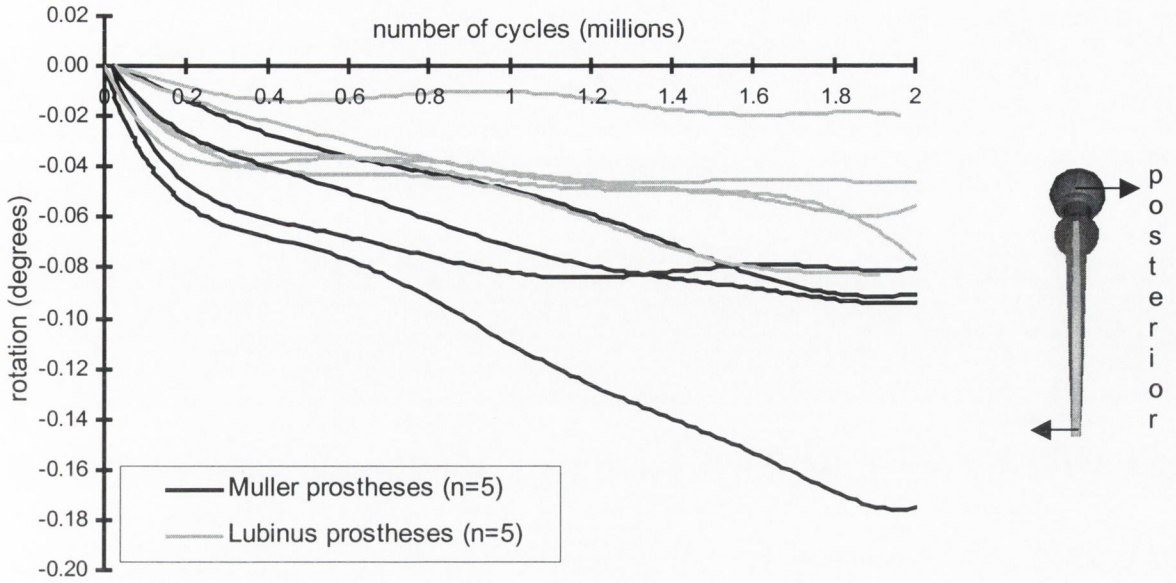


Figure 4.24: Rotation of the Müller (n=5) and Lubinus (n=5) prostheses into varus during cyclic loading.

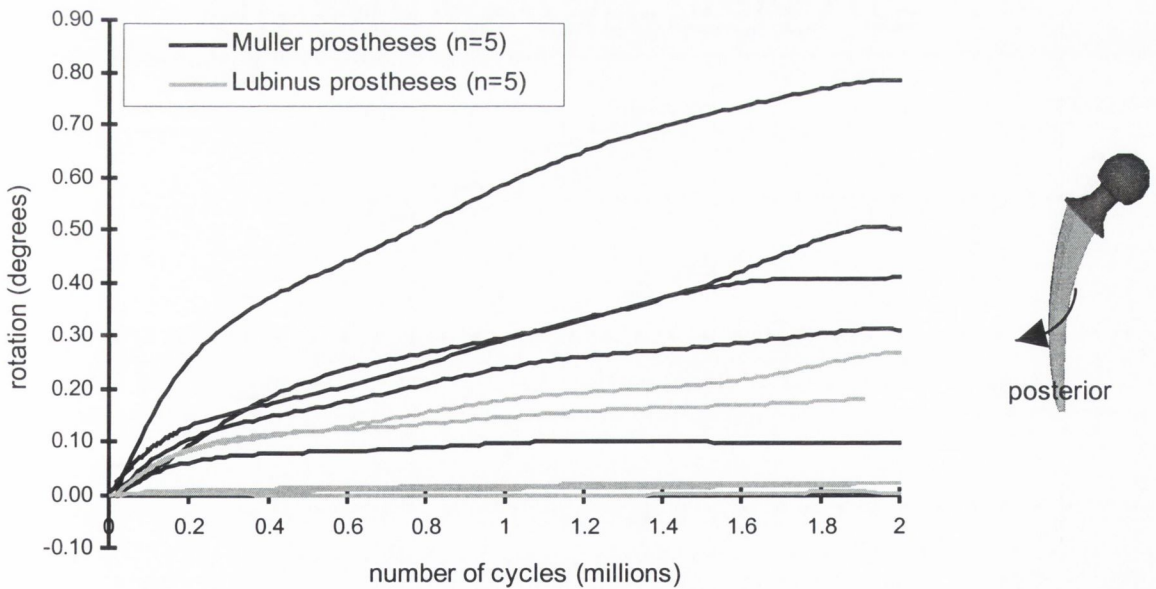


Figure 4.25: Rotation of the Müller (n=5) and Lubinus (n=5) prostheses about the longitudinal axis so that the medial face rotates posteriorly and the lateral face rotates anteriorly, during cyclic loading.

4.3.2 Total migration at 0.2 million cycles

A one tailed Student's t test found that after 0.2 million cycles the Müller prostheses head centres migrated significantly more than the Lubinus prostheses head centres in the z' direction, at a significance level of $p = 0.03$ (see Figure 4.26), and rotated more about the z axis at a significance level of $p = 0.03$ (see Figure 4.27).

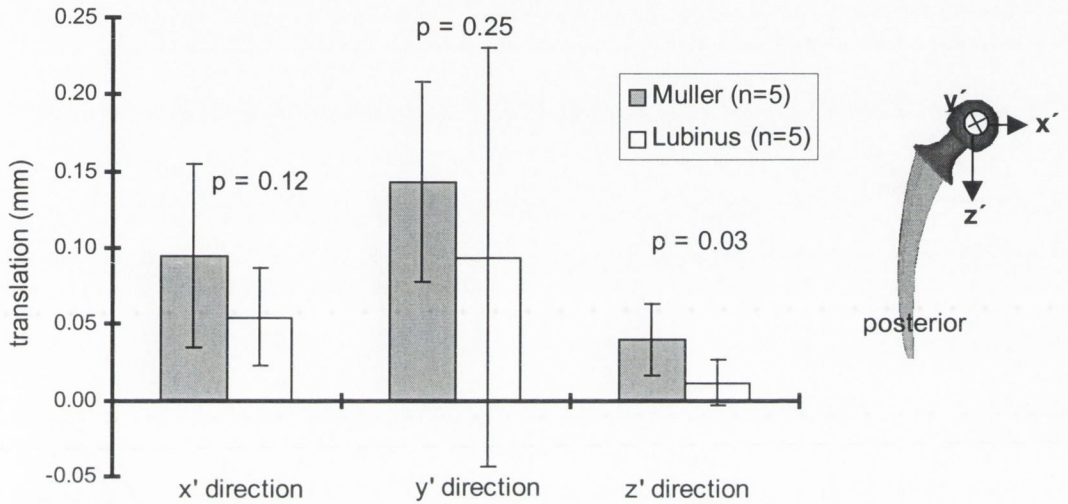


Figure 4.26: The average translations of the Müller and Lubinus head centres after 0.2 million loading cycles.

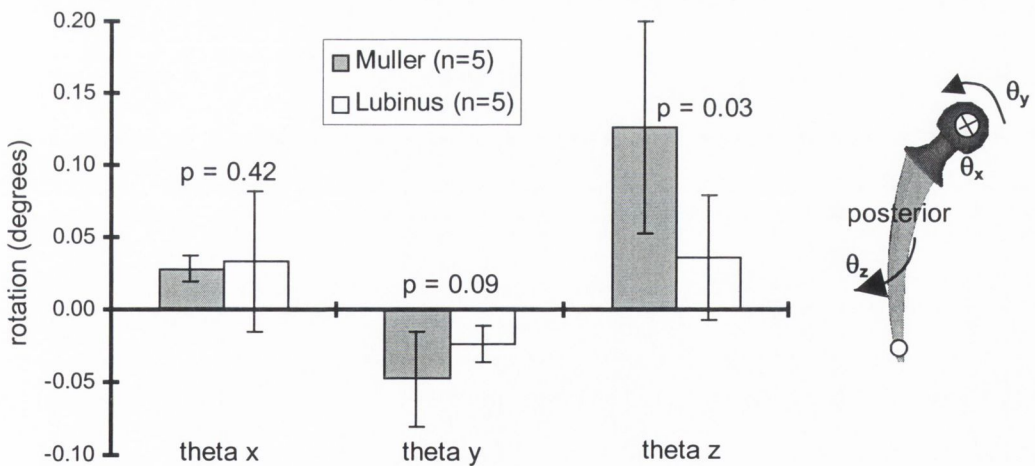


Figure 4.27: The average rotations of the Müller and Lubinus head centres after 0.2 million loading cycles.

4.3.3 Total migration at 1 million cycles

The Müller prostheses migrated significantly more than the Lubinus in the x' , y' and z' directions, at a significance level of $p = 0.04$, $p = 0.06$ and $p = 0.05$ respectively, after 1 million loading cycles (see Figure 4.28). The Müller rotated more than the Lubinus about the y and z axes at a significance level of $p = 0.04$ and 0.02 , respectively (see Figure 4.29).

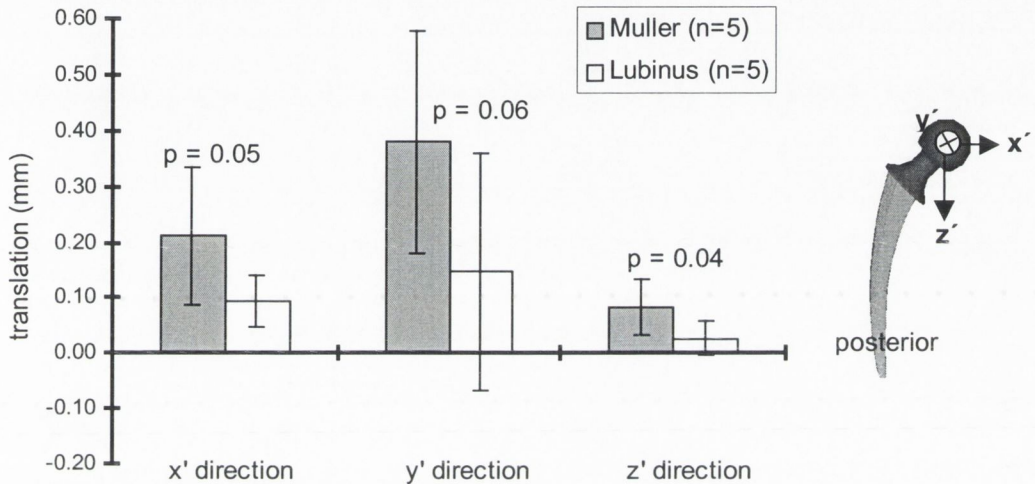


Figure 4.28: The average translations of the Müller and Lubinus head centres after 1 million loading cycles.

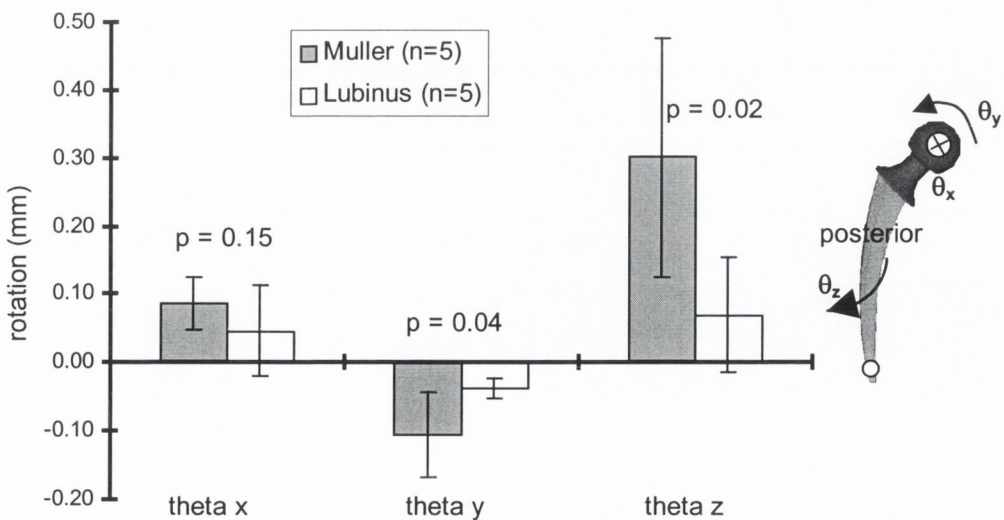


Figure 4.29: The average rotations of the Müller and Lubinus head centres after 1 million loading cycles.

4.3.4 Total migration at 2 million cycles

After 2 million cycles, the Müller prostheses migrated 294 microns, 547 microns and 113 microns in the x' , y' and z' directions respectively, whereas the Lubinus prostheses migrated 139 microns, 223 microns and 44 microns in the x' , y' and z' directions respectively, see Figure 4.30. Despite the variability, Student's t test revealed that the Müller prosthesis translated significantly more than the Lubinus prosthesis in the x' , y' and z' directions at $p = 0.06$, $p = 0.07$ and $p = 0.06$ level of significance, respectively (see Figure 4.30). The Müller prosthesis rotated significantly more than the Lubinus prosthesis about the y and z axes at $p = 0.04$, $p = 0.02$ level of significance, respectively (see Figure 4.31).

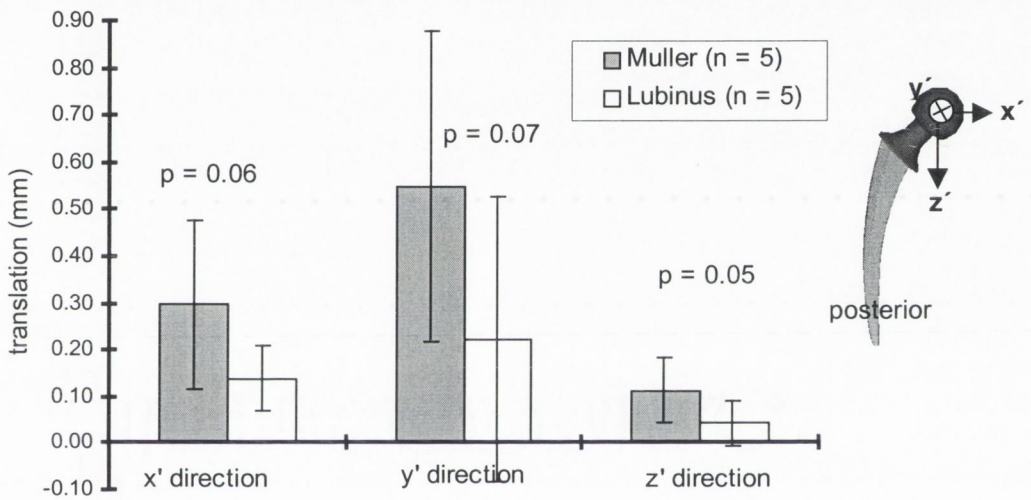


Figure 4.30: The average and standard deviation of the migrations of the Müller and Lubinus head centres at the end of 2 million loading cycles.

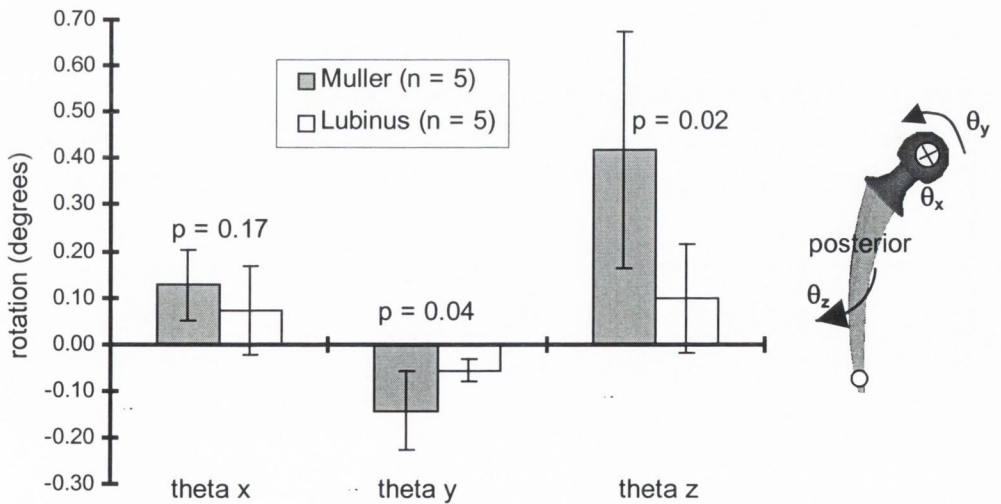


Figure 4.31: The average and standard deviation of the rotations of the Müller and Lubinus head centres at the end of 2 million loading cycles.

4.3.5 Total migration of the Müller and Lubinus prostheses, with migration over the first 0.2 million loading cycles discounted

When migrations over the first 200,000 loading cycles were subtracted from the final migrations, the difference between the Müller and Lubinus prosthesis migrations in the z' direction decreased in significance (from $p = 0.06$ to $p = 0.08$), see Figure 4.32. There was little difference in translations in the x' and y' directions.

Subtraction of prosthesis migration in the first 200,000 loading cycles had little affect on the significance of the differences in rotation about the y and z axis, however the difference between the rotation of the two prosthesis types about the x axis increased (with p decreasing from $p = 0.17$ to $p = 0.12$), see Figure 4.33.

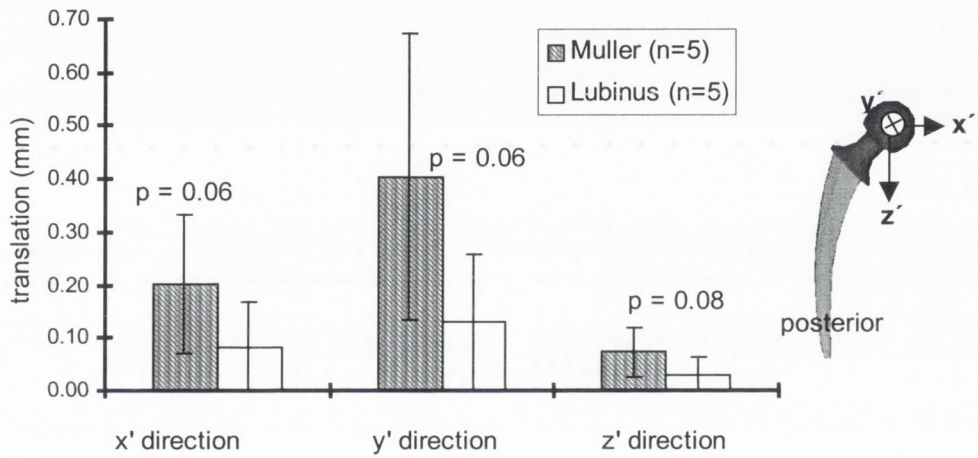


Figure 4.32: The translation of the Müller and Lubinus head centres when migration over the first 0.2 million cycles was subtracted.

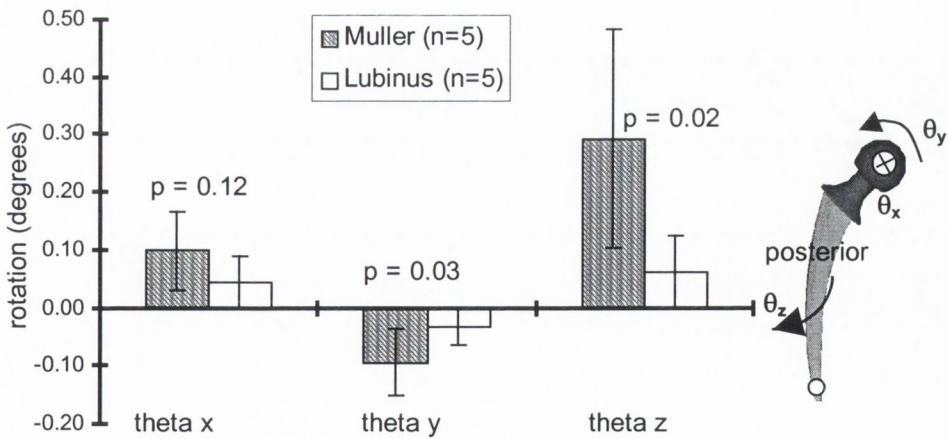


Figure 4.33: The rotation of the Müller and Lubinus head centres when migration over the first 0.2 million cycles was subtracted.

The ‘p’ values as computed by the Student’s t test for the differences in Müller and Lubinus migrations at different stages throughout the loading history, are listed in Table 4.6.

Table 4.6: The p values as computed by the Student’s t test for the differences between the migration of the Müller and Lubinus prostheses as measured at different stages during the cyclic loading history.

	θ_x	θ_y	θ_z	x'	y'	z'
200,000	0.42	0.09	0.03	0.12	0.25	0.03
1,000,000	0.15	0.04	0.02	0.05	0.06	0.04
200,000 - 2,000,000	0.12	0.03	0.02	0.06	0.06	0.08
2,000,000	0.17	0.04	0.02	0.06	0.07	0.05

4.3.6 Rate of migration at 1 million cycles (steady state migration rate)

Steady state migration rate was evaluated at 1 million loading cycles. The migration rates at different stages during the loading history for each prosthesis tested are given in Appendix E. The Müller prosthesis was migrating at least three times faster than the Lubinus in all directions. The largest difference in migration rates was seen in rotation about the y axis — where the Müller was rotating an order of magnitude faster than the Lubinus — and about the z axis, where the Müller migrated at a rate of five times faster than the Lubinus prosthesis, see Table 4.7.

Table 4.7: The average steady state migration rate of the cement mantle around the Müller prostheses (n=5) and Lubinus prostheses (n=5), evaluated at 1 million cycles. The significance of the difference between the two data sets computed by the Student’s t test are also presented.

	Lubinus migration rate	Müller migration rate	Significance of difference (p)
x'	$5.53 \times 10^{-5} \mu\text{m}/\text{cycle}$	$15.94 \times 10^{-5} \mu\text{m}/\text{cycle}$	0.07
y'	$8.50 \times 10^{-5} \mu\text{m}/\text{cycle}$	$27.86 \times 10^{-5} \mu\text{m}/\text{cycle}$	0.05
z'	$1.91 \times 10^{-5} \mu\text{m}/\text{cycle}$	$4.99 \times 10^{-5} \mu\text{m}/\text{cycle}$	0.08
θ_x	$2.65 \times 10^{-5} \mu^\circ/\text{cycle}$	$7.71 \times 10^{-5} \mu^\circ/\text{cycle}$	0.07
θ_y	$-2.34 \times 10^{-5} \mu^\circ/\text{cycle}$	$-70.46 \times 10^{-5} \mu^\circ/\text{cycle}$	0.06
θ_z	$3.56 \times 10^{-5} \mu^\circ/\text{cycle}$	$17.52 \times 10^{-5} \mu^\circ/\text{cycle}$	0.03

4.4 COMPARISON OF THE MIGRATION OF THE LUBINUS AND MÜLLER PROSTHESES WITH AND WITHOUT RESORPTION.

4.4.1 Comparison of the migration curves

In all stems that were tested for 4 million cycles — 2 million without resorption simulated and 2 million with resorption simulated — a discontinuity in the migration pattern is evident (see Figures 4.34 to 4.40). The discontinuity occurs during the initial period of the resorption phase of cyclic loading, and comprises of an initial rapid migration (see Figures 4.34, 4.35), after which migration progresses at a slower, steady state rate. For Müller 1 (Figure 4.34 and 4.35) and Müller 3 (Figure 4.36 and 4.37) the steady state resorption migration is similar to the pre-resorption steady state migration rate. Although this is generally true for the two Lubinus prostheses, the migration behaviour of both Lubinus 2 and Lubinus 3 is more erratic, particularly in rotation (see Figure 4.39 for Lubinus 2 and Figure 4.40 for Lubinus 3).

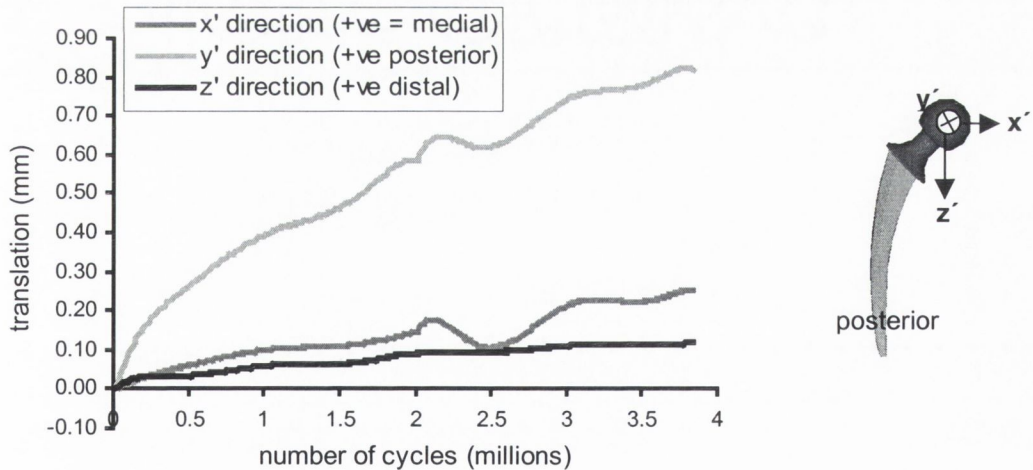


Figure 4.34: Translation of Müller 1 after 4 million loading cycles. For 0 - 2 million cycles, the cemented prosthesis was tested without resorption. For 2 - 4 million cycles, resorption was simulated.

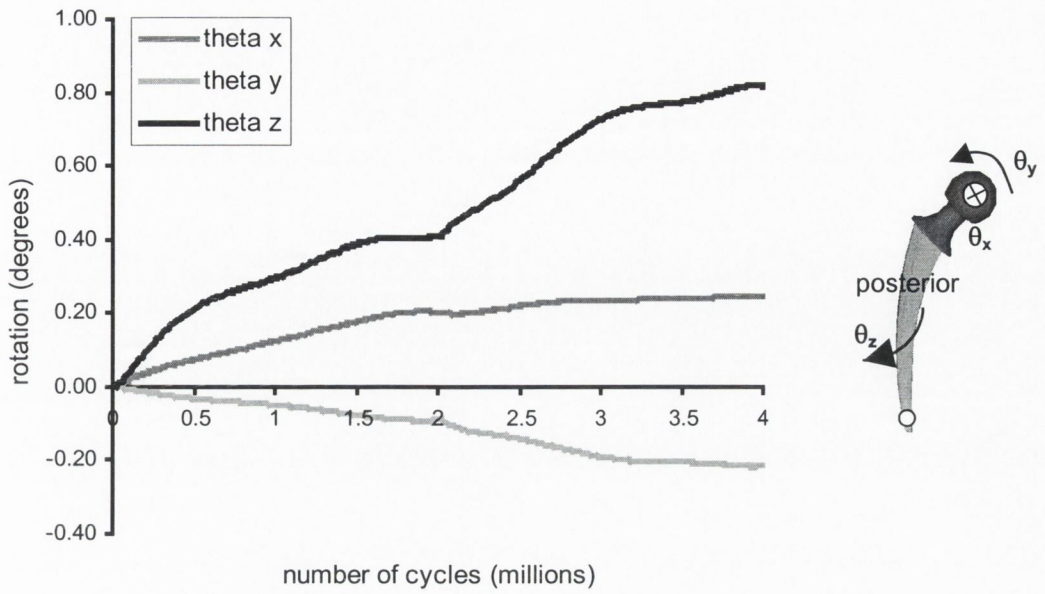


Figure 4.35: Rotation of Müller 1 after 4 million loading cycles. For 0 - 2 million cycles, the cemented prosthesis was tested without resorption. For 2 - 4 million cycles, resorption was simulated.

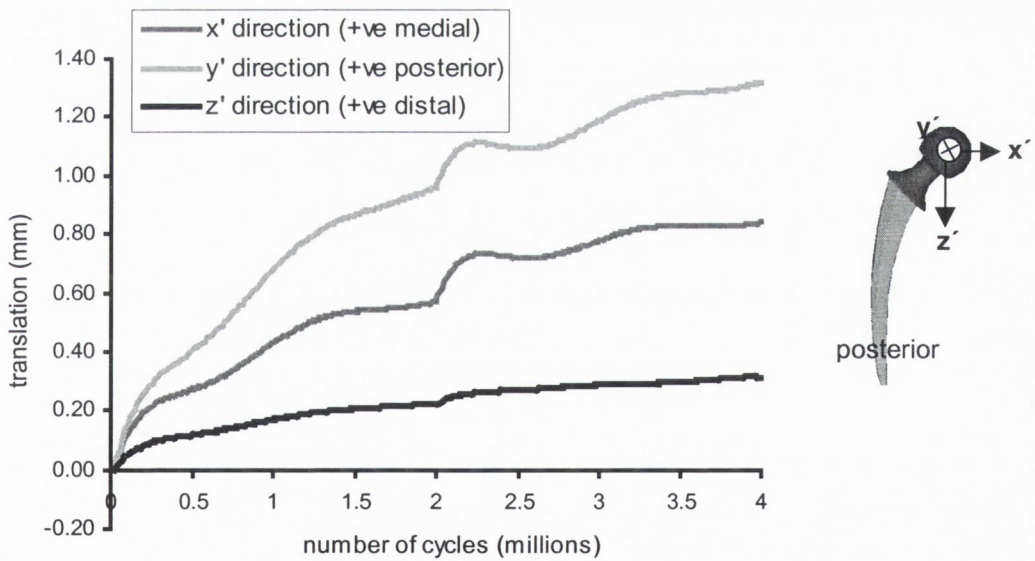


Figure 4.36: Translation of Müller 3 after 4 million loading cycles. For 0 - 2 million cycles, the cemented prosthesis was tested without resorption. For 2 - 4 million cycles, resorption was simulated.

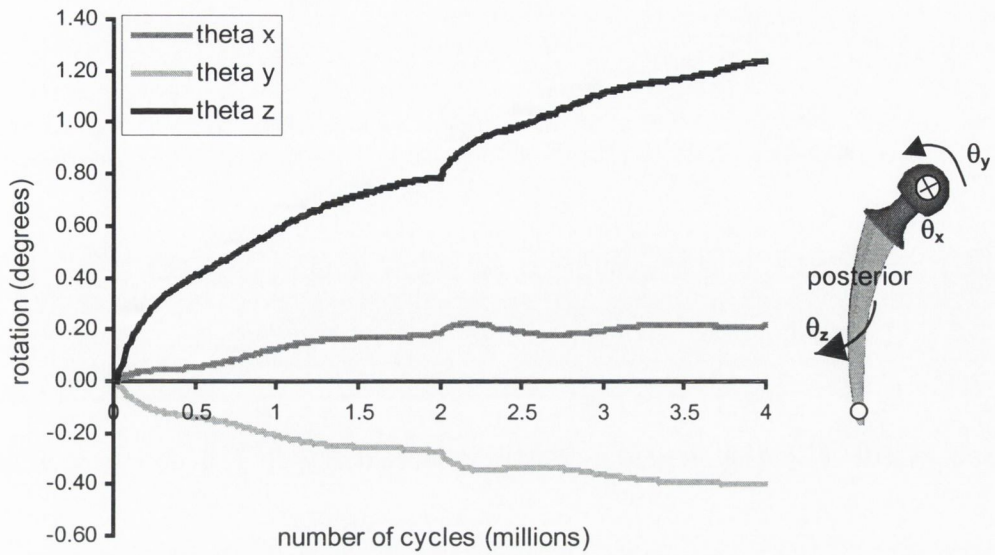


Figure 4.37: Rotation of Müller 3 after 4 million loading cycles. For 0 - 2 million cycles, the cemented prosthesis was tested without resorption. For 2 - 4 million cycles, resorption was simulated.

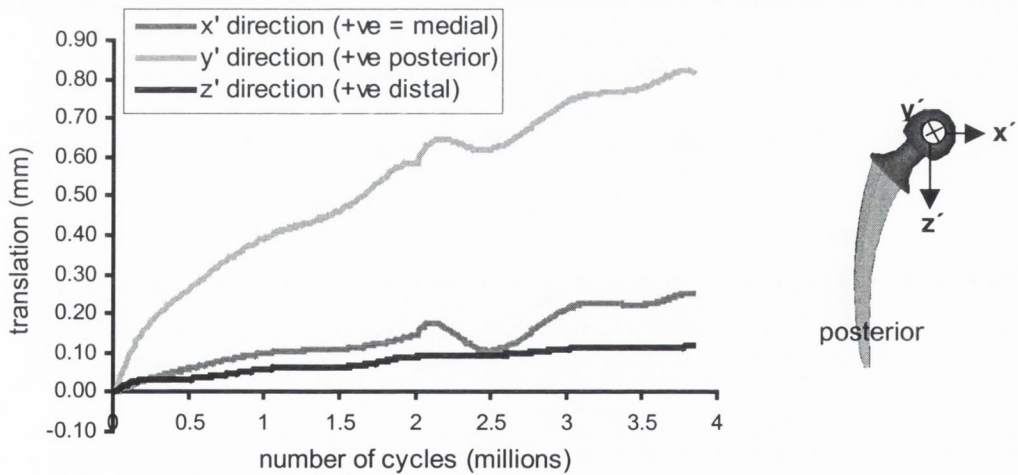


Figure 4.38: Translation of Lubinus 2 after 4 million loading cycles. For 0 - 2 million cycles, the cemented prosthesis was tested without resorption. For 2 - 4 million cycles, resorption was simulated.

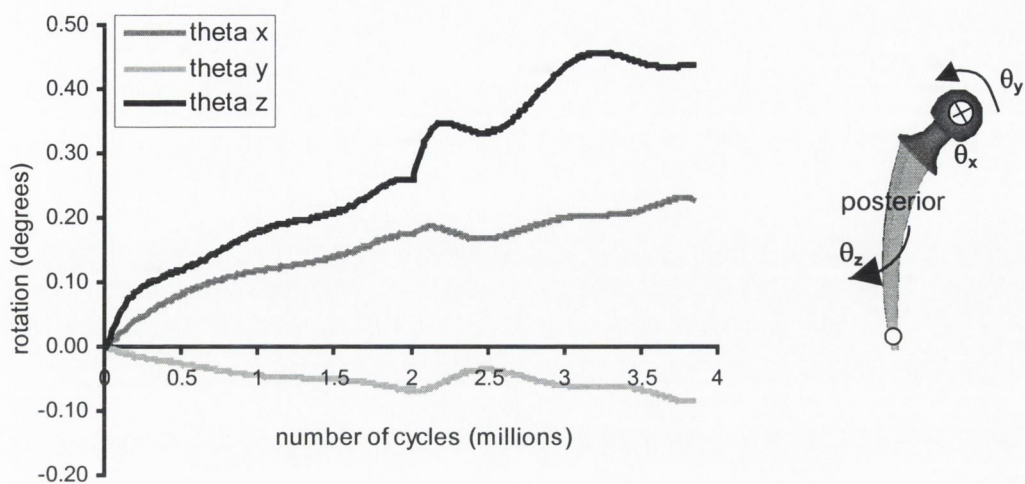


Figure 4.39: Rotation of Lubinus 2 after 4 million loading cycles. For 0 - 2 million cycles, the cemented prosthesis was tested without resorption. For 2 - 4 million cycles, resorption was simulated.

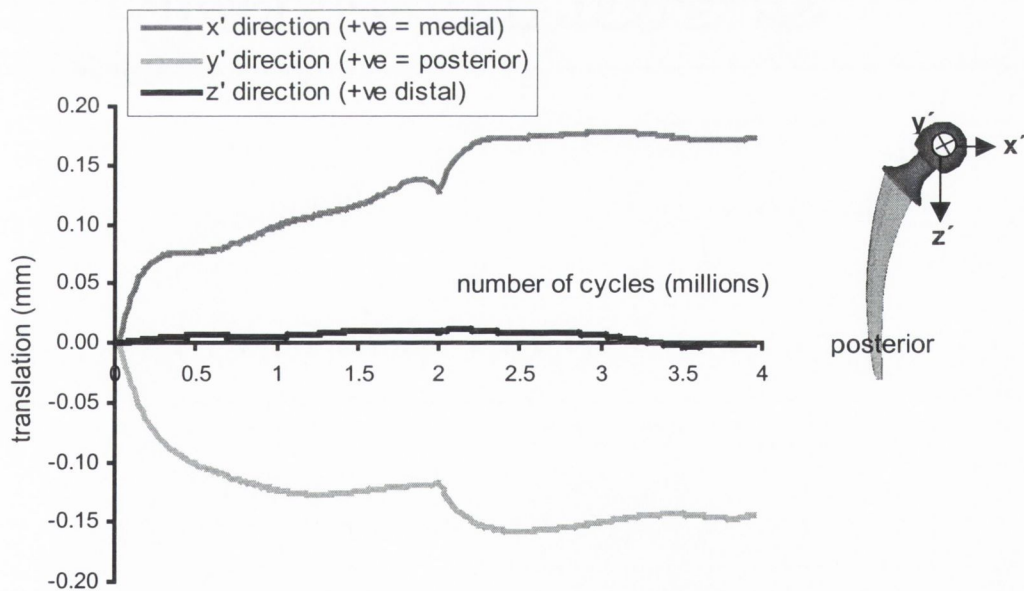


Figure 4.40: Translation of Lubinus 3 after 4 million loading cycles. For 0 - 2 million cycles, the cemented prosthesis was tested without resorption. For 2 - 4 million cycles, resorption was simulated.

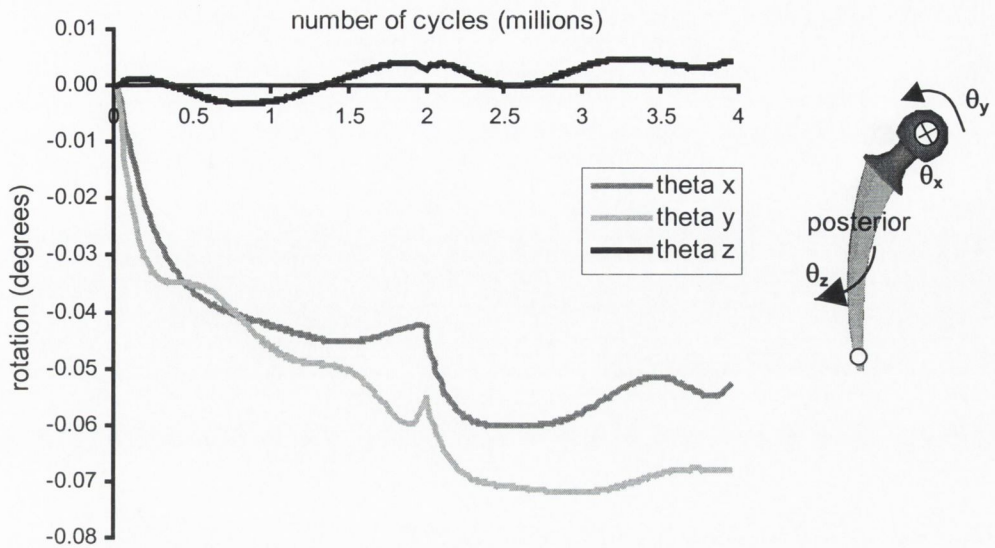


Figure 4.41: Rotation of Lubinus 3 after 4 million loading cycles. For 0 - 2 million cycles, the cemented prosthesis was tested without resorption. For 2 - 4 million cycles, resorption was simulated.

4.4.2 Comparison of Total Migration

A comparison was made between the total migration from 0 – 2 million cycles (without resorption) and the total migration from 2 – 4 million cycles (with resorption) for each prosthesis tested. The absolute migrations, before and after resorption, in translation in the x' and z' directions and in rotation about the z axis were comparable for Müller 1. The prosthesis rotated slightly more about the y axis after resorption was simulated (see Figure 4.42). Müller 3 migrated almost half as much during the 2 – 4 million phase as it did during the initial 2 million loading cycles in all directions (see Figure 4.43).

A decrease was found in the total migration of Lubinus 2 in all directions (see Figure 4.44), after resorption was simulated, however translation in the x' direction and rotation about the z axis, were comparable. Similarly, Lubinus 3 rotated more about the z axis in the 2 – 4 million cycles of the resorption phase of testing, than in the initial 2 million cycles. Translation measured in the x' direction before and after resorption was comparable (see Figure 4.45).

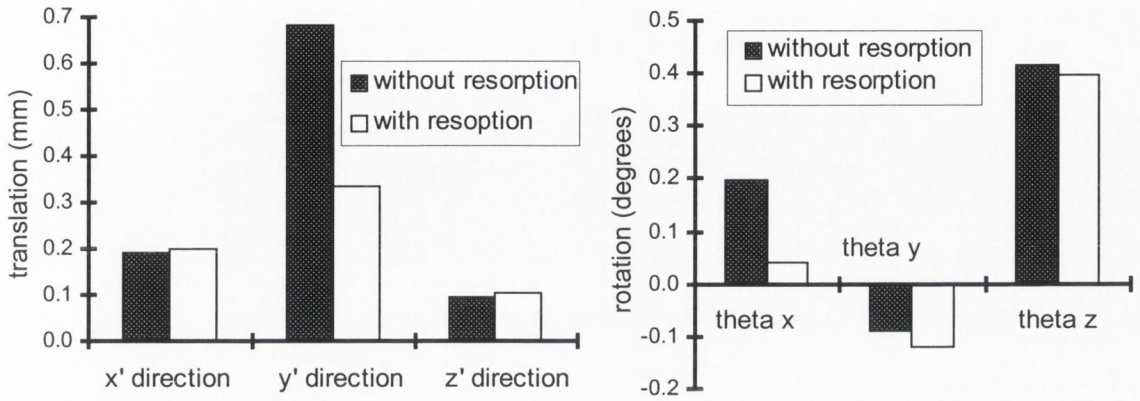


Figure 4.42: Migration of Müller 1 with and without resorption at 2 million cycles.

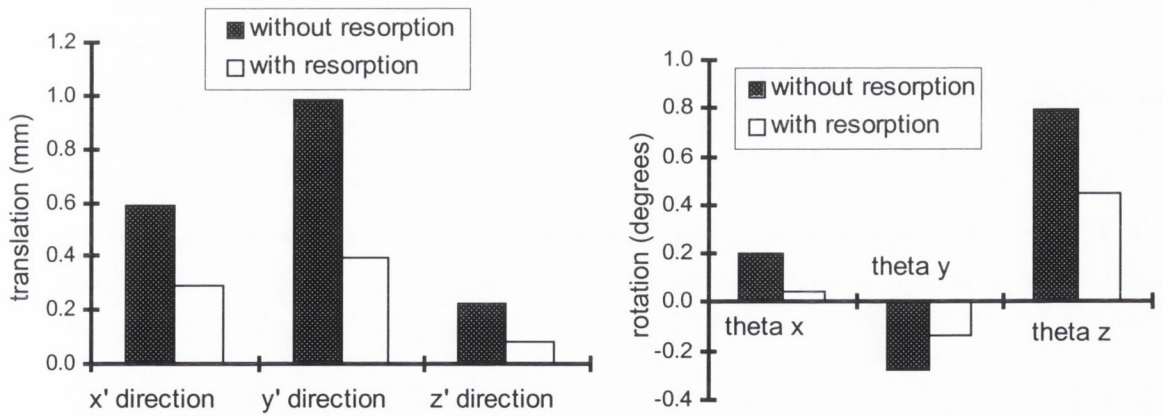


Figure 4.43: Migration of Müller 3 with and without resorption at 2 million cycles.

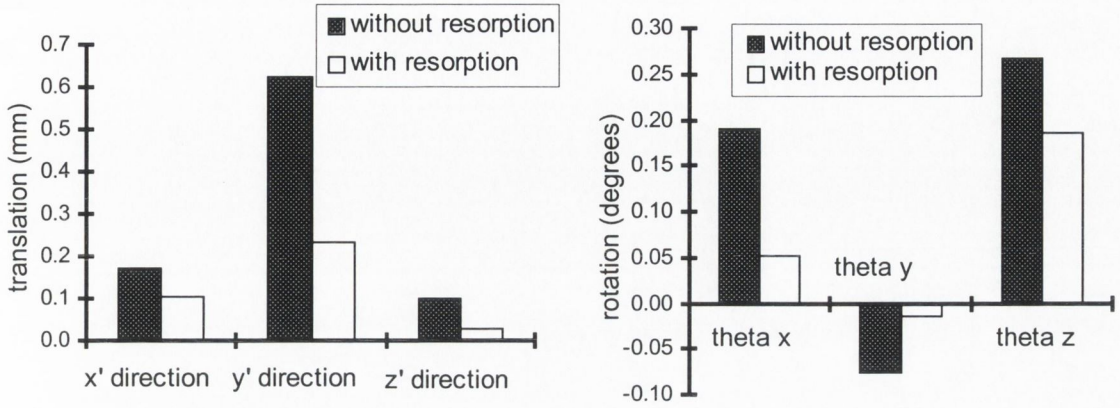


Figure 4.44: Migration of Lubinus 2 with and without resorption at 2 million cycles.

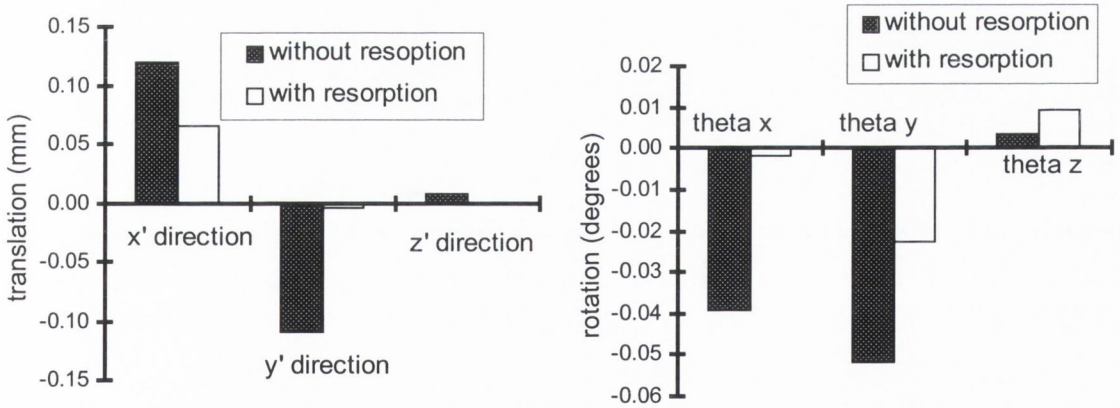


Figure 4.45: Migration of Lubinus 3 with and without resorption at 2 million cycles.

4.4.3 Comparison of the steady state migration

A comparison was made between the steady state migration at 1 million cycles and at 3 million cycles for the four prostheses where resorption was modelled. The wide variability in migration rates is apparent (see Table 4.8) and makes comparisons difficult. This is particularly evident for the Lubinus prostheses, where no trends in the steady state migration rates before and after bone resorption simulation are evident. However, both Müller prostheses show an increase in migration rates in the y' direction and in rotation about the z axis, (these values are highlighted in Table 4.8).

Table 4.8: The steady state migration at 1 million and 3 million loading cycles for the prostheses tested to 4 million cycles, 0 – 2 million was without resorption and 2 – 4 million was with resorption modelled. The units of the steady state migration rate are $\times 10^{-5} \mu\text{m}/\text{cycle}$ or $10^{-5} \mu\%/\text{cycle}$.

	x'	y'	z'	θ_x	θ_y	θ_z
Müller 1	9.3	32.0	3.6	10.5	-4.1	16.1
Müller 1 resorption	11.6	16.6	5.1	0.7	-7.3	21.4
Müller 3	36.8	57.9	11.0	15.6	-15.7	35.0
Müller 3 resorption	20.2	31.6	31.6	88.4	-98.1	20.6
Lubinus 2	5.4	18.9	4.7	4.6	-2.5	9.6
Lubinus 2 resorption	19.7	2.1	3.4	-6.3	2.1	5.1
Lubinus 3	5.0	-2.7	0.3	-0.8	-2.1	0.5
Lubinus 3 resorption	0.4	2.4	-1.5	1.5	0.2	1.0

4.5 THE CEMENT/METAL INTERFACES OF SECTIONED SAMPLES

Sectioned femora were inspected for damage using dye penetrant techniques. Cracks emanating from the corners of the Müller prosthesis were macroscopically visible (see Figures 4.46), however macroscopically no damage was visible around the Lubinus prostheses (see Figure 4.47).

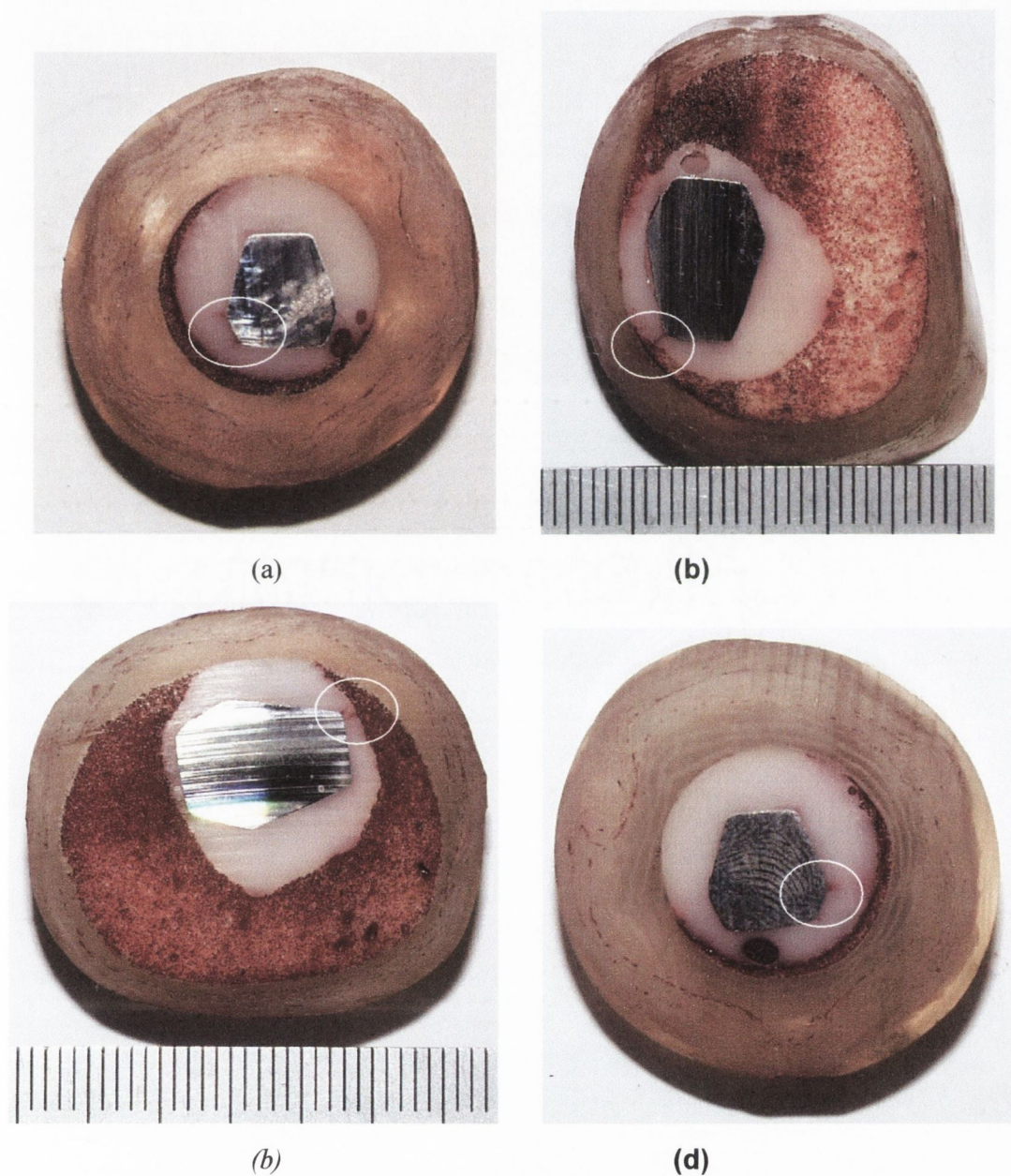


Figure 4.46: Four sections of the Müller prosthesis where cracks were evident. The cracks are highlighted with dye penetrant which colours them red, and for clarity areas where cracks were seen are circled.

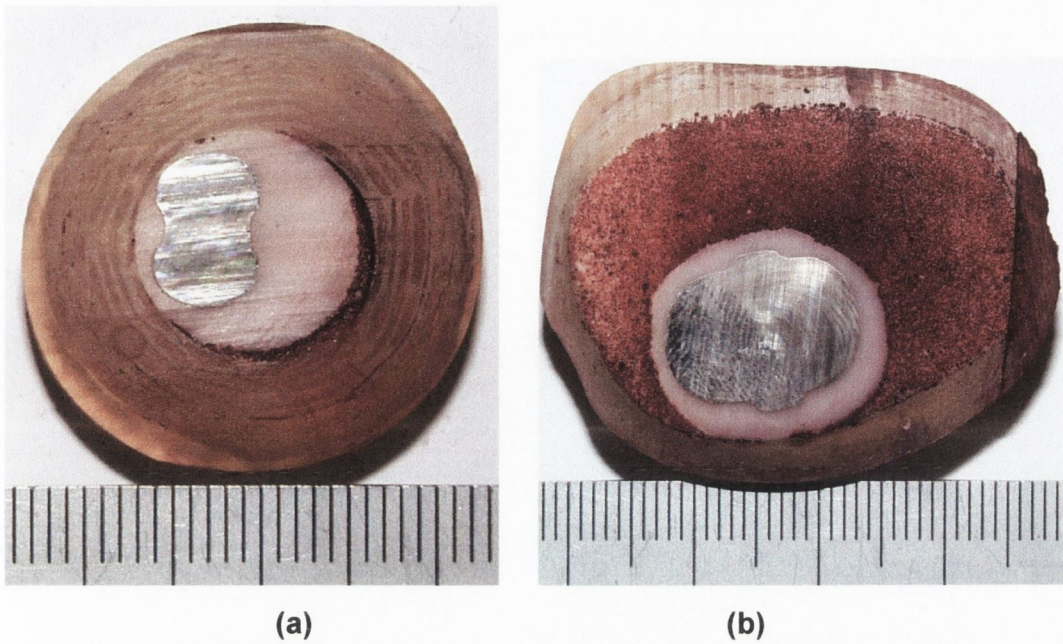


Figure 4.47: Two sections taken through Lubinus prostheses. No cracks in the cement mantle were evident.

Push out tests were performed on the sliced sections. Students t test revealed that on average, the cement/metal interfacial strength was significantly higher for the Lubinus prostheses than for the Müller, without resorption ($p = 0.09$) and with resorption ($p = 0.08$), see Figure 4.48. However there was no significant difference in the push out strength before and after bone resorption for either prosthesis.

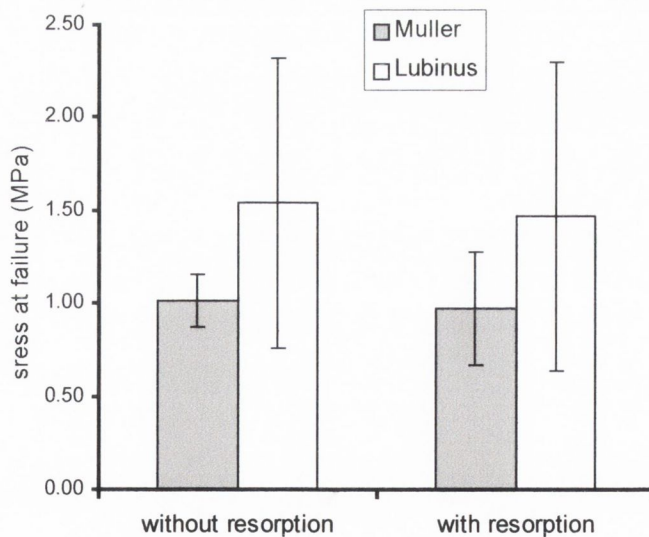


Figure 4.48: The stress at failure during push out tests carried out on two sectioned Lubinus prostheses.

4.6 INDUCIBLE DISPLACEMENT

The inducible displacement (*i.e.* the amplitude of displacement during a loading cycle) in the form of an inducible translation and an inducible rotation for each Müller and Lubinus prosthesis was quantified. An example of the inducible rotation of a Müller prosthesis as a function of number of cycles is illustrated in Figure 4.49.

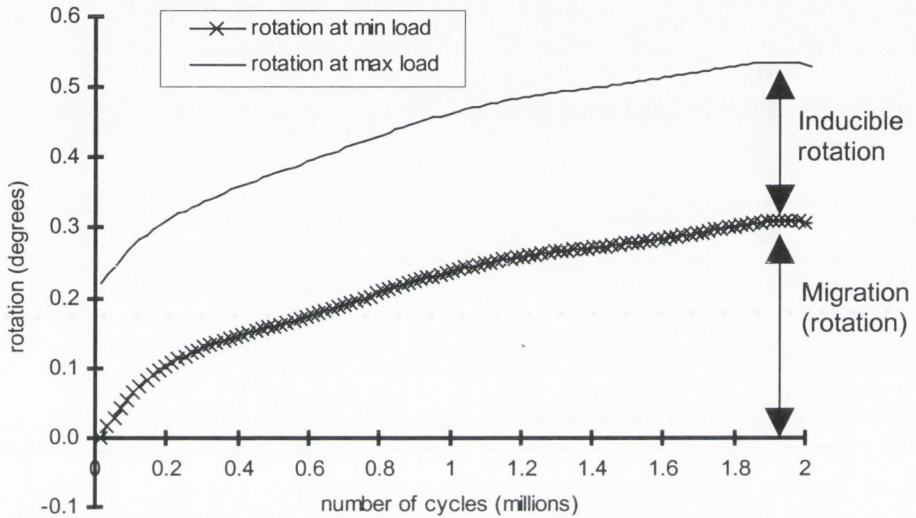


Figure 4.49: The migration and inducible rotation in θ_z of Müller 2 throughout its loading history is illustrated.

4.6.1 Comparison between the average inducible displacement of the Müller prostheses and the Lubinus prostheses

Applying a one tailed Student's t test, the average inducible rotation of the Müller prosthesis was found to be significantly larger than that of the Lubinus prosthesis about the x and z axes, at a significance level of $p = 0.02$ and $p = 0.04$ (see Figure 4.50). The inducible translation of the point of contact between the subsidence device and the prosthesis was found to be significantly greater in the y' and z' directions at a significant level of $p = 0.04$ and $p = 0.03$ respectively (see Figure 4.51)

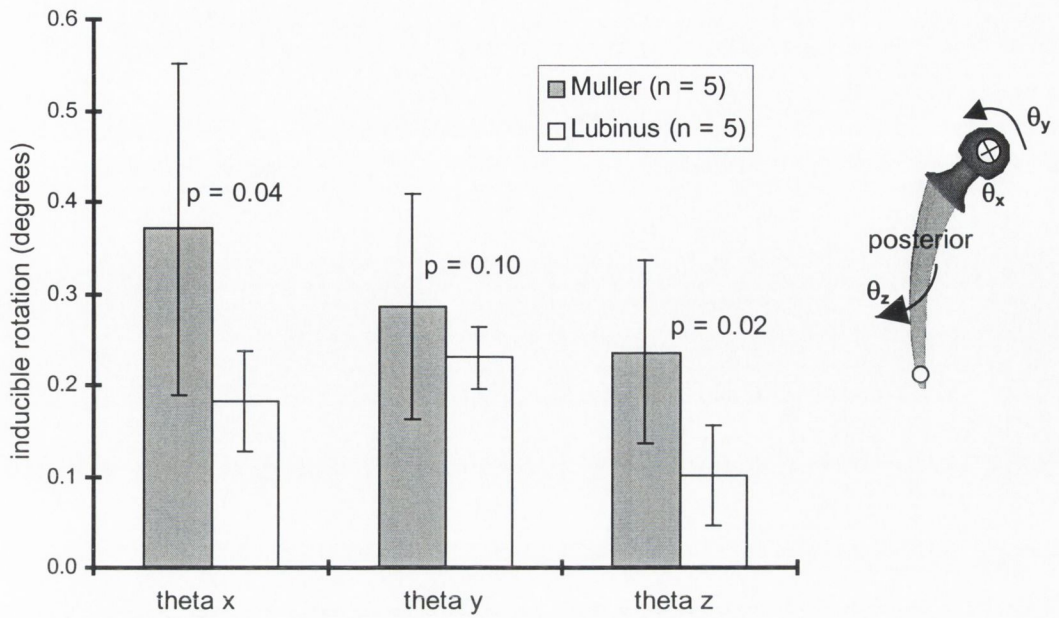


Figure 4.50: The average inducible rotation of the Müller and the Lubinus prostheses about the x, y and z axes.

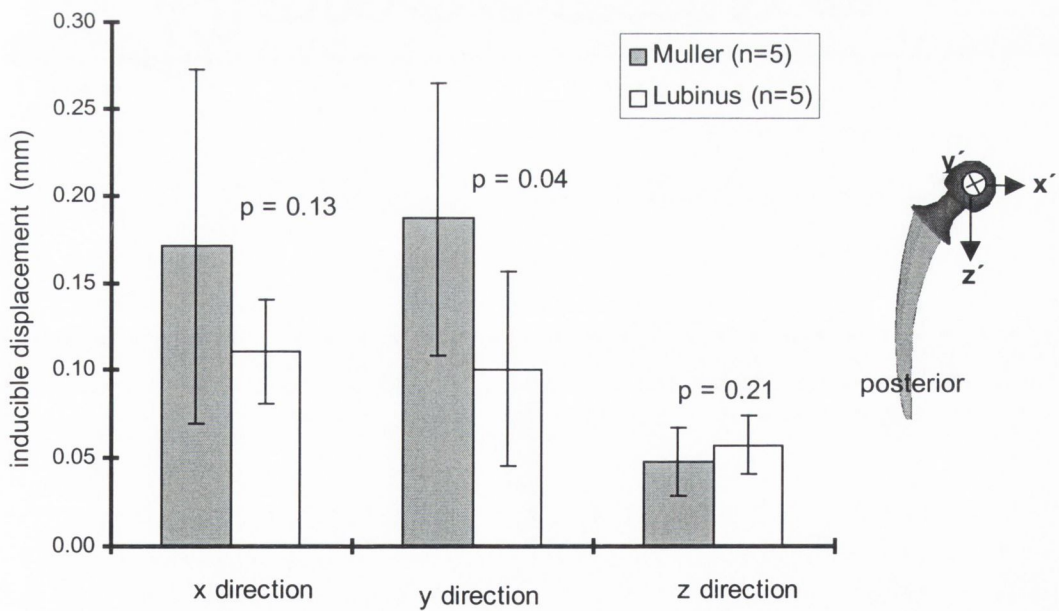


Figure 4.51: The average inducible displacement of the point of contact between the migration measurement device and the prosthesis for the Müller and Lubinus prostheses along the x', y' and z' axes

The change in displacement throughout loading was investigated using the Pearson's correlation coefficient. A positive coefficient, with a value close to 1 indicated an increasing inducible displacement with increasing number of cycles. A negative correlation coefficient close to -1 indicated a decreasing inducible displacement with increasing number of cycles. The Pearson's correlation coefficient revealed that all Lubinus prostheses, without resorption, bar one, exhibited a reduction in inducible displacement as testing progressed, whereas the opposite was the case for the Müller prostheses, see Table 4.9. The Lubinus stems for which resorption was simulated showed a positive correlation between increasing amplitude and number of loading cycles, in general; whereas the effect of resorption on the inducible displacement of the Müller prostheses was variable.

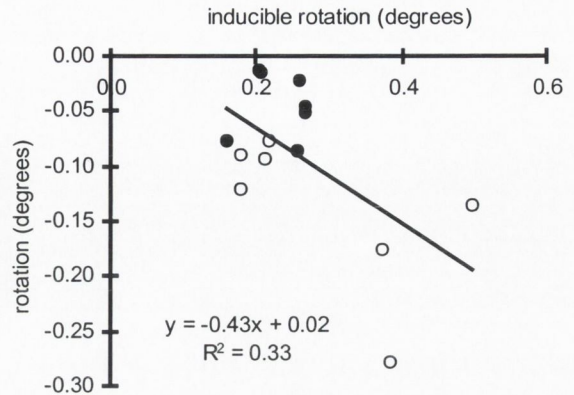
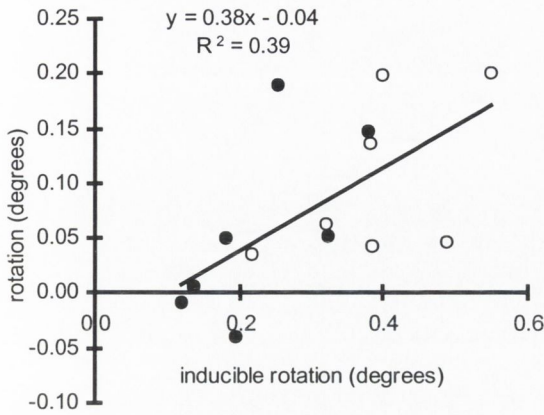
Table 4.9: The Pearson's correlation coefficient for the variation in inducible rotation and translation for each prosthesis throughout its loading history. The samples with a correlation coefficient greater than 0.9 are highlighted.

	θ_x	θ_y	θ_z	u	v	w
Lubinus 1	0.793	-0.934	-0.876	-0.920	-0.892	-0.234
Lubinus 2	-0.171	0.018	0.663	0.661	0.552	0.472
Lubinus 3	-0.167	-0.649	-0.405	-0.789	-0.043	-0.326
Lubinus 4	0.132	-0.403	-0.464	-0.750	0.243	-0.224
Lubinus 5	-0.692	-0.465	-0.618	-0.353	-0.671	-0.749
Lubinus 2 with resorption	0.861	0.807	0.818	0.740	0.768	-0.260
Lubinus 3 with resorption	-0.095	0.621	0.568	0.650	0.810	-0.901
Müller 1	0.486	0.724	0.710	0.748	0.507	0.320
Müller 2	0.645	0.813	0.713	0.914	0.081	0.661
Müller 3	0.953	0.955	0.970	0.955	0.933	0.905
Müller 4	-0.614	-0.606	-0.493	-0.472	-0.531	0.769
Müller 5	0.912	0.946	0.967	0.999	0.913	-0.938
Müller 1 with resorption	-0.897	0.890	0.225	-0.280	-0.895	-0.830
Müller 3 with resorption	0.575	0.679	0.652	0.624	0.740	0.340

4.6.2 Correlation between the inducible displacement at different stages throughout the loading history and the migration at 2 million cycles

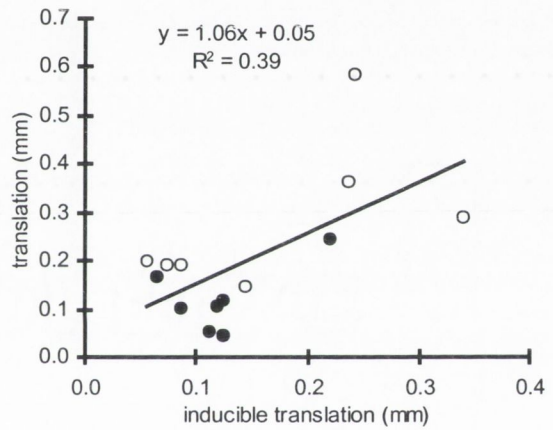
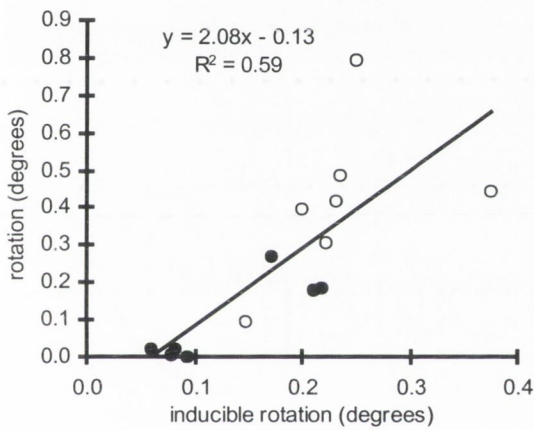
To determine if there was any relationship between inducible displacement and migration, the inducible displacement at different times during testing was plotted against total migration at 2 million loading cycles. The inducible displacements were computed at 0.02 million cycles (Figure 4.52), 0.2 million cycles (Figure 4.53), 1 million cycles (Figure 4.54) and averaged over the 2 million loading cycles (Figure 4.55). Despite considerable scatter, there was a general trend whereby stems with higher inducible translations in any direction (either in rotation or translation) tended to produce larger migrations after 2 million cycles, in that particular direction. The inducible displacement and the final migration of the

Müller prostheses (illustrated by the circles filled in white) tended to be higher than that of the Lubinus prostheses (illustrated as filled circles).



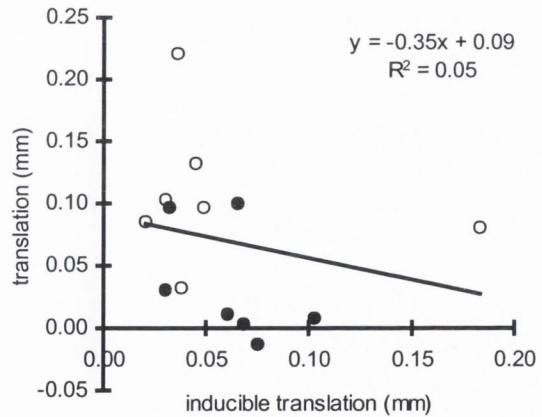
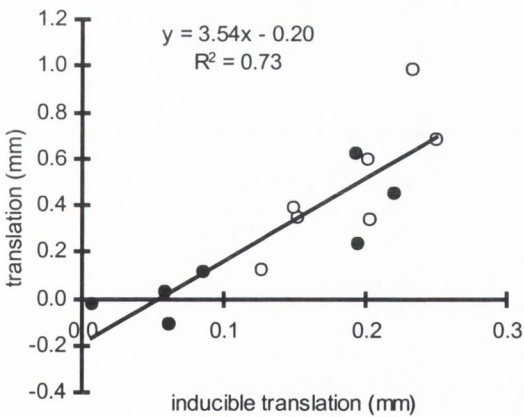
(a): rotation about θ_x

(b): rotation about θ_y



(c): rotation about θ_z

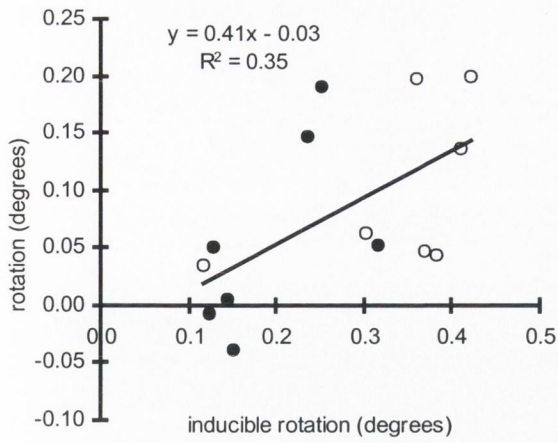
(d): translation in x' direction



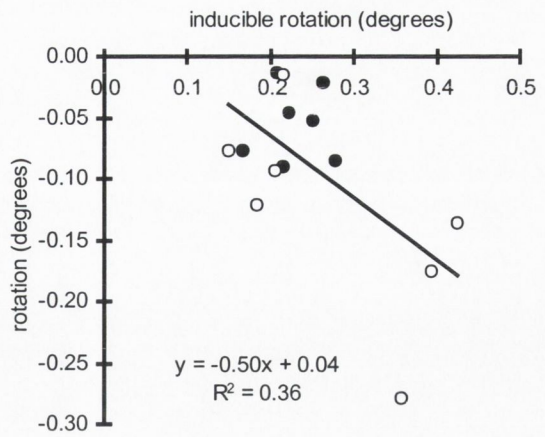
(e): translation in y' direction

(f): translation in z' direction

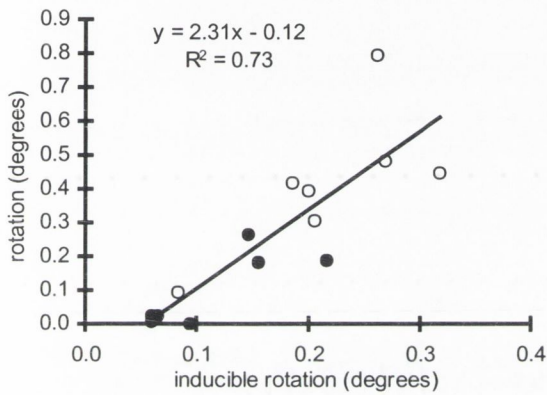
Figure 4.52: The inducible displacement at 0.02 million cycles versus migration at 2 million cycles. Note: circles filled in white = Müller prostheses, blackened circles = Lubinus prostheses.



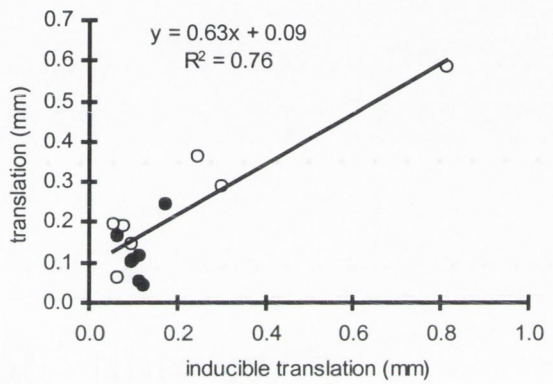
(a): rotation about θ_x



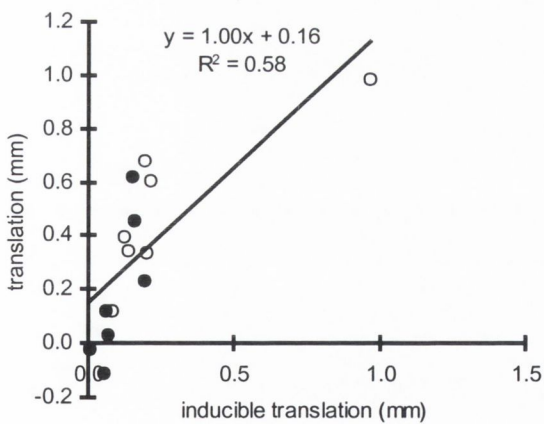
(b): rotation about θ_y



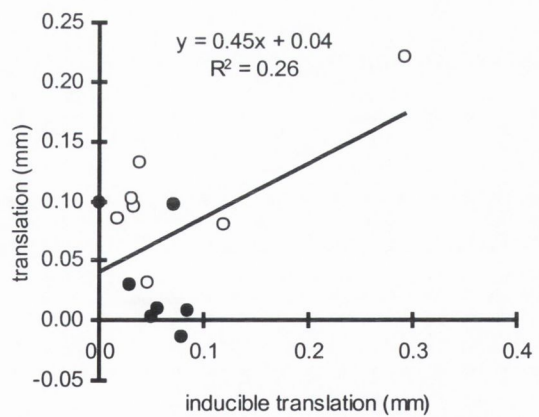
(c): rotation about θ_z



(d): translation in x' direction

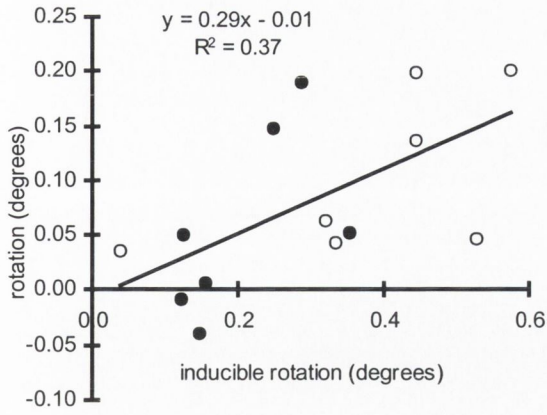


(e): translation in y' direction

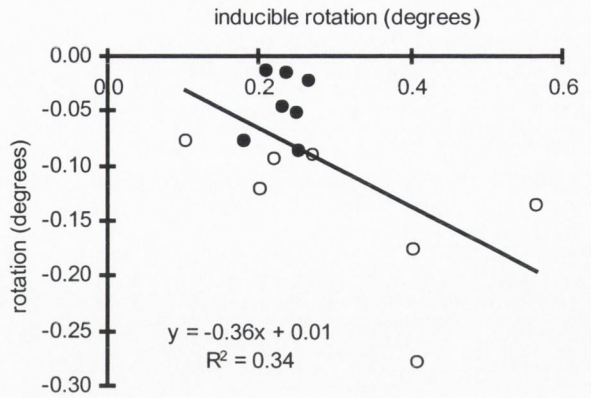


(f): translation in z' direction

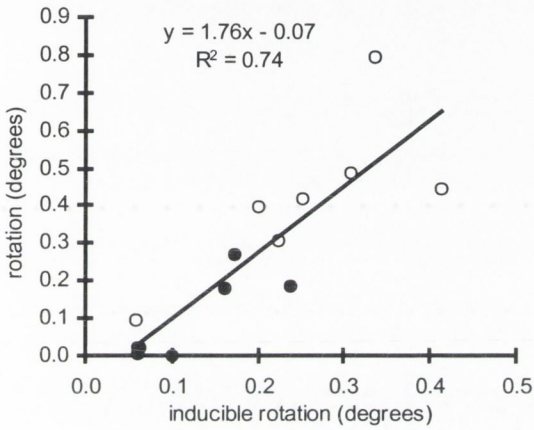
Figure 4.53: The inducible displacement at 0.2 million cycles versus migration at 2 million cycles. Note: circles filled in white = Müller prostheses, blackened circles = Lubinus prostheses.



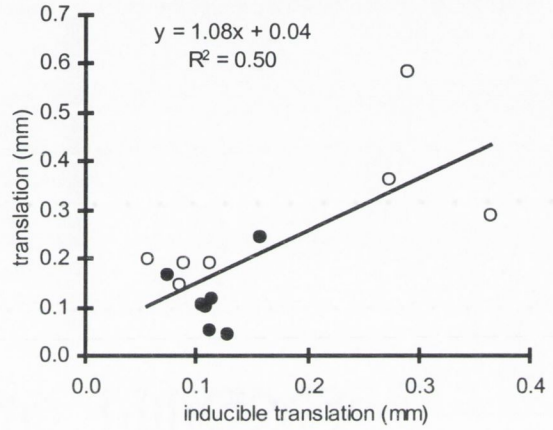
(a): rotation about θ_x



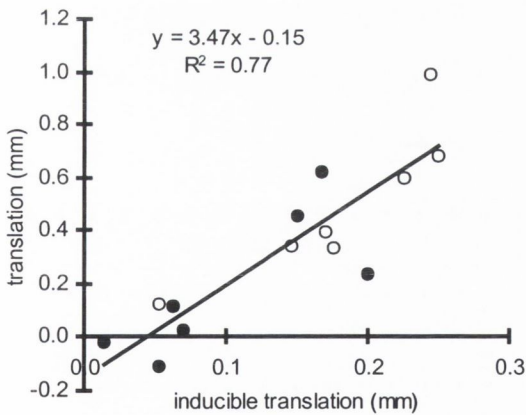
(b): rotation about θ_y



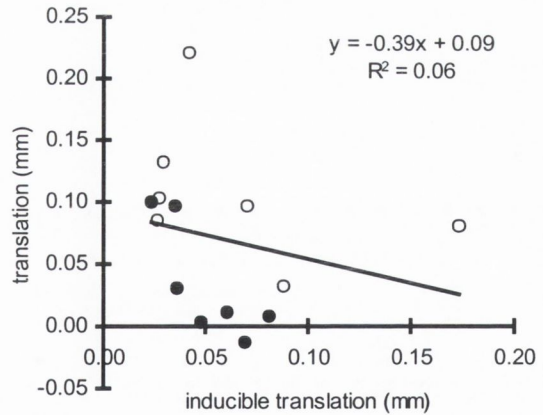
(c): rotation about θ_z



(d): translation in x' direction

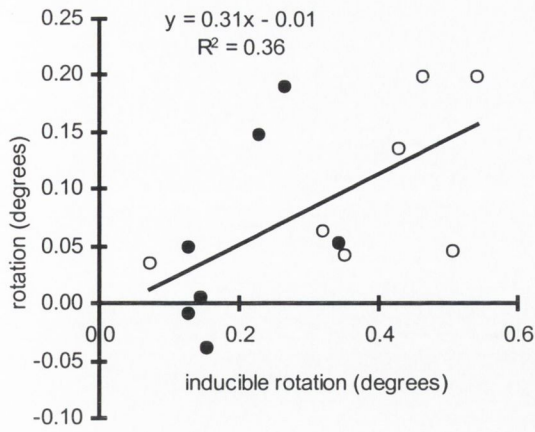


(e): translation in y' direction

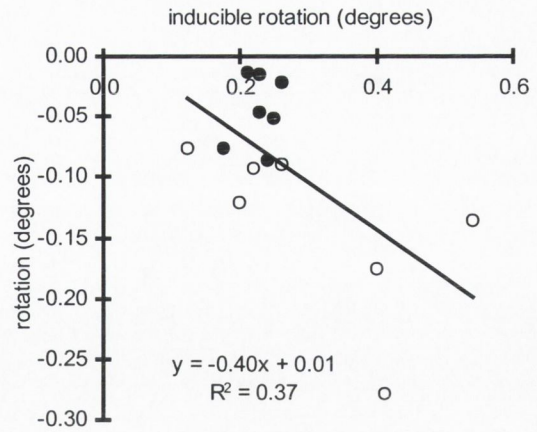


(f): translation in z' direction

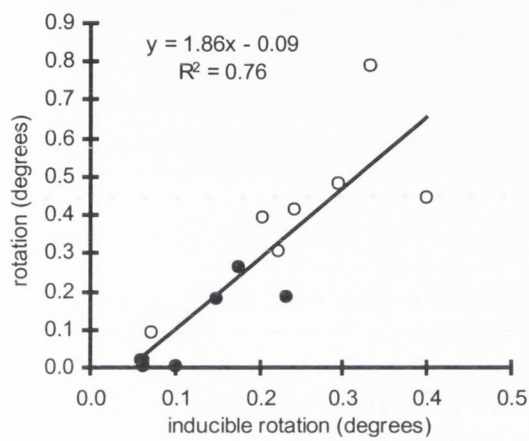
Figure 4.54: The inducible displacement at 1 million cycles versus migration at 2 million cycles. Note: circles filled in white = Müller prostheses, blackened circles = Lubinus prostheses.



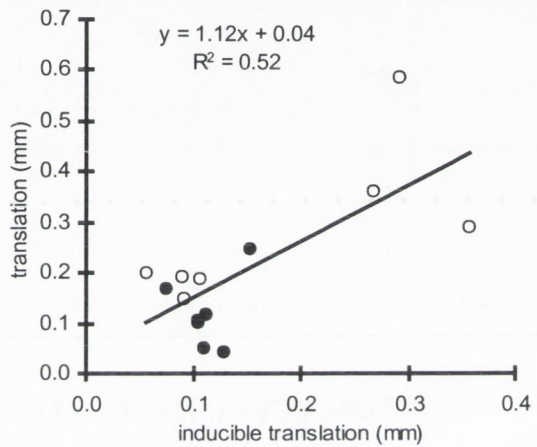
(a): rotation about θ_x



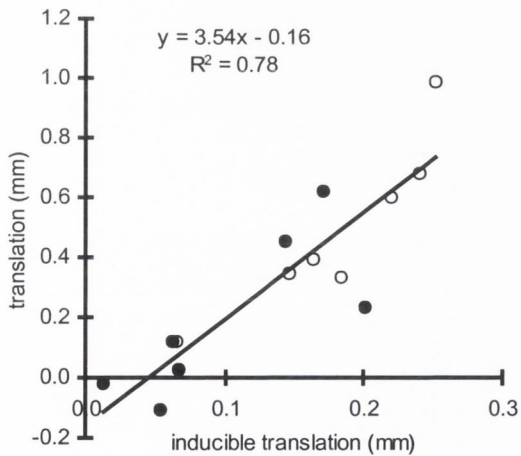
(b): rotation about θ_y



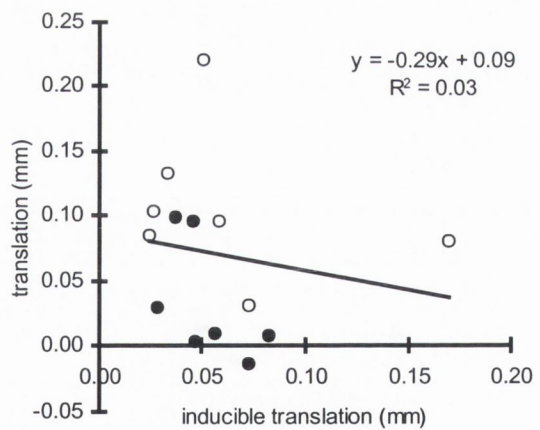
(c): rotation about θ_z



(d): translation in x' direction



(e): translation in y' direction



(f): translation in z' direction

Figure 4.55: The average inducible over 2 million cycles versus migration at 2 million cycles. Note: circles filled in white = Müller prostheses, blackened circles = Lubinus prostheses.

4.7 THE 'COOLDOWN' AFFECT

For, on average, ten hours after completion of testing, the output voltages from the LVDTs were recorded. On average 12%, 11% and 15% of the total migration measured over two million loading cycles was recovered in the x' , y' and z' directions (see Table 4.10). 21%, 41% and 57% of the total rotations measured about the x , y and z axes respectively, were recovered. In general, a higher percentage of the rotational migrations measured for the Lubinus prostheses are recovered upon the removal of load, compared to that recovered by the Müller prostheses.

Table 4.10: The Percentage of total migration (translation of the head centre in the x' , y' and z' directions and rotation of the prosthesis about the x , y and z axes) that is recovered up to ten hours after the removal of load. Note: - indicates that the measured translation was within the error of the system.

	x'	y'	z'	θ_x	θ_y	θ_z
Müller 2	10	11	20	15	7	6
Müller 3	11	10	10	16	10	5
Lubinus 3	11	20	-	42	10	22
Lubinus 5	14	2	-	11	14	24

5: Discussion

5.1	INTRODUCTION	121
5.2	SHAPE OF THE MIGRATION CURVES	121
5.2.1	Damage accumulation and crack growth	121
5.2.2.1	<i>Micro-damage accumulation in the bulk mantle and along the interfaces</i>	122
5.2.2.2	<i>Macroscopic crack growth in the cement mantle</i>	123
5.2.2.3	<i>Interfacial debonding</i>	124
5.2.2.4	<i>Summary</i>	125
5.2.2	Creep	125
5.2.3	Damage and Creep Interaction	126
5.2.4	Proposal for Failure Mechanism	129
5.3	LIMITATIONS	130
5.4	CLINICAL SIGNIFICANCE OF RESULTS	132
5.4.1	Clinical significance of migrations	132
5.4.2	Migration as a measure of failure	135
5.4.3	Failure mechanisms	136
5.5	EFFECT OF BONE RESORPTION SIMULATION	137
5.5.1	Shapes of the migration curves	137
5.5.2	Steady-state creep rate and total migration	138
5.5.3	Cement/metal interfacial strength	138
5.6	DESIGNING A PRE-CLINICAL TEST: ESSENTIAL FEATURES	139
5.6.1	Number of loading cycles	139
5.6.2	Inducible Displacement	139

5.1 INTRODUCTION

In the opening chapter of this thesis, it was argued that pre-clinical tests should be developed as an integral part of the implant innovation process. Current testing methods do not allow for prostheses to be differentiated on the basis of known failure modes — as a result the potential performance of new implants cannot be tested relative to implants in clinical use. In this thesis, a testing protocol to address this need has been designed, and it has been applied to two hip prosthesis designs that are known to loosen at different rates when implanted using similar cementing techniques, *viz.* the Müller and the Lubinus prostheses.

The results of the tests allow differentiation of prosthesis performance on the basis of absolute migrations, steady-state migration rates, and inducible displacements. The minimum number of loading cycles required before differences in implant performances can be established is suggested. The migration profiles give an indication of the mechanism of failure of cemented hip prostheses, in particular with regard to the interaction of creep and fatigue.

5.2 SHAPE OF THE MIGRATION CURVES

The time-course of prostheses migration has never before been reported in laboratory tests. The salient characteristics of the migration curves are that they are non-linear, with significant variability between specimens. Rapid movement of the prosthesis relative to the bone occurs over the first 0.2 million cycles, and a steady-state migration pattern sets in thereafter. In the following section, the implications of this result for our understanding of the failure mechanisms of cemented hip replacement will be discussed.

5.2.2 Damage accumulation and crack growth

Clinically, both micro-damage (cracks of the order of microns) and macro-damage (cracks of the order of millimeters) have been found in autopsy-retrieved femora (Jasty et al., 1991). Can damage accumulation in cemented reconstructions explain the observed migration behaviour? To answer this question we need to look closer at the fundamental mechanism of damage accumulation.

5.2.2.1 Micro-damage accumulation in the bulk mantle and along the interfaces

In uniaxial tensile fatigue tests of bone cement, microcracks were found to accumulate non-linearly throughout testing, depending on the stress applied (Murphy and Prendergast, 1999; see Figure 5.1).

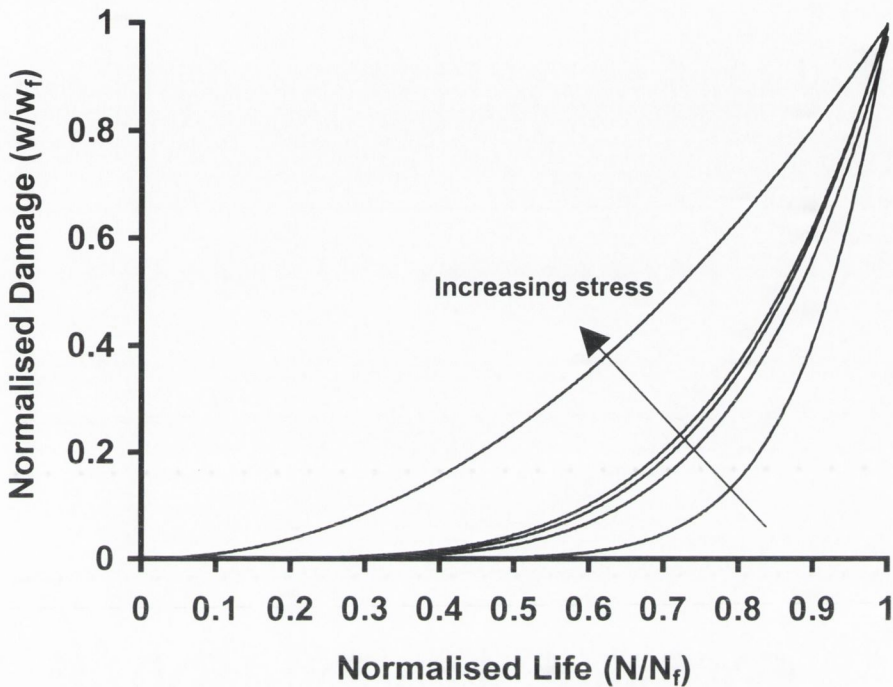


Figure 5.1: The non-linear damage accumulation in 5 bone cement samples (Murphy and Prendergast, 1999). As the stress increases, the non-linearity of damage accumulation decreases.

Micro-damage can also be expected to occur along the interfaces between the cement and the prosthesis and bone. In flexion, McCormack and Prendergast (1999) found damage to originate from the pores within the bulk cement, whereas in torsion McCormack et al. (1999) found damage to emanate mainly from the prosthesis/cement interface. This suggests that under combined flexion/torsion, damage along interfaces may accumulate. However, if it is assumed that cement and interfacial micro-damage are responsible for prosthesis migration, migration should follow a path similar to that of Figure 5.1 — *i.e.* a slow rate of migration at the beginning of testing, followed by an increasing migration rates leading to eventual rapid migration at failure. However the migration patterns of the prostheses tested were the opposite of this. Therefore, no direct link between the accumulation of micro-damage and prosthesis migration can be proposed.

5.2.2.2 Macroscopic crack growth in the cement mantle

Macroscopic cracks were not seen in the cement mantle of the Lubinus prostheses (see Figure 4.47). Macroscopic cracks were found in the sectioned Müller implants in the form of occasional radial cracks through the cement mantles. If crack growth were to affect migration, the Müller prosthesis should migrate more than the Lubinus — and indeed this was found in the experimental tests. Is it possible that the presence of a few cracks could influence migration rates? Consider the schematic of a cemented Müller stem illustrated in Figure 5.2.

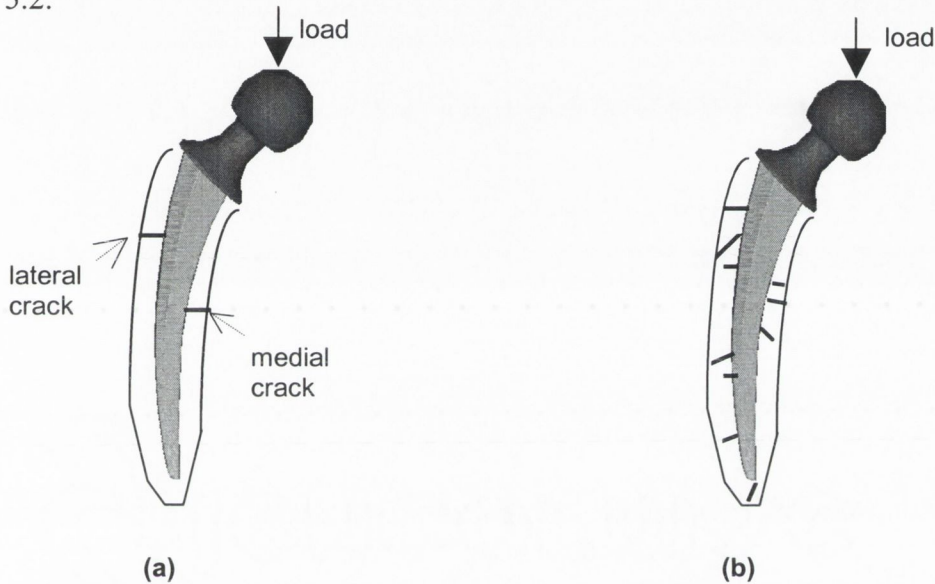


Figure 5.2: The cement mantle for a Müller prosthesis at various stages along the path to failure. (a) Only two cracks are present in the mantle. The rest of the mantle is intact: prosthesis migration will not be much affected. (b) The cement mantle is fractured at numerous locations. Migration is more likely.

The load direction is such that varus rotation (*i.e.* clockwise rotation when looking from this view) of the prosthesis may be expected. In Figure 5.2(a), a through-cement crack on the medial and lateral side are illustrated. If the remaining cement mantle is intact, upon loading it will hold the prosthesis in its position, and prevent any tendency for it to migrate further into varus. For migration to be *allowed* by the mantle, more crack than just occasional cracks must exist. In the scenario illustrated in Figure 5.2(b), a significant number of cracks have accumulated. The cement mantle is less stable, and more prone to allowing prosthesis migration. Since the damage quantified in the sectioned samples was not deemed as extreme as that illustrated in Figure 5.2 (b), it seems that crack growth cannot explain the migration behaviour found over the testing period. It is more likely that

an accumulation of through mantle macroscopic cracks will contribute to implant instability during the later stages of testing, beyond the range tested in this study. In further support of this conclusion, Maloney et al. (1989) found cement cracks in the mantles of radiographically stable (as measured by migrations) and mechanically stable autopsy-retrieved implants.

5.2.2.3 Interfacial debonding

It is conceivable that the migrations measured resulted from debonding of the cement/bone interfaces, or from failure of the cancellous/cortical interfaces. The interfaces of the sectioned femora were difficult to inspect with dye penetrant, due to the porous nature of the cancellous bone. However, in both preliminary tests (see section 3.4.1) and in the samples from which the migration histories were measured, the proximal cancellous/cortical interface appeared intact, although some gaps along the interface were evident distally. In an RSA study, Huiskes et al. (1998) found that after 344,000 cycles very little migration occurred between the cement and cancellous replica of the synthetic femora. Similarly, in this study, the cement/cancellous bone junction appeared to be intact. Because both the cement/cancellous bone and the cancellous/cortical bone interfaces appeared intact, this indicates that neither cement/bone nor cancellous bone/cortical bone separation significantly influenced the migration patterns measured.

For prosthesis/cement debonding to occur, the cement/metal interfacial strengths must be exceeded and the bond broken. Debonding may be manifested by longitudinal cracks along the cement/metal interface of the kind seen for both prostheses in appendix F (see pages 207 and 208), or by fracture of cement at the distal tip. The push out strength of the cement/metal interfaces measured in this study (ranging from 0.6 to 2.7 MPa, see Figure 4.52) were lower than that quoted in literature for bonded interfaces (ranging from 3 MPa to 12 MPa, Stone et al., 1989), suggesting that the metal/cement interfaces were debonded. To investigate exactly when debonding took place, samples would need to be sectioned at various stages throughout the loading history and push out tests performed. Since this could not be done, it is difficult to estimate the time of debonding. However, breakdown of the interface would allow the prosthesis to slip relative to the cement and to stabilise in a new migrated position. This might manifest itself as a rapid migration of the kind measured in the first 0.2 million loading cycles in this study. It is suggested that prosthesis debonding most likely occurred during the initial stages of cyclic loading.

5.2.2.4 Summary

Although crack growth and damage accumulation occurred during the cyclic tests, they cannot explain the observed migration behaviour. Initial rapid migration could in part be explained by prosthesis/cement debonding. However, some other failure mechanism must influence the migration paths.

5.2.3 Creep

The prosthesis migration histories have a similar profile to a bone cement creep curve, of the kind recorded by Chwirut (1984) for the compressive loading of various commercial bone cements, see Figure 5.3. The cement tested in the current study (Cemex Low Viscosity) was closest to cement type B (Zimmer Low Viscosity). Figure 5.3 suggests that the cement should still be in its primary phase of creep after approximately 100 hours of static loading (note: 100 hours is the equivalent of 1.8 million cycles).

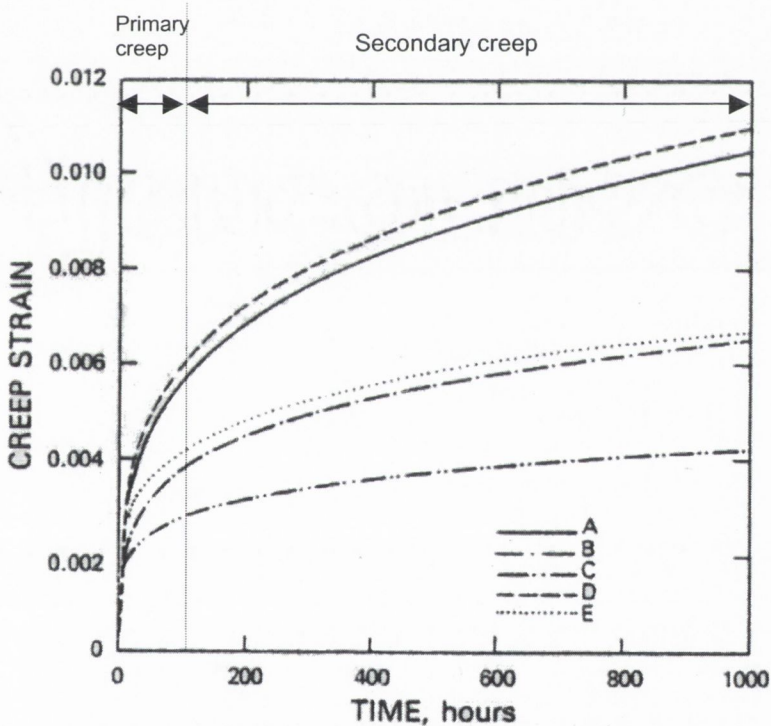


Figure 5.3: A cement creep curve for static compressive stress of 12.1 MPa tested at 37°C, from Chwirut (1984). Note: A - E indicate the different cements that were tested. The division between the primary and secondary phases of creep for cement B, which is closest to the cement used in the current study, is shown.

In the current experimental tests, migration of the prosthesis over the first 0.2 to 0.3 million loading cycles was rapid (see in particular the Lubinus migration curves in Appendix D, page 181): this correlates with the primary phase of creep. Two million cycles corresponds to approximately 11 hours of testing, whereas the duration of primary creep for a similar cement is estimated as 100 hours by Chwirut (1984). Differences occur because Chwirut (1984) tested at 37°C in saline solution, whereas the current tests were carried out in air at room temperature. Also, the creep curves generated by Chwirut were static, but the current tests were subjected to a cyclic load.

From 0.2 - 2 million cycles, in the current study, deformation occurred at a slower, constant rate: this correlates with secondary creep. The rate of migration at 1 million loading cycles may be taken as the steady-state creep rate (see Figures 4.20 to 4.25). A tertiary creep phase consisting of rapid elongation leading to rupture, was not seen in the migration curves.

5.2.3 Damage and Creep Interaction

Verdonschot and Huiskes (1994), recorded what they termed a *dynamic creep* curve during the fatigue of bone cement samples comprising of a primary, secondary and tertiary phase of creep, see Figure 5.4.

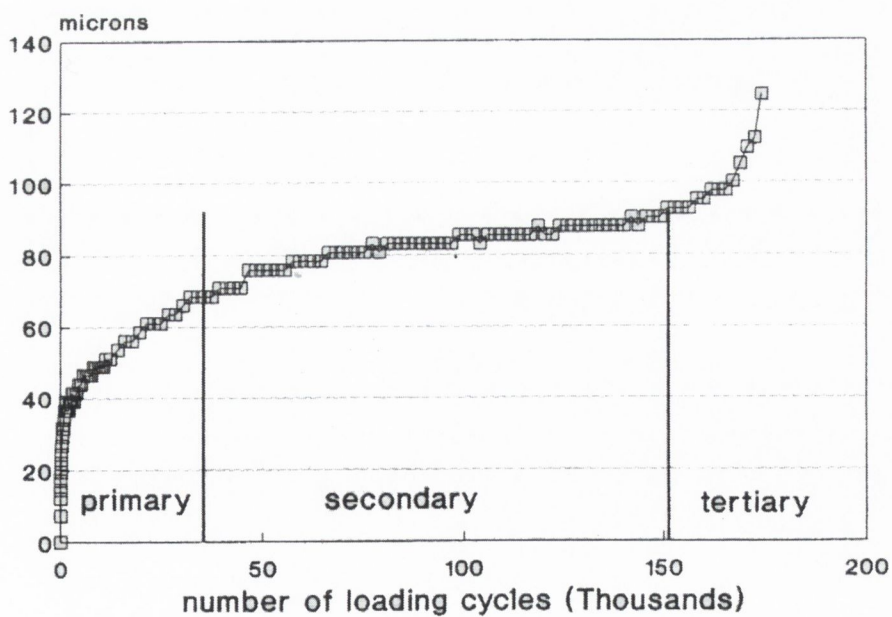


Figure 5.4: A typical dynamic creep curve for bone cement, from Verdonschot and Huiskes (1994).

The *creep curve* is in fact the result of combined damage *and* creep because the sample is subjected to cyclic loading (Murphy and Prendergast, 1999). The strong similarities between Figure 5.3, Figure 5.4, and the migrations observed in the experimental tests, suggest that PMMA creep and not damage accumulation is the major phenomenon contributing to the migrations measured in the tests.

A simple calculation may serve to compute the migrations that may be expected from creep of the bone cement. The maximum cement stresses generated by different stem profiles in the proximal 10 mm of a cement mantle were computed in a 3D finite element model by Crownshield et al. (1980). The model interfaces were assumed to be fully bonded and stress distributions were not presented. Nonetheless, it is the only analytical study in literature where comparisons are made between the stresses generated around stem profiles of the kind tested in this research. The maximum compressive stresses generated by a Müller and Lubinus type profile were 6.7 MPa and 5.1 MPa respectively (see Figure 2.1(a)). These stresses are comparable to that estimated around a debonded polished stem by Verdonschot and Huiskes (1997) using finite element techniques. Applying equation (5.1) from Verdonschot and Huiskes (1995):

$$\varepsilon_c = CN^{b_0} 10^{S\sigma} \quad (5.1)$$

where ε_c denotes the strain in compression, $C = 1.255 \times 10^{-5}$, $b_0 = 0.314$, $S = 0.033$, σ denotes the stress amplitude, N denotes the number of cycles, dynamic creep strain at 2 million loading cycles was computed as:

$$\varepsilon_c = 1.225 \times 10^{-5} (2 \times 10^6)^{0.314} 10^{(0.033 \times 6.7)} = 1987 \mu\varepsilon \text{ for the Müller prosthesis and,}$$

$$\varepsilon_c = 1.225 \times 10^{-5} (2 \times 10^6)^{0.314} 10^{(0.033 \times 5.1)} = 1714 \mu\varepsilon \text{ for the Lubinus prosthesis.}$$

Maximum tensile stresses generated in the cement mantle were lower at 1.4 MPa for both prosthesis designs, and applying equation (5.2), from Verdonschot and Huiskes, 1994

$$\varepsilon_T = CN^b \sigma^{S_s} N^{S_n \text{Log} \sigma} \quad (5.2)$$

where ε_T is the strain in tension, $C = 7.985 \times 10^{-7}$, $b = 0.4113$, $S_s = 1.9063$, $S_n = -0.116$, $\sigma =$ stress amplitude, and $N =$ the number of cycles, a dynamic creep strain of

$$\varepsilon_T = (7.985 \times 10^{-7}) (2 \times 10^6)^{0.4113} 1.4^{1.9063} (2 \times 10^6)^{-0.116(\text{Log}(1.4))} = 463 \mu\varepsilon \text{ was computed.}$$

Consider a transverse slice through a cemented Müller prosthesis, with a 2 mm thick cement mantle medially (see Figure 5.5).

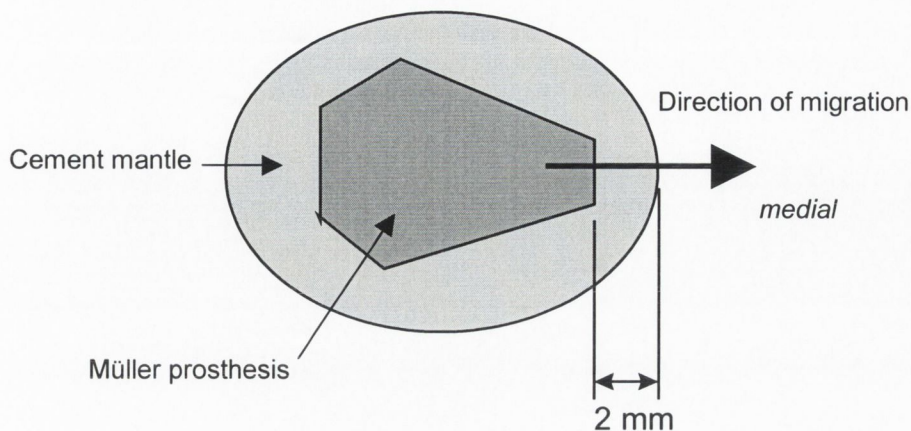


Figure 5.5: Schematic of a transverse slice through a Müller prosthesis.

Migration in the direction shown can be evaluated by substituting the computed compressive creep strain, $\epsilon = 1900 \mu\epsilon$, and the original length of bone cement $L = 2 \text{ mm}$ into equation (5.3)

$$\epsilon = \frac{\Delta L}{L} \tag{5.3}$$

$$\Delta L = \epsilon L : 1987 \mu\text{m} \times 2 \text{ mm} = 3.97 \text{ microns}$$

From this simple calculation, a small medial migration of 4 microns results. Head centre migrations computed in this study were due to a combination of translation and rotation of the prostheses, so that direct comparisons cannot be made. However, medial translations of the migration measurement device at the point of contact with the prosthesis ranged from a minimum of 15 microns (for Lubinus 4) to a maximum of 163 microns for Müller 3. Although the translations measured are somewhat higher than the theoretically estimated migrations of 4 microns, the scatter in the experimental results are too wide to allow this method to fully confirm that migrations are a result of creep.

Using equation (5.1), a creep rate can be analytically computed at 1 million cycles. Assuming again that a compressive stress of 6.7 MPa acts medially, the dynamic creep strain (ϵ_C) at 1 million cycles is computed as 0.101×10^{-5} microns/cycle. If the migrations are caused by cement creep, the creep rate should equate with the migration rate. Steady-state medial migration rates ranged from 0.045×10^{-5} microns/cycle to 0.368×10^{-5}

microns/cycle for the Müller prosthesis and from 0.0043×10^{-5} microns/cycle to 0.197×10^{-5} microns/cycle for the Lubinus prosthesis. There are three possible reasons for these differences:

- (i) The creep strain equations were generated from fatigue tests performed in water at 37 °C at a frequency of 1Hz (Verdonschot and Huiskes, 1997), whereas experimental migration rates were measured at room temperature in air.
- (ii) The stresses quantified by Crowninshield et al. (1980) could underestimate of the stresses generated in the current experimental test set-up.

In summary, creep cannot fully explain the migrations and a more thorough stress analysis of the stresses around the cement mantle is necessary to fully quantify expected migrations due to creep¹.

5.2.4 Proposal for Failure Mechanism

Following from the analysis of damage accumulation (section 5.2.3 above) and the analysis of creep (section 5.2.4 above), it is proposed that prosthesis migration measured in an *in vitro* test can be explained in the following way, with three distinct stages:

- (i) A primary stage, which extends approximately over the first 0.2 million loading cycles. The prosthesis debonds from the cement, the cement stresses increase (as shown in FEA studies by Lennon et al. (2000b) and others), prosthesis migration is rapid and controlled by creep of the bone cement, (stage A, see Figure 5.6).
- (ii) A secondary stage, where the prosthesis debonding is complete and the stress in the mantle becomes stable. The prosthesis begins to migrate at a constant rate. The cement creeps at a steady-state rate, damage has initiated and is accumulating, but it is not sufficiently high to contribute to prosthesis migration, (stage B, see Figure 5.6).

¹ A three dimensional finite element model is being developed by J. Stolk, Katholieke Universiteit Nijmegen, The Netherlands, to investigate the damage/creep interaction in cyclic loading tests.

- (iii) A tertiary stage, defined by an accumulation of cracks. Mechanical integrity is lost and gross loosening of the prosthesis occurs (stage C, see Figure 5.6). None of the samples tested in this study entered the tertiary phase of creep.

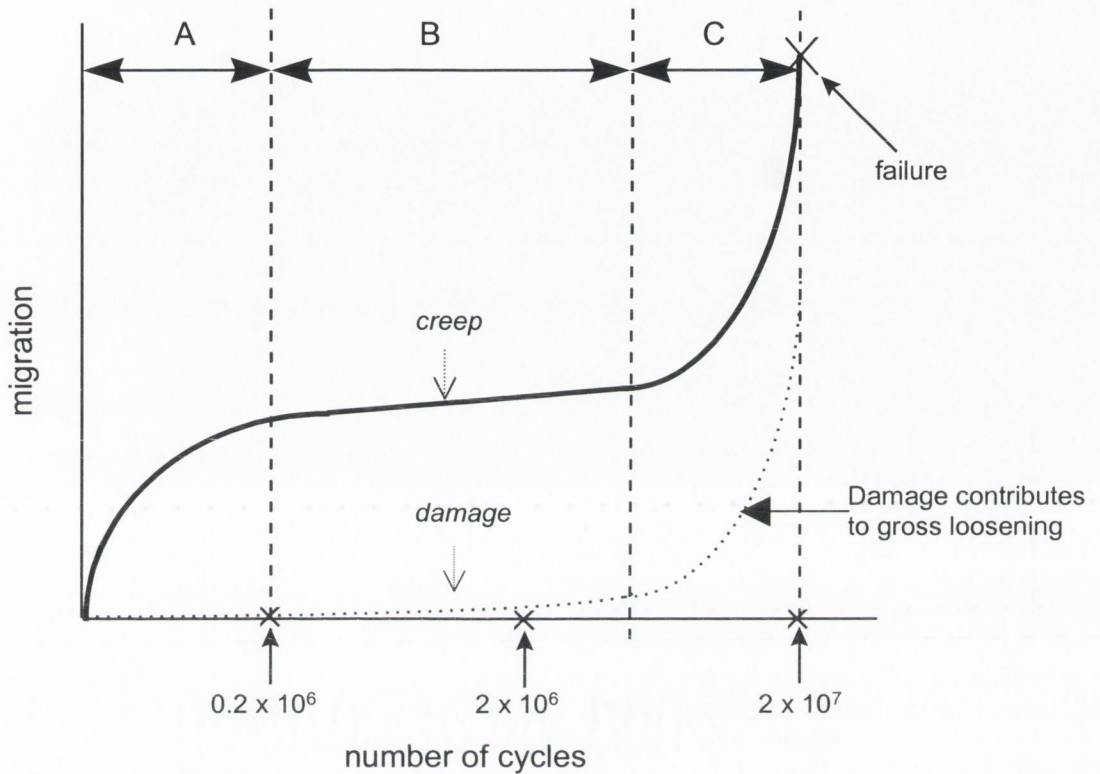


Figure 5.6: Proposal for the failure mechanism of the prostheses tested.

5.3 LIMITATIONS

The absolute migrations quantified in this study were lower than those clinically recorded. This can be attributed to some features of the test.

- (i) Biological Effects: In testing synthetic composite femora, not all biological adaptations of bone can be included.

For example, the initial post-operative migration may be partially caused by tissue damage during polymerisation (Mjoberg 1986) and it was not included in the tests. Cracks found at the cement/metal interface (Figures 4.50 and 4.51) could generate debris which could also initiate a biological response and result in fibrous tissue formation (Jasty et al., 1992). This could accelerate the rate of loosening, and again was not modelled in this test.

- (ii) Specimen preparation protocol: To explore the influence of prosthesis design on migration rates, it was necessary to control other variables that could influence migration.

For example, creep behaviour is sensitive to variations in bone cement polymerisation. Strain rate during primary creep is produced by stretching of polymer molecular chains and secondary creep is caused by polymeric molecules sliding relative to each other. The nature of bone cement preparation is such that inter sample variations in polymer chain orientation, molecular weight, internal stresses and porosity will exist (Verdonschot and Huiskes, 1995), but to minimise the variability in this study, cement was prepared using controlled vacuum mixing and gun injection techniques.

Cementing pressures during prosthesis insertion, cement polymerisation (Stone et al., 1991), and prosthesis orientation (Savino et al., 1982; Kobayashi et al., 1992, Wirta et al., 1993), can influence cement stresses, and hence creep rates. All prosthesis designs have been inserted along controlled paths into repeatable and ideal final seated positions using the Insertion Machine (see section 3.2). In a clinical setting, control of prosthesis positioning is more difficult to achieve. Some prostheses are more *forgiving* to misalignment, whereas the performance of others is reliant on the prosthesis being inserted as close as possible to its intended seated position (McBeath and Foltz, 1979). In using an automated method of insertion, the influence of mal-alignment on migration has not been investigated and the variability due to it has been obviated.

- (iii) Testing Protocol: Simplified loading conditions were applied and testing was done in air at room temperature.

The cyclic loads applied do not include the influence of muscles. Because of the stabilising effect that the muscles would have on the flexural bending of the femur, larger cement stresses may be generated and larger *distal* migrations may result. This may produce migrations that are closer to that achieved clinically. Nonetheless, the migration trends of distal, medial and posterior migration, were consistent with that measured clinically. Because the cemented femora were stored and tested in air and not in fluid media, the cement mantle should act in a more brittle manner than may be expected physiologically (Hailey et al., 1994). It has been found experimentally that specimens stored at 37 °C were more ductile than those stored at 21 °C (Hailey et al., 1994). This has been attributed to an increase in the diffusion and mobility of residual monomer. This suggests that the two

differences (*i.e.* room temperature and saline solution) between the *in vivo* and the *in vitro* storage and testing conditions could offset each other.

(iv) Prostheses tested: Cemented type I implants were tested in this study.

Prior to acceptance of a bench test as a method to differentiate between prosthesis performance, the test should be validated with implants designed with a range of fixation principles that represent — sometimes contrasting — design methodologies. Cemented type II implants were not tested in this study and their behaviour compared to that of the cemented type I implants tested is still the subject of some controversy. For example, it can be expected that type II implants will migrate early, as they are designed to do. In this case, migration may not be associated with early loosening, however parameters such as the prosthesis steady-state migration, or inducible displacement may (see section 5.4 below).

(v) Curve fitting: To prevent small fluctuations in the LVDT voltages from erroneously distorting the migration data, curve fitting techniques were employed to smoothen the data.

The nature of the curve fitting techniques used in this study was such that the polynomial fitted captured the overall shape of the LVDT data based on the voltage measured from 0 - 2 million cycles. Nonetheless, some of the migration curves exhibited fluctuations. For example, there is an end effect associated with measuring the migration at two million cycles (see Lubinus 3, Figure 4.14). The polynomial fitted to the data would best estimate migration at 2 million cycles if testing had continued beyond 2 million cycles. In prostheses where migrations measured were small, fluctuations close to the accuracy of the measurement techniques used (as defined in section 4.1.4.3) are found (see Lubinus 4 in Appendix D, page 185). Larger variations in migration are more likely to be associated with temporary fluctuations in the load applied to the implanted femora by the materials testing machine.

5.4 CLINICAL SIGNIFICANCE OF RESULTS

5.4.1 Comparison with clinical measurements

It is worthwhile to reiterate that the migration measurement device is designed to measure the relative movement of the prosthesis and bone. The relative movement may originate between the cement/metal interface, between the cement/bone interface, or in creep of the bulk cement mantle and they cannot be differentiated. Notably, this is also the case for

many of the RSA studies (Karrholm et al., 1994) and radiographic studies (Walker et al., 1995) on which the concept of measuring migration during an *in vitro* test is based.

Recalling Chapter 2, considerable evidence from both radiological and RSA studies exists to suggest that, for cemented Type I implants, distal migration of over 2 mm at 2 years is a good predictor of loosening. Assuming that 1 million loading cycles is a realistic estimate of the number of walking cycles endured by the hip joint annually (Huiskes and Verdonschot, 1997, Zahari et al., 1998), the femora in this research were cyclically loaded for the equivalent of 2 years. In the experiments, no prosthesis migrated by an amount even approaching the 2 mm threshold. This disparity is a cause for concern; it is due perhaps to the fact that 1 million cycles per year may not be a good estimate of the loading on the hip joint (Bergmann et al., 1999), or due to the simplified nature of the loading, as discussed above. Nonetheless, comparatively, the Müller prosthesis subsided significantly more than the Lubinus prosthesis at $p = 0.05$ level of significance, see Table 4.6. Therefore the objective of comparative analysis (if not quantitative analysis) has been achieved.

The damage found in the sectioned Müller cement mantles at 2 million cycles, indicated that the mantles were closer to the tertiary phase of failure, hence further advanced along the hypothetical failure curve depicted in Figure 5.6. The increased presence of cracks in the cement of the Müller prostheses, combined with the differences in absolute migrations at 2 million cycles, could be expected to further diverge the migrations of the two designs if cyclic loading were to continue beyond 2 million cycles.

In an experimental test, as in clinical reality, two outcomes of an implantation are possible: failure; where the prosthesis will loosen and success; where it will remain stable. Experimentally, it is unlikely that all prosthesis designs tested will fall into a single category. It is more realistic to expect that of the prostheses that perform well clinically, some tested will fail the experimental test, whereas some will pass, and vice versa for prostheses that perform poorly when implanted. For example, Lubinus 1 and Lubinus 2 subside at a much lower level than that experienced by the remaining prostheses, see Figure 4.16. This may indicate that clinically, Lubinus 1 and 2 would remain stable, whilst the other Lubinus prostheses would not. In a study of the migration and loosening patterns of Lubinus prostheses, Karrholm et al. (1994) group the prostheses into those which subsequently failed and those which did not. They found a substantial range of migrations at two years, spanning up to 3.5 mm medially, 2 mm distally and 7 mm posteriorly. In comparing the experimental data to the clinical data (assuming that 1 year = 1 million

cycles), it becomes apparent that the average migrations measured in this study are similar to those prostheses that remained stable, see Table 5.1.

Table 5.1: Comparison of the average migration of the centre of the head of the Lubinus prosthesis computed from the clinical measurements of Karrholm et al., 1994) and experimentally in five cyclic tests of this study.

Direction	Clinical migration - stems not revised (microns)	Clinical migration - stems revised (microns)	Experimental migration (microns)
Medial	131	2500	139
Posterior	1049	4500	223
Distal	80	2000	44

Similarly, for the Müller prostheses tested, in Figure 4.10, Müller 4 appears to have migrated along a path that is quite different to that of Muller 3. Comparison between the experimentally measured migrations of the Müller prostheses and that which occurs clinically is difficult, since no RSA data exists for this stem. However, radiologically, Sutherland et al. (1982) correlated varus drift and distal subsidence of the Müller prostheses with loosening. A combination of varus drift (see Figure 4.12) and distal subsidence (see Figure 4.10) for the Müller prostheses was seen. If it is assumed that all the Lubinus prostheses tested would remain stable, the fact that the Müller prostheses migrated significantly more than the Lubinus prostheses would indicate that the Müller prostheses would be more likely to loosen.

From this analysis it can be concluded that:

- (i) The migration *directions* measured for both the Müller prosthesis and the Lubinus prosthesis are similar to those quantified clinically.
- (ii) The *total* migrations measured are not directly comparable to those quantified clinically.
- (iii) A significant difference in distal migration between a Lubinus and Müller prosthesis has been quantified. This is considered predictive of loosening rates.

5.4.2 Migration as a measure of failure

The fundamental premise of this work is that migration can be used as a predictor of failure. If we accept that the underlying mechanism of steady-state migration is cement creep, a theoretical basis for the connection between migration and failure can be proposed.

The steady-state creep rate has been correlated with time-to-failure for the creep of metals, by the well-known Monkman-Grant relationship (Nabarro and de Villiers, 1995). The Monkman-Grant relationship states that for a given material in a certain range of stress and strain that:

$$\dot{\epsilon}_{\min} t_f = C \quad (5.3)$$

where $\dot{\epsilon}_{\min}$ is the minimum steady-state creep rate, t_f is the time to failure and C is a material dependent constant. In other words, a higher steady-state creep rate will result in a lower time-to-failure, see Figure 5.6 for a graphical illustration of this concept. Following from this idea, the Müller cement mantle will have a shorter time to failure because it had a steady-state creep rate and a total migration that was significantly higher than of Lubinus cement mantle. Early migration is, in effect, a measure of the creep strain endured by the cement mantle; and large strains lead more quickly to a damage accumulation process and loosening.

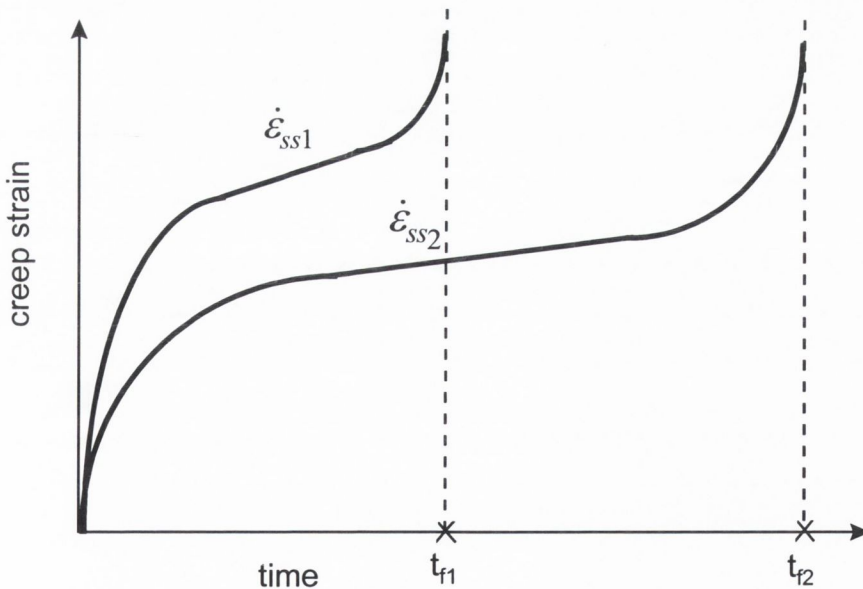


Figure 5.6: Graph illustrating the concept of the Monkman-Grant relationship, where the product of the steady-state creep rate and the time-to-failure are constant for a material. A high steady-state creep rate, indicates that the time to failure will be low.

5.4.3 Failure Mechanisms

Damage has been found in clinically retrieved cement mantles. Maloney et al. (1989) found fractures in the cement mantles of Charnley-Müller prostheses that had been in place for 3.3 years or longer. Cracks were found at the cement/metal interface particularly around the sharp corners of the prosthesis. In the samples sectioned in this study, macroscopic cracks were also found primarily at the cement/prosthesis interface of the Müller prosthesis, emanating from the sharp corners of the prosthesis (see Figure 4.46a, 4.46d) and at sections where the cement mantle was thin (Figure 4.46b, 4.46c). Some cracks extended through the cement mantle to the cement/bone interface, see Figure 4.46c, but others stretched for only fractions of a millimeter into the cement (see Figure 4.46d). Longitudinal cracks along the cement/prosthesis interface of both prostheses were found, consistent with prosthesis debonding. Large, randomly distributed pores, with diameters of up to 2 mm, were found in some of the sectioned samples. This appears to be an artifact of using a vacuum mixing cement preparation procedure *in vitro* (Murphy and Prendergast, 2000), and because the prostheses were inserted along clinically relevant insertion paths, large pores can be expected to occur *in vivo*. Some cracks were found by Maloney et al. (1989) originating from pores along the cement/bone interface. However, in this study no cracks were macroscopically seen to emanate from pores. Scanning electron microscopy techniques of the sort used by Jasty et al. (1991) may be necessary to detect such cracks. The nature of the damage found in the samples tested in this research indicates that although the samples have not been fatigued to destruction, that two million cycles was sufficient to generate clinically relevant damage in the samples.

The initial interfacial strength achieved between the cement and prosthesis will be determined, in part, by the microscopic roughness of the stem (Crowninshield et al., 1998), by the macroscopic features on the stem — i.e. the presence of grooves, like those on the Lubinus prosthesis which might enhance the strength of the cement/metal interface, compared to the sharp corners of the Müller prosthesis which would not, and by the viscosity of the cement during prosthesis insertion. The Lubinus prosthesis R_a value was measured to range from 1.15 to 1.37 μm , whereas the Müller prosthesis was found to have an R_a value ranging from 0.42 to 0.49 μm . The prosthesis/cement interfaces for both the Müller and Lubinus stems were found to be debonded, although the Lubinus interface was significantly stronger than the Müller interface. The rougher Lubinus surface, combined with its geometrical features explain the higher cement/stem strength that was found.

5.5 EFFECT OF BONE RESORPTION SIMULATION

It is possible that the smaller migrations measured for the Lubinus prostheses compared to the Müller prostheses, were due to the stabilising effect of the collar. By simulating the loss of collar/calcar contact the significance of the collar in determining migration patterns were assessed.

5.5.1 Shapes of the migration curves

At 2 million cycles, the cemented reconstructions were removed from the testing machine, bone resorption was simulated (see section 3.2.4.3) and the samples were tested for a further 2 million cycles. Consequently, the migration curves exhibited a discontinuity at 2 million cycles (see Figures 4.34 to 4.41). The migration curves for the resorption phase were comprised of an initial rapid migration followed by migration at a slower steady-state (see in particular Figure 4.37 and 4.40). However, the migratory behaviour of the Lubinus prostheses appeared more erratic. This is particularly evident in Lubinus 2, where the prosthesis appeared to migrate and rotate in one direction, to reverse directions, then to return to its original direction of migration. It is possible that a *stick-slip* phenomenon is active in this phase of testing. Because the Lubinus stem has a rougher surface (Ra: 1.16 - 1.37) compared to the Müller prosthesis (Ra: 0.40 - 0.49), this may explain why the stick-slip phenomena is less apparent in the migratory curves of the Müller prosthesis.

5.5.2 Steady-state creep rate and total migration

If migration is influenced by collar/bone contact, it should be expected that in removing bone under the collar that a larger difference in the migration of the Lubinus would occur, compared with that expected with the Müller which had a smaller collar.

Although no patterns for the Lubinus prostheses emerged, Lubinus 3 showed an increase in total rotation about the z axis (see Figure 4.45) over the 2 - 4 million cycles stage, compared that measured over 0 - 2 million cycles combined with an increase in the steady-state migration rate in that direction (see Table 4.8). An increase in steady-state migration rate for both Müller prosthesis in the z' direction and in rotation about the y axis (see Table 4.8), combined with an increase in the total migration of Müller 1 in the z' direction, and in rotation about the y axis (see Figure 4.42) was found. This suggests that

accelerated failure of both Müller implants in the z' direction, and in rotation about the y axis may result, and that accelerated failure of one of the Lubinus implants in rotation about the z axis may result. However, the sample sizes were too small to allow for comparison of pre and post resorption to be made on a statistically significant basis.

Since differences in migration patterns for the Lubinus prosthesis were small and were not consistent for both implants tested, this supports the clinical evidence that proximal calcar resorption is not necessarily linked with an increase in loosening rates (Kelley et al., 1998, Sutherland et al., 1982). It also would suggest that the collar is not necessary to prevent migration. This was also concluded from a clinical study by Mjöberg et al., 1986 (for the Lubinus prosthesis). Although a collar may be useful in pressurising the cement mantle during prosthesis insertion and may assist with locating the prosthesis within the cemented cavity, its effectiveness in preventing loosening is not apparent.

5.5.3 Cement/metal interfacial strength

If more damage was generated at the cement/prosthesis interface as testing progressed, it was expected that because the stems in which resorption was simulated were tested for an extra 2 million cycles, that the interfaces would have a lower push out strength. However, no significant difference between the cement/metal interfacial strength for either prosthesis design was found before and after bone resorption. This indicates that no additional damage was generated along the cement/metal interfaces of either prosthesis and further suggests that it is not necessary to model bone resorption to quantify the migration rates of prostheses.

5.6 DESIGNING A PRE-CLINICAL TEST: ESSENTIAL FEATURES

5.6.1 Number of loading cycles

Little data exists in literature to suggest the minimum number of cycles that cemented implants should be tested for *in vitro*. Currently, cyclic tests on cemented femora vary in duration from 3000 to 5000 loading cycles (see section 2.6.2), with little scientific evidence that this is sufficient to capture *in vivo* failure modes, or to validly compare prosthesis migrations. The femora reported in this study were cyclically loaded for 2 million cycles, on the basis that distal migration at two years is a good indicator of loosening. Significant differences in migrations were found at 2 million cycles. However, significant differences

were also found at various stages during testing (see Table 4.6). This suggests that to capture the expected clinical behaviour of prostheses, it may not be necessary to test to 2 million cycles.

At 0.2 million cycles, (i.e. at the end of primary creep) significant differences in total migration of the Müller and Lubinus prosthesis were found in the in the z' direction ($p = 0.03$), and in the θ_z direction ($p = 0.03$), see section 4.3.2. In clinical terms, movement over the first 0.2 million cycles corresponds to the rapid migration over the first 4 months post operatively similar to that found clinically (Mjoberg et al., 1986). If comparisons between prostheses migration is made at a time where one prosthesis is still in primary creep, but at the same time another has entered its steady-state creep, the differences between prostheses migrations will be inaccurate. If the predictive nature of steady-state creep rate proposed in section 5.3.2 is accepted, testing must continue until a realistic estimate of the steady-state creep rate can be made. For the prostheses tested, creep rate at 1 million loading cycles was found to be a good stage at which to estimate steady-state creep. Little comparative difference was found between the migrations of the Lubinus and Müller prostheses at 2 million and at 1 million cycles (see Table 5.3). Therefore, one million loading cycles is proposed as a suitable cut-off point for cyclic loading tests of the kind reported in this research.

5.6.2 Inducible Displacement

As cyclic loading progressed, the inducible displacement of the Lubinus prostheses had a tendency to decrease (see Table 4.9). Contrary to this there was a correlation between an increase in the inducible displacement of the Müller prostheses as testing progressed. The correlation was particularly strong for Müller 3 and Müller 5, which migrated by amounts that were in the upper limits of the migrations quantified for all the Müller prostheses (see Figures 4.8 to 4.13). A decrease in inducible displacement during testing was seen for Müller 4. Correspondingly, this prosthesis migrates least of all the Müllers tested in all directions at 2 million cycles (see Figures 4.8 to 4.13). This suggests that some correlation between inducible displacement and migration exists. This may be explained by the increased damage found around the Müller prosthesis compared to that of the Lubinus (see section 5.2.2.2).

To explore this possible correlation further, the inducible displacement at various stages through the loading history was compared to the total migration at 2 million cycles.

Although there was considerable scatter in results, there appeared to be a linear relationship between the inducible displacement of a prosthesis in a particular direction, measured at any stage during its loading history, and its final migration in that direction. It can be seen that generally the Müller prostheses exhibited higher inducible displacements and higher total migrations than the Lubinus (see in particular Figures 4.52e and Figure 4.54c). However, the overlap between the Müller and Lubinus points on the graphs, also underline the inherent variability in such tests.

There was a good correlation (as indicated by the R^2 value on the graphs) between the average inducible translation in the y' direction and the final translation in that direction when the inducible displacement was measured at 0.2 million loading cycles, at 1 million loading cycles, and averaged over 2 million cycles. There was also a good correlation between the average inducible rotation about the z axis at 0.2 million, 1 million and averaged over 2 million, and the final rotation in that direction. These correlations further underline the possible inter-dependency between inducible displacement and the total migration. In fact, it opens the possibility that inducible displacement may be a sufficient indicator of cemented THR success. If inducible displacement could be measured in RSA studies, 'at risk' reconstructions could be rapidly identified post-operatively.

6: Conclusions

6.1	CONCLUSIONS	142
6.2	RECOMMENDATIONS FOR FUTURE WORK	143

6.1 CONCLUSIONS

The conclusions reached are as follows:

- (i) A machine which can insert femoral hip prostheses along a user defined controlled insertion path has been designed and validated.
- (ii) The Müller prosthesis migrated significantly more than the Lubinus prosthesis after 2 million loading cycles.
- (iii) Migration at two years is correlated with early failure. Hence this test qualitatively predicts that the Müller prosthesis is more likely to loosen than the Lubinus prosthesis.
- (iv) The migration patterns measured in this study are similar to those measured clinically, although quantitatively there are differences.
- (v) To quantitatively produce more relevant migrations, the inclusion of muscles and of a fibrous tissue that forms along the cement/metal interface may be necessary.
- (vi) Testing to one million cycles was sufficient to generate damage in the cement mantle similar to that found in autopsy-retrieved cement implants.
- (vii) All prostheses migrated at a fast rate from 0 - 0.2 million loading cycles (approximately), and thereafter at a slower, steady-state rate.
- (viii) The change in the rate of prosthesis migration during the testing period, suggests that bone cement creep predominantly determines prosthesis migration.
- (ix) The relative contributions of damage and creep in determining migrations cannot be definitively answered without further analytical studies.
- (x) The average Müller steady-state migration rate was three fold larger than that of the Lubinus.
- (xi) Point (ix) combined with application of the Monkman-Grant relationship suggests that the rate of migration can be used as a predictor of time to failure.
- (xii) Steady-state rate of migration for both prosthesis designs was reached at 1 million loading cycles.

- (xiii) The significant difference in absolute migrations at 1 million cycles was similar to that at 2 million cycles.
- (xiv) Both (xi) and (xii) indicate that, to differentiate between implant performance, it is sufficient to test to 1 million cycles.
- (xv) There is an approximately linear relationship between the inducible displacement in a particular direction and the final migration in that direction, indicating the potential of inducible displacement as a post-operative measure of potential implant longevity.
- (xvi) The large collar of the Lubinus prosthesis appears to have a negligible effect in preventing prosthesis migration.
- (xvii) One might argue that with existing fixation methods implant longevity has reached its limit. Until this is definitively proven in a pre-clinical test, like that presented in this thesis the evolution of new designs will continue, even if each step is only a marginal, if any, improvement over its predecessor.

6.2 RECOMMENDATIONS FOR FUTURE WORK

To quantify migrations of the order of that measured clinically, tests including fibrous tissue and physiological loads (with muscles included) should be performed. This should attenuate the migrations measured, and in doing so allow for many prostheses to be ranked according to their clinical performance¹.

To fully evaluate the ability of this pre-clinical to differentiate between prosthesis performance, it should be applied to a cemented type I implant, *e.g.* the Exeter design. It may be expected that the total migration of this prosthesis design may be higher, however its steady-state migration rate may be low, suggesting that its time to failure will also be low. However, testing must be done to explore these possible scenarios further. To explore the validity of migration rate as predictor of loosening, cyclic tests to destruction for the two designs in this study should be performed.

¹ This is currently being undertaken by the Trinity Bioengineering Group as part of the SMT funded project to which the research presented in this thesis also contributes.

REFERENCES

- Andriacchi, T.P., Galante, J.O., Belytschko, T.B., Hampton, S., 1976**, 'A Stress Analysis of the Femoral Stem in Total Hip Prostheses', *Journal of Bone and Joint Surgery*, Vol. 58A(5), pp. 618 - 624.
- Askew, M.J., Steege, J.W., Lewis, J.L., Ranieri, J.R., Wixson, R.L., 1984**, 'Effect of Cement Pressure and Bone Strength on Polymethylmethacrylate Fixation', *Journal of Orthopaedics Research*, Vol 1(4), pp. 412 - 420.
- Bannister, G.C., Miles, A.W., 1988**, 'The Influence of Cementing Technique and Blood on the Strength of the Bone-Cement Interface', *Engineering in Medicine*, Vol. 17, pp. 131 - 133.
- Bargar, W.L., Bauer, A., Borner, M., 1998**, 'Primary and Revision Total Hip Replacement Using the Robodoc System', *Clinical Orthopaedics and Related Research*, No. 354, pp. 82 - 91.
- Barrack, R.L., Mulroy, R.D., Harris, W.H., 1992**, 'Improved Cementing Techniques and Femoral Component Loosening in Young Patients with Hip Arthroplasty', *Journal of Bone and Joint Surgery*, Vol. 74-B, pp. 285 - 289.
- Basalla, G., 1996**, 'The Evolution of Technology', Cambridge University Press, Cambridge History of Science Series, ISBN 0-521-29681-1.
- Bergamnn, G., Deuretzbacher, G., Morlock, M., 1999**, 'Development of the loading Configuration', Progress report of the third year on contract SMT4-CT96-2076, 'Preclinical Testing of Cemented Hip Replacement Implants: Pre-Normative Research for a European Standard'.
- Bergmann, G., Graichen, F., Rohlmann, A., 1995**, 'Is Staircase Walking a Risk For the Fixation of Hip Implants', *Journal of Biomechanics*, Vol. 28, pp. 535 - 553.
- Bergmann, G., Graichen, F., Rohlmann, A., 1993**, 'Hip Joint Loading During Walking and Running Measured in Two Patients', *Journal of Biomechanics*, Vol. 26, pp. 969 - 900.
- Berry, D.J., Harmsen, W.S., Ilstrup, D.M., 1998**, 'The Natural History of Debonding of the Femoral Component from the Cement and its Effect on Long-Term Survival of Charnley Total Hip Replacements', *Journal of Bone and Joint Surgery*, Vol. 80A, pp. 715 - 721.
- Berzins, A., Sumner, D.R., Andriacchi, T.P., Galante, J.O., 1993**, 'Stem Curvature and Load Angle Influence the Initial relative Bone-Implant Motion of Cementless Femoral Stems', *Journal of Orthopaedics Research*, Vol. 11, pp. 758 - 769.

- Brand R.A., Pedersen D.R., Yoder S.A., 1986**, 'How Definition of 'Loosening' Affects the Incidence of Loose Total Hip Reconstructions', *Clinical Orthopaedics and Related Research*, No. 210, pp.185 - 191.
- Britton, A.R., Murray, D.W., Bulstrode, C.J., McPherson, K., Denham, R.A., 1996**, 'Long Term Comparison of Charnley and Stanmore Design Total Hip Replacement', *Journal of Bone and Joint Surgery*, Vol. 78-B, pp. 802 - 808.
- Brown, S.A., 1991**, 'Polymers', Chapter 3 in 'Total Joint Replacement', Edited by William Petty, Published by W.B. Saunders Company.
- Browne, A.O., Sheehan, J.M., 1986**, 'Trochanteric Osteotomy in Charnley Low-Friction Arthroplasty of the Hip', *Clinical Orthopaedics and related Research*, No. 211, pp. 128 - 133.
- Buhler, D.W., Oxland, T.R., Nolte L.-P., 1997a**, 'Design and Evaluation of a Device for Measuring Three-Dimensional Micromotions of Press-Fit Femoral Stem Prostheses', *Medical Engineering Physics*, Vol. 19, No. 2, pp. 187 - 199.
- Buhler, D.W., Berlemann, U., Lippuner, K., Jaeger, P., Nolte, L.P., 1997b**, 'Three-dimensional Primary Stability of Cementless Femoral Stems', *Clinical Biomechanics*, Vol. 12, pp. 75 - 86.
- Burke, D.W., P'Connor, D.O., Zalenski, E.B., Jasty, M., Harris, W.H., 1991**, 'Micromotion of Cemented and Uncemented Femoral Components', *Journal of Bone and Joint Surgery*, Vol. 73-B, pp. 33 - 37.
- Callaghan, J.J., Fulgham, C.S., Glisson, R.R., Stranne, S.K., 1992**, 'The Effect of Femoral Stem Geometry on Interface Motion in Uncemented Porous-Coated Total Hip Prostheses', *Journal of Bone and Joint Surgery*, Vol. 74A, 1992, pp. 839 - 847.
- Chafetz, N., Baumrind, S., Murray, W.R., Genant, H.K., Korn, E.L., 1985**, 'Subsidence of the Femoral Prosthesis: A Stereophotogrammetric Evaluation', *Clinical Orthopaedics and Related Research*, No. 201, pp. 60 - 67.
- Chang, P.B., Mann, K.A., Bartel, D.L., 1998**, 'Cemented Femoral Stem Performance. Effects of Proximal Bonding, Geometry and Neck Length', *Clinical Orthopaedics and Related Research*, No. 355, pp. 57 - 69.
- Charnley, J., Kettlewell, J., 1965**, 'The Elimination of Slip Between Prosthesis and Femur', *Journal of Bone and Joint Surgery.*, Vol. 47B, pp. 56 - 60.
- Charnley, J., 1961**, 'Arthroplasty of the Hip. A New Operation', *The Lancet*, Vol. 1, pp. 1129 - 1132.
- Charnley, J., 1960**, 'Anchorage of the Femoral Head Prosthesis to the Shaft of the Femur', *Journal of Bone and Joint Surgery*, Vol. 42-B, pp.28 - 30.

- Chwirut, D.J., 1984**, 'Long-term Compressive Creep Deformation and Damage in Acrylic Bone Cements', *Journal of Biomedical Materials Research*, Vol. 18, pp. 25 - 37.
- Collis, D.K., Mohler, C.G., 1998**, 'Loosening Rates and Bone Lysis With Rough Finished and Polished Stems', *Clinical Orthopaedics Related Research*, No. 355, pp. 113 - 122.
- Cristofolini, L., 1997**, 'A critical Analysis of Stress Shielding Evaluation of Hip Prostheses', *Critical Reviews in Biomedical Engineering*, 25(4+5), pp. 409 - 483.
- Crowninshield, R.D., Jennings, J.D., Laurent, M.L., Maloney, W.J., 1998**, 'Cemented Femoral Component Surface Finish Mechanics', *Clinical Orthopaedics and Related Research*, No. 355, pp. 90 - 102.
- Crowninshield, R.D., Brand, R.A., Johnston, R.C., Milroy, J.C., 1980**, 'The Effect of Femoral Stem Cross-Sectional Geometry on Cement Stresses in Total Hip Reconstruction', *Clinical Orthopaedics and Related Research*, No. 146, pp. 71 - 77.
- Davies, J.P., O'Connor, D.O., Burke, D.W., Jasty, M., Harris, W.H., 1988**, 'The Effect of Centrifugation on the Fatigue Life of Bone Cement in the Presence of Surface Irregularities', *Clinical Orthopaedics and Related Research*, No. 229, pp. 156 - 161.
- Davies, J.P., Harris, W.H., 1993**, '*In Vitro* and *In Vivo* Studies of Pressurization of Femoral Cement in Total Hip Arthroplasty', *The Journal of Arthroplasty*, Vol. 8, No. 6, pp. 585 - 591.
- Dobbs, H.S., 1980**, 'Survivorship of Total Hip Replacements', *Journal of Bone and Joint Surgery*, Vol. 62B, No. 2, pp. 160 - 173.
- Ebramzadeh, E., Sarimento, A., McKellop, H.A., Llinas, A., Gogan, W., 1994**, 'The Cement Mantle in Total Hip Arthroplasty', *Journal of Bone and Joint Surgery*, Vol. 76A, pp. 77 - 87.
- Engh, C.A., O'Connor, D., Jasty, M., McGovern, T.F., Bobyn, J.D., Harris, W.H., 1992**, 'Quantification of Implant Micromotion, Strain Shielding, and Bone Resorption With Porous Coated Anatomic Medullary Locking Femoral Prostheses', *Clinical Orthopaedics and related Research*, NO. 285, pp. 13 - 29.
- Fowler, J.L., Gie, G.A., Lee, A.J.C., Ling, R.S.M., 1988**, 'Experience with the Exeter Total Hip Replacement Since 1970', *Clinical Orthopaedics of North America*, Vol. 19(3), pp. 477 - 489.
- Freeman, M.A.R., Plante-Bordeneuve, P., 1994**, 'Early and Late Aseptic failure of Proximal Femoral Prostheses', *Journal of Bone and Joint Surgery*, Vol. 76B, No. 3, pp. 432 - 437.
- Freitag, T.A., Cannon, S.L., 1977**, 'Fracture Characteristics of Acrylic Bone Cements. II Fatigue', *Journal of Biomedical Materials Research*, Vol. 11, pp. 609 - 624.

- Gait98**, version June 1999, Internal CD produced by Biomechanics Laboratory, Berlin, as part of SMT project Nr. SMT4-CT96-2076.
- Gardiner, R.C., Hozack, W.J., 1994**, 'Failure of the Cement-Bone Interface. A Consequence of Strengthening the Cement-Prosthesis Interface?', *Journal of Bone and Joint Surgery*, Vol. 76B, pp. 49 - 52.
- Gibson, L.J., 1985**, 'The Mechanical Behaviour of Cancellous Bone', *Journal of Biomechanics*, Vol. 18(5), pp. 317 - 328.
- Gilbert, J.L., Bloomfield, R.S., Lautenschlager, E.P., Wixson, R.L., 1992**, 'A Computer-Based Biomechanical Analysis of the Three Dimensional Motion of Cementless Hip Prostheses', *Journal of Biomechanics*, Vol. 25, No. 4, pp. 329 - 340.
- Haas, S.S., Brauer, G.M., Dickson, G., 1975**, 'A Characterisation of Polymethylmethacrylate Bone Cement', *Journal of Bone and Joint Surgery*, Vol. 57A, pp. 380 - 391.
- Haboush, E.J., 1953**, 'A New Operation for Arthroplasty of the Hip Based on Biomechanics, Photoelasticity, Fast-setting Dental Acrylic, and Other Considerations', *Bulletin for the Hospital for Joint Diseases*, Vol. 14, pp. 242 - 277.
- Hailey, J.L., Turner, I.G., Miles, A.W., 1994**, 'An In Vitro Study of the Effect of Environment and Storage Time on the Fracture Properties of Bone Cement', *Clinical Materials*, Vol. 16, pp. 211 - 216.
- Halawa, M., Lee, A.J.C., Ling, R.S.M., Vangala, S.S., 1978**, 'The Shear Strength of Trabecular Bone from the Femur, and some Factors Affecting the Shear Strength of the Cement-Bone Interface', *Acta Orthopaedica of Traumatic Surgery*, Vol. 92, pp 19 - 30.
- Hardinge, K., 1983**, 'Hip Replacement. The Facts', Published by Oxford University Press, 1983, ISBN 0-19-261393-6.
- Harman, M.K., Toni, A., Cristofolini, L., Viceconti, M., 1995**, 'Initial Stability of Uncemented Hip Stems: An In Vitro Protocol to measure torsional interface motion', *Medical Engineering Physics*, Vol. 17(3), pp. 163 - 171.
- Harris, W.H., McCarthy, J.C., O'Neill, D.A., 1982**, 'Femoral Component Loosening Using Contemporary Techniques of Femoral Cement Fixation', *Journal of Bone and Joint Surgery*, 64-A, pp. 1063 - 1067.
- Hori, R.Y., Lewis, J.L., 1982**, 'Mechanical Properties of the Fibrous Tissue Found at the Bone-Cement Interface Following Total Joint Replacement', *Journal of Biomedical Materials Research*, Vol. 16, pp. 911 - 927.
- Howie, D.W., Middleton, R.G., Costi, K., 1998**, 'Loosening of Matt and Polished Cemented Femoral Stems', *Journal of Bone and Joint Surgery*, Vol. 80-B, pp. 573 - 576.

- Hua, J., Walker, P.S., 1994**, 'Relative Motion of Hip Stems Under Load', *Journal of Bone and Joint Surgery*, Vol.76A, pp. 95 - 103.
- Huiskes, R., Verdonschot, N., Nivbrant, B., 1998**, 'Migration, Stem Shape, and Surface Finish in Cemented Total Hip Arthroplasty', *Clinical Orthopaedics and Related Research*, No. 355, pp. 103 - 112.
- Huiskes, R., Verdonschot, N., 1997**, 'Biomechanics of Artificial Joints: The Hip', Chapter 10 in 'Basic Orthopaedic Biomechanics', 2nd Edition, Edited by Mow, V.C., and Hayes, W.C., published by Lippincott-Raven.
- Huiskes, R., 1993**, 'Failed Innovation in Total Hip Replacement', *Acta Orthopaedica Scandinavia*, 64, pp. 699 - 716.
- International Standard, 1988**, 'Implants for surgery – Partial and Total Hip Joint Prostheses – Part 3: Determination of Endurance Properties of Stemmed Femoral Components With Application of Torsion', ISO 7206-3: 1988(E).
- Jacobsson, S-A., Ivarsson, I., Djerf, K., Wahlstrom, O., 1995**, 'Stem Loosening more Common with ITH than Lubinus Prosthesis: A 5 year clinical and radiographic follow-up of 142 patients', *Acta Orthopaedica Scandinavia*, 66(5), pp. 425 - 431.
- James, S.P., Jasty, M., Davies, J., Piehler, H., Harris, W.H., 1992**, 'A Fractographic Investigation of PMMA Bone Cement Focusing on the Relationship Between Porosity Reduction and Increased Fatigue Life', *Journal of Biomedical Materials Research*, Vol. 26, pp. 651 - 662.
- Jasty, M., Maloney, W.J., Bragdon, C.R., O'Connor, D., Haire, T., Harris, W.H., 1991**, 'The Initiation of Failure in cemented Femoral Components of Hip Arthroplasties', *Journal of Bone and Joint Surgery*, Vol. 73B, pp. 551 - 550.
- Kabo, M., 1991**, 'Biomaterials for Use in Orthopaedic Surgery', Chapter 3 in 'Hip Arthroplasty', edited by Amstutz, H.C., Published by Churchill Livingstone, pp. 25 - 36.
- Karrholm J., Borssen B., Lowenhielm G., Snorrason F., 1994**, 'Does early micromotion of femoral stem prostheses matter - 4-7 year stereoradiographic follow-up of 84 cemented prostheses', *Journal of Bone and Joint Surgery*, Vol. 76-B, pp. 912 - 916.
- Kelley, S.S., Fitzgerald, R.H., Rand, J.A., Ilstrup, D.M., 1993**, 'A Prospective Randomized Study of a Collar Versus a Collarless Femoral Prosthesis', *Clinical Orthopaedics and Related Research*, No 294, pp. 114 - 122.
- Kindt-Larsen, T., Smith, D.B., Jensen, J.S., 1995**, 'Innovations in Acrylic Bone Cement and Application Equipment', *Journal of Applied Biomaterials*, Vol. 6, 75 - 83.
- Koybayashi S., Takaoka K., Saito N., Hisa K., 1997a**, 'Factors Affecting Aseptic Failure of Fixation After Primary Charnley Total Hip Arthroplasty', *Journal of Bone and Joint Surgery*, 79A, pp. 1618 - 1627.

- Kobayashi, A., Donnelly, W.J., Scott, G., Freeman, M.A.R., 1997b**, 'Early Radiological Observations May Predict the Long-Term Survival of Femoral Hip Prostheses', *Journal of Bone and Joint Surgery*, Vol. 79B, pp. 583 - 589.
- Kobayashi, S., Terayama, K., 1992**, 'Factors Influencing Survivorship of the Femoral Component After Primary Low-Friction Hip Arthroplasty', *Journal of Arthroplasty*, Vol. 7, Supplement, pp. 327 - 338.
- Kotzar, G.M., Davy, D.T., Goldberg, V.M., 1995**, 'Torsional Loads in the Early Postoperative Period Following Total Hip Replacement', *Journal of Orthopaedic Research*, Vol. 13, pp. 945 - 955.
- Krismer, M., Klar, M., Klestil, T., Frischut, B., 1991**, 'Aseptic Loosening of Straight- and Curved-Stem Müller femoral prostheses', *Archives of Orthopaedic Trauma in Surgery*, Vol. 110, pp. 190 - 194.
- Lee, A.J.C., 1994**, 'Rough or Polished Surface on Femoral Anchorage Stems?', In *Technical Principles, Design and Safety of Joint Implants*, Edited by Buchhorn, G.H., Willert H.G., Published by Hogrefe and Huber, pp. 209 - 211.
- Lennon, A.B., Prendergast, P.J., Whelan, M.P., Forne, C., 2000a**, 'Use of Grating Interferometry for Validation of Finite Element Models and to Investigate Residual Strain in PMMA', *Proceedings of the Fourth International Symposium on Computer Methods in Biomechanics and Biomedical Engineering*, Edited by Middleton, J.P., and Jones, M., in press.
- Lennon, A.B., Prendergast, P.J., Lacroix, D., Revie, I., Pfliderer, M., 2000b**, 'Stress analysis of cement mantle of a polished femoral hip replacement', submitted for presentation at the European Society of Biomechanics conference, 2000.
- LeVay, D., 1990**, 'The History of Orthopaedics. An Account of the Study and Practice of Orthopaedics from the Earliest Times to the Modern Era', The Parthenon Publishing Group, ISBN 1850701458.
- Ling, R.S., 1992**, 'The Use of a Collar and Precoating on Cemented Femoral Stems is Unnecessary and Detrimental', *Clinical Orthopaedics and Related Research.*, No. 285, pp. 73 - 83.
- Maher, S.A., Prendergast, P.J., Reid, A.J., Waide, D.V., 2000**, 'Design and Validation of a Machine for Reproducible Precision Insertion of Prostheses for Preclinical Testing', *Journal of Biomechanical Engineering*, Vol. 122.
- Maher, S.A., McCormack, B.A.O., 1999**, 'Quantification of Interdigitation at Bone Cement/Cancellous Bone Interfaces in Cemented Femoral reconstructions', *Proceedings of the Institute of Mechanical Engineers (Part H: Engineering in Medicine)*, Vol. 213, pp. 347 - 354.

- Majkowski, R.S., Miles, A.W., Bannister, G.C., Perkins, J., Taylor, G.J.S., 1993**, 'Bone Surface Preparation in Cemented Joint Replacement', *Journal of Bone and Joint Surgery*, 73-B (check that 73 is correct number), No. 3, 1993, pp. 459 - 463.
- Malchau H., Herberts P., 1998**, 'Prognosis of Total Hip Replacement. Revision and Re-Revision Rate in THR: A Revision-Risk Study of 148,359 Primary Operations', Scientific Exhibition presented at the 65th Annual Meeting of the AAOS.
- Malchau, H., 1995**, 'On the Importance of Stepwise Introduction of New Hip Implant Technology', Ph.D. Thesis from the Department of Orthopaedics, Institute of Surgical Sciences, Göteborg University, Göteborg, Sweden.
- Malchau, H., Karrholm, J., Wang, Y.X., Herberts, P., 1995**, 'Accuracy of Migration Analysis in Hip Arthroplasty. Digitized and Conventional Radiography, Compared to Radiostereometry in 51 Patients', *Acta Orthopaedica Scandinavia*, Vol. 66(5), pp. 418 - 424.
- Malchau, H., Herberts, P., Ahnfelt, L., 1993**, 'Prognosis of Total Hip Replacement in Sweden. Follow-up of 92,675 Operations Performed 1978 - 1990', *Acta Orthopaedica Scandinavia*, Vol. 64(5), pp. 497 - 506.
- Maloney, W.J., Jasty, M., Burke, D.W., O'Connor, D.O., Zalenski, E.B., Bragdon, C., Harris, W.H., 1989**, 'Biomechanical and Histologic Investigations of Cemented Total Hip Arthroplasties', *Clinical Orthopaedics and Related Research*, No. 249, pp. 129 - 140.
- Manley M., Stern L.S., Kotzar G., Stulberg B.N., 1987**, 'Femoral component loosening in hip arthroplasty: Cadaver study of subsidence and hoop strain', *Acta Orthopaedica Scandinavia*, 58, pp.485 - 490.
- Mann, K.A., Bartel, D.L., Wright, T.W., Ingraffe, A.R., 1991**, 'Mechanical Characteristics of the Stem-Cement Interface', *Journal of Orthopaedic Research*, Vol. 9, pp. 798 - 808.
- Markolf, K.L., Amstutz, H.C., 1976**, 'In Vitro Measurement of Bone-Acrylic Interface Pressure During Femoral Component Insertion', *Clinical Orthopaedics and Related Research*, No. 121, pp. 60 - 66.
- McBeath, A.A., Foltz, R.N., 1979**, 'Femoral Component Loosening After Total Hip Replacement', *Clinical Orthopaedics and Related Research*, No. 141, pp. 66 - 70.
- McCormack, B.A.O., Prendergast, P.J., 1999**, 'Microdamage Accumulation in the Cement Layer of Hip Replacements Under Flexural Loading', *Journal of Biomechanics*, Vol. 32, pp. 467 - 475.
- McCormack, B.A.O., Prendergast, P.J., O'Dwyer, B., 1999**, 'Fatigue of Cemented Hip Replacements Under Torsional Loads', *Fatigue and Fracture of Engineering Materials and Structures*, Vol. 22, pp. 467 - 475.

- McElfresh, E., 1991**, 'History of Arthroplasty', Chapter 1 in 'Total Joint Replacement', edited by W. Petty, Published by W.B.Saunders Company, ISBN 0-7216-3367-6, pp. 3 - 18.
- McKellop, H., Ebramzadeh, E., Niederer, P.G., Sarimento, A., 1991**, 'Comparison of the Stability of Press-Fit Prosthesis Femoral Stems Using a Synthetic Model Femur', Journal of Orthopaedics. Research., 9:297 - 305.
- Meyer, P.R., Lautenschlager, E.P., Moore, B.K., 1973**, 'On the Setting Properties of Acrylic Bone Cement', Journal of Bone and Joint Surgery, Vol. 55-A, pp. 149 - 156.
- Middleton, R.G., Howie, D.W., Costi, K., Sharpe, P., 1998**, 'Effects of Design Changes on Cemented Tapered Femoral Stem Fixation', Clinical Orthopaedics and Related Research, No. 355, pp. 47 - 56.
- Mjöberg B., Franzen H., Selvik G., 1990**, 'Early detection of prosthetic-hip loosening', Acta Orthopaedica Scandinavia, Vol. 61(3), pp. 273 - 274.
- Mjöberg, B., 1986**, 'Loosening of the Cemented Hip Prosthesis. The Importance of Heat Injury', Acta Orthopaedica Scandinavica, Supplementum No. 221, Vol. 57.
- Mjöberg, B., Selvik, G., Hansson, L.I., Rosenqvist, R., Önerfält, R., 1986** "Mechanical Loosening of Total Hip Prostheses. A Radiographic and Roentgen Stereophotogrammetric Study", Journal of Bone and Joint Surgery, Vol. 68B, No. 5, pp. 770 - 773.
- Mjöberg B., Brismar J., Hansson LI, Pettersson H., Selvik G., Önerfält R., 1985**, 'Definition of Endoprosthetic Loosening - Comparison of arthrography, scintigraphy and roentgenstereophotogrammetry in prosthetic hips', Acta Orthopaedica Scandinavia 56, pp. 469 - 473.
- Mulroy, R.D., Harris, W.H., 1990**, 'The Effect of Improved Cementing Techniques on Component Loosening in Total Hip Replacement', Journal of Bone and Joint Surgery, Vol. 72-B, pp. 757 - 760.
- Murphy, B.P., Prendergast, P.J., 2000**, 'The Probability of Failure of Acrylic Bone Cement as a Function of Stress and Porosity', International Journal of Fatigue, *in press*.
- Murphy, B.P., Prendergast, P.J., 1999**, 'Measurement of Non-Linear Microcrack Accumulation Rates in Polymethylmethacrylate Bone Cement Under Cyclic Loading', Journal of Materials Science: Materials in Medicine, Vol. 10, pp. 779 - 781.
- Murray, D.W., Carr, A.J., Bulstrode, C.J., 1995**, 'Which Primary Total Hip Replacement', Journal of Bone and Joint Surgery, 77B, pp 520 - 527.
- Murray, D.W., Carr, A.J., Bulstrode, C., 1993**, 'Survival Analysis of Joint Replacements', Journal of Bone and Joint Surgery, 75-B, pp. 697 - 704.

- Nabarro, F.R.N., de Villiers, H.L., 1995**, 'The Physics of Creep', published by Taylor & Francis, ISBN 085066 852 2.
- National Institutes of Health, 1994**, 'National Institutes of Health Consensus Statement', NIH Consensus Statement, Vol. 12, pp. 1 – 31.
- Niederer, P.G., Chiquet, C., Frey, O., Semlitsch, M., 1978**, 'Artificial Proximal Femur of Fiber Reinforced Polyester for the Study of Load Transmission of Cemented Hop Prostheses: The Prosthesis Cement Interface', *Journal of Biomaterials*, pp. 88-89.
- Nilsson, K.G., Karrholm, J., 1996**, 'RSA in the Assessment of Aseptic Loosening', *Journal of Bone and Joint Surgery*, Vol. 78B, pp. 1 - 2.
- Nobel, P.C., Swarts, E., 1983**, 'Penetration of Acrylic Bone Cements Into Cancellous Bone', *Acta Orthopaedica Scandinavia*, Vol. 54, pp. 566 - 573.
- Nunn, D., Freeman, M.A.R., Tanner, K.E., Bonfield, W., 1989**, 'Torsional Stability of the Femoral Component of Hip Arthroplasty', *Journal of Bone and Joint Surgery*, Vol., 71-B, pp. 452 - 455.
- O'Hara, J.N., McMinn, D.J., 1991**, 'Calcar Resorption Beneath a Well Fitting Flanged Femoral Prosthesis', *Journal of Arthroplasty*, 6, pp. 147 - 150.
- Ohlin A., Önsten I., 1990**, 'Loosening of the Lubinus hip: 202 cases followed for 3 - 6 years', *Acta Orthopaedica Scandinavia*, Vol. 361(3), pp. 244 - 247.
- Oishi, C.S., Walker, R.H., Colwell, C.W., 1994**, 'The Femoral Component in Total Hip Arthroplasty', *Journal of Bone and Joint Surgery*, Vol. 76-A, pp. 1130 - 1136.
- Olsson, S.S., 1987**, 'Loosening and Femoral Neck Resorption 5 years after CAD hip replacement', *Acta Orthopaedica Scandinavia*, Vol. 58, pp. 491 - 493.
- Otani, T., Whiteside, L.A., White, S.E., McCarthy, D.S., 1995**, 'Reaming Technique of the Femoral Diaphysis in Cementless Total Hip Arthroplasty', *Clinical orthopaedics and Related Research*, NO. 311, pp. 210 - 211.
- Paul, J.P., 1997**, 'Development of Standards for Orthopaedic Implants', *Proceedings of the Institute of Mechanical Engineers, Part H: Engineering in Medicine*, Vol. 211, pp. 119 - 126.
- Paul, H.A., Bargar, W.L., Mittlestadt, B., Musits, B., Taylor, R.H., Kazanzides, P., Williamson, B., Hanson, W., Zuhars, J., 1992**, 'Development of a Surgical Robot for Cementless Total Hip Arthroplasty', *Clinical Orthopaedics and Related Research*, Vol. 285, pp. 57 - 66.
- Pellicci, P.M., Salvati, E.A., Robinson, H.J., 1979**, 'Mechanical Failures in Total Hip replacement Requiring Re-operation', *Journal of Bone and Joint Surgery*, Vol. 61A, pp. 28 - 30.

- Petty, W., 1991**, 'Prostheses for Total Hip Arthroplasty', Chapter 25 in 'Total Joint Replacement', Edited by Petty, W., Published by W.B. Saunders and Co., ISBN 0-7216-3367-6.
- Phillips, T.W., Nguyen, L.T., Munro, S.D., 1991**, 'Loosening of Cementless Femoral Stems: A Biomechanical Analysis of Immediate Fixation With Loading Vertical, Femur Horizontal', *Journal of Biomechanics*, Vol. 24 (1), pp 37 - 48.
- Pilliar, R.M., Lee, J.M., and Maniopoulos, C., 1986**, 'Observation of the Effect of Movement on Bone Ingrowth into Porous-Surfaced Implants', *Clinical Orthopaedics and Related Research*, Vol. 208, pp. 108 - 113.
- Prendergast, P.J., Birthistle, P., Waide, D.V., Girish Kumar, N.V., 1999**, 'An Investigation of the Performance of Biostop G and Hardinge Bone Plugs', *Proceedings of the Institution of Mechanical Engineers*, Vol. 213, Part H, pp. 361 – 365.
- Prendergast, P.J., Maher, S.A., 1999**, 'Issues in Pre-Clinical Testing of Implants', *Proceedings of the International Conference on Advances in Materials and Processing Technologies, AMPT'99 and 16th Annual Conference of the Irish Manufacturing Committee, IMC16, Volume II*, pp. 1195 – 1202, Edited by Hashmi, M.S.J., and Looney, L, Dublin City University, Dublin.
- Prendergast, P.J., Monaghan, J., Taylor, D., 1989**, 'Materials Selection in the Artificial Hip Joint Using Finite Element Stress Analysis', *Clinical Materials*, Vol. 4, pp. 361 – 376.
- Rho, J.Y., Ashman, R.B., Turner, C.H., 1993**, 'Young's Modulus of Trabecular and Cortical Bone Material: Ultrasonic and Microtensile Measurements', *Journal of Biomechanics*, Vol. 26, pp. 111 - 119.
- Ritter, M.A., Albohm, M.J., 1997**, 'Overview: Maintaining Outcomes for Total Hip Arthroplasty', *Clinical Orthopaedics and Related Research*, No. 344, pp. 81 - 87.
- Rockborn P., Olsson, S.S., 1993**, 'Loosening and Bone Resorption in Exeter Hip Arthroplasties. Review at a Minimum Five Years', *Journal of Bone and Joint Surgery* 75B, pp. 865 - 868.
- Roesler, H., 1987**, 'The History of Some Fundamental Concepts in Bone Biomechanics', *Journal of Biomechanics*, Vol. 20, pp. 1025 - 1034.
- Røkkum, M., Bye, Kjell, Hetland, K.R., Reigstad, A., 1995**, 'Stem Fracture with the Exeter Prosthesis. 3 of 27 hips followed for 10 years', *Acta Orthopaedica Scandinavica*, Vol. 66(5), pp.435 - 439.
- Rydell, N.W., 1966**, 'Forces Acting on the Femoral Head-Prosthesis. A Study on Strain Gauge Supplied Prosthesis in Living Persons', *Acta Orthopaedica Scandinavica*, Supplementum 88.

- Sarmiento, A., 1991**, 'Staying the Course', *Journal of Bone and Joint Surgery*, Vol. 73-A, No. 4, pp. 479 - 483.
- Savino, A.W., Andersson, G.B.J., Andriacchi, T.P., Hampton, S., Galante, J.O., 1982**, 'The Influence of Femoral Stem Thickness and Implantation Technique on the Strength of the Bone Cement Bond', *Acta Orthopaedica Scandinavica*, Vol. 53, pp. 23 - 27.
- Schmidt, J., Steur, G., Specht, R., Kumm, D., 1994**, 'Computer Controlled Experimental Implantation Techniques Comparing the Quality of Different Types of Cement Application into the Femoral Canal in cemented Hip Arthroplasty', *Biomedizinische Technik*, Vol. 39(4), pp. 79 - 84.
- Schneider, E., Eulenberger, J., Steiner, W., Wyder, W., Friedman, R.J., Perren, S.M., 1989**, 'Experimental Method for the In Vitro Testing of the Initial Stability of Cementless Hip Prostheses', *Journal of Biomechanics*, Vol. 22, pp. 735 - 744.
- Schneider E., Kinast C., Eulenberger J., Wyder D., Eskilsson G., Perren S.M., 1989**, 'A Comparative Study of The Initial Stability of Cementless Hip Prostheses', *Clinical Orthopaedics and Related Research*, No. 248, pp. 200 - 209.
- Selvik, G., 1989**, 'Roentgen Stereophotogrammetry: A Method for the Study of the Kinematics of the Skeletal System', *Acta Orthopaedica Scandinavica*, Supplementum No. 232, Vol. 60.
- Semlitsch, M., Panic, B., 1983**, 'Ten Years of Experience with Test Criteria for Fracture-Proof Anchorage Stems of Artificial Hip Joints', *Engineering in Medicine*, Vol. 12, pp.185 - 193.
- Søballe, K., Toksvig-Larsen, S., Gelinek, J., Fruensgaard, S., Hansen, E.S., 1993**, 'Migration of Hydroxyapatite Coated Femoral Prostheses', *Journal of Bone and Joint Surgery*, Vol.75-B, 1993.
- Song, Y., Goodman, S.B., Jaffe, R.A., 1994**, 'An In Vitro Study of Femoral Intramedullary Pressures During Hip Replacement Using Modern Cementing Technique', *Clinical Orthopaedics and Related Research.*, No 302, pp 297 - 304.
- Spector, M., Shorttroff, S., Hsu, H-P., Lane, N., Sledge, C.B., Thornhill, T.S., 1990**, 'Tissue Changes Around Loose Prostheses', *Clinical Orthopaedics and Related Research*, No. 261, pp. 140 - 152.
- Speirs, A.D., Slomczkowski, M.A., Orr, T.E., Sibenrock, K., Nolte, L.-P., 2000**, 'Three Dimensional Measurement of Cemented Femoral Stem Stability: An In Vitro Cadaver Study', *Clinical Biomechanics*, Vol. 15, pp. 548 - 255.
- Star, M.J., Colwell, C.W., Kelman, G.J., Ballock, R.T., Walker, R.H., 1994**, 'Suboptimal (Thin) Distal Cement Mantle Thickness as a Contributory Factor in Total Hip Arthroplasty Femoral Component Failure', *Journal of Arthroplasty*, Vol. 9(2), pp. 143 - 149.

- Stone, M.H., Wilkinson, R., Stother, I.G., 1991**, 'Variation in Applied Force During Insertion of Cemented Femoral Prostheses', *International Communication*, Vol. 14, pp. 709 - 803.
- Stone, M.H., Wilkinson, R., Stother, I.G., 1989**, 'Some Factors Affecting the Strength of the Cement-Metal Interface', *Journal of Bone and Joint Surgery*, 71B, pp. 217 - 221.
- Sutherland, C.J., Wilde, A.H., Borden, L.S., Marks, K.E., 1982**, 'A Ten Year Follow-up of One Hundred Consecutive Muller Curved-Stem Total Hip-Replacement Arthroplasties', *Journal of Bone and Joint Surgery* 64A, pp. 970 - 982,.
- Szivek, J.A., Gealer, R.L., 1991**, 'Comparison of the Deformation Response of Synthetic Femora During Simulated One-Legged Stance', *Journal of applied Biomaterials*, Vo.1, pp. 277 - 280.
- Szivek, J.A., Weng, M., Karpman, R., 1990**, 'Variability in the Torsional and Bending Response of a Commercially Available Composite Femur', *Journal of Applied Biomaterials*, Vol. 1, pp. 183 - 186.
- Taylor, S.J.G., Perry, J.S., Meswania, J.M., Donaldson, N., Walker, P.S., Cannon, S.R., 1997**, 'Telemetry of Forces from Proximal Femoral Replacements and Relevance to Fixation', *Journal of Biomechanics*, Vol. 30, No. 3, pp. 225 - 234.
- Thompson, F.R., 1952**, 'Vitallium Intramedullary Hip Prosthesis: Preliminary Report', *New York Journal of Medicine*, Vol. 52, pp. 301 - 3020.
- Turner, R.H., Scheller, A.D., McKay, W.F., VanSyckle, P.B., 1983**, 'Cement Intrusion Pressure as a Function of Stem Design', 29th Annual ORS, pp. 333.
- Vander Sloten, J., Labey, L., Van Audekercke, R., Helsen, J., Van der Perre, G., 1993**, 'The Development of a Physiological Hip Prosthesis: The Influence of Design and Materials', *Journal of Materials Science: Materials in Medicine*, Vol. 4, pp. 407 - 414.
- Vanderby, R., Manley, P.A., Kohles, S.S., McBeath, A.A., 1992**, 'Fixation Stability of Femoral Components in a Canine Model', *Journal of Orthopaedic Research*, Vol. 10, pp.300 - 309.
- Verdonschot, N., Huiskes, R., 1997**, 'Acrylic Cement Creeps But Does Not Allow Much Subsidence of Femoral Stems', *Journal of Bone and Joint Surgery*, Vol. 74-B, No. 4, pp. 665 - 669.
- Verdonschot, N., Huiskes, R., 1995**, 'Dynamic Creep Behaviour of Acrylic Bone Cement', *Journal of Biomedical Materials Research*, Vol. 29, pp. 575 - 581.
- Verdonschot, N., Huiskes, R., 1994**, 'Creep Behavior of Hand-Mixed Simplex P Bone Cement Under Cyclic Tensile Loading', *Journal of Applied Biomaterials*, Vol. 5, pp. 235 - 243.

- Viceconti, M., Casali, M., Massari, B., Cristofolini, L., Bassini, S., Toni, A., 1996**, 'The 'standardized femur program' proposal for a reference geometry to be used for the creation of finite element models of femur', *Journal of Biomechanics*, Vol. 29 (9), pp. 1214 - 1241.
- Walker P.S., Mai S.F., Cobb A.G., Bentley G., Hua J., 1995**, 'Prediction of Clinical Outcome of THR from migration measurements on standard radiographs', *Journal of Bone and Joint Surgery*, Vol. 77-B, pp. 705 - 714.
- Walker, P.S., Schneeweist, D., Murphy, S., Nelson, P., 1987**, 'Strains and Micromotions of Press-Fit Femoral Stem Prostheses', *Journal of Biomechanics*, Vol. 20, pp. 693 - 702.
- Weightman, B., Freeman, M.A.R., Revell, P.A., Braden, M., Albrektsson, B.E.J., Carlson, L.V., 1987**, 'The Mechanical Properties of Cement and Loosening of the Femoral Component of Hip Replacements', *Journal of Bone and Joint Surgery*, Vol. 69-B, pp. 558 - 564.
- Wiles, P., 1958**, 'The Surgery of the Osteo-Arthritic Hip', *British Journal of Surgery*, Vol. 45, pp. 488 - 497.
- Whiteside L.A., Easley J.C., 1989**, 'The Effect of Collar and Distal Stem Fixation on Micromotion of Femoral Stem in Uncemented Total Hip Arthroplasty', *Clinical Orthopaedics Related Research*, No. 239, pp.145 -153.
- Willert, H.-G., Broback, L.-G., Buchhorn, G.H., Jensen, P.H., Koster, G., Lang, I., Ochsner, P., Schenk, R., 1996**, 'Crevice Corrosion of Cemented Titanium Alloy Stems in Total Hip Replacement', *Clinical Orthopaedics and Related Research.*, No. 333, pp 51 - 75.
- Wirta, J., Eskola, A., Hoikka, V., Honkanen, V., Lindholm, S., Santavirta, S., 1993**, 'Revision of Cemented Hip Arthroplasties. 101 hips followed for 5 (4 - 9) years', *Acta Orthopaedica Scandinavia*, Vol. 64(3), pp. 263 - 267.
- Witt, J.D., Swann, M., 1991**, 'Metal Wear and Tissue Response in Failed Titanium Alloy Total Hip Replacements', *Journal of Bone and Joint Surgery*, Vol. 73-B, No. 4, pp. 559 - 563.
- Wixson, R.L., 1992**, 'Do We Need to Vacuum Mix or Centrifuge Cement?', *Clinical Orthopaedics and Related Research*, No. 285, pp. 84 - 90.
- Wright, T.M., Robinson, R.P., 1982**, 'Fatigue Crack Propagation in Polymethy Methacrylate Bone Cements', *Journal of Materials Science*, Vol. 17, pp. 2463 - 2468.
- Zahiri, C.A., Schmalzried, T.P., Szuszczewick, S., Amstutz, C., 1998**, 'Assessing Activity in Joint Replacement Patients', *Journal of Arthroplasty*, Vo. 13, No. 8, pp. 890 - 895.

APPENDIX A

Table A1: Protocol for determination of the cam profile.

Step	Description
1.	Import the frontal two dimensional profile of the insertion machine, the femoral clamp and the composite femur into 3D Studio™ (hereafter called 3DS).
2.	Import a profile of the prosthesis into 3DS. Typically this profile will be constructed in a drawing package such as Autocad™.
3.	Position the prosthesis into the clamped composite femur, in the required final orientation.
4.	Clone the prosthesis, and shade it. This will act as a <i>shadow</i> which will help in designing the insertion path.
5.	Draw a circle of radius 17.5 mm (this is the radius of the roller that will eventually follow the cam) at the centre of the head of the prosthesis; <i>circle A</i> .
6.	Draw a circle of diameter 150 mm (<i>circle B</i>), with its edge placed on the centre of <i>circle A</i> .
7.	Place a circle of radius 17.5 mm (<i>circle C</i>) along the perimeter of circle B. The exact position of <i>circle C</i> along the radius of <i>circle B</i> , is not critical to subsequent steps, as it can be altered later. As an initial step, position <i>circle C</i> 45 degrees counter clockwise from the vertical, as drawn through the centre of circle B.
8.	Link the two circles, as <i>children</i> of the prosthesis, in 3DS terminology, this means that the circles will follow the motion of the prosthesis.
9.	When the prosthesis profile is imported into 3DS, its pivot point is automatically fixed at its geometrical centre. Adjust the pivot point of the prosthesis so that it is no longer at the geometrical centre, but at a point mid way along the length of the collar. In reality, any position for the pivot point of the prosthesis can be chosen; however iteratively, it has been found that this point allows the user greatest flexibility in rotating the prosthesis into its required final seated position.
10.	Animate a path of deinsertion, where the prosthesis is incrementally removed from the femur. During deinsertion 10 key points 10 steps apart are defined: these are the positions through which the prosthesis is constrained to go through. Throughout deinsertion, an attempt should be made to keep the prosthesis within the <i>shadow</i> of its final position, whilst ensuring that the path of removal is as smooth as possible. This can be achieved by maintaining a feature of the prosthesis, such as the lateral face, aligned with a feature of the shadow throughout its deinsertion.
11.	Plot the trajectories of circle A - TrajA
12.	Plot the trajectories of circle C - TrajC
13.	If the trajectories have a rough undulating surface, edit the animated path of deinsertion to smoothen the undulations. This is an iterative process.
14.	When the trajectories are as smooth as considered possible, convert both trajectories to splines.

15.	Move the prosthesis to its fully deinserted position.
16.	Move the cheek plate (see Figure 3.12) so that the centre of the bearing which runs along TrajA is centered with the centre of <i>circle A</i> .
17.	Rotate the cheek plate so that the centre of the bearing which runs along TrajC is centered with the centre of <i>circle C</i> .
18.	Draw a circle (<i>circle D</i>), diameter 35 mm, centered on the <i>circle A</i> .
19.	Draw a circle (<i>circle E</i>), diameter 35 mm, centered on <i>circle C</i> .
20.	Draw a third circle (<i>circle F</i>), diameter xmm, on the bearing attaching the cheek plate and the end of the roller arm.
21.	Make <i>circle D</i> a child of <i>circle A</i> .
22.	Make <i>circle E</i> a child of <i>circle C</i> .
23.	Make <i>circle F</i> a child of <i>circle C</i> .
24.	Make the cheek plate a child of <i>circle C</i> .
25.	Run an animation. The cheek plate should remain attached to circle A and circle C, so that the cheek plate follows the path of insertion as it would in reality.
26.	There is a possibility that in determining a path of insertion, that the cheek plate may collide with the perpendicular slide rails. Run the animation step by step, and measure the minimum gap that exists between the cheek plate and the guide rail during the insertion. If this gap is less than 0.5mm, crashing will occur. To prevent this from happening, the cam must be redesigned.
27.	Draw a vector indicating the line of action of the pneumatic cylinders. Follow this line of action throughout the animation. If the line of action acts outside the either circle A or circle C, the cam must be redesigned.
28.	To redesign the cam, consider circle B. Pick another point on the perimeter of this circle.
29.	Construct a circle of diameter 35mm at the chosen point.
30.	Unlink any children from <i>circle C</i> and delete <i>circle C</i> .
31.	Repeat the procedure from step 6.
32.	When a suitable profile has been designed, export the two trajectories, trajA and trajB, and the insertion machine to a drawing package.
33.	Offset each of the trajectories by 17.5 mm, downwards.
34.	Offset the trajectory created by <i>circle A</i> by 17.5 mmm upwards (<i>trajoff</i>). This will assist in constructing the cam profile, by creating a barrier below which the material of the cam cannot exist. This ensures that the roller will not crash into the profiled plate.
35.	Construct the cam profile. The profile should not impinge on the <i>trajoff</i> , six pillars should be used to attach the profile to the backplate of the insertion machine, the holes to be drilled through the cam, should pickup on any pre-existing holes in the backplate. If the cam is of such a different shape that the preexisting position of the holes in the backplate cannot be used, ensure that the new holes are offset by the original ones, by at least 20mm.
36.	Export the cam profile in .dxf format to APS software.

37.	Move the cam profile, so that one of its edges are centered at (0,0,0).
38.	Break the profile at certain junctions, depending on the method of machining that will be used. For example it is sometimes necessary to machine the cam profile in two separate runs - one run for the top trajectory, and a second for the lower trajectory. The way in which the profile is broken down in separate sections will also depend on the way in which the plate will be clamped in the milling machine.
39.	Choose a slot drill type, the number of passes of the cutting tool in which to manufacture the cam , decide on the method of clamping, and design the appropriate cutting program.
40.	Download the program to the CNC milling machine, and machine the profile from mild steel plate.

Table A2: Alignment Femur Set-up Procedure.

Step	Description
1.	Place a composite femur on the alignment plate. Pin and bolt the casting bracket onto the alignment plate.
2.	Fill the casting bracket with PMMA and allow the PMMA to set.
3.	Pin and bolt two measurement brackets (see Figure 3.9) to the alignment plate.
4.	Resect the femoral head, drill, and ream the medullary cavity, using the locator cylinder as a drilling guide.
5.	Mill out the alignment slots along the medial, lateral, anterior and posterior sides of the composite femur
6.	Remove the alignment femur from the alignment plate.

Table A3: A protocol to perform an insertion of a prosthesis into a composite femur using the femoral insertion machine

Some terminology that is used in Table 3 with reference to the femoral insertion machine:

insertion machine	specially designed machine for insertion of a prosthesis into a composite femur along a defined path, with a predetermined final seated-position;
alignment femur	a composite femur with a reamed medullary cavity, a resected femoral head, alignment slots milled along its coronal and sagittal planes and a <i>casting bracket</i> bonded to it using PMMA
casting bracket	a bracket made of mild steel containing a PMMA casting around the <i>alignment femur</i> so that when it is pinned and bolted to the <i>alignment plate</i> , it reproducibly positions the <i>alignment femur</i> ;
alignment plate	a plate which reproducibly locates a composite femur

alignment slots	longitudinal slots on the sides of a composite femur
cam	a profiled plate which describes the insertion path and final orientation of a prosthesis within a femoral cavity in the coronal plane
carriage	two rollers connected via front and back cheek plates, onto which a prosthesis is clamped. The two rollers rest on the cam profile, and are moved along the cam via pneumatic cylinders
measurement bracket	a bracket which is located around the alignment femur and fixed to the alignment plate. It has holes on its four orthogonal sides which allow the prosthesis to be pushed into the specified position as determined in the animation software.
positioning pins	pins with pointed ends, which are placed through orthogonal holes in the measurement brackets. Micrometer heads push the pins against the prosthesis during the alignment procedure. When the prosthesis has been pushed into the position as defined in the animation software, the positioning pins are locked in place.
spherical joint	a lockable ball and socket joint onto which a toolmaker's clamp is mounted. It allows rotational freedom of motion so that the toolmakers clamp can be positioned around the prosthesis head after the prosthesis has been aligned in the alignment femur.
locator cylinder	a mild steel cylinder that is fixed to the <i>alignment plate</i> , through which the drill must pass before contacting the composite femur that is clamped on the <i>alignment plate</i> .
xy table:	positioning table used for fine adjustment of the <i>alignment plate</i> during set up of the prosthesis for insertion.
test femur	a composite femur that is clamped to the alignment plate. Its cancellous cavity is reamed, and its femoral head is resected
LVDT holder	aluminium bracket which is attached to a <i>test femur</i> (co-planar with the <i>subsidence measurement target device</i>) which holds the six measurement LVDTs;
Migration measurement device mechanism	device used to measure subsidence of prosthesis relative to the outer cortex of a <i>test femur</i> —consists of <i>subsidence measurement target device</i> and <i>LVDTs holder</i> ;
migration target device:	device attached to a test prosthesis by means of press-fit pins, against which LVDTs measure displacement;

Step	Description
1.	Pin and bolt the <i>alignment femur</i> and the two <i>measurement brackets</i> to the <i>alignment plate</i> .
2.	Pin and bolt the <i>alignment plate</i> to an xy table.
3.	Insert the <i>adjustable base</i> through the xy table so that it is sticking up through

	the <i>alignment femur</i> .
4.	Place the prosthesis in the cavity of the <i>alignment femur</i> so that its tip is resting on the <i>adjustable base</i> .
5.	Activate the pneumatics so that the <i>head coupling</i> is in its end position along the <i>cam</i> profile.
6.	Place four positioning pins through the holes in the distal <i>measurement bracket</i> . Place four micrometer heads in the <i>measurement bracket</i> in predefined positions.
7.	Adjust the distal four micrometer heads and vary the height of the tip using the adjustable base, until the micrometer heads read the predetermined values, as determined in the animation.
8.	When the readout from the four micrometer heads are equivalent to that determined in 3DS, tighten the <i>positioning pins</i> in place using grub screws.
9.	Retract the adjustable base so that it is no longer in contact with the tip of the prosthesis.
10.	Place four micrometers into the proximal measurement bracket in predefined positions.
11.	Adjust the four micrometer heads until they read the predetermined values.
12.	When the readout from the four micrometer heads are similar to that estimated in 3DS, tighten the positioning pins in place using grub screws.
13.	Open the <i>femoral head clamp</i> . Adjust the xy table, so that the head of the prosthesis is loosely positioned within the <i>femoral head clamp</i> .
14.	Clamp the xy table.
15.	Loosen the <i>head coupling</i> , and tighten the <i>femoral head clamp</i> around the head of the prosthesis; ensuring that the surfaces of the clamp contact all sides of the head of the prosthesis.
16.	Tighten the <i>head coupling</i> .
17.	Release the grub screws that are holding the <i>positioning pins</i> in place.
18.	Deinsert the prosthesis.
19.	Remove the <i>alignment plate</i> from the insertion machine, and remove the <i>alignment femur</i> from the <i>alignment plate</i> .
20.	Position the <i>test femur</i> on the <i>alignment plate</i> .
21.	Resect the test femoral head and drill the medullary cavity.
22.	Manually rasp the proximal medullary cavity using the surgical instruments as supplied by the manufacturers of the prosthesis that will be inserted..
23.	Pin the <i>alignment plate</i> to the xy table. Check that the xy table has not moved.
24.	Mix the bone cement and insert it into the prepared medullary cavity of the test femur.
25.	Activate the pneumatics to push the prosthesis along the cam profile into the prepared test femur.
26.	Remove the alignment plate and implanted test femur. Remove the implanted test femur from the alignment plate.

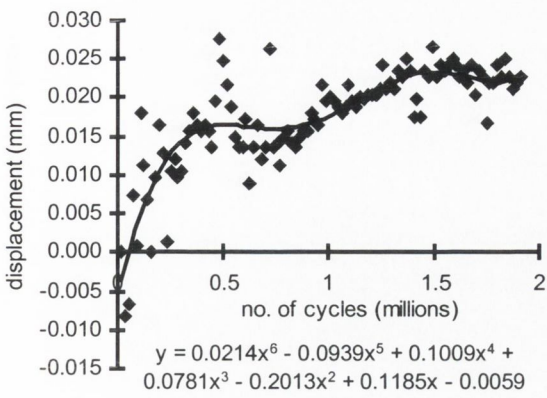
APPENDIX B

Table B: Protocol for use of the migration measurement device.

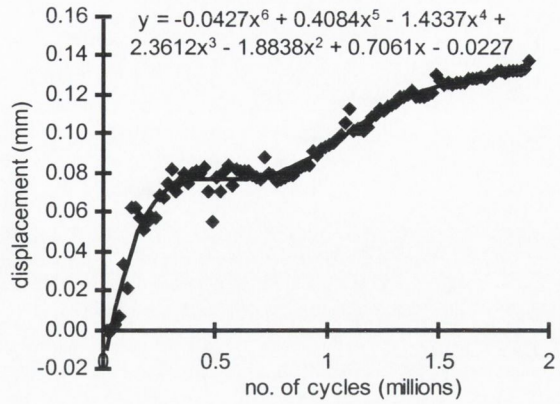
Step	Description
1.	The prosthesis is mounted in a suitable holding jig see Figure 3.20 and Figure 3.21.
2.	If the anterior face of the prosthesis is not flat, the surface is milled to produce a horizontal flat - typical depth of machining is 0.2mm.
3.	Two holes each 1.95 mm diameter for attachment of the device are drilled normal to the machined flat.
4.	The drilled holes are plugged with silicone rubber to prevent the ingress of cement into the holes during insertion of the prosthesis.
5.	The prosthesis can now be prepared for insertion as per the steps defined in table A3.
6.	After step 16 in Table A3, measure the position of the drilled hole in the prosthesis relative to known features on the alignment plate. Although this is a crude measurement, if the prosthesis has been located correctly, the user will know here these holes should be located.
7.	Continue with steps 17 - 19 from Table A3.
8.	Mount the test femur in a milling machine. Machine a cavity 8mm in diameter through the femur in the position that will be coincident with the drilled holes in the prosthesis.
9.	Plug the hole on the anterior face with a PTFE solid cylinder, and plug the hole on the posterior face with a tapered cylinder of PTFE.
10.	Continue with step 20 - 26 from Table A3
	<u>AFTER STEM INSERTION:</u>
11.	Remove the PTFE plugs, revealing a thin cement layer that covers the plugged holes.
10	Carefully machine away the cement mantle covering the subsidence measurement device holes.
11	Remove the silicone rubber plugs from the stem of the prosthesis exposing the holes for press-fitting the subsidence measurement target device.
12	Mount the specimen on a drilling machine and press fit the attachment cylinder (see Figure 3.19) into the two holes on the prosthesis. Pressure is applied in a uniform manner, to minimise any damage that may be induced in the sample.
13	Remove the inserted femur from the alignment plate and cement its distal end into a mild steel cylindrical holder.
14	Fit the subsidence measurement target device to the attachment cylinder.
15	Locate the aligner over the migration measurement device
16	Pin and bolt the LVDT bracket to the underside of the aligner
17	Move the slider linkers and main tie so that the LVDT bracket is loosely joined with the femoral ring.
18	Place four pointed bolts through the femoral ring, tighten them into the wall of the femur, then lock them against the femoral ring
19	Tighten the grub screws against the ties, and afterwards lock the ball and socket joints in place.

- | | |
|----|---|
| 20 | Remove the aligner. |
| 21 | Attach the LVDTs to the data acquisition system.. |
| 22 | Adjust the LVDTs so that they give a reading that is as close to zero as possible.
This represents the mid range of the LVDTs. |
| 23 | Record the readings from the LVDTs. |

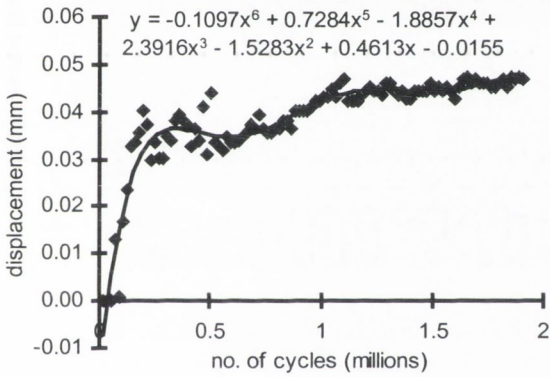
APPENDIX C



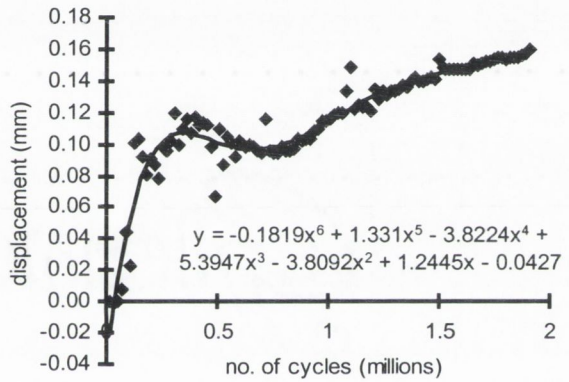
(a) LVDT1



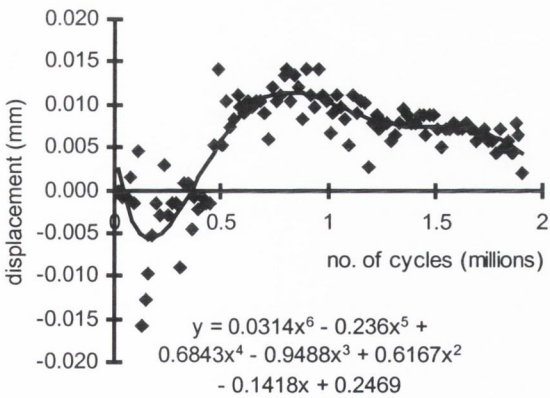
(b) LVDT2



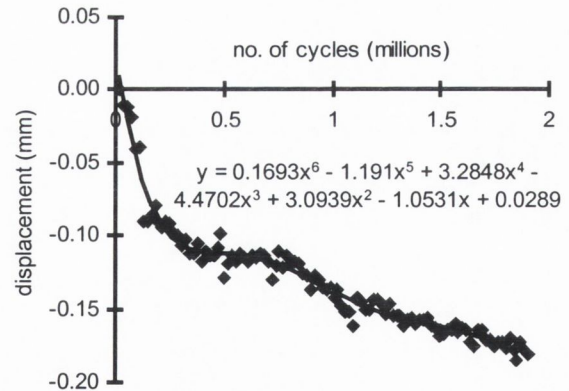
(c) LVDT3



(d) LVDT4

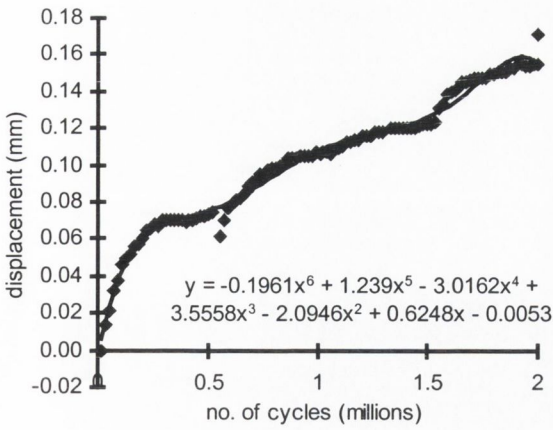


(c) LVDT5

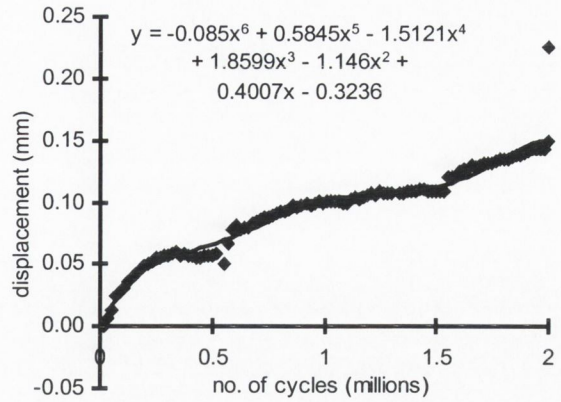


(d) LVDT6

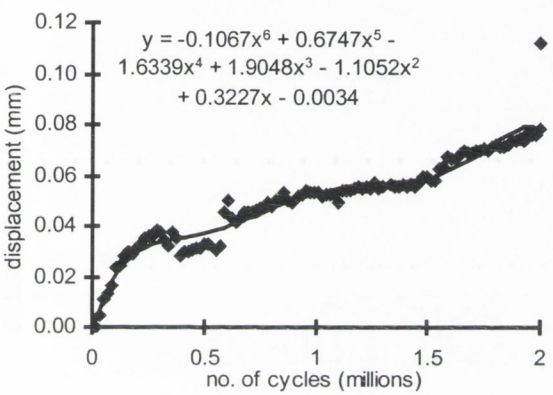
Figure C1: The displacements computed from the LVDTs as labeled in Figure 3.18 during the cyclic loading of Lubinus 1. Sixth order polynomial curves have been fitted to the data.



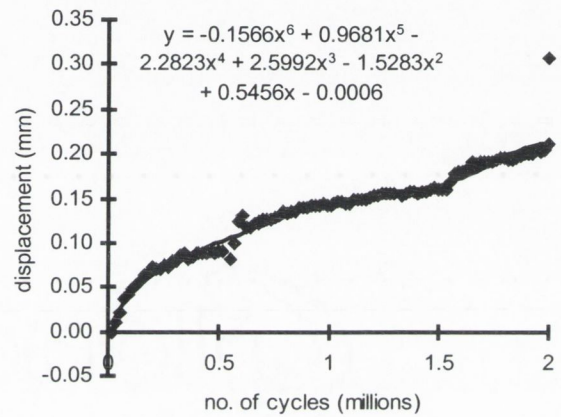
(a) LVDT1



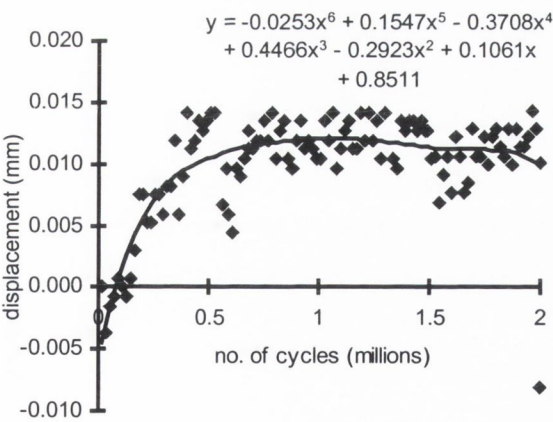
(b) LVDT2



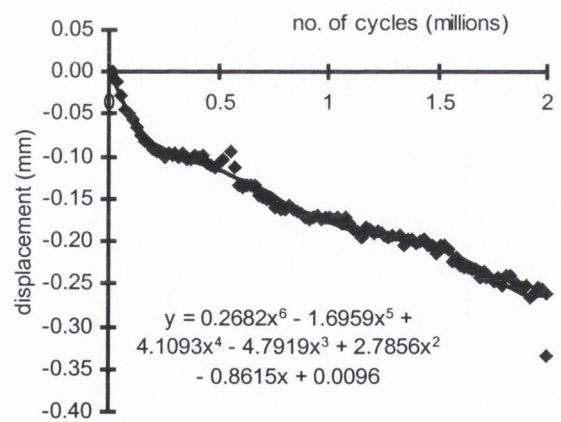
(c) LVDT3



(d) LVDT4

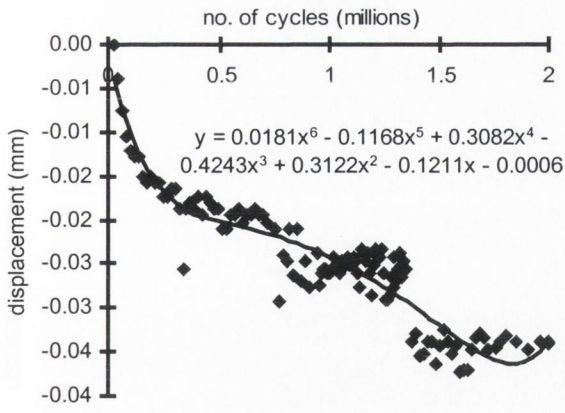


(e) LVDT5

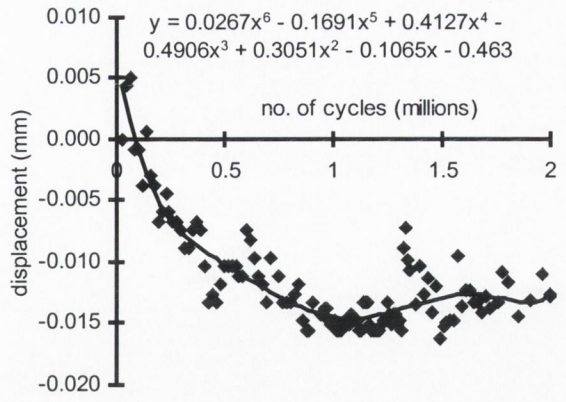


(f) LVDT6

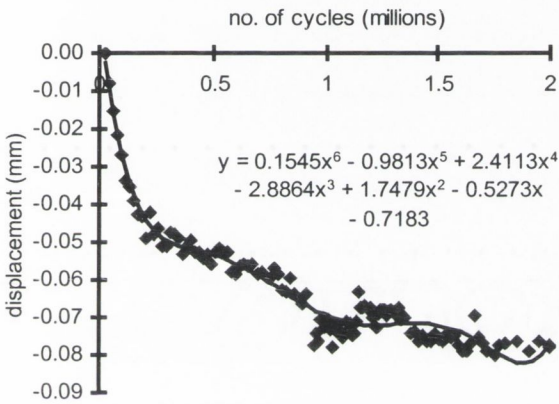
Figure C2: The displacements computed from the LVDTs as labeled in Figure 3.18 during the cyclic loading of Lubinus 2. Sixth order polynomial curves have been fitted to the data.



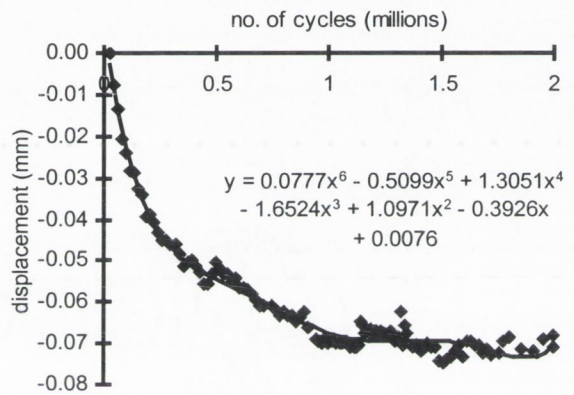
(a) LVDT1



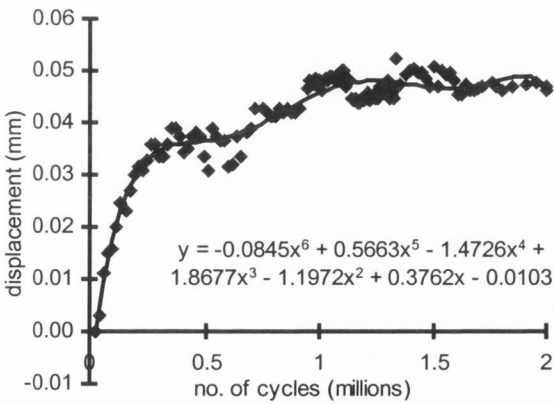
(b) LVDT2



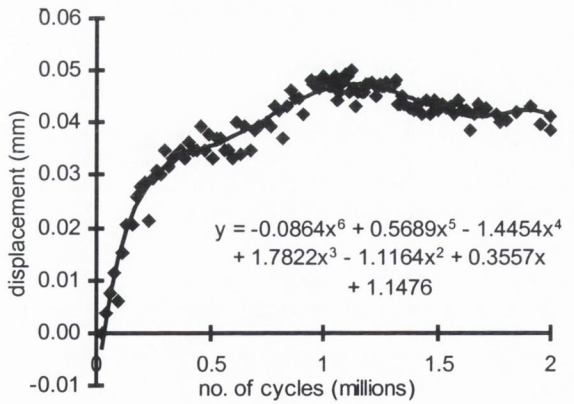
(c) LVDT3



(d) LVDT4

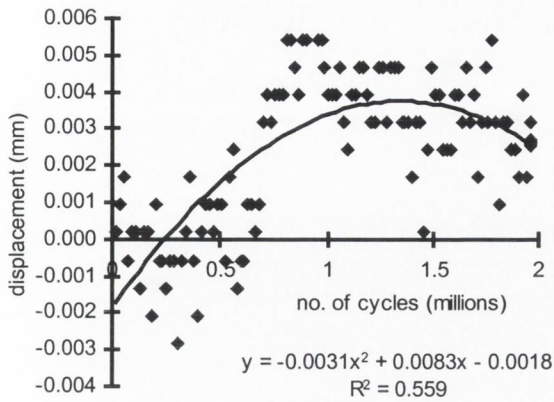


(e) LVDT5

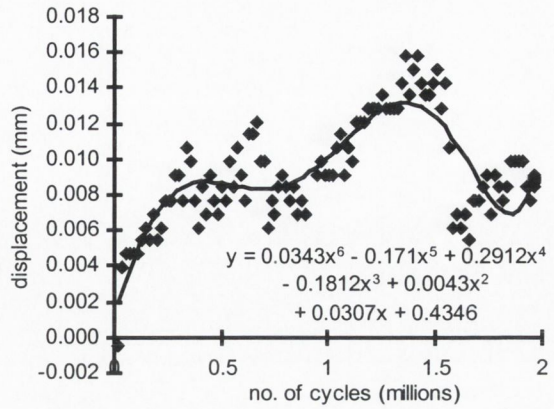


(f) LVDT6

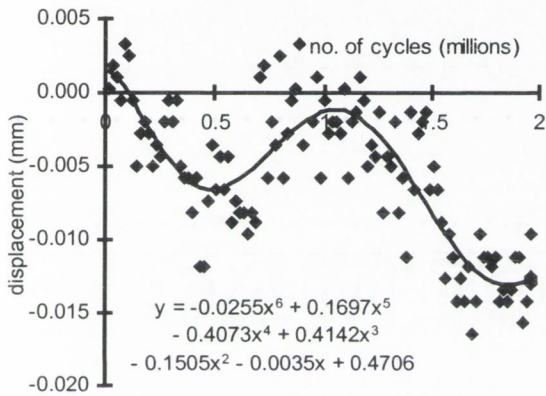
Figure C3: The displacements computed from the LVDTs as labeled in Figure 3.18 during the cyclic loading of Lubinus 3. Sixth order polynomial curves have been fitted to the data.



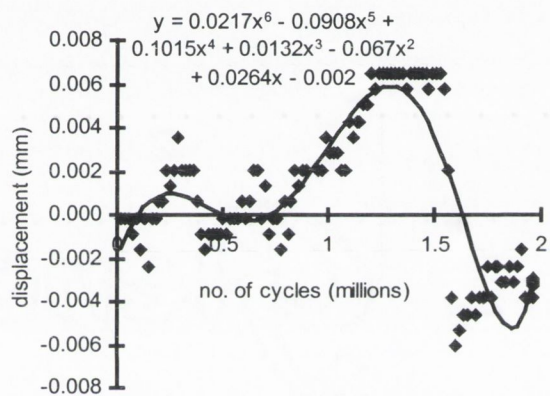
(a) LVDT1



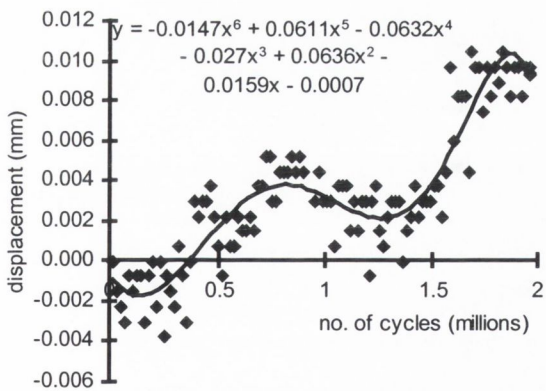
(b) LVDT2



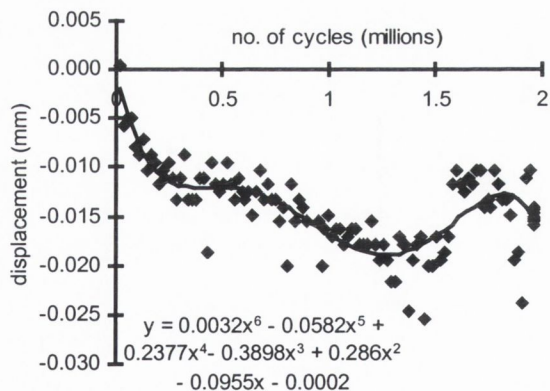
(c) LVDT3



(d) LVDT4

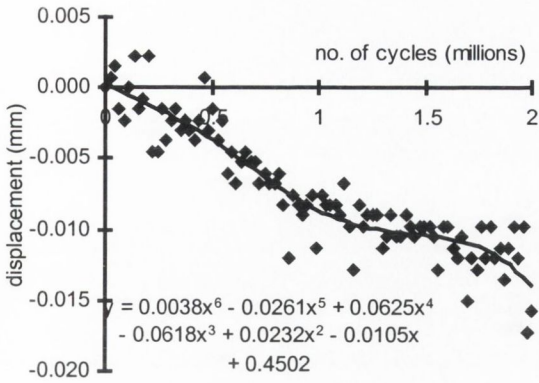


(e) LVDT5

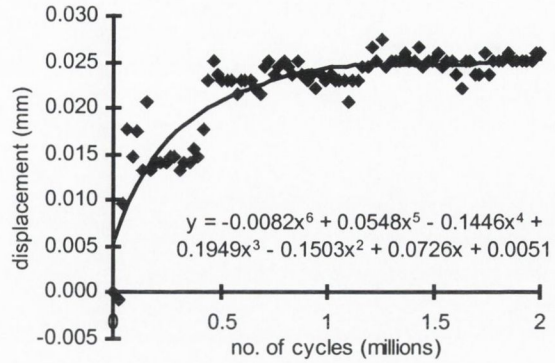


(f) LVDT6

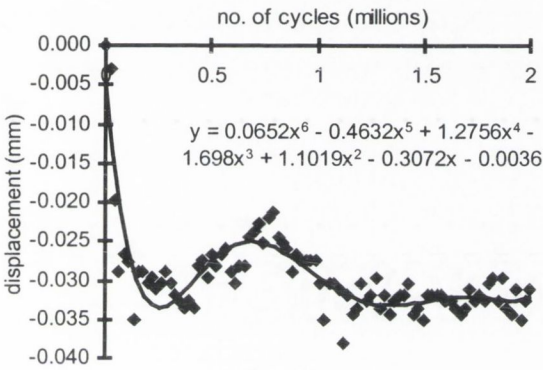
Figure C4: The displacements computed from the LVDTs as labelled in Figure 3.18 during the cyclic loading of Lubinus 4. Sixth order polynomial curves have been fitted to the data.



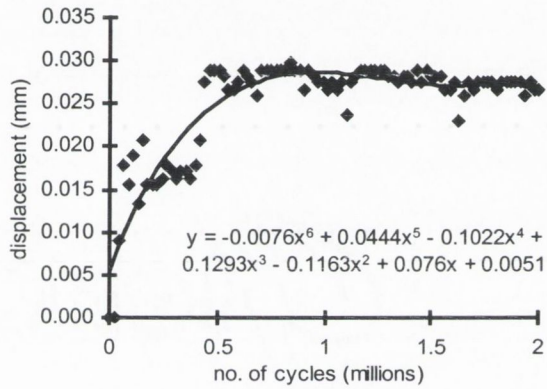
(a) LVDT1



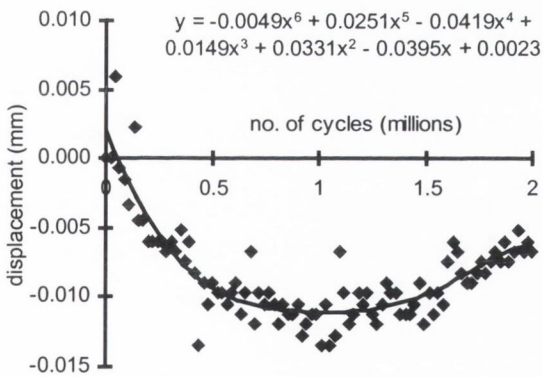
(b) LVDT2



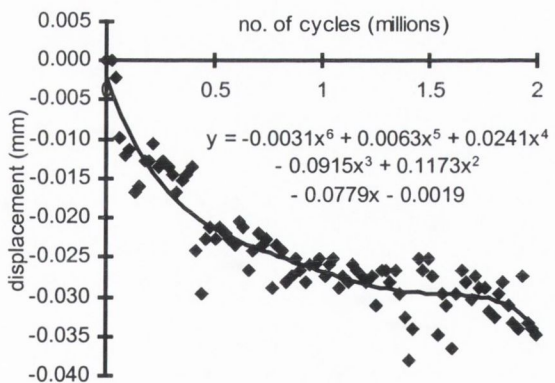
(c) LVDT3



(d) LVDT4

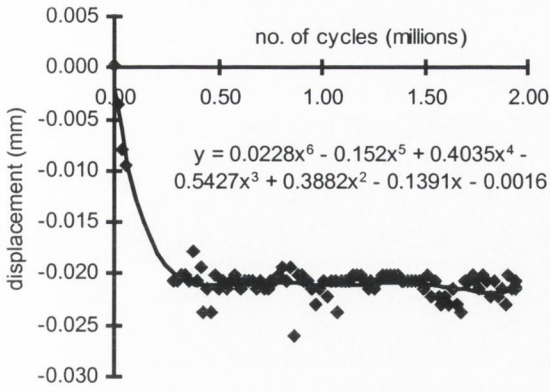


(e) LVDT5

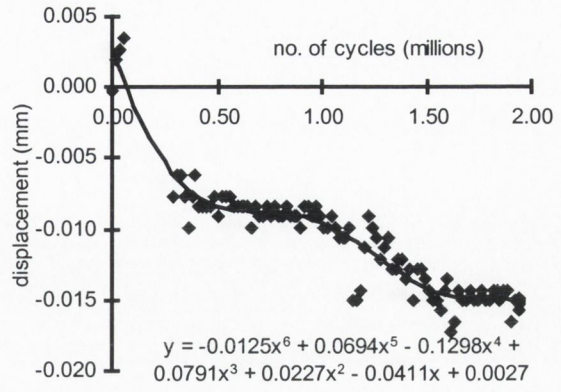


(f) LVDT6

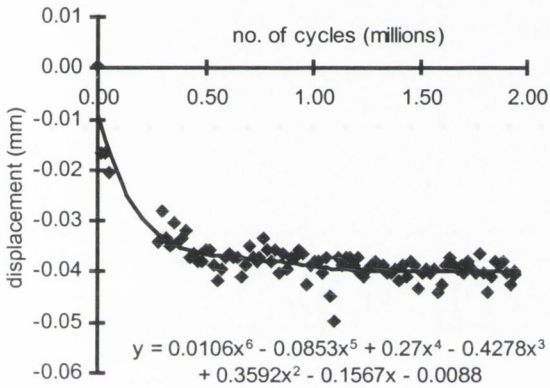
Figure C5: The displacements computed from the LVDTs as labelled in Figure 3.18 during the cyclic loading of Lubinus 5. Sixth order polynomial curves have been fitted to the data.



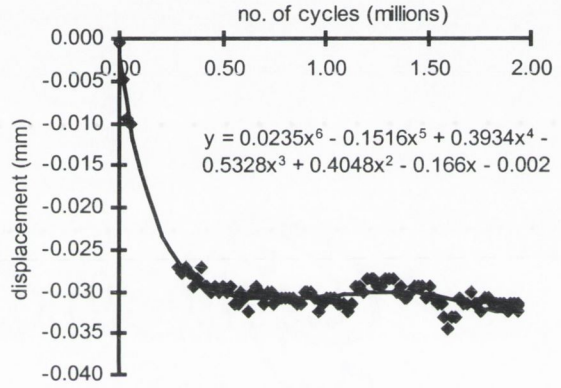
(a) LVDT1



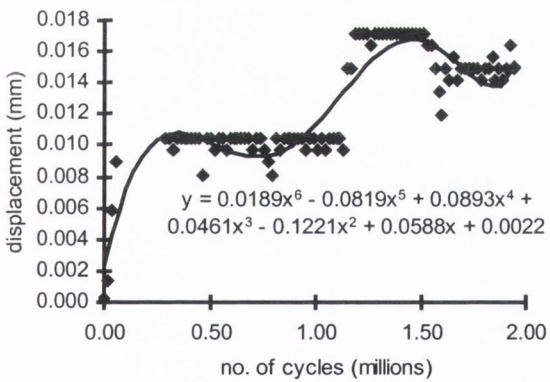
(b) LVDT2



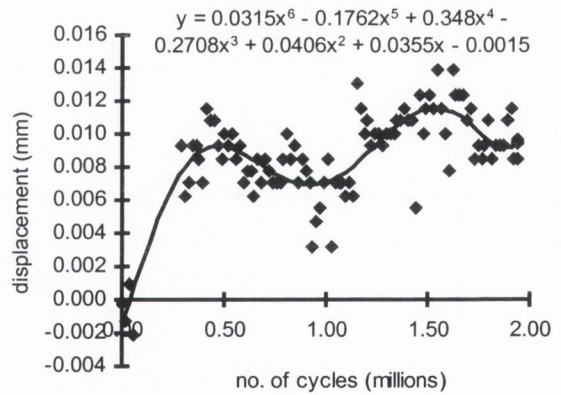
(c) LVDT3



(d) LVDT4

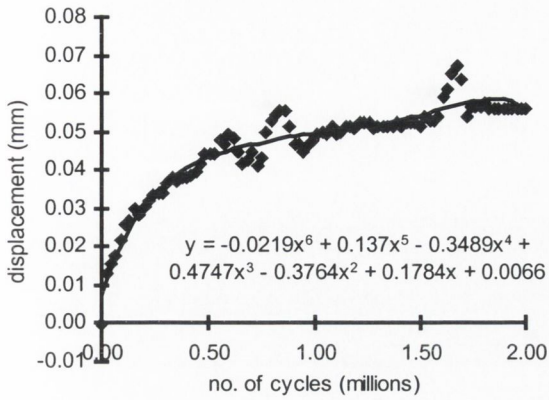


(e) LVDT5

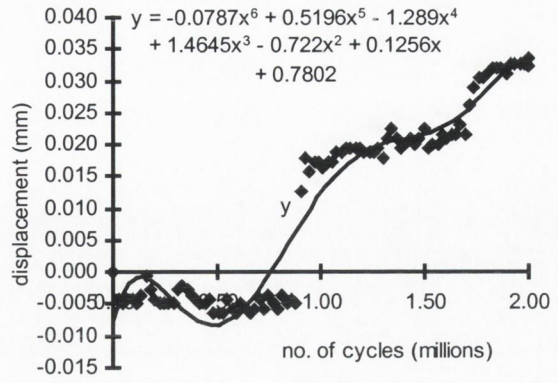


(f) LVDT6

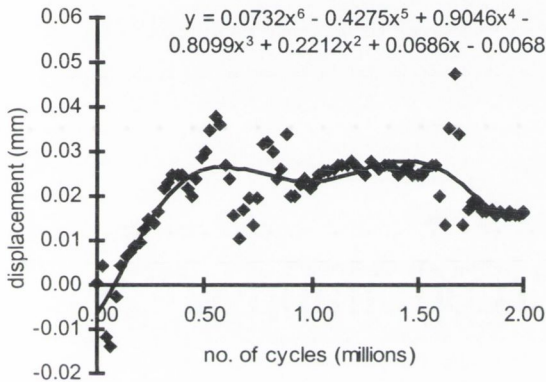
Figure C6: The displacements computed from the LVDTs as labelled in Figure 3.18 during the cyclic loading of Lubinus 3 with resorption. Sixth order polynomial curves have been fitted to the data.



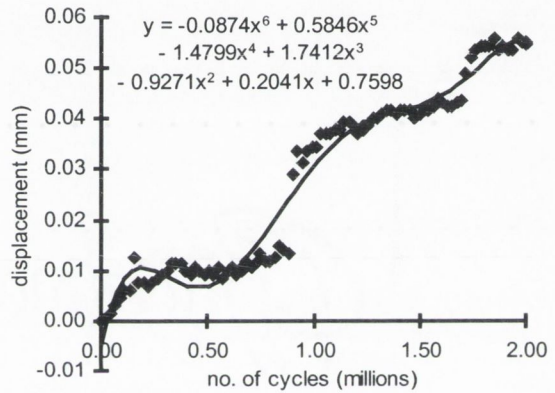
(a) LVDT1



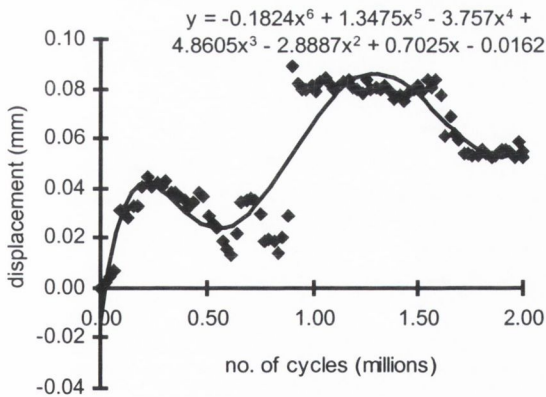
(b) LVDT2



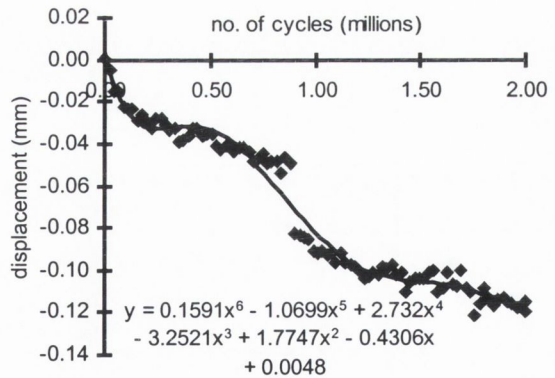
(c) LVDT3



(d) LVDT4

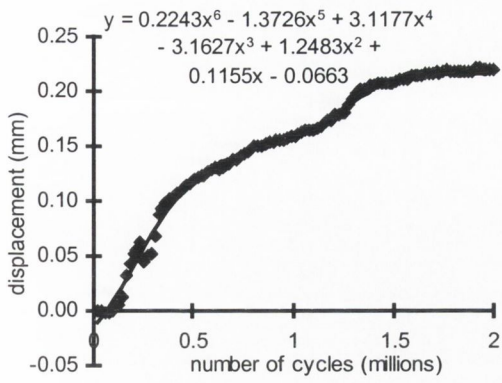


(e) LVDT5

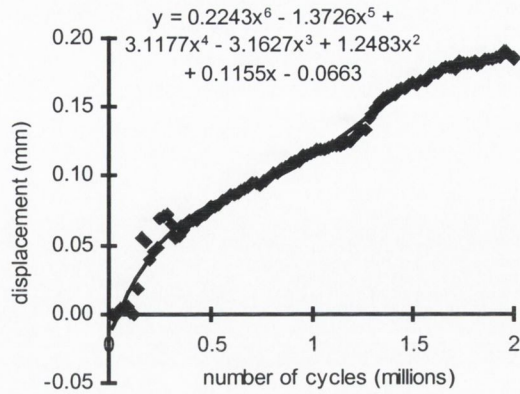


(f) LVDT6

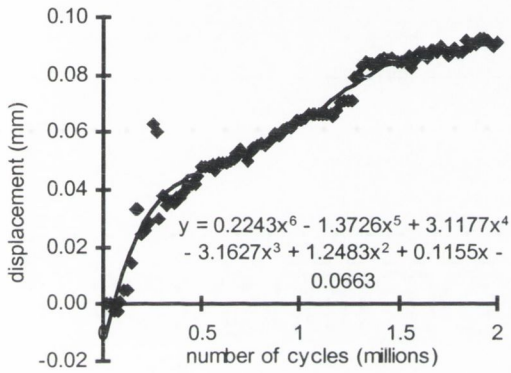
Figure C7: The displacements computed from the LVDTs as labelled in Figure 3.18 during the cyclic loading of Lubinus 2 with resorption. Sixth order polynomial curves have been fitted to the data.



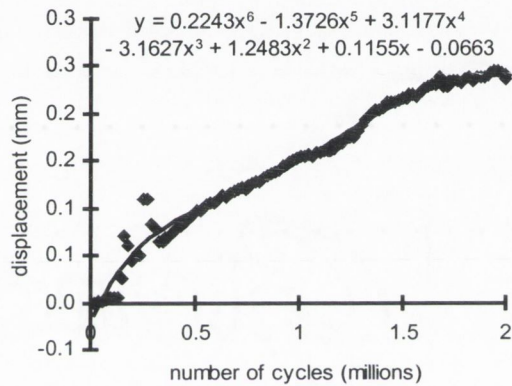
(a) LVDT1



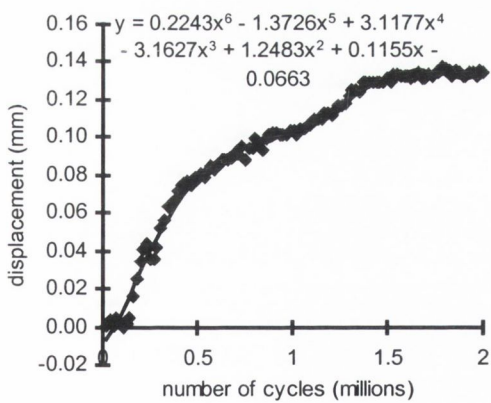
(b) LVDT2



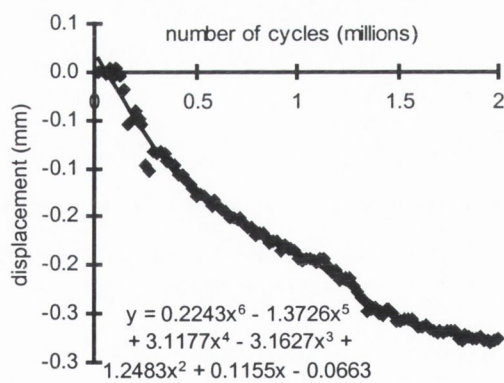
(c) LVDT3



(d) LVDT4

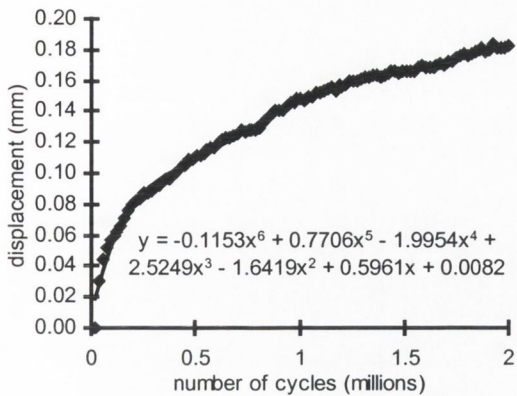


(e) LVDT5

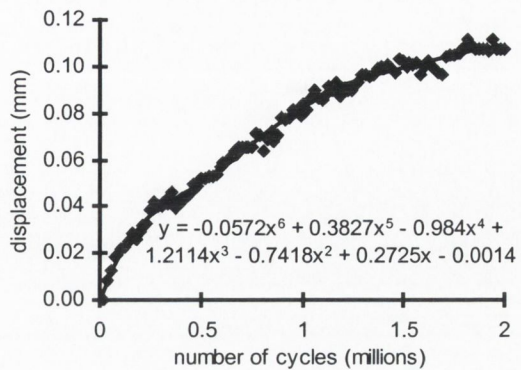


(f) LVDT6

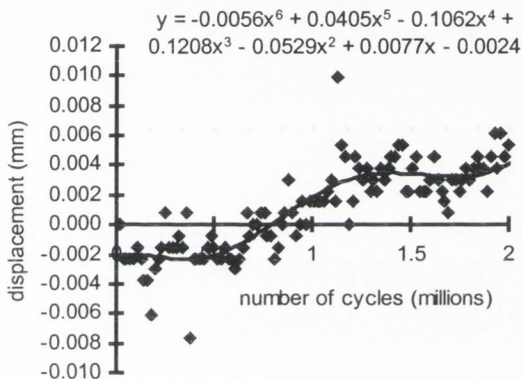
Figure C8: The displacements computed from the LVDTs as labelled in Figure 3.18 during the cyclic loading of Müller 1. Sixth order polynomial curves have been fitted to the data.



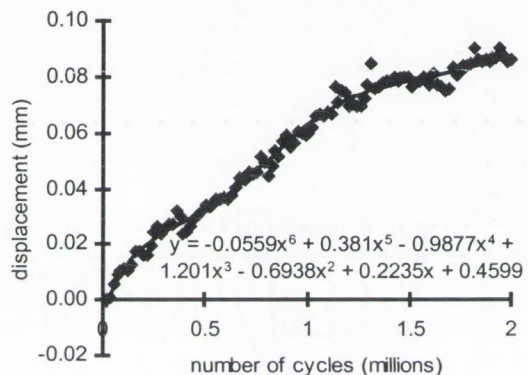
(a) LVDT1



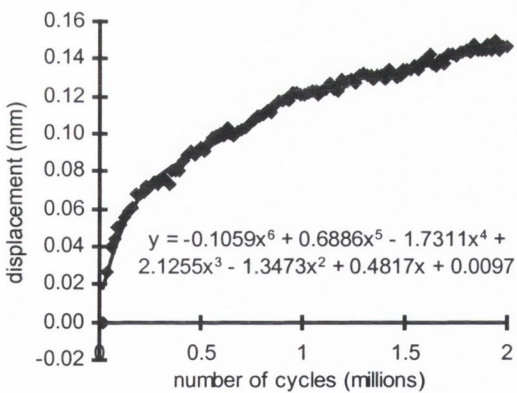
(b) LVDT2



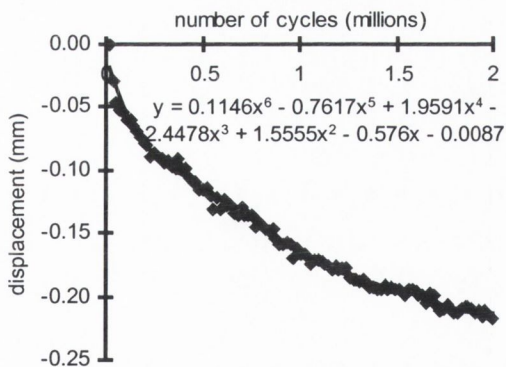
(c) LVDT3



(d) LVDT4

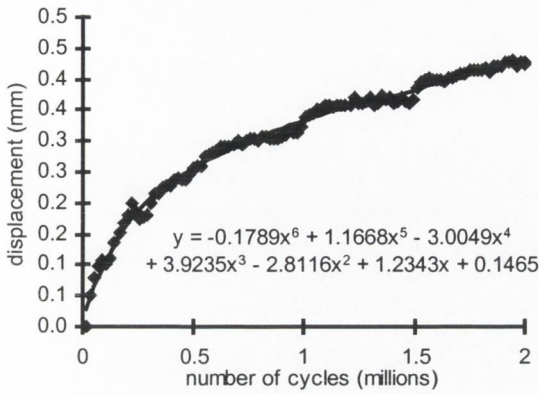


(e) LVDT5

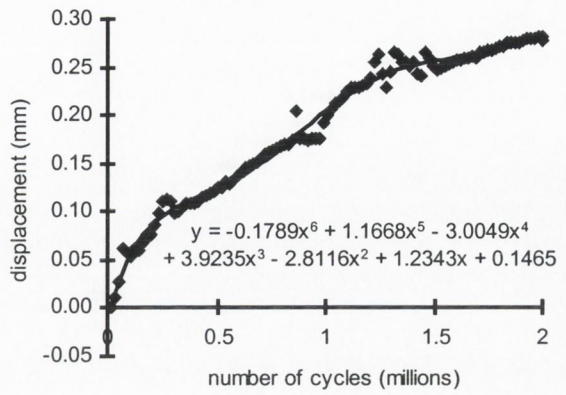


(f) LVDT6

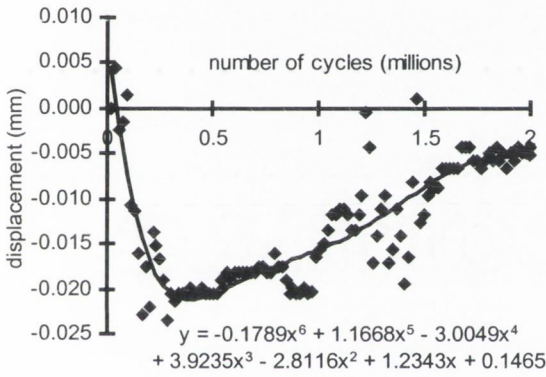
Figure C9: The displacements computed from the LVDTs as labelled in Figure 3.18 during the cyclic loading of Müller 2. Sixth order polynomial curves have been fitted to the data.



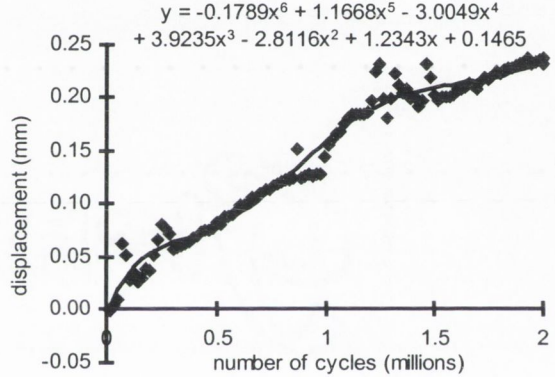
(a) LVDT1



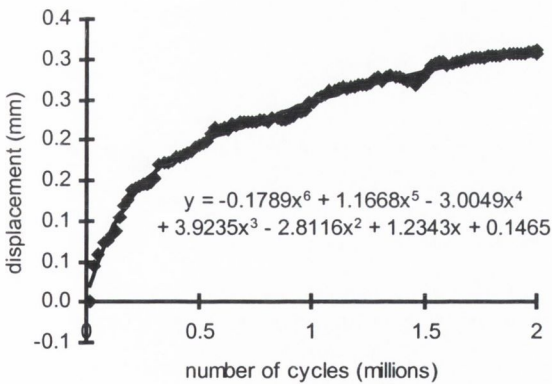
(b) LVDT2



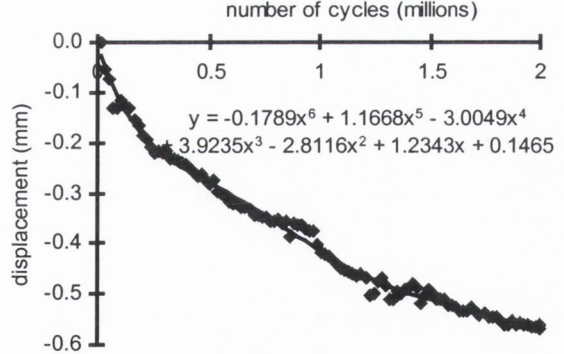
(c) LVDT3



(d) LVDT4

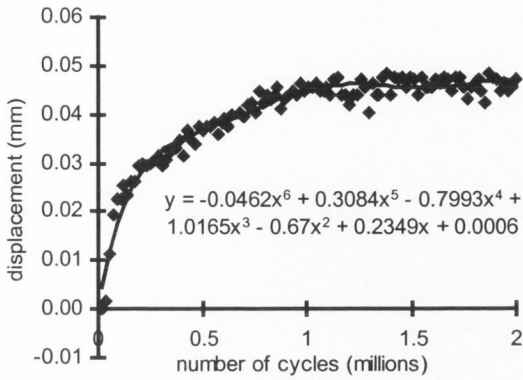


(e) LVDT5

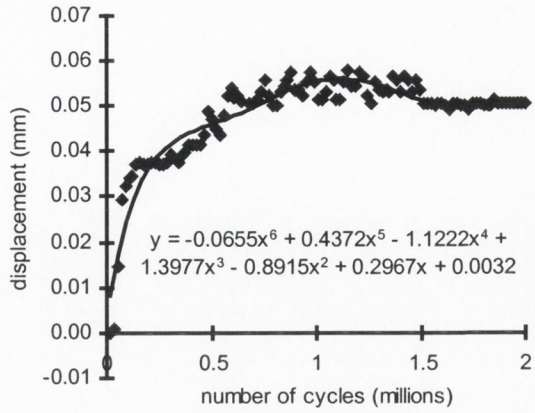


(f) LVDT6

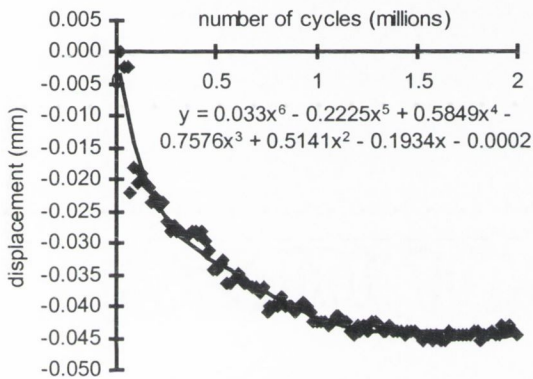
Figure C10: The displacements computed from the LVDTs as labelled in Figure 3.18 during the cyclic loading of Müller 3. Sixth order polynomial curves have been fitted to the data.



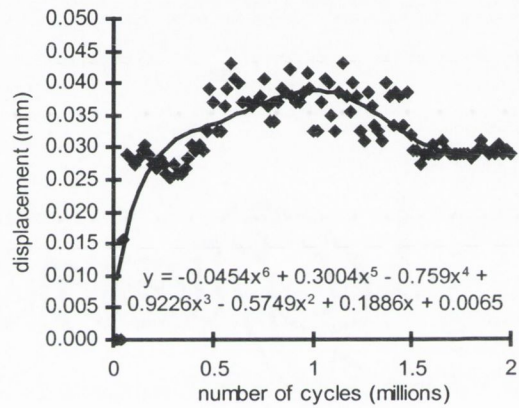
(a) LVDT1



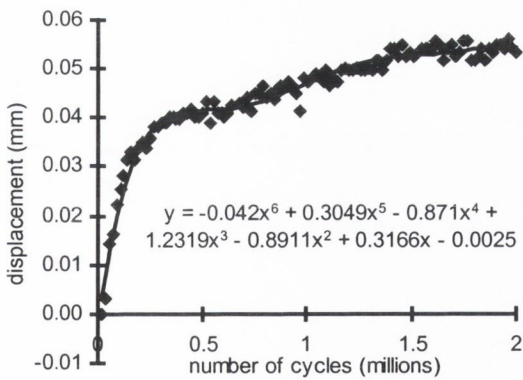
(b) LVDT2



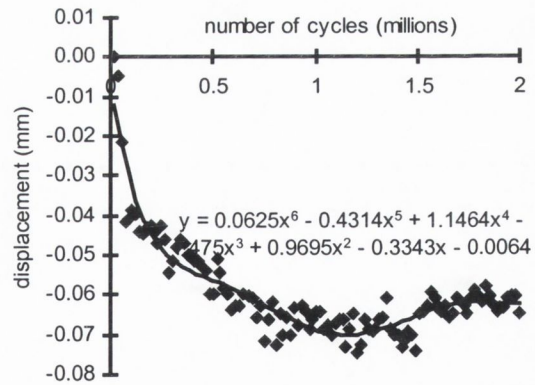
(c) LVDT3



(d) LVDT4

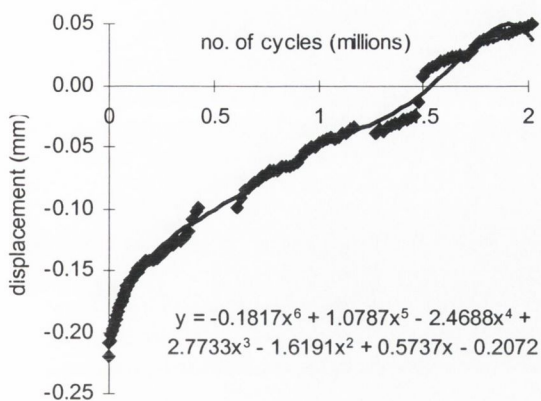


(e) LVDT5

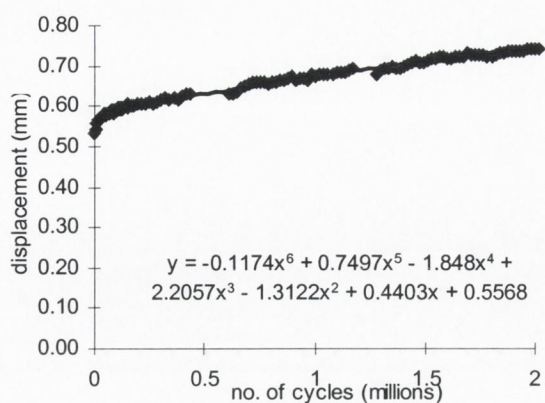


(f) LVDT6

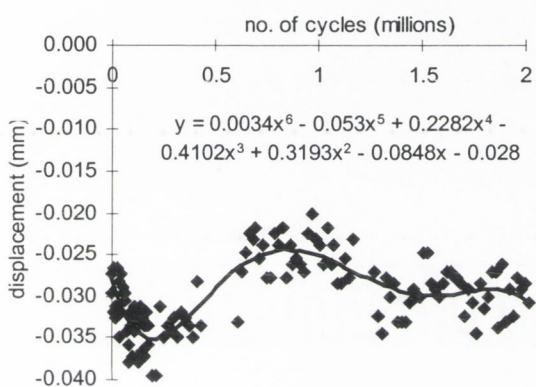
Figure C11: The displacements computed from the LVDTs as labelled in Figure 3.18 during the cyclic loading of Müller 4. Sixth order polynomial curves have been fitted to the data.



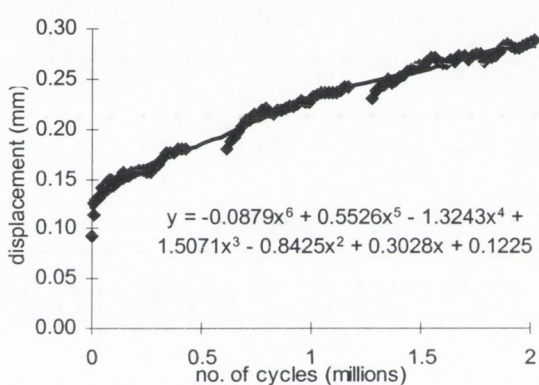
(a) LVDT1



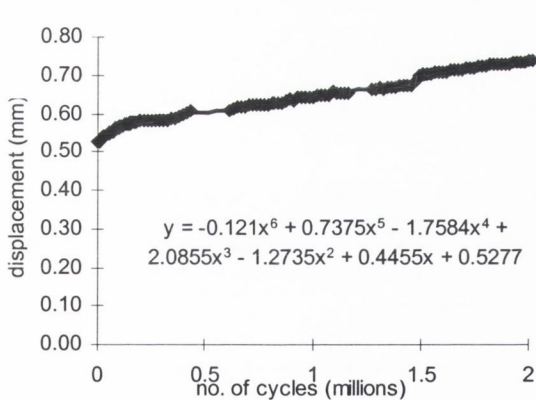
(b) LVDT2



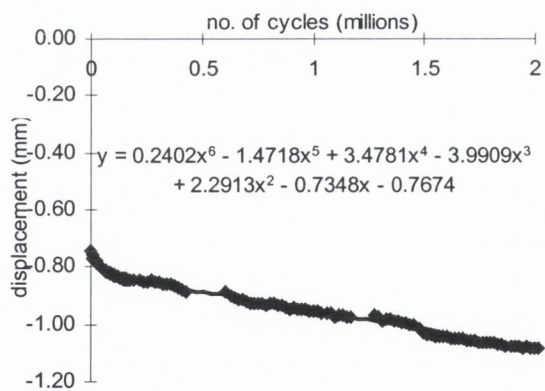
(c) LVDT3



(d) LVDT4

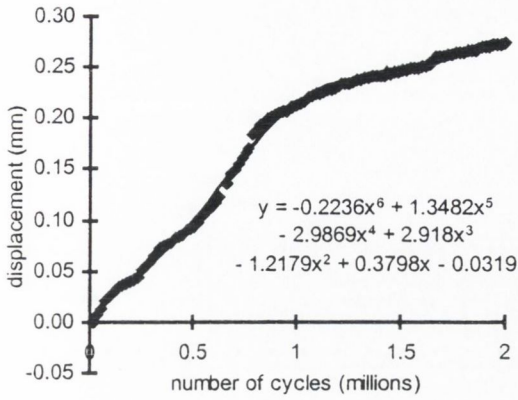


(e) LVDT5

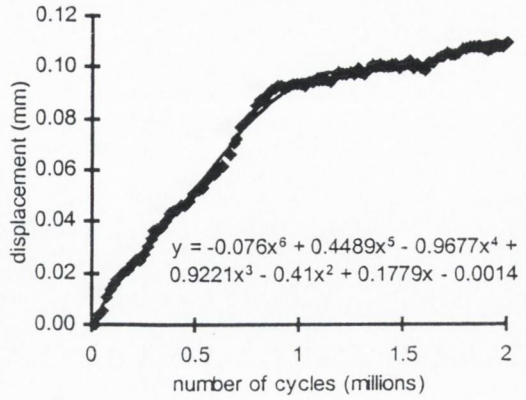


(f) LVDT6

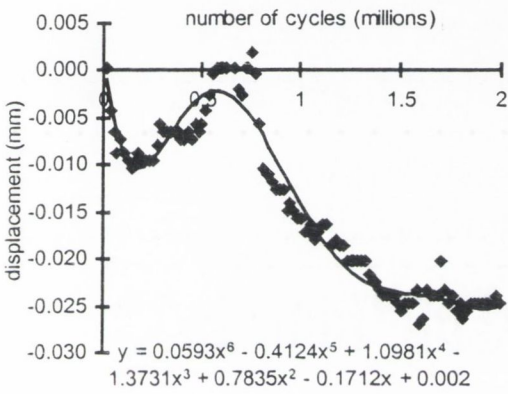
Figure C12: The displacements computed from the LVDTs as labelled in Figure 3.18 during the cyclic loading of Müller 5. Sixth order polynomial curves have been fitted to the data.



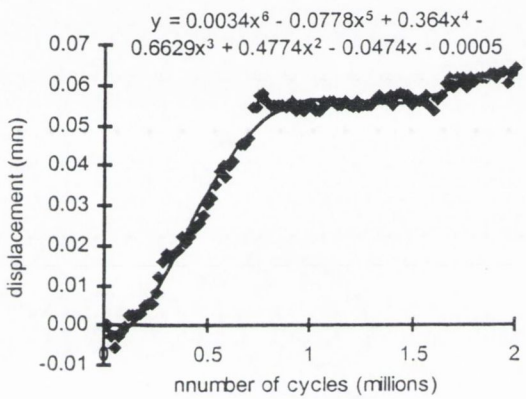
(a) LVDT1



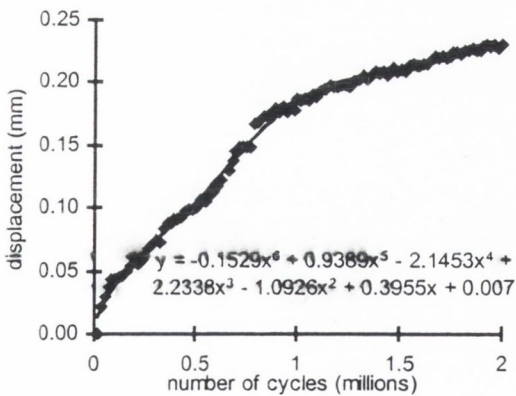
(b) LVDT2



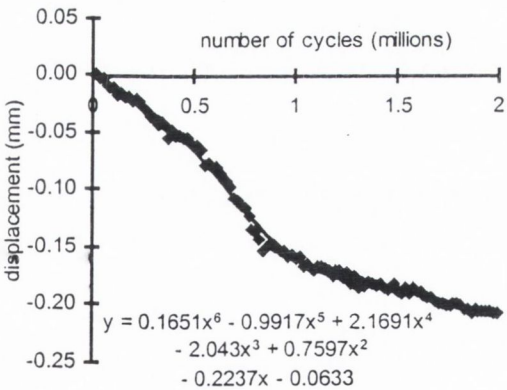
(c) LVDT3



(d) LVDT4

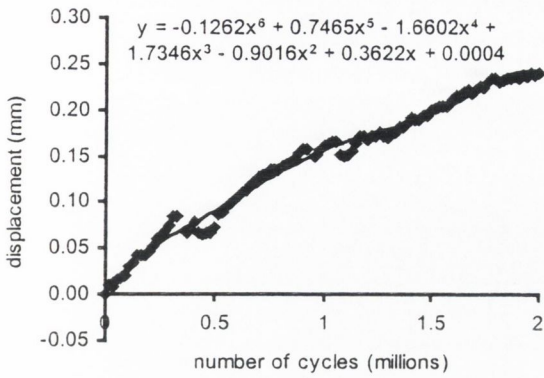


(e) LVDT5

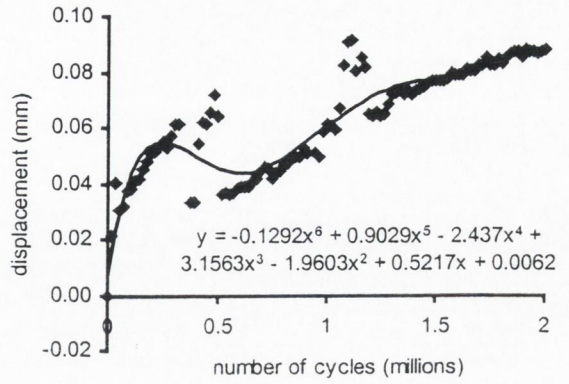


(f) LVDT6

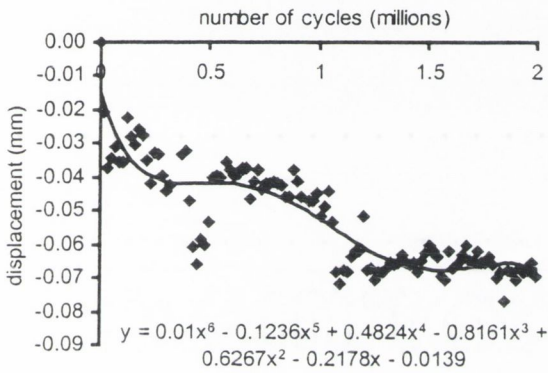
Figure C13: The displacements computed from the LVDTs as labelled in Figure 3.18 during the cyclic loading of Müller 1 with resorption. Sixth order polynomial curves have been fitted to the data.



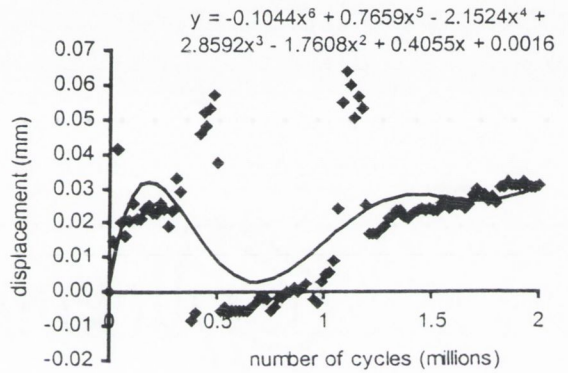
(a) LVDT1



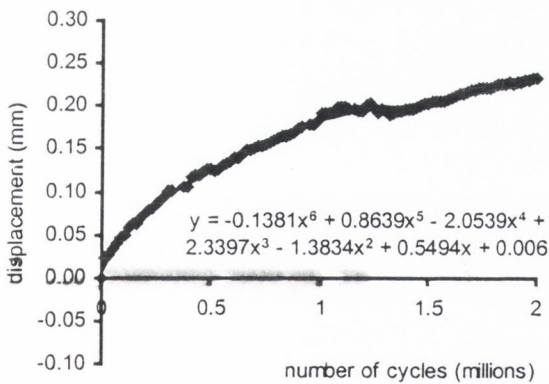
(b) LVDT2



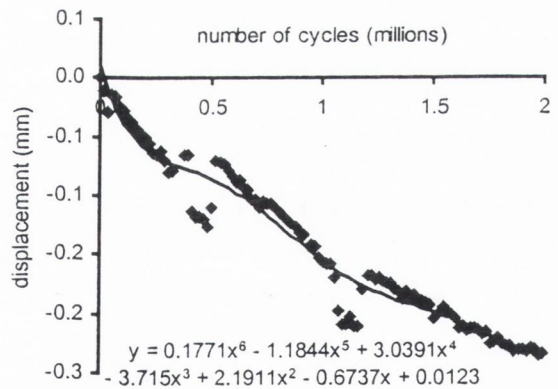
(c) LVDT3



(d) LVDT4



(e) LVDT5



(f) LVDT6

Figure C14: The displacements computed from the LVDTs as labelled Figure 3.18 during the cyclic loading of Müller 3 with resorption. Sixth order polynomial curves have been fitted to the data.

APPENDIX D

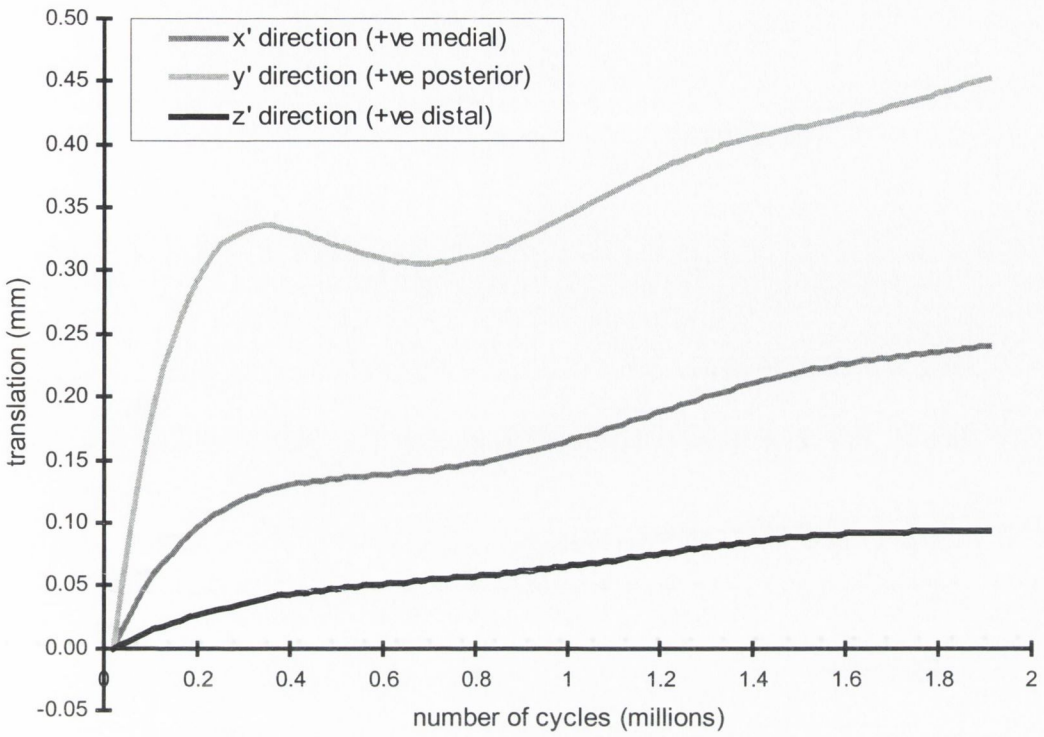


Figure D1: Translation of Lubinus 1 head centre in the x', y' and z' directions.

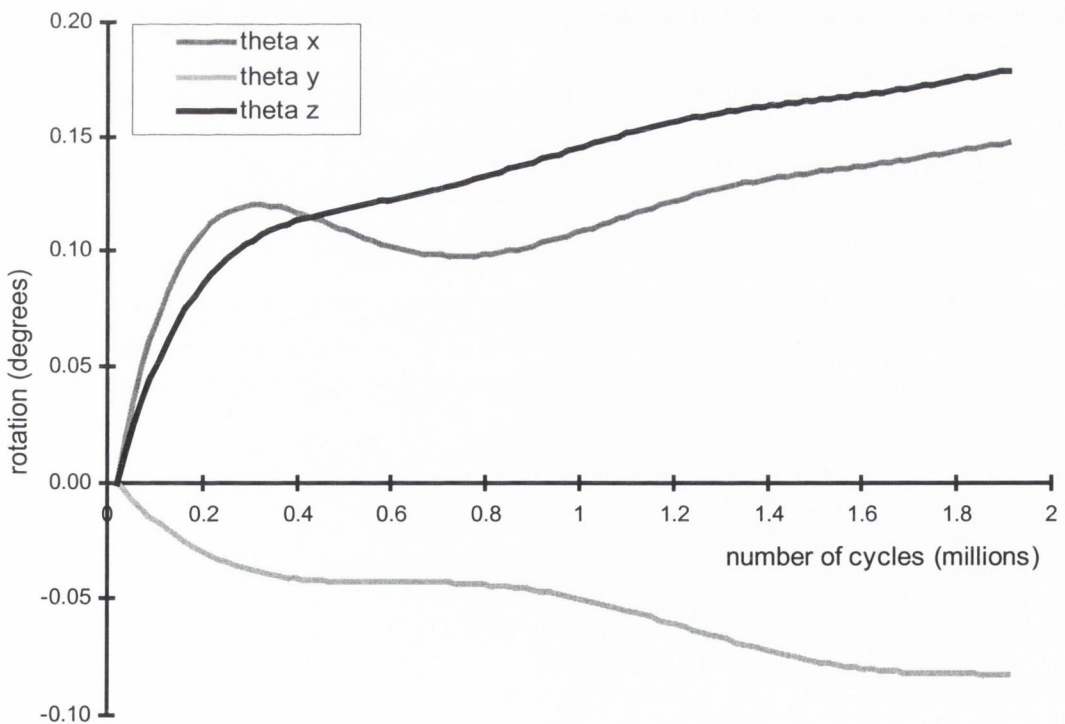


Figure D2: Rotation of Lubinus 1 about the x,y and z axes.

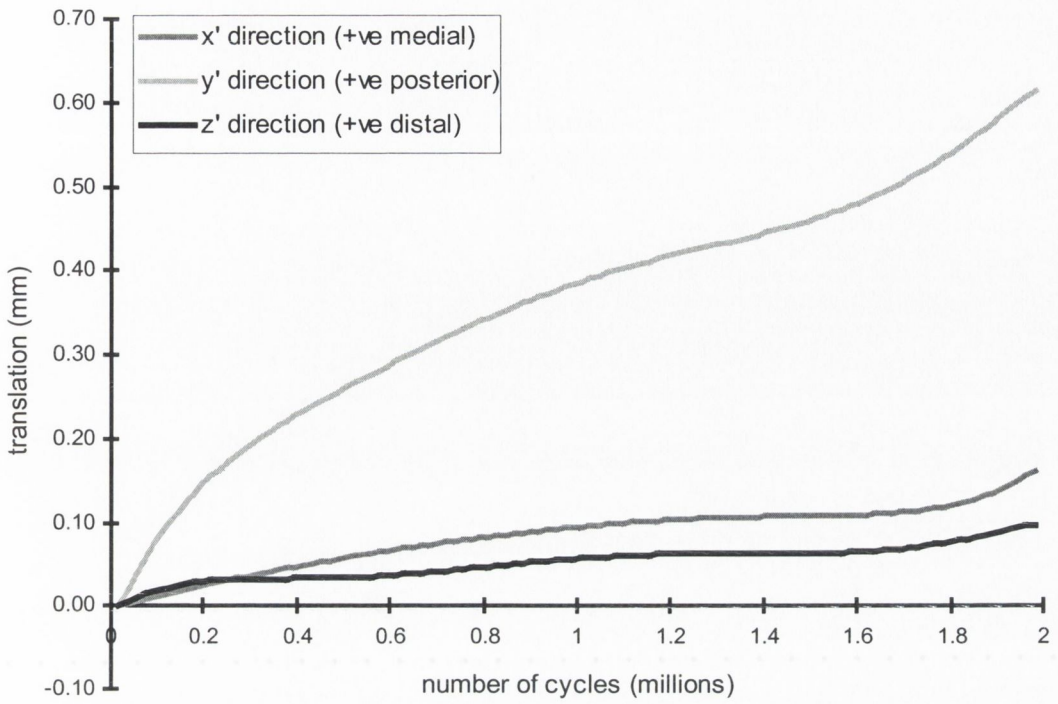


Figure D3: Translation of Lubinus 2 head centre in the x', y' and z' directions.

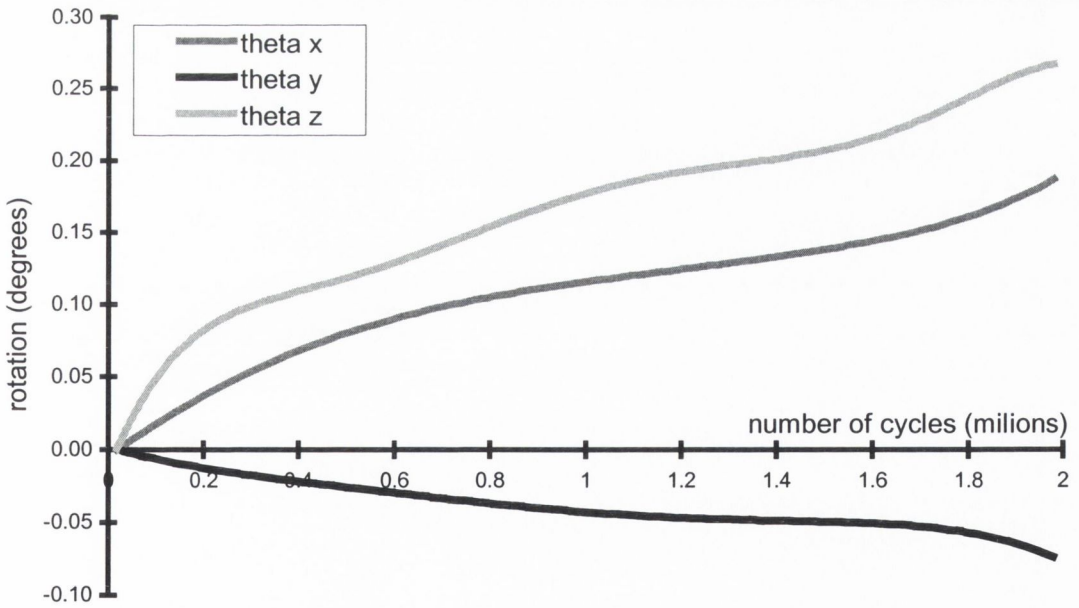


Figure D4: Rotation of Lubinus 2 about the x,y and z axes.

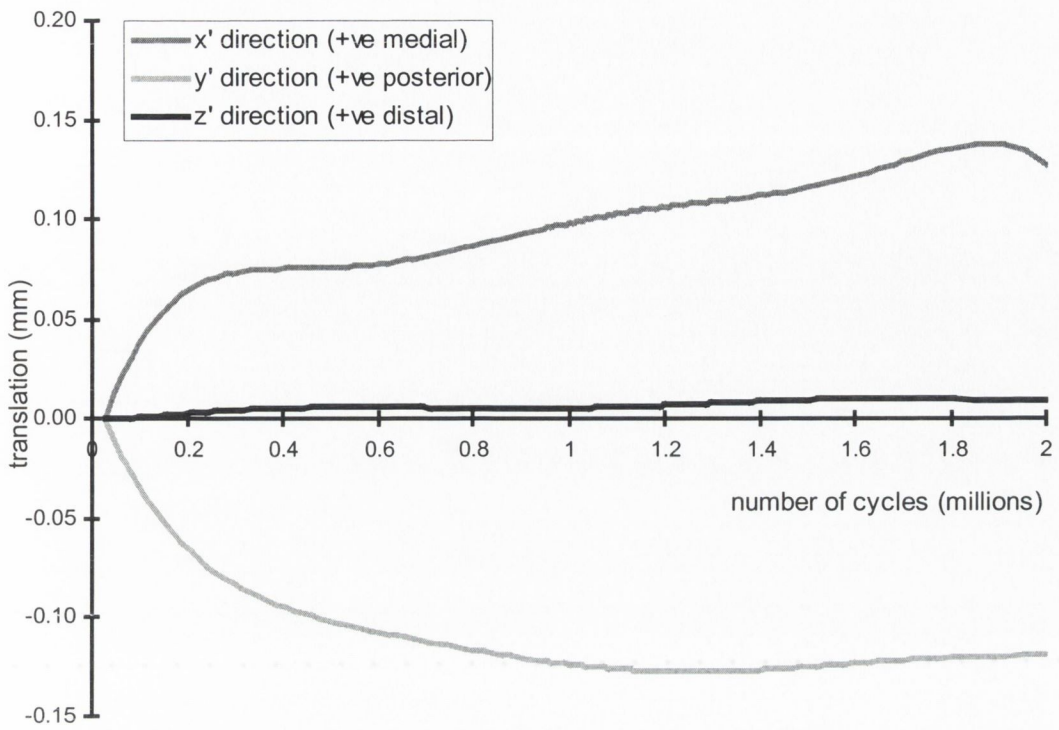


Figure D5: Translation of Lubinus 3 head centre in the x' , y' and z' directions.

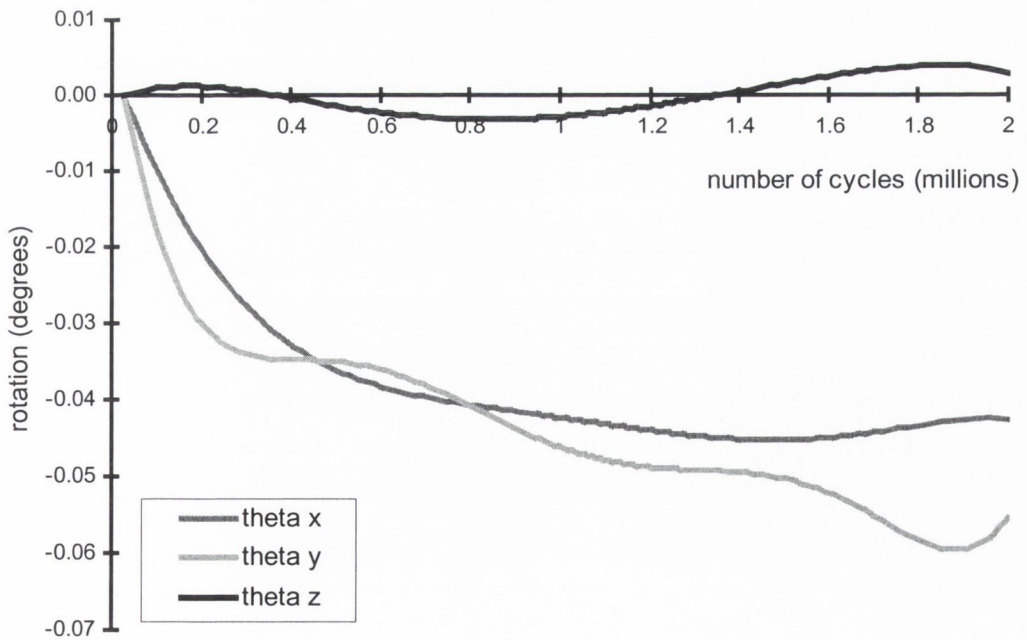


Figure D6: Rotation of Lubinus 3 about the x , y and z axes.

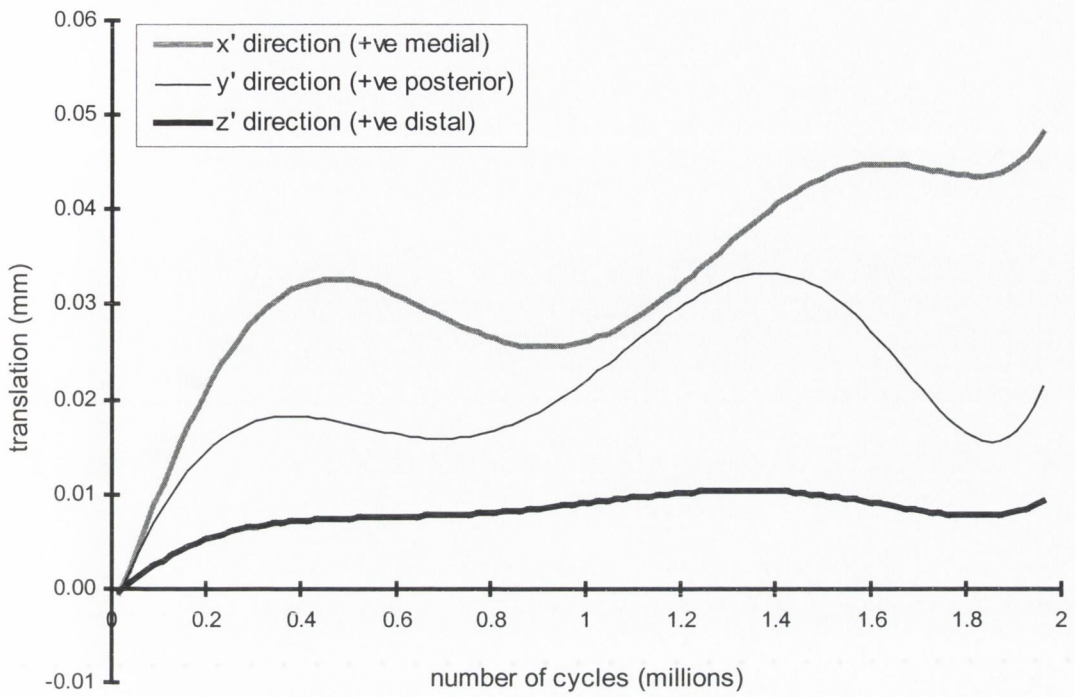


Figure D7: Translation of Lubinus 4 head centre in the x', y' and z' directions.

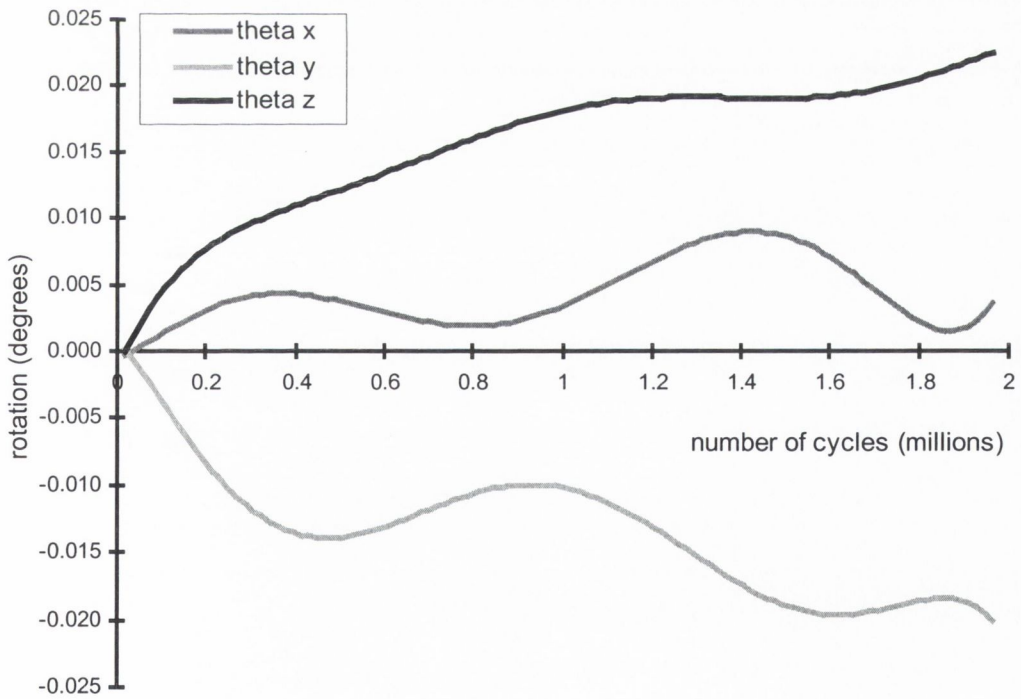


Figure D8: Rotation of Lubinus 4 about the x, y and z axes.

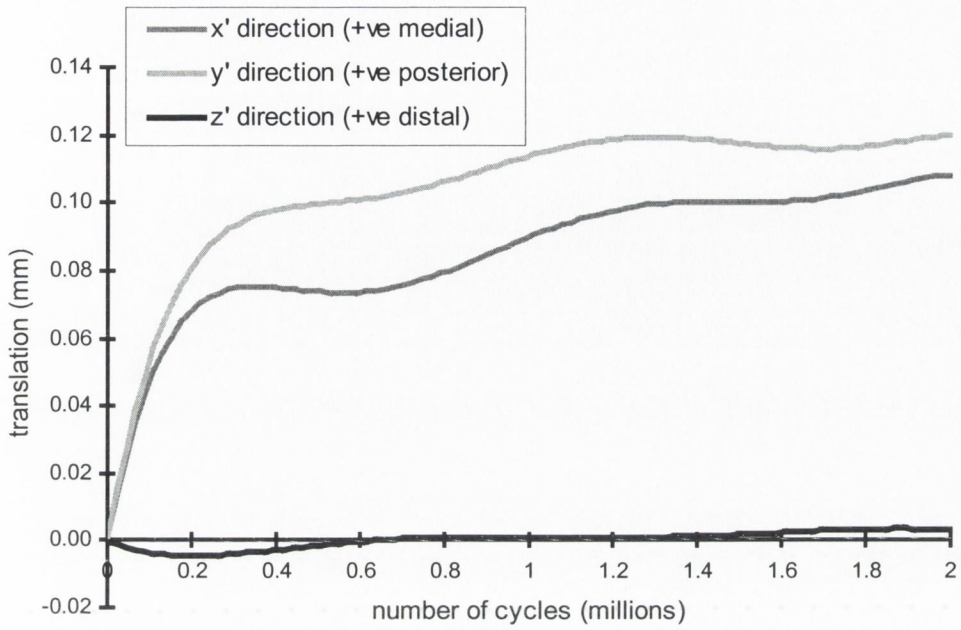


Figure D9: Translation of Lubinus 5 head centre in the x' , y' and z' directions.

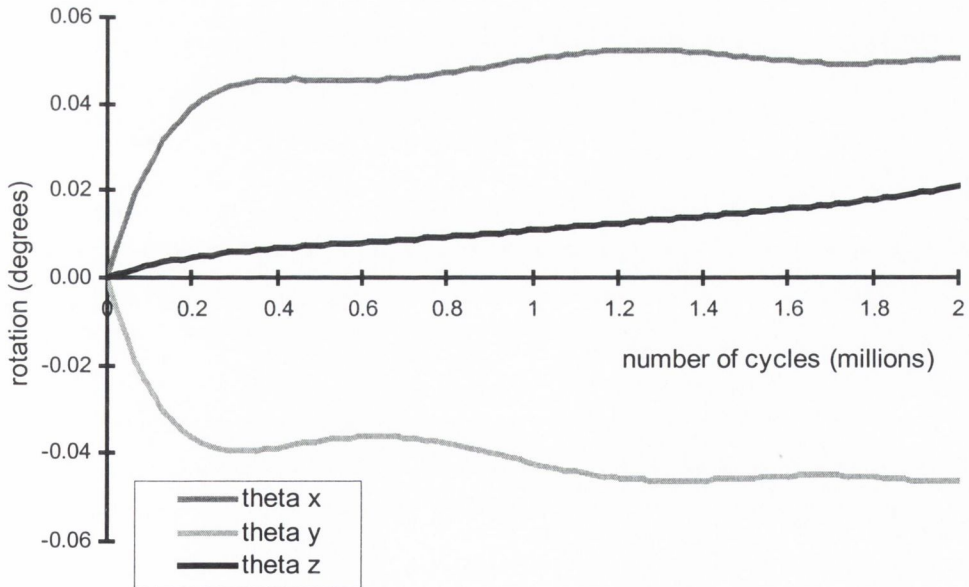


Figure D10: Rotation of Lubinus 5 about the x , y and z axes.

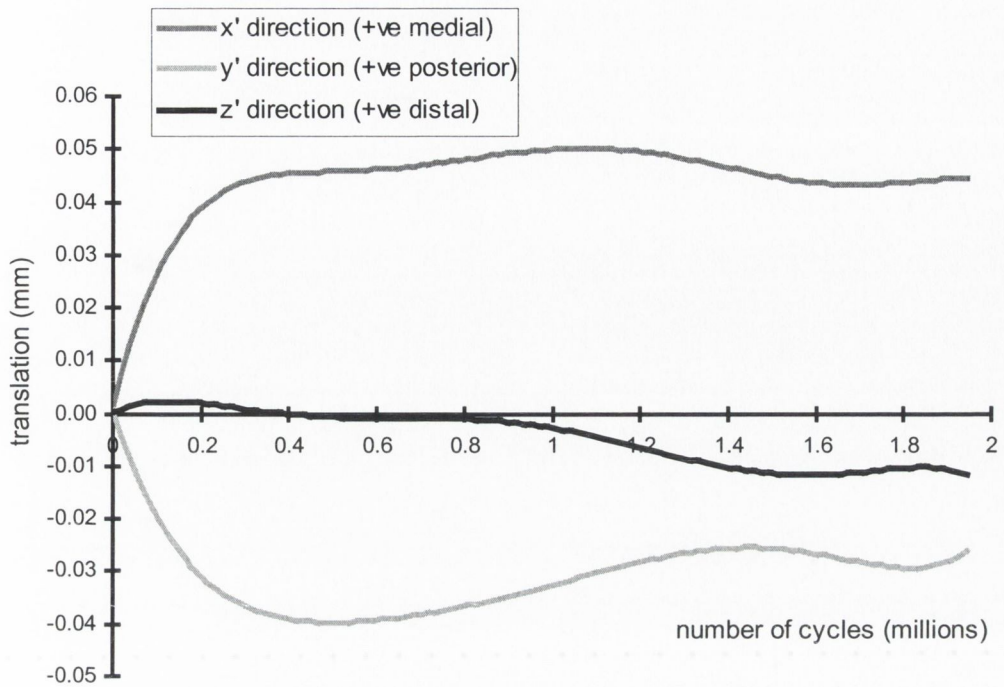


Figure D11: Translation of Lubinus 3 (with resorption) head centre in the x' , y' and z' directions.

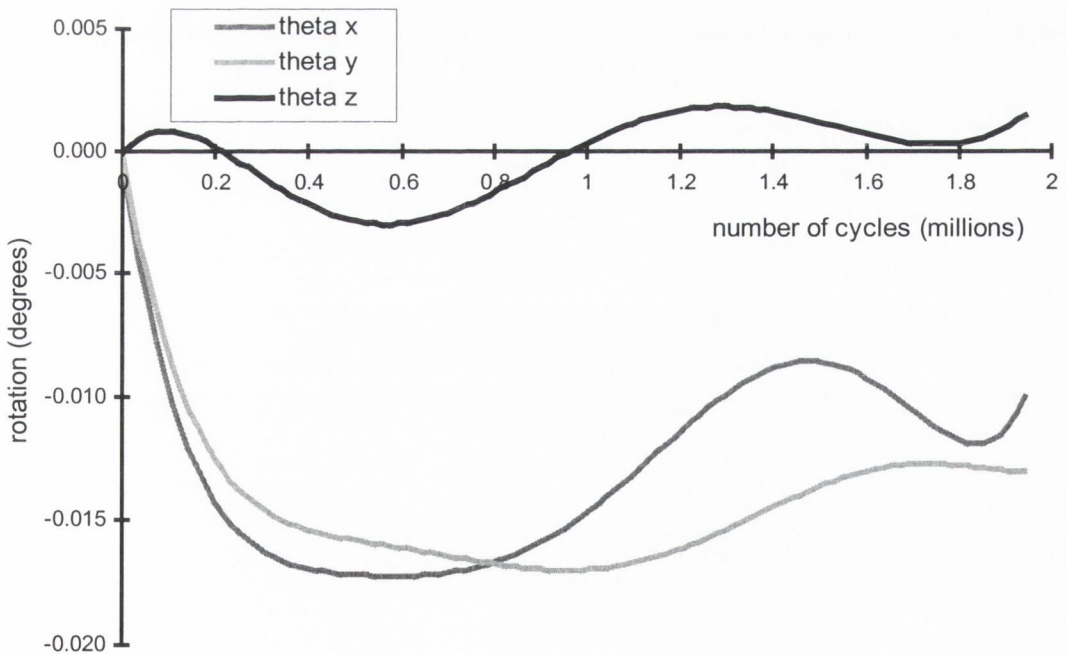


Figure D12: Rotation of Lubinus 3 (with resorption) about the x , y and z axes.

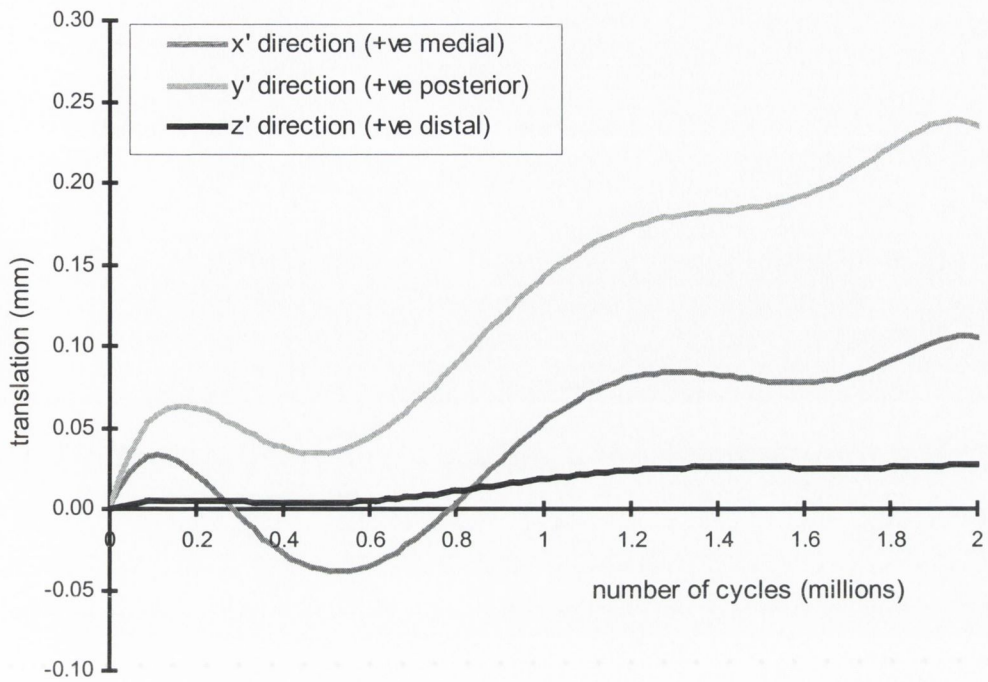


Figure D13: Translation of Lubinus 2 (with resorption) head centre in the x' , y' and z' directions.

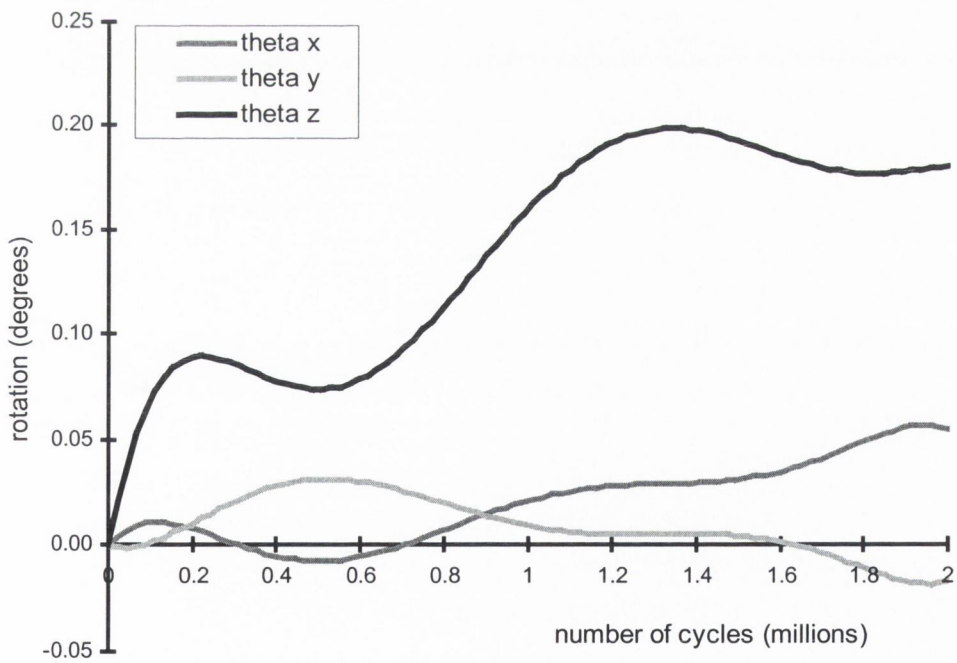


Figure D14: Rotation of Lubinus 2 (with resorption) about the x , y and z axes.

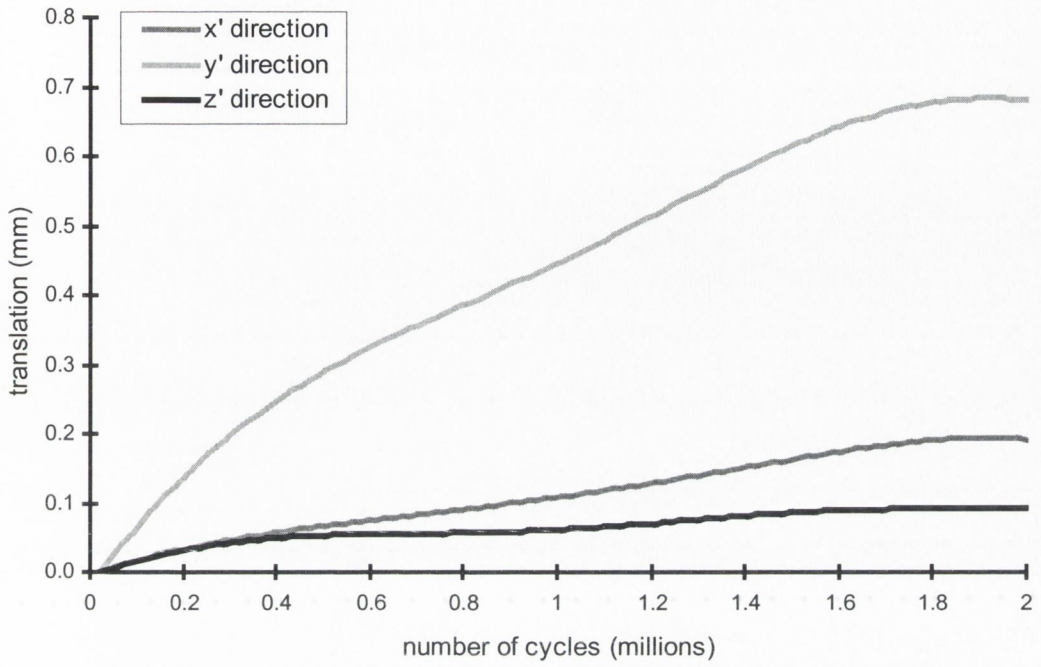


Figure D15: Translation of Müller 1 head centre in the x' , y' and z' directions.

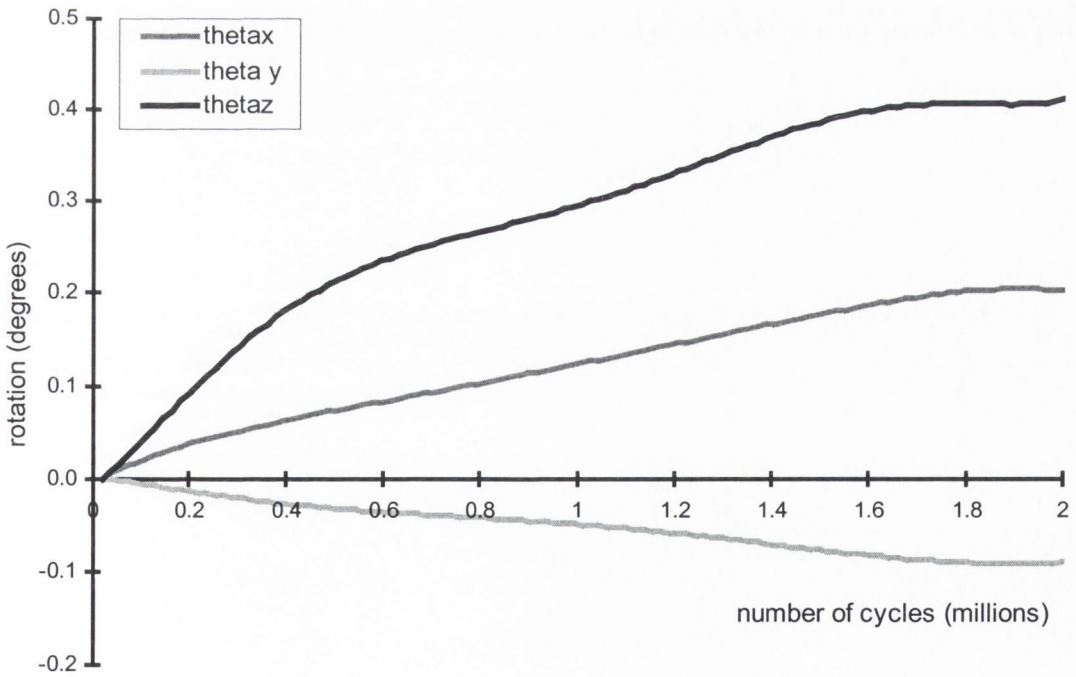


Figure D16: Rotation of Müller 1 about the x , y and z axes.

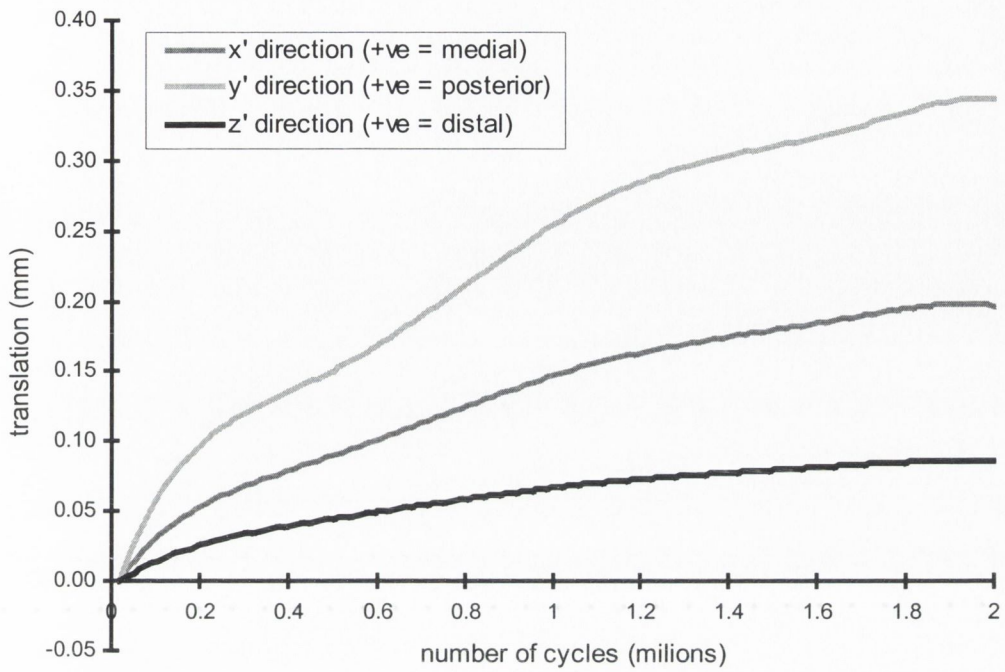


Figure D17: Translation of Müller 2 head centre in the x' , y' and z' directions.

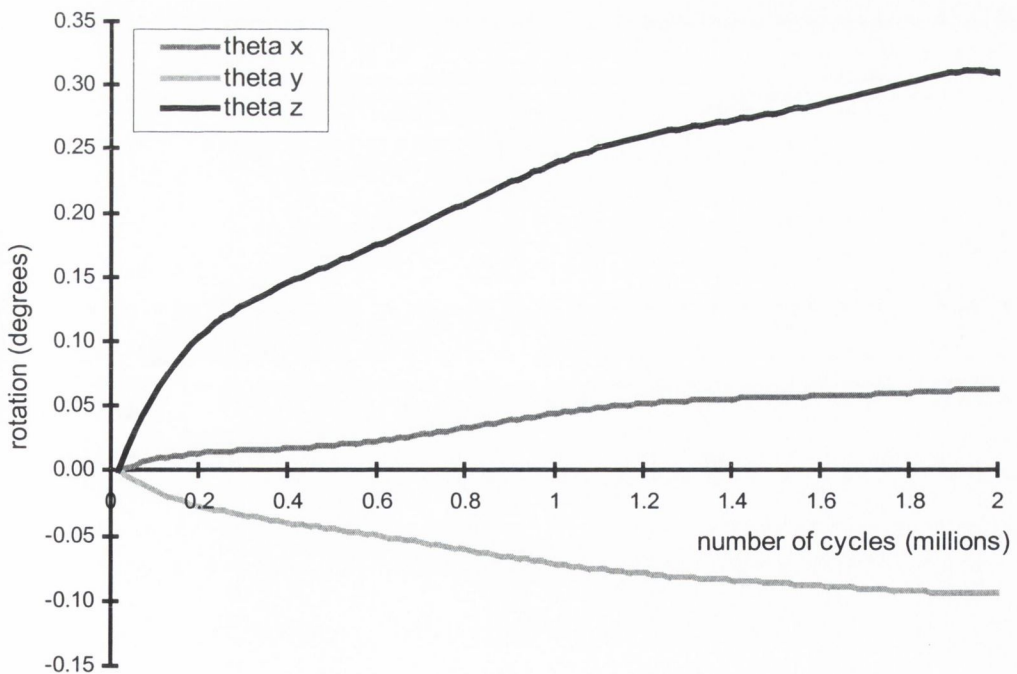


Figure D18: Rotation of Müller 2 about the x , y and z axes.

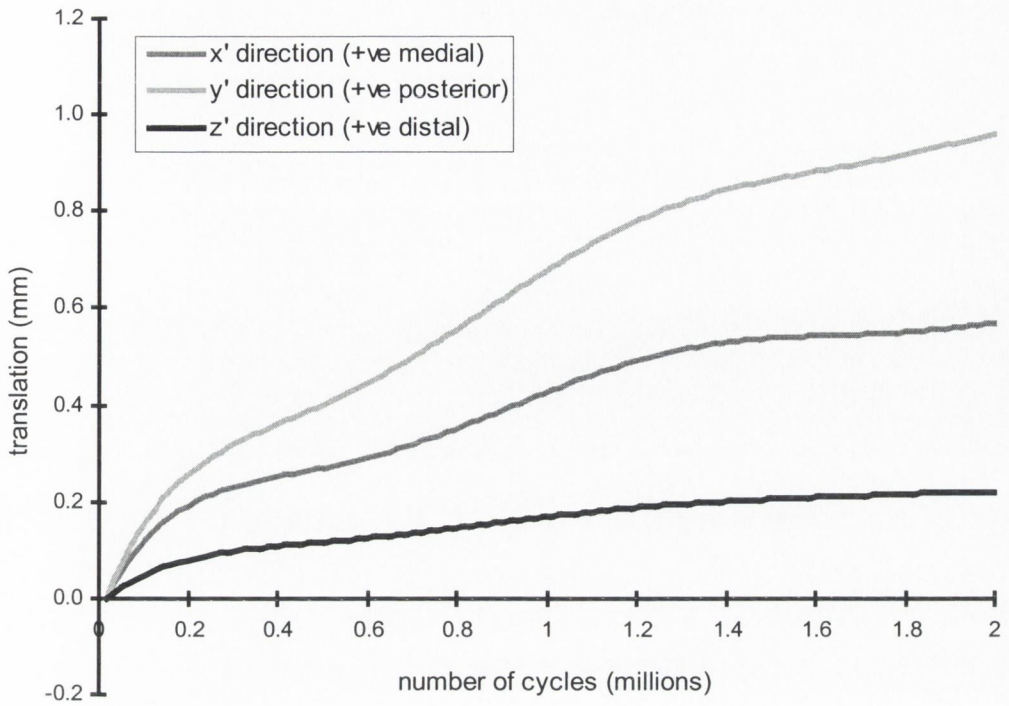


Figure D19: Translation of Müller 3 head centre in the x' , y' and z' directions.

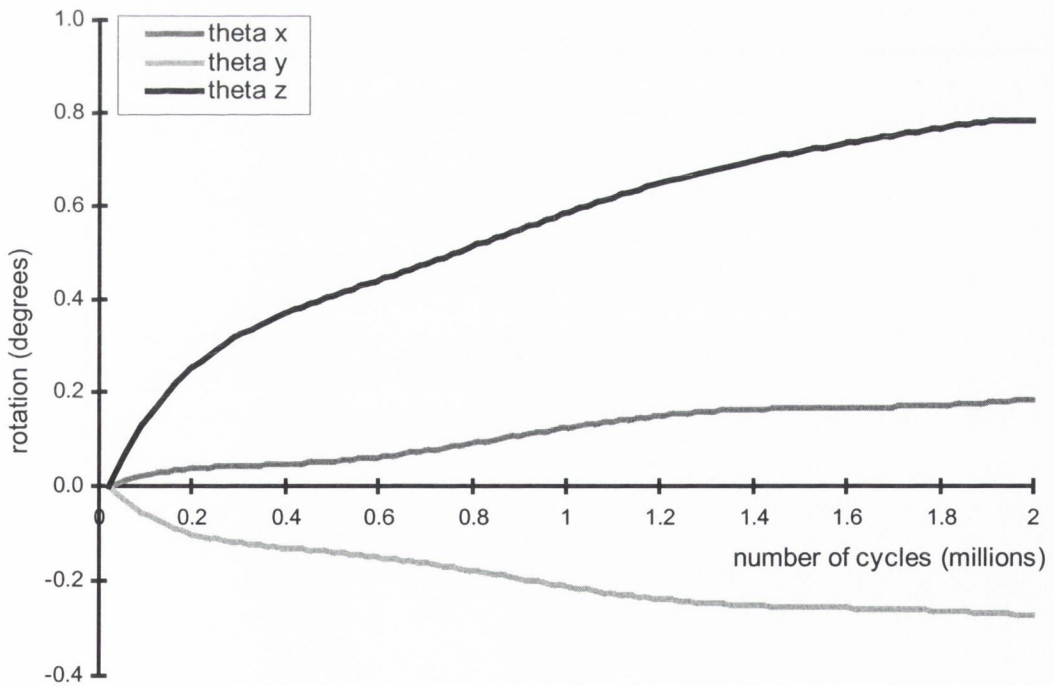


Figure D20: Rotation of Müller 3 about the x , y and z axes.

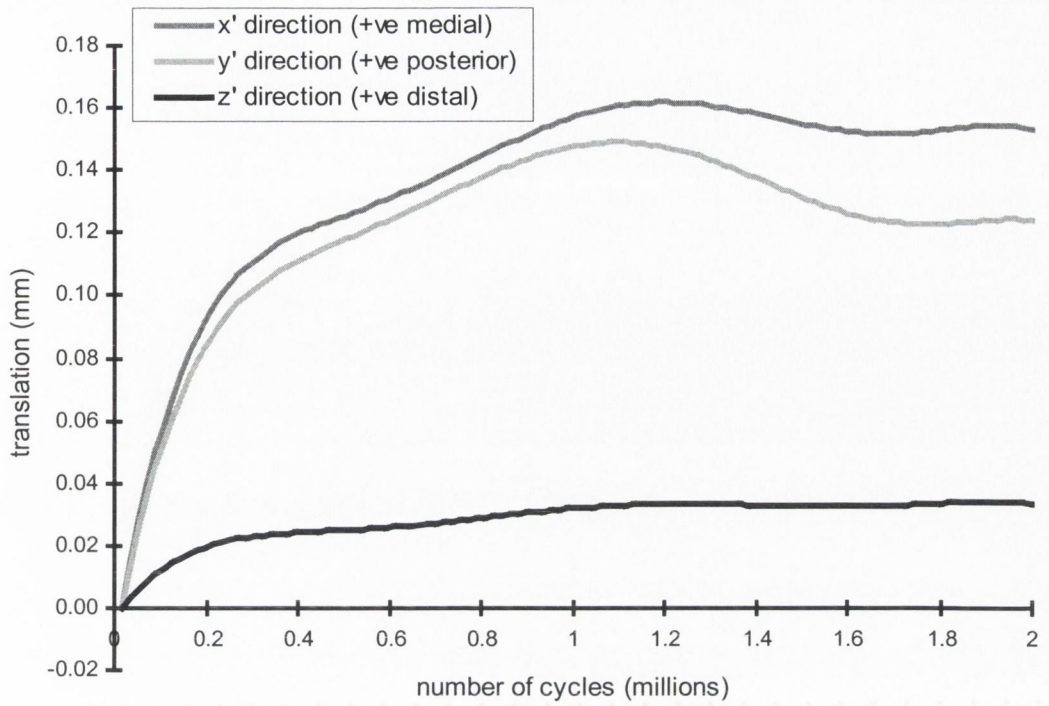


Figure D21: Translation of Müller 4 head centre in the x' , y' and z' directions.

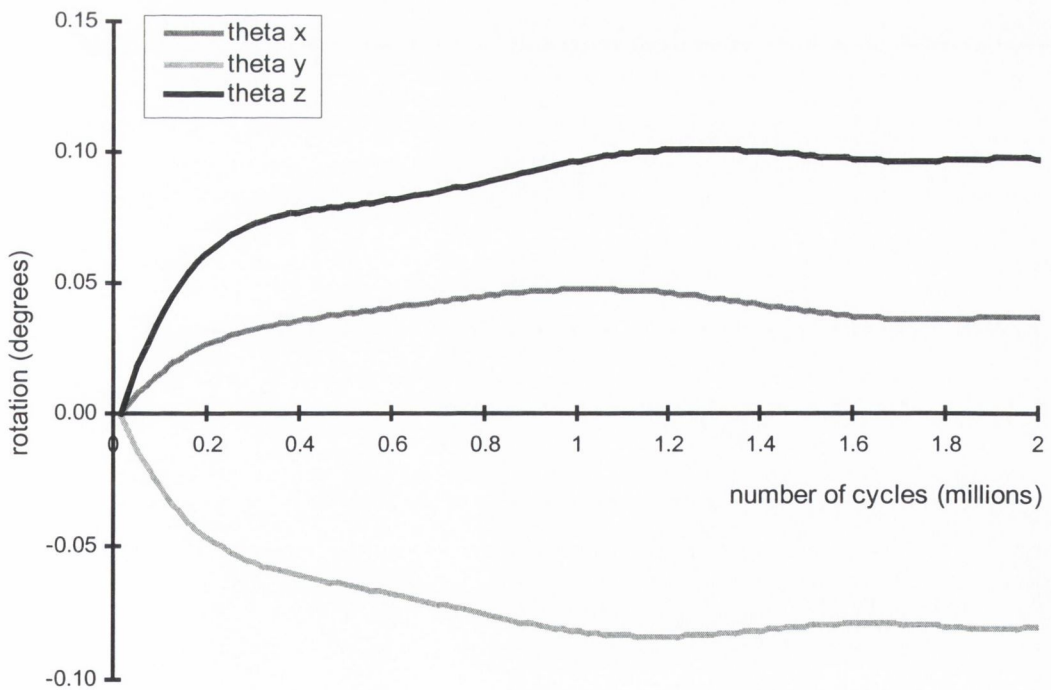


Figure D22: Rotation of Müller 4 about the x , y and z axes.

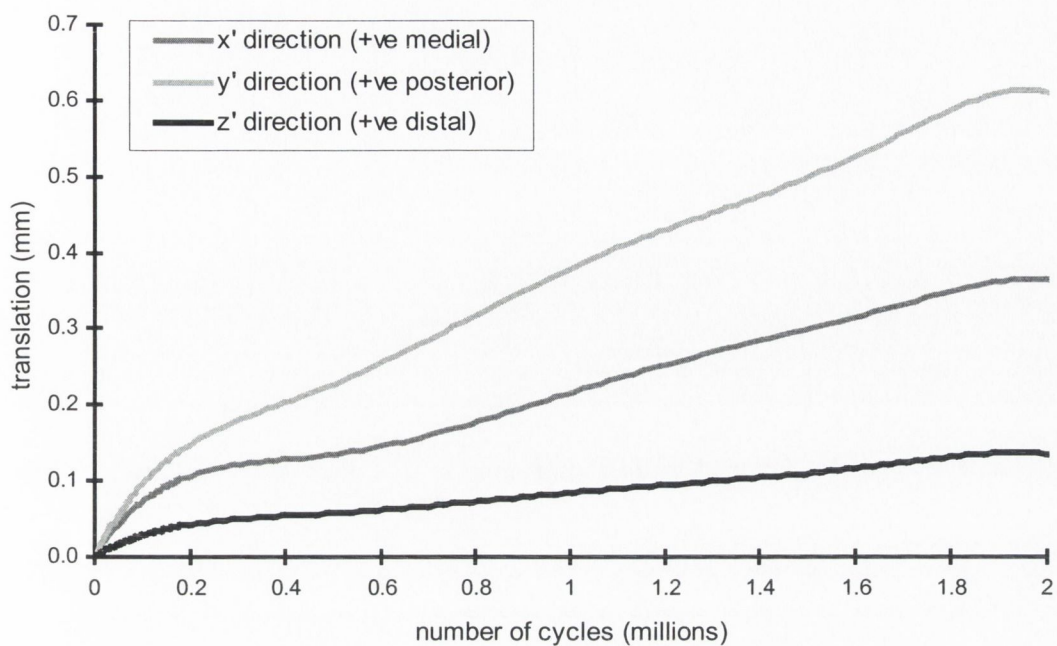


Figure D23: Translation of Müller 5 head centre in the x' , y' and z' directions.

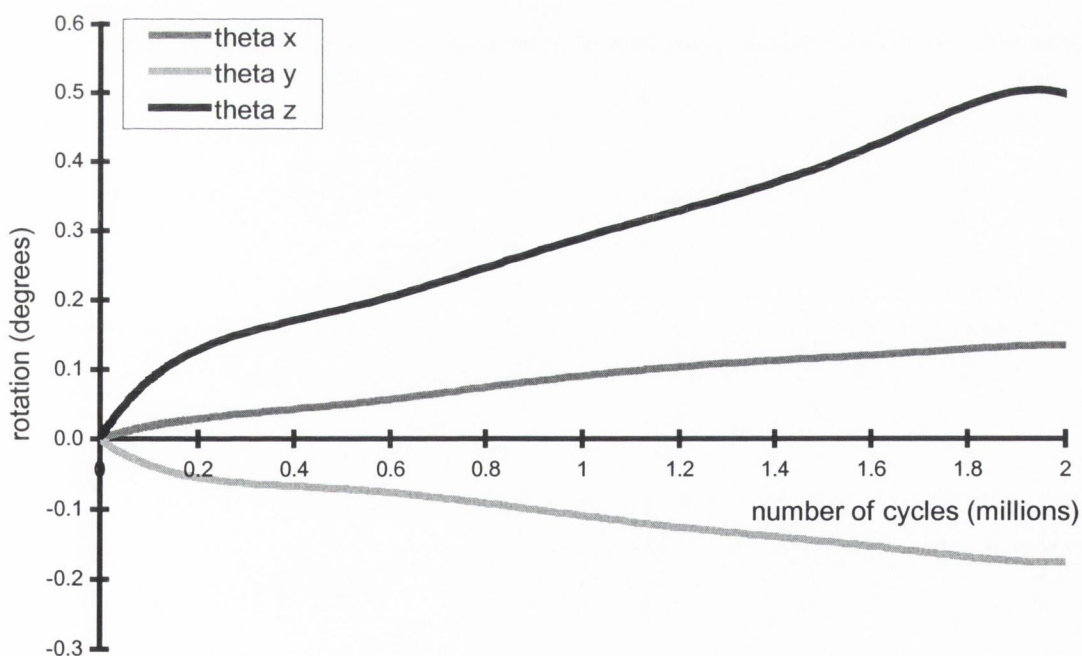


Figure D24: Rotation of Müller 5 about the x , y and z axes.

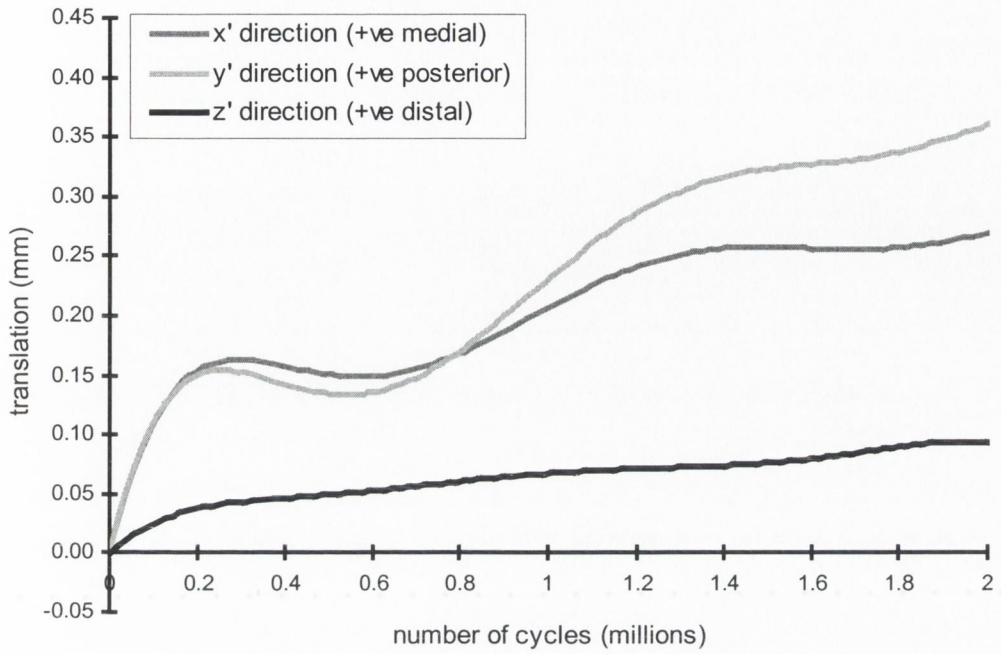


Figure D25: Translation of Müller 3 (with resorption) head centre in the x' , y' and z' directions.

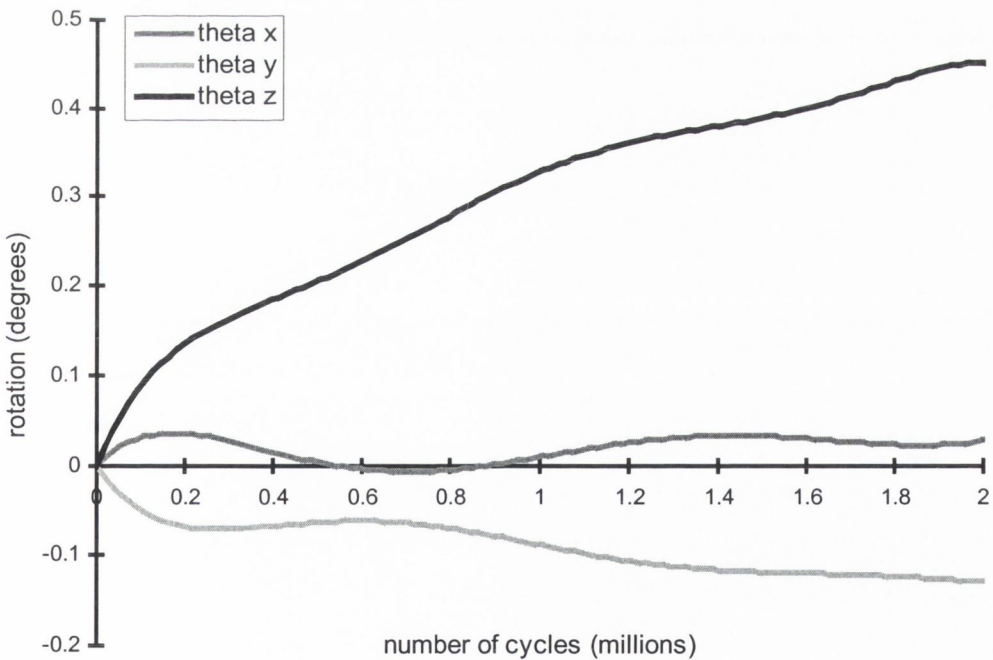


Figure D26: Rotation of Müller 3 (with resorption) about the x , y and z axes.

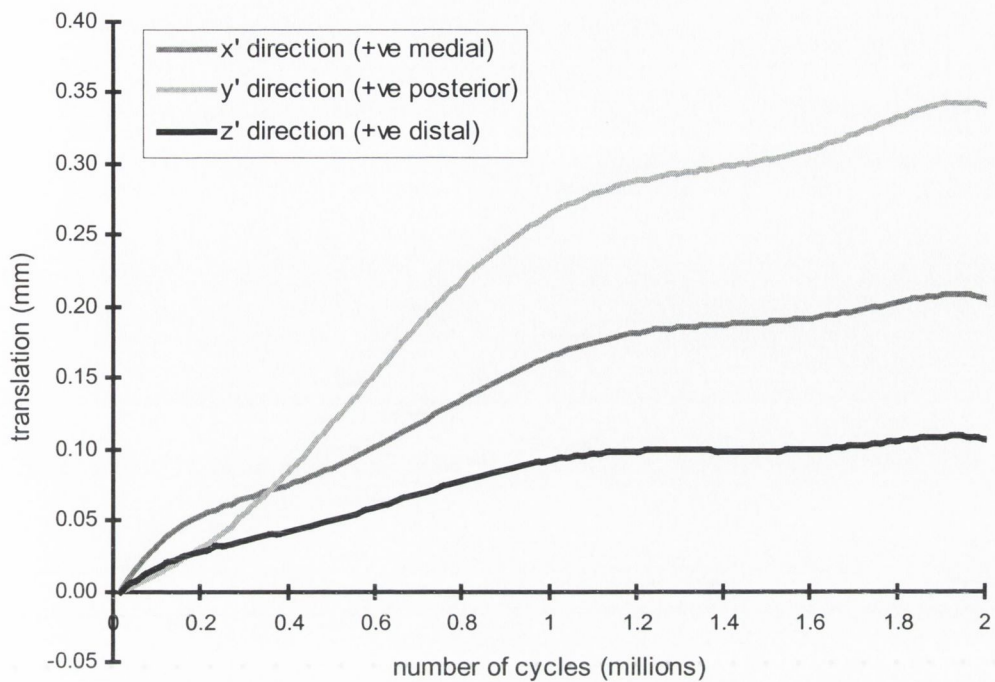


Figure D27: Translation of Müller 1 (with resorption) head centre in the x' , y' and z' directions.

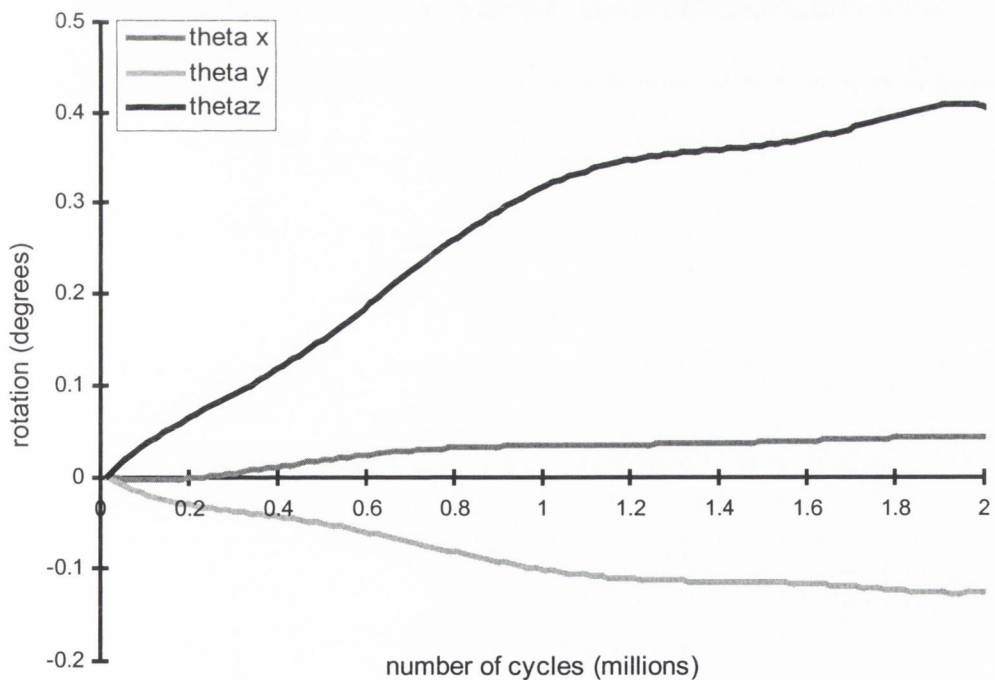


Figure D28: Rotation of Müller 1 (with resorption) about the x , y and z axes.

APPENDIX E

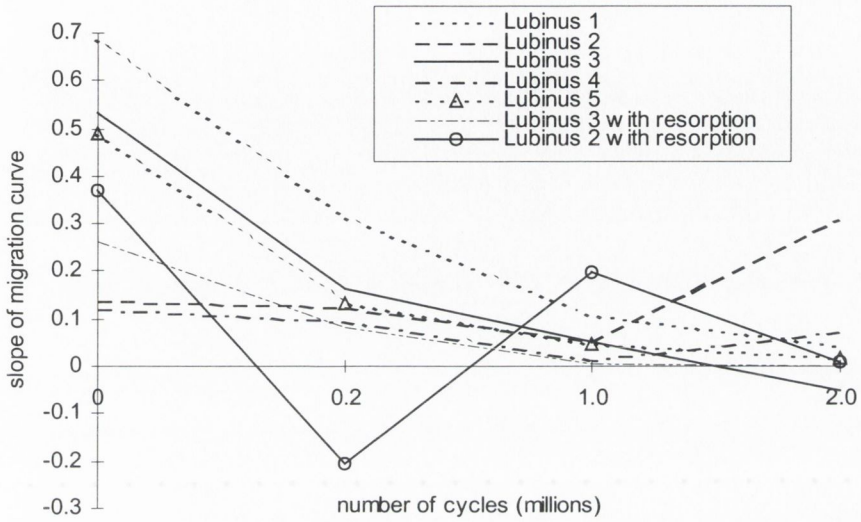


Figure E1: The slope of the curve describing translation of the Lubinus prostheses in the x' direction at 1800 cycles, 200000 cycles, 1000000 cycles and 2000000 cycles.

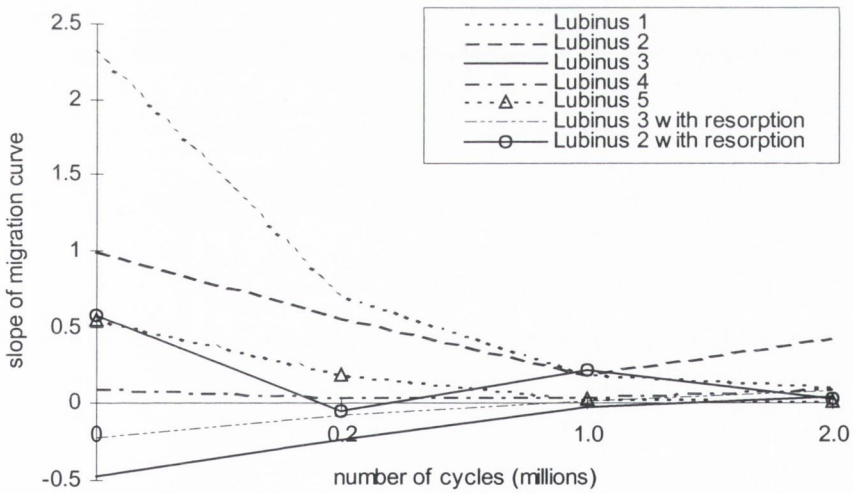


Figure E2: The slope of the curve describing translation of the Lubinus prostheses in the y' direction at 1800 cycles, 200000 cycles, 1000000 cycles and 2000000 cycles.

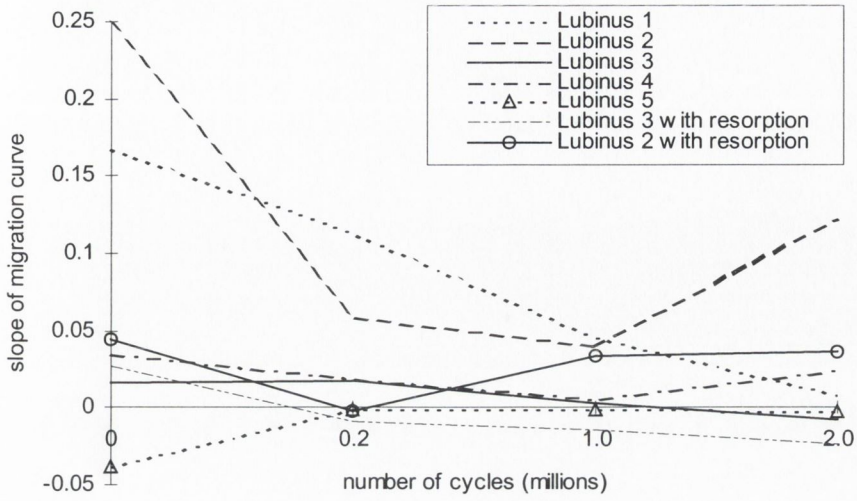


Figure E3: The slope of the curve describing translation of the Lubinus prostheses in the z' direction at 1800 cycles, 200000 cycles, 1000000 cycles and 2000000 cycles.

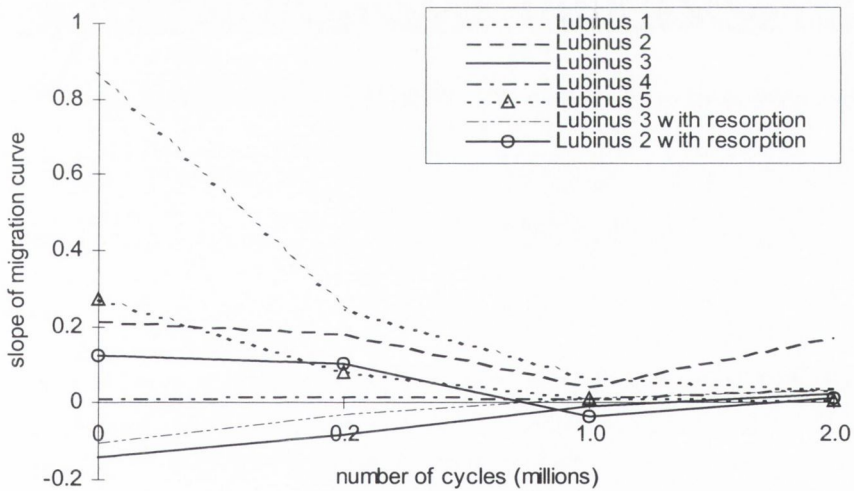


Figure E4: The slope of the curve describing rotation of the Lubinus prostheses in θ_x at 1800 cycles, 200000 cycles, 1000000 cycles and 2000000 cycles.

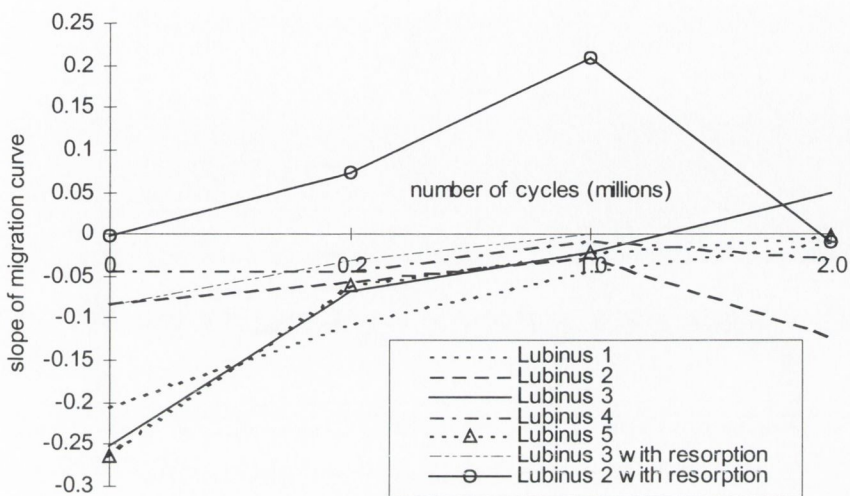


Figure E5: The slope of the curve describing rotation of the Lubinus prostheses in θ_y at 1800 cycles, 200000 cycles, 1000000 cycles and 2000000 cycles.

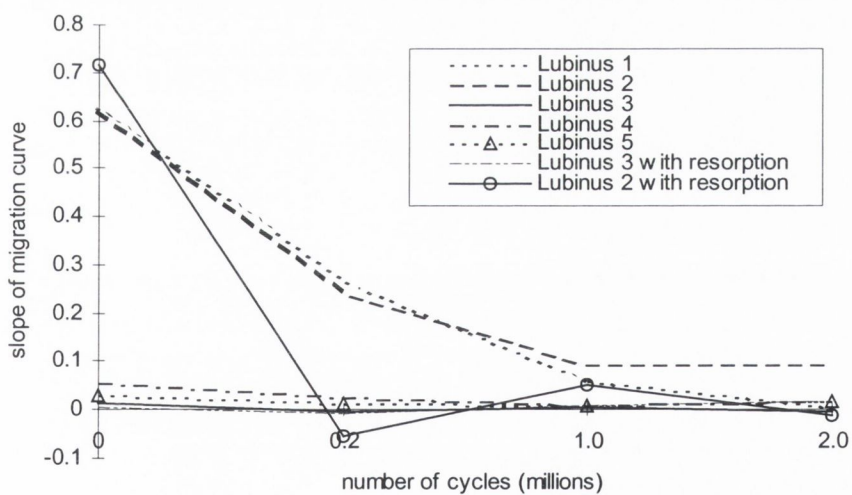


Figure E6: The slope of the curve describing rotation of the Lubinus prostheses in θ_z at 1800 cycles, 200000 cycles, 1000000 cycles and 2000000 cycles.

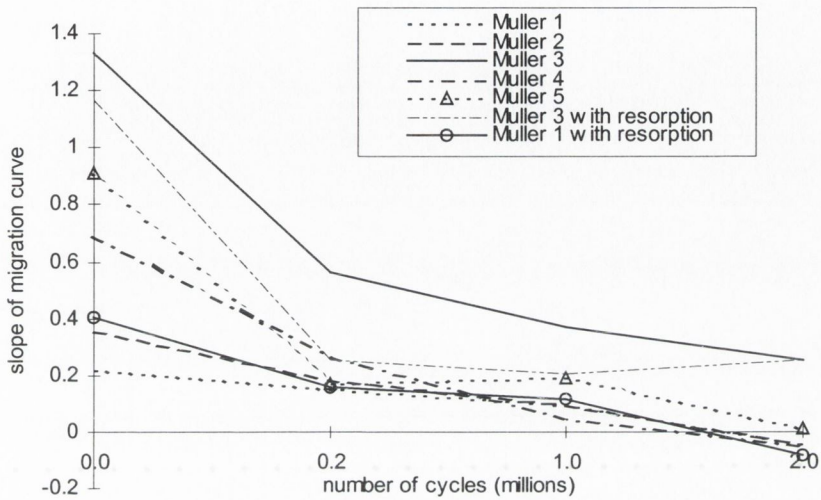


Figure E7: The slope of the curve describing translation of the Müller prostheses in the x' direction at 1800 cycles, 200000 cycles, 1000000 cycles and 2000000 cycles.

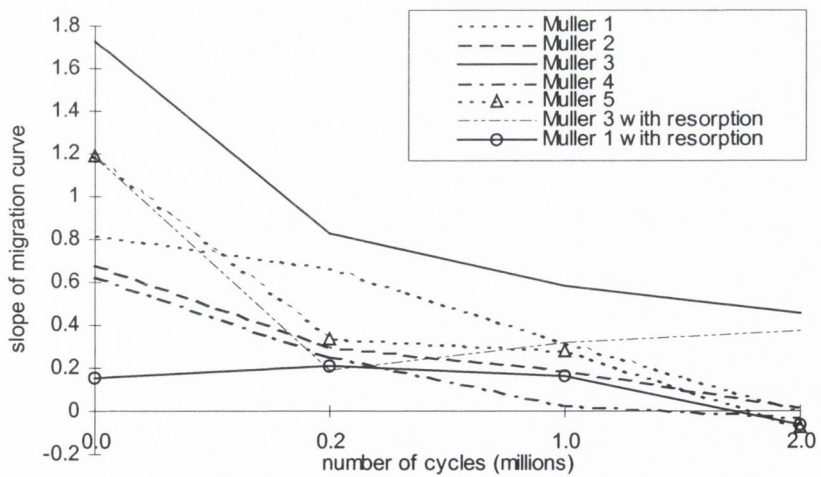


Figure E8: The slope of the curve describing translation of the Müller prostheses in the y' direction at 1800 cycles, 200000 cycles, 1000000 cycles and 2000000 cycles.

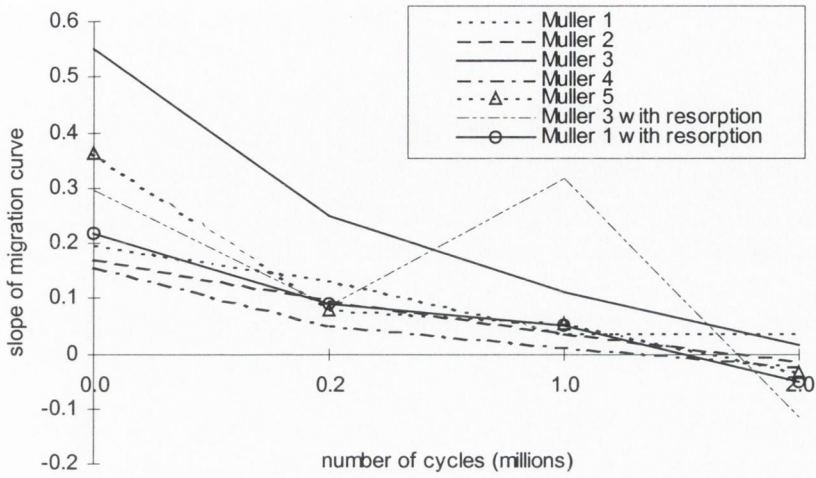


Figure E9: The slope of the curve describing translation of the Müller prostheses in the z' direction at 1800 cycles, 200000 cycles, 1000000 cycles and 2000000 cycles.

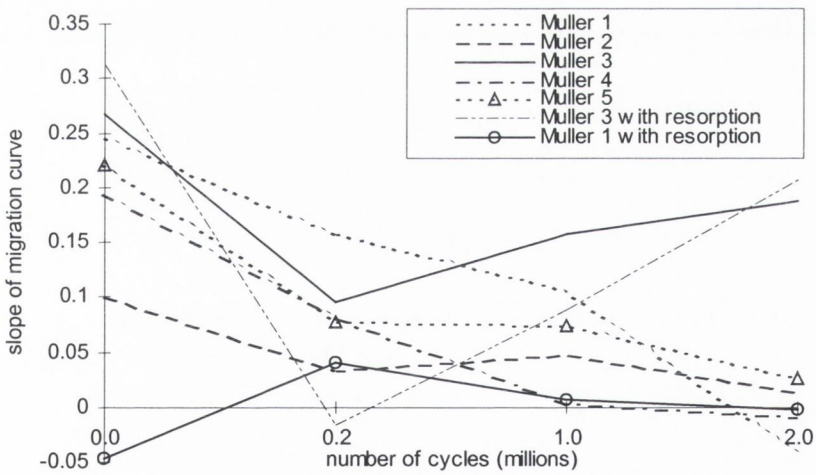


Figure E10: The slope of the curve describing rotation of the Müller prostheses in θ_x at 1800 cycles, 200000 cycles, 1000000 cycles and 2000000 cycles.

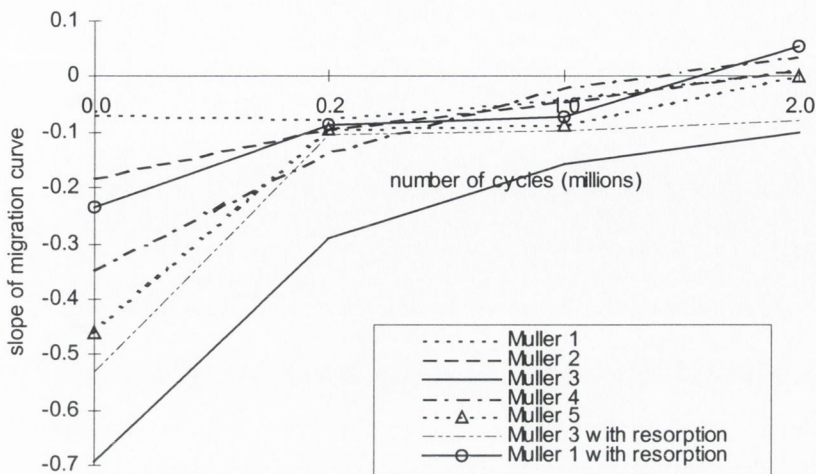


Figure E11: The slope of the curve describing rotation of the Müller prostheses in θ_y at 1800 cycles, 200000 cycles, 1000000 cycles and 2000000 cycles.

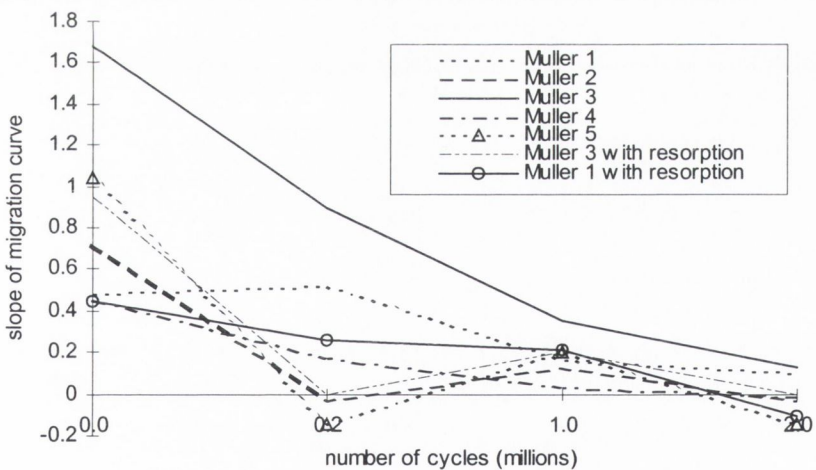


Figure E12: The slope of the curve describing rotation of the Müller prostheses in θ_z at 1800 cycles, 200000 cycles, 1000000 cycles and 2000000 cycles.

APPENDIX F

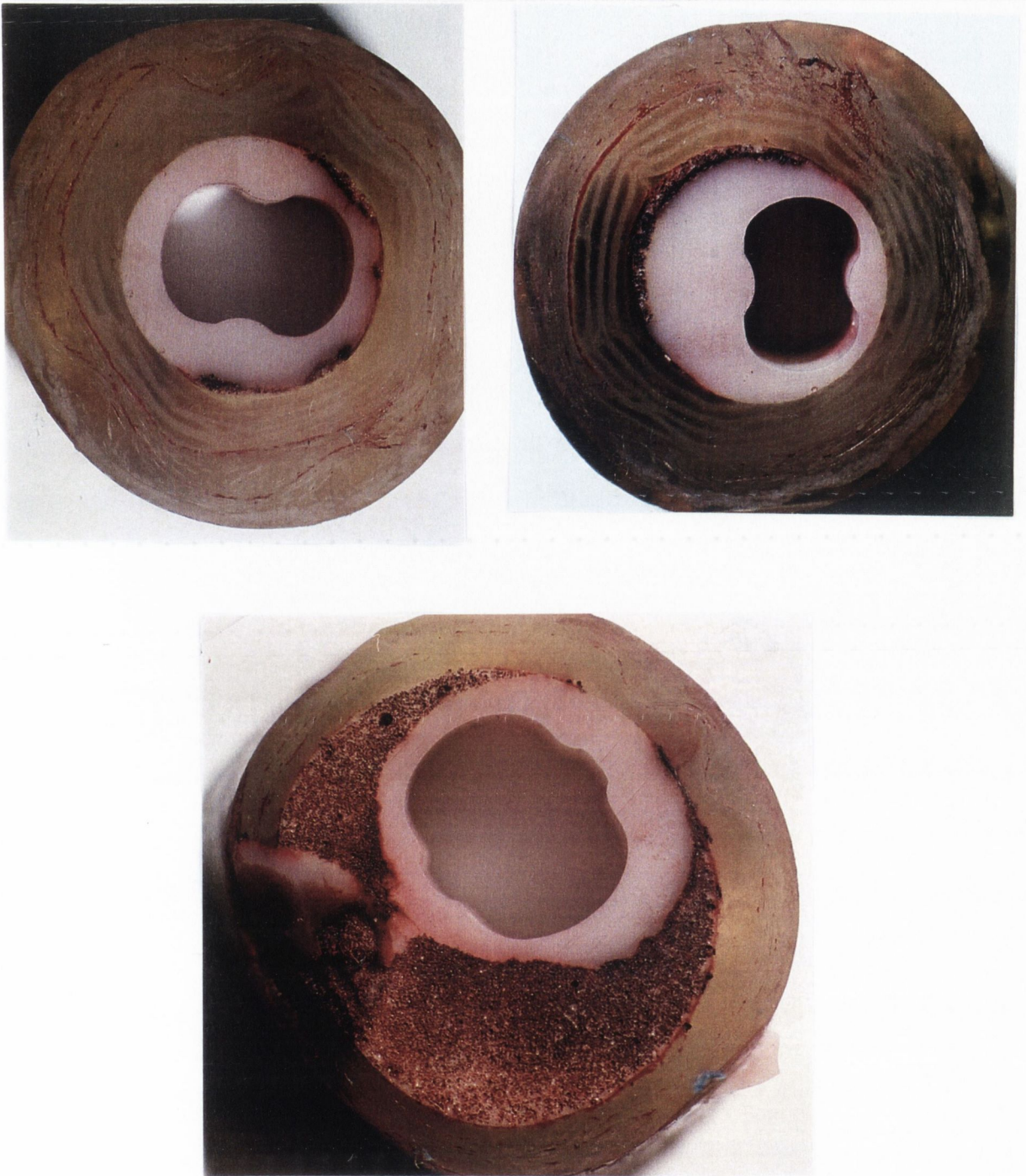


Figure F1: Photographs of the Lubinus cement mantles. The samples have been cyclically loaded, sectioned and push out tests have been performed. Little damage in the cement mantle is apparent.

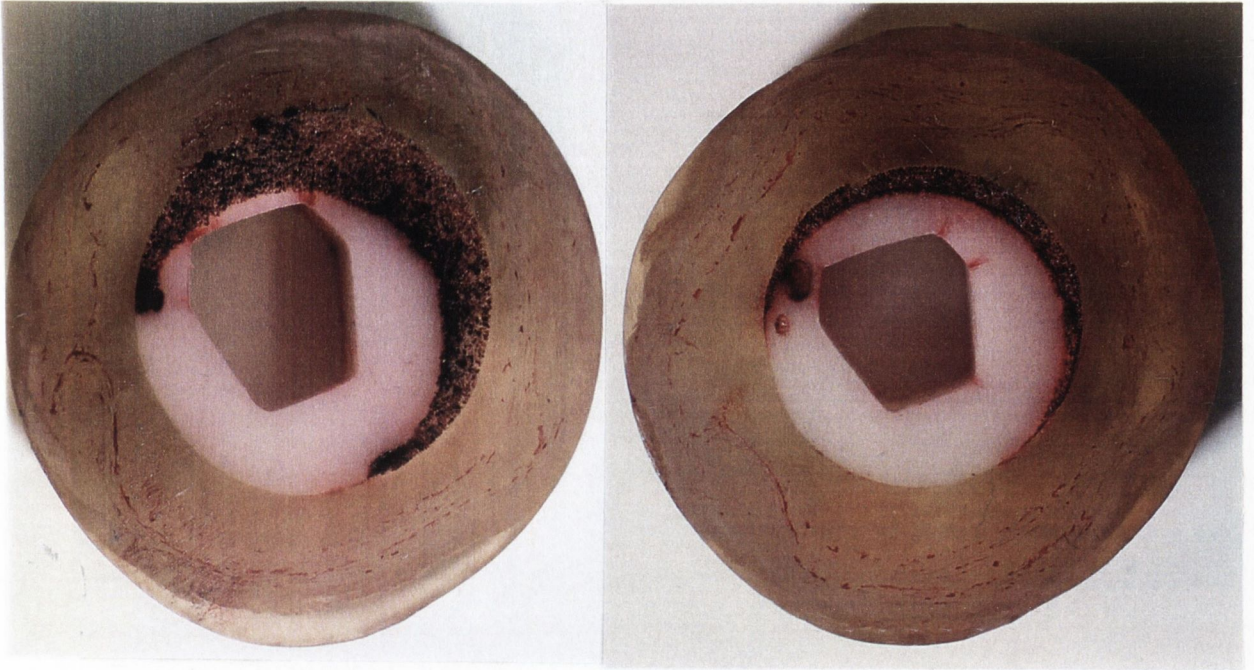


Figure F2: Photographs of the Müller cement mantles. The samples have been cyclically loaded, sectioned and push out tests have been performed. Damage in the cement mantle and along the interfaces is apparent.

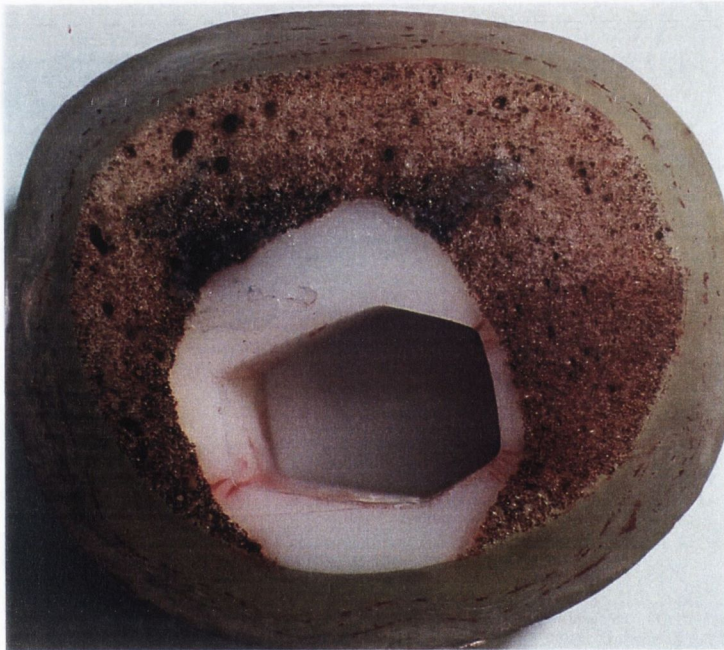
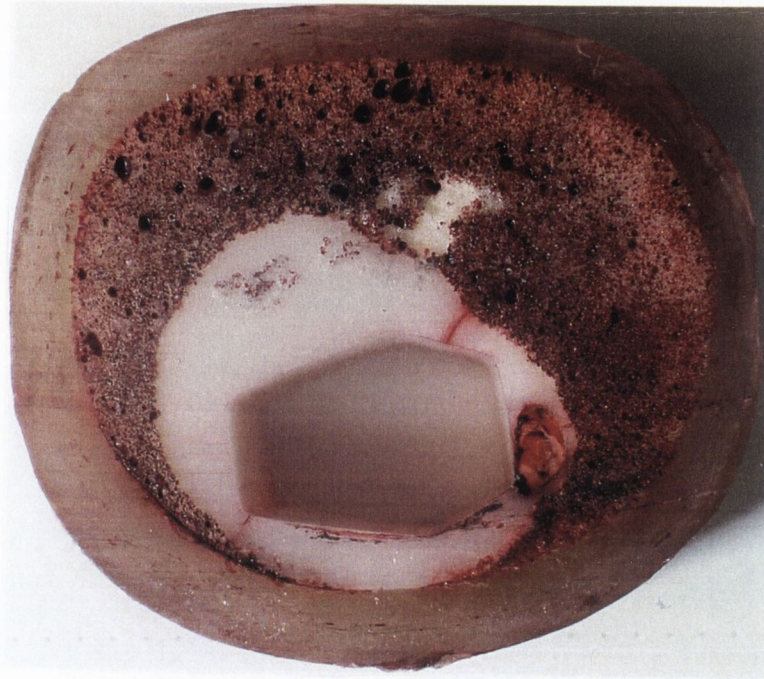


Figure F3: Additional photographs of the Müller cement mantles. The samples have been cyclically loaded, sectioned and push out tests have been performed. Damage in the cement mantle and along the interfaces is apparent.



Figure F4: Photographs of the Lubinus inner cement mantles. The samples have been cyclically loaded, sectioned and push out tests have been performed. Damage along the cement/prosthesis interface is evident.

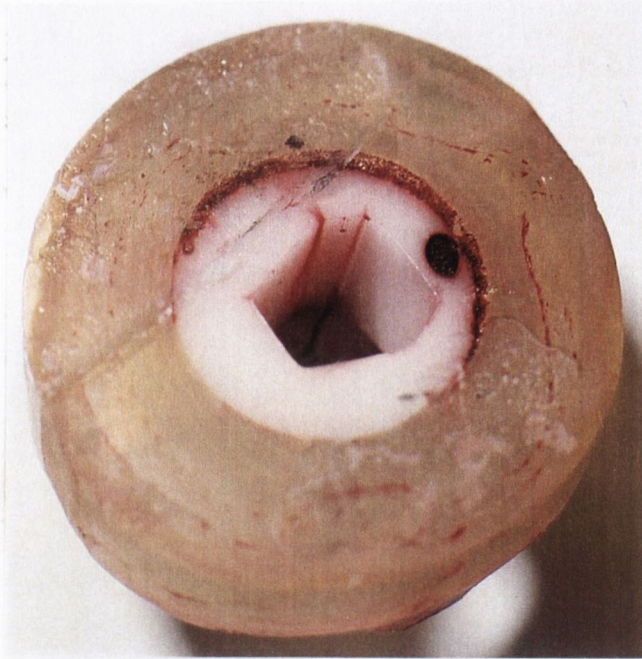
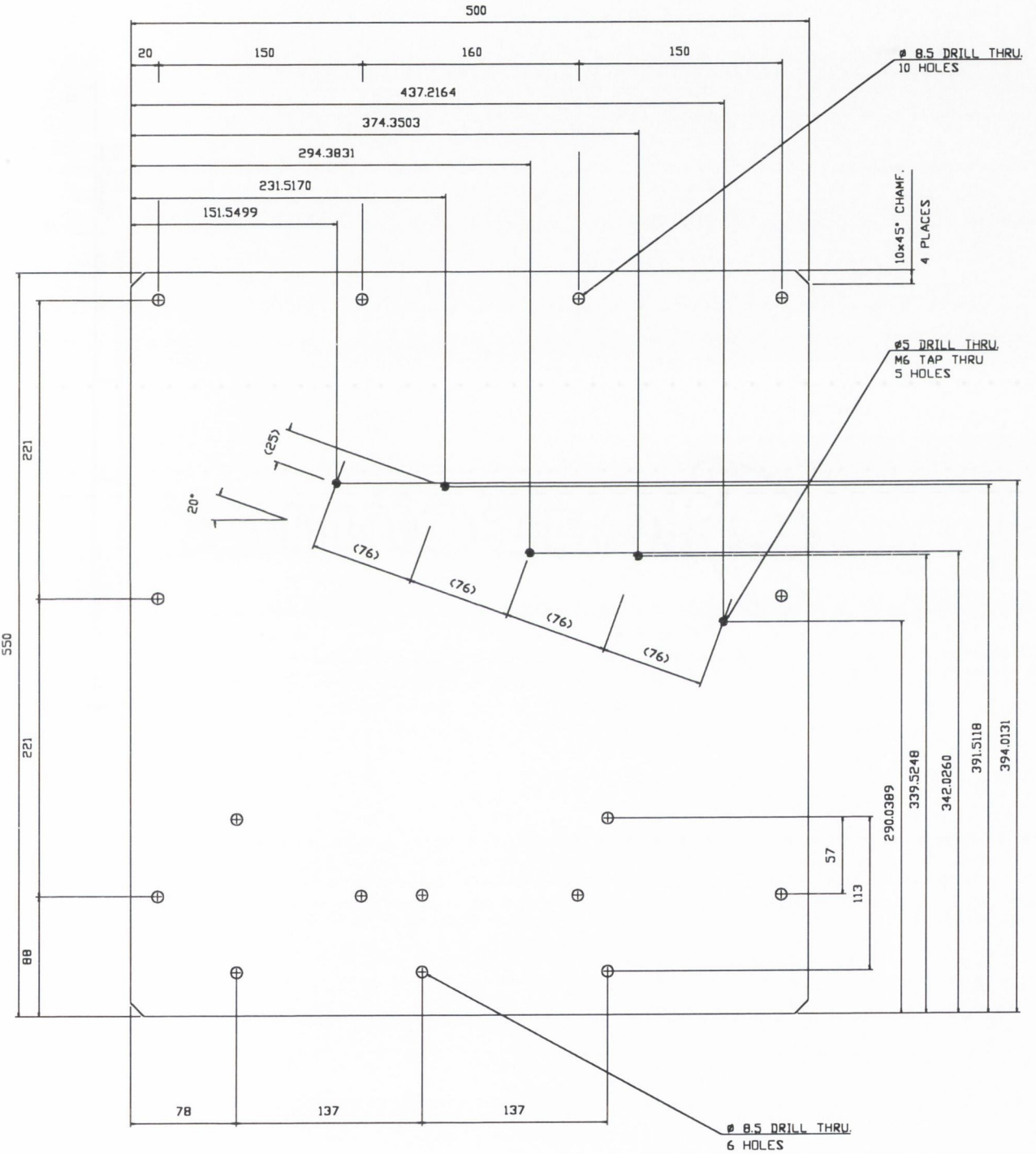


Figure F5: Photographs of the Müller inner cement mantles. The samples have been cyclically loaded, sectioned and push out tests have been performed. Damage along the cement/prosthesis interface is evident.

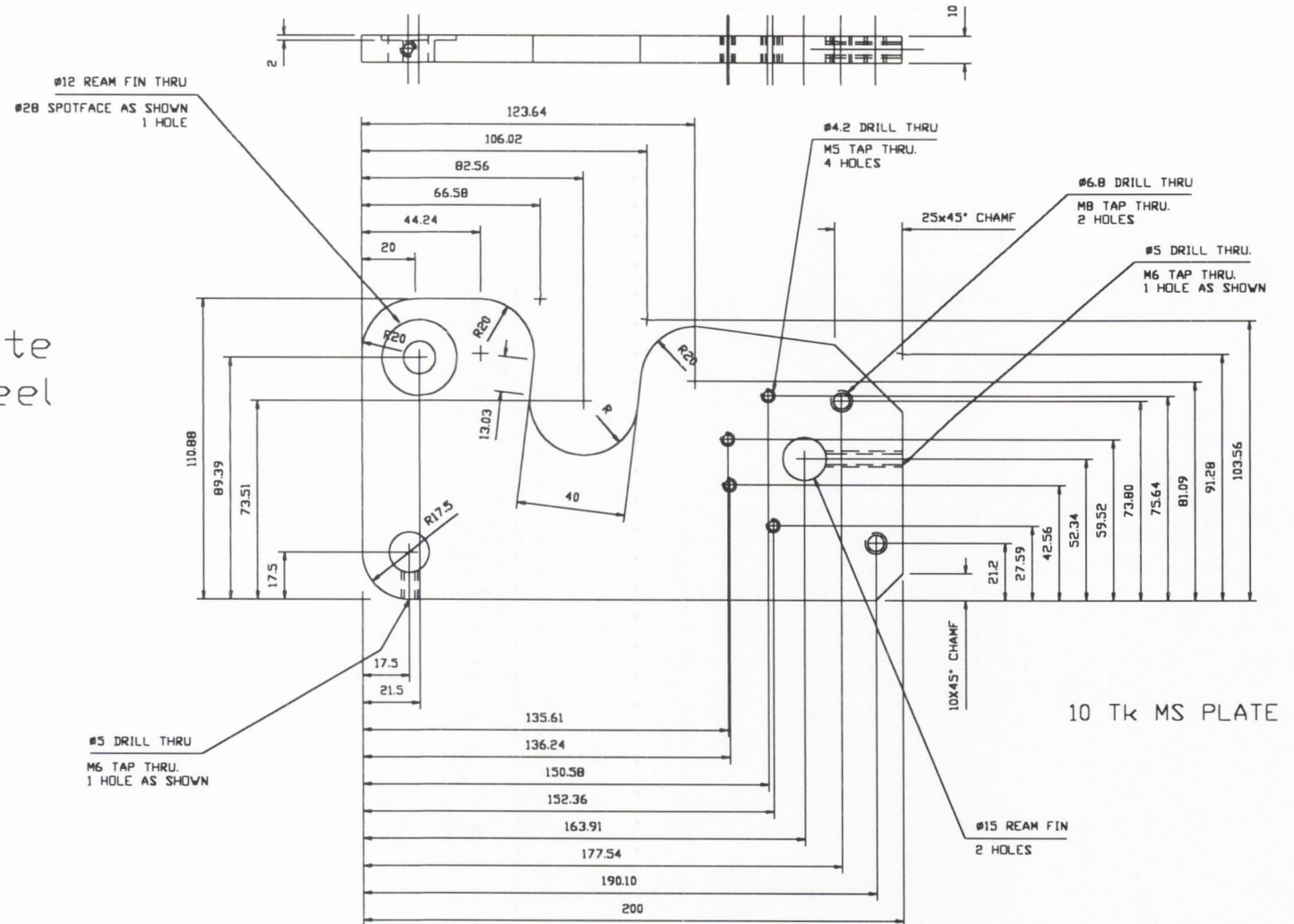
APPENDIX G

*Note: These drawings have been produced by Suzanne Maher, Alan Reid and
Victor Waide*

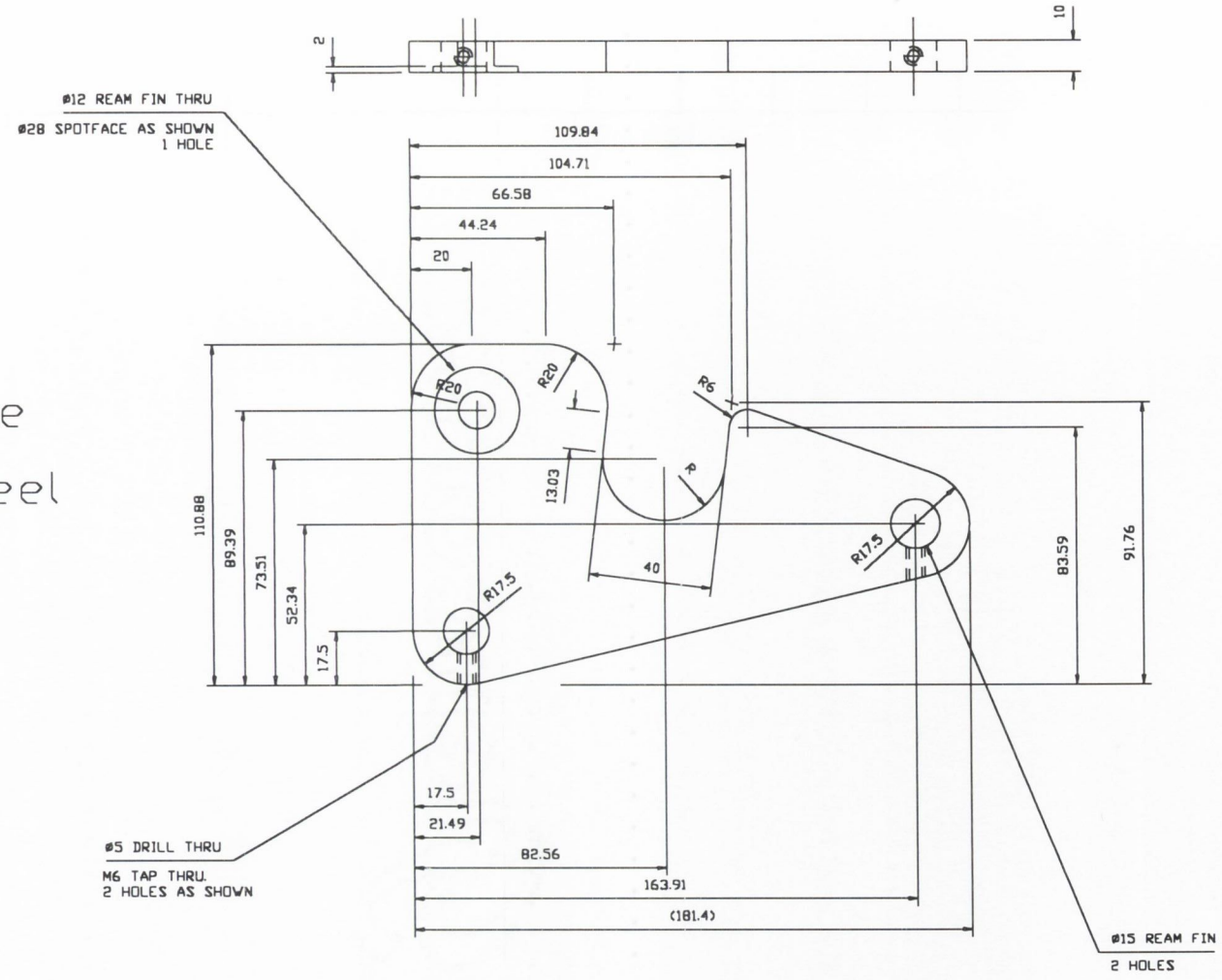
Backplate
Material: Mild Steel

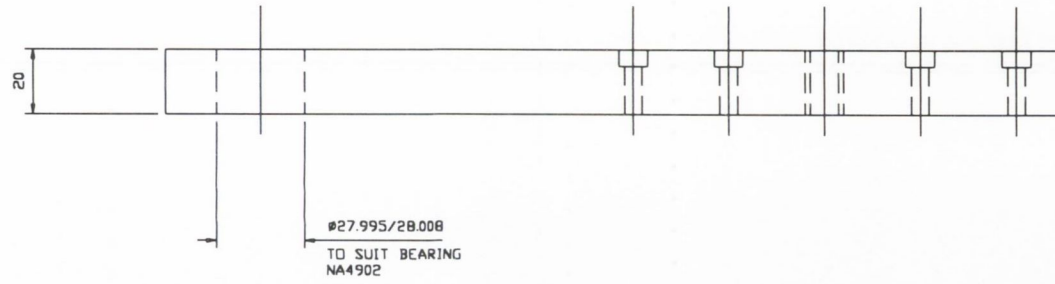


Outer Cheek Plate
Material: Mild Steel

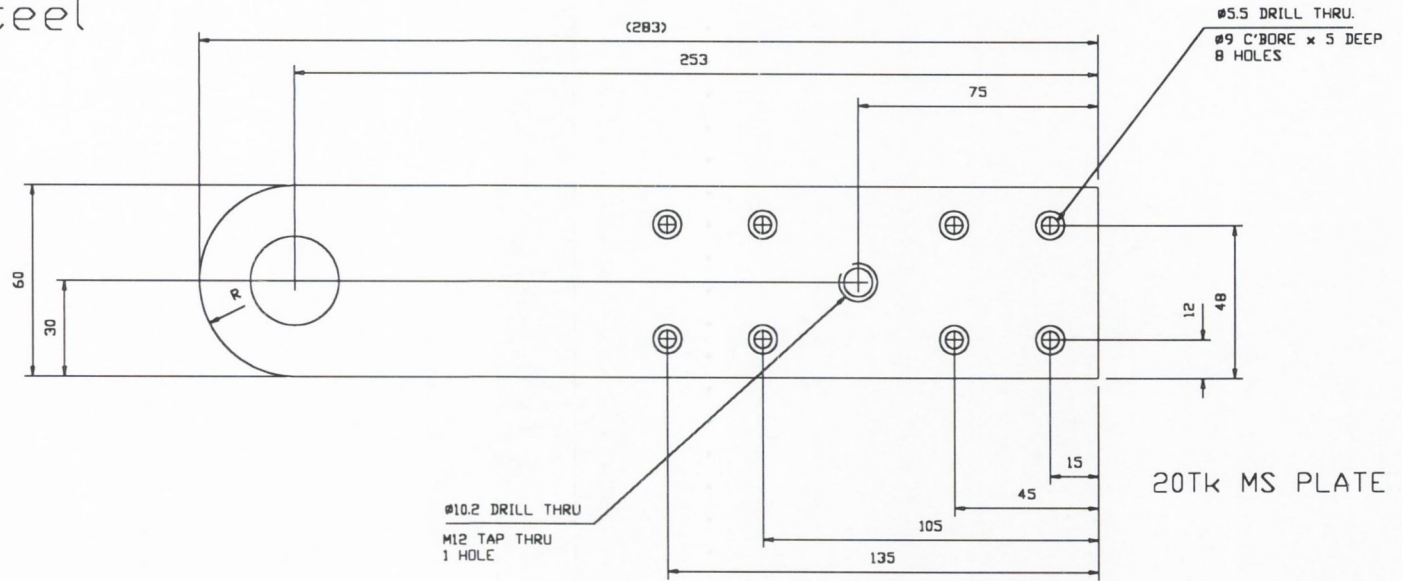


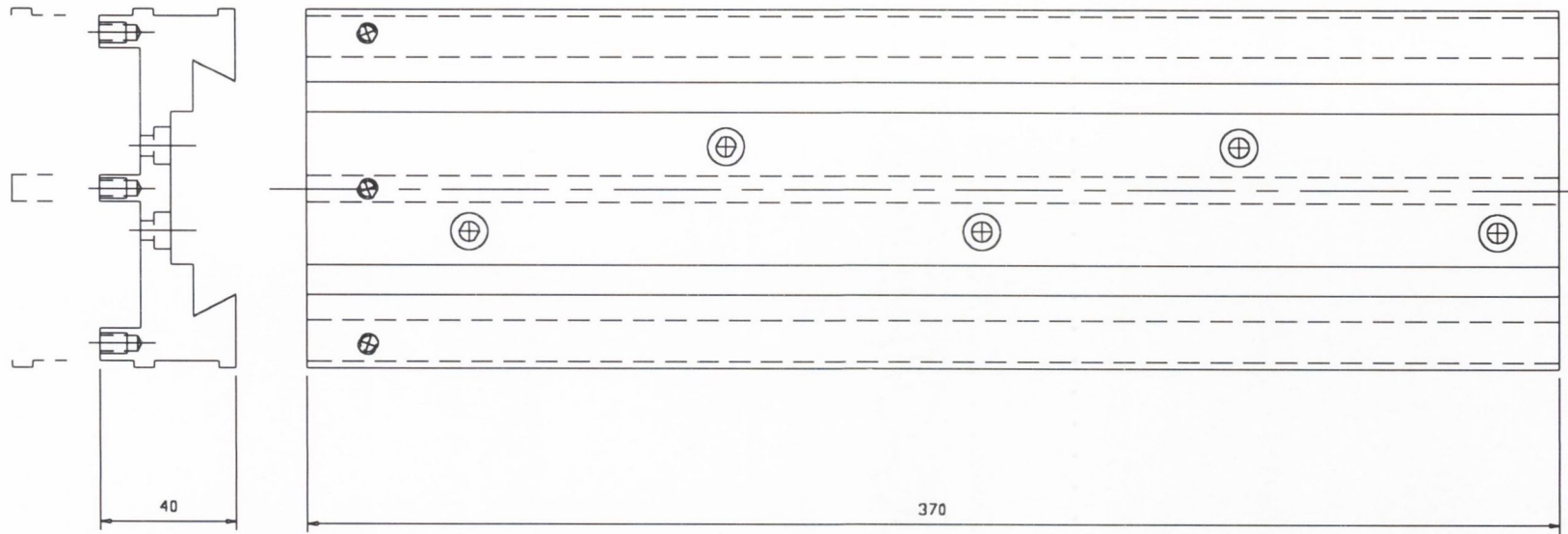
Back cheek plate
Material: mild steel





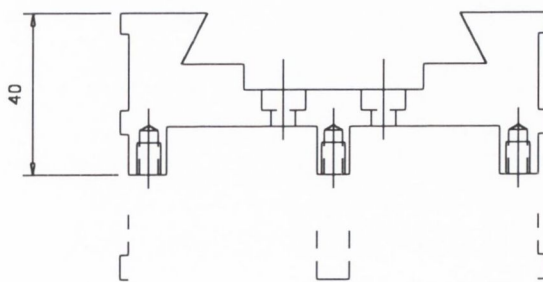
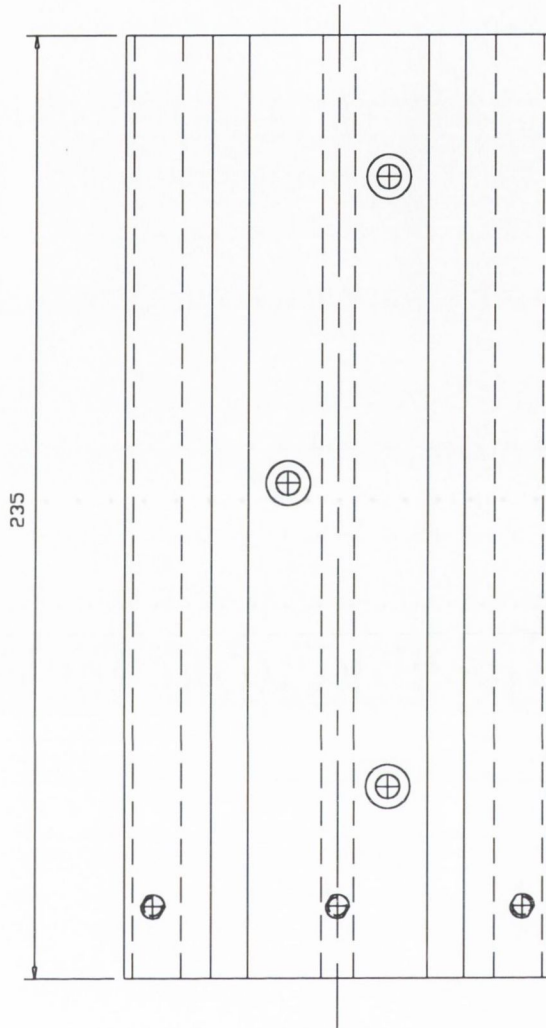
Roller Arm
 Material: mild steel



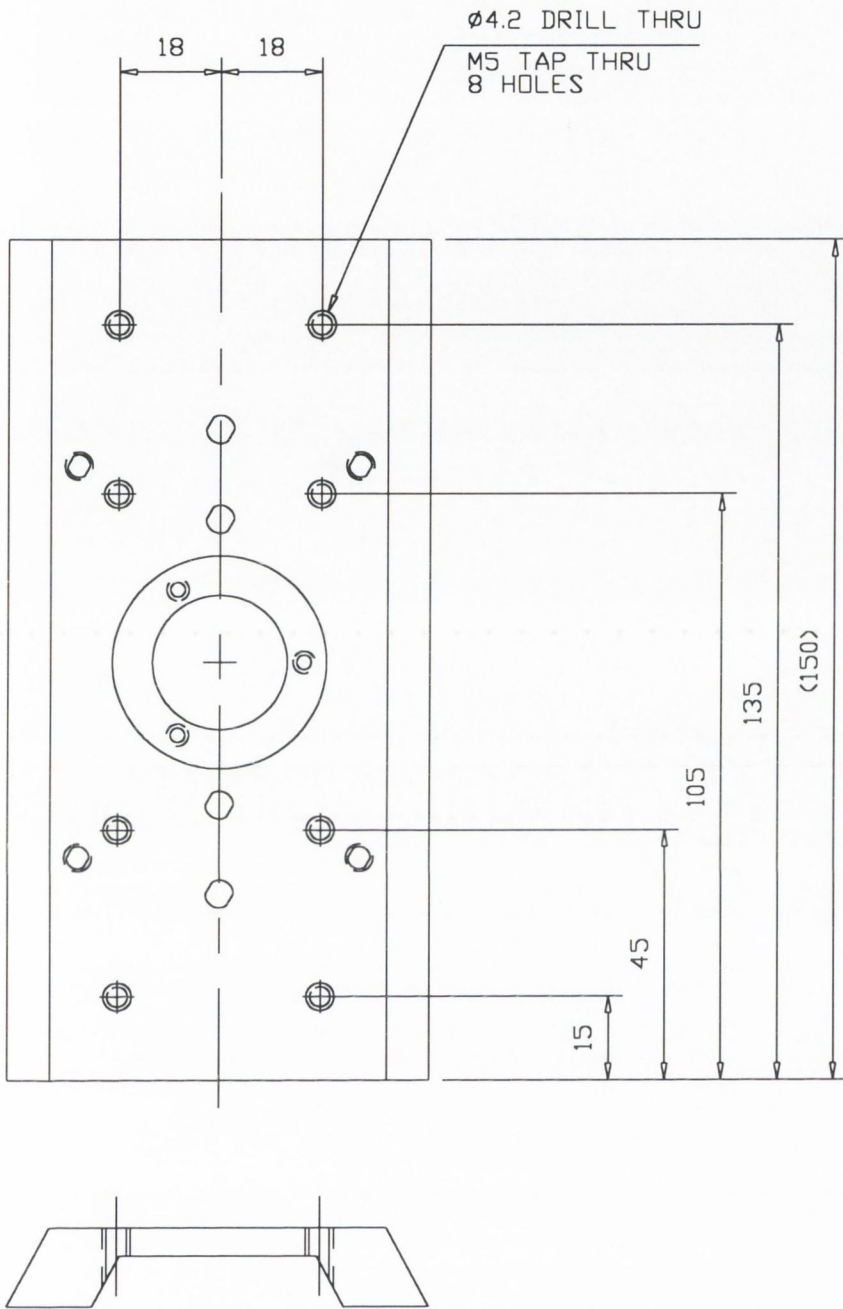


Lower slideway: modify from pre-existing slideway as shown

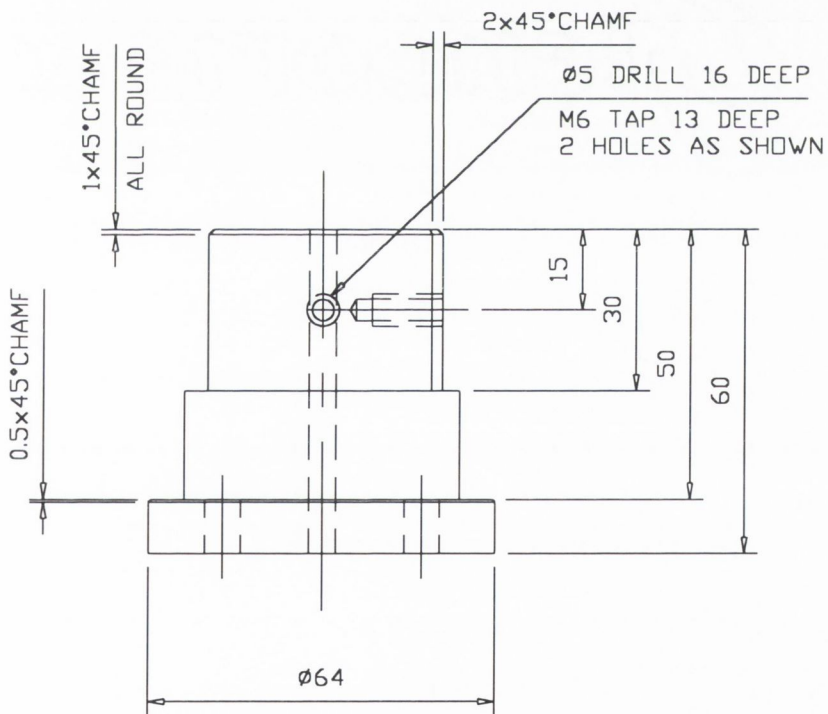
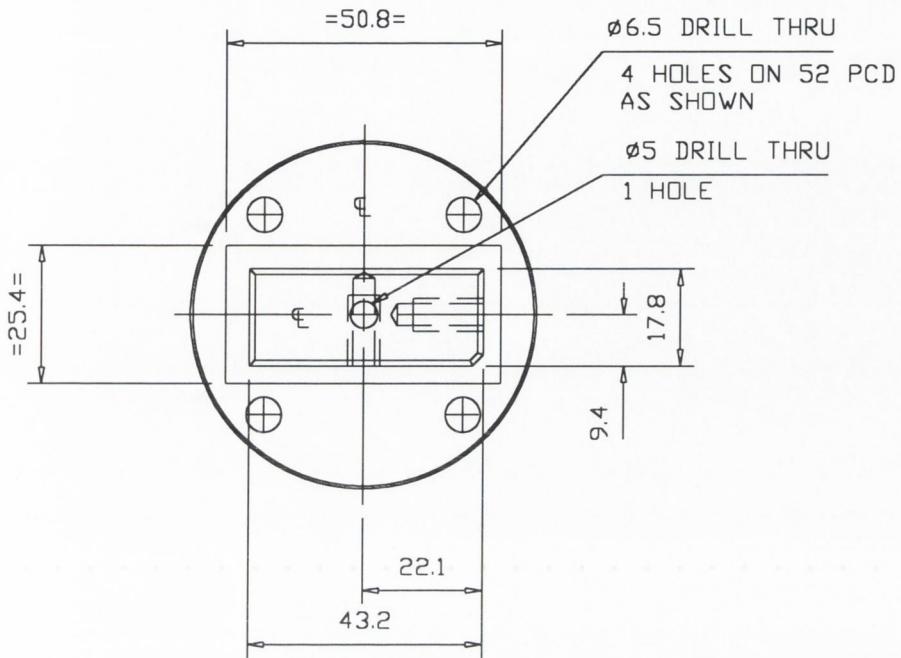
Upper Slideway: modify from pre-existing slideway, as shown



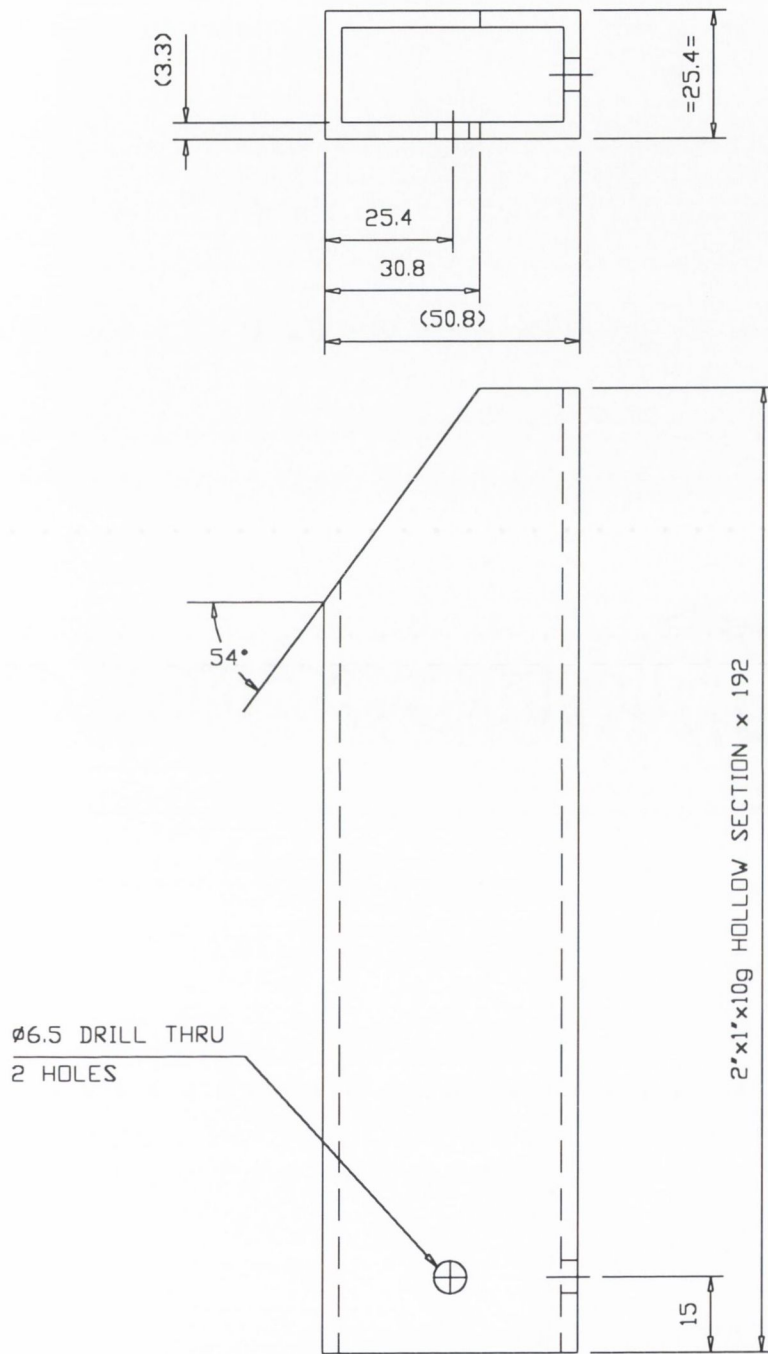
Slider



Dummy Hip Holder for validation

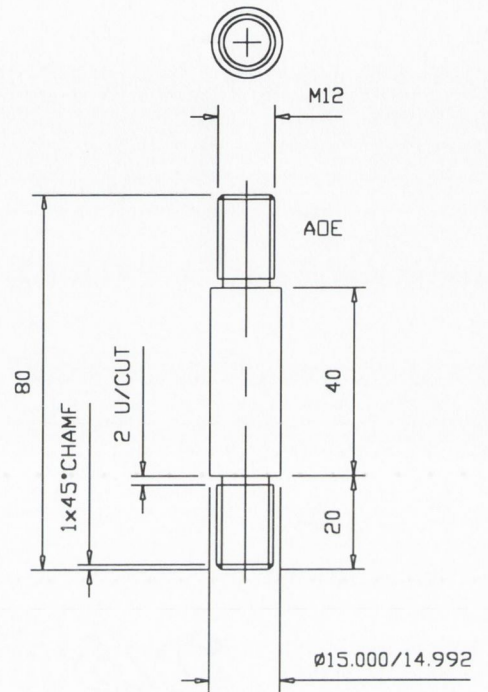


Dummy Hip for validation
Material: aluminium box section



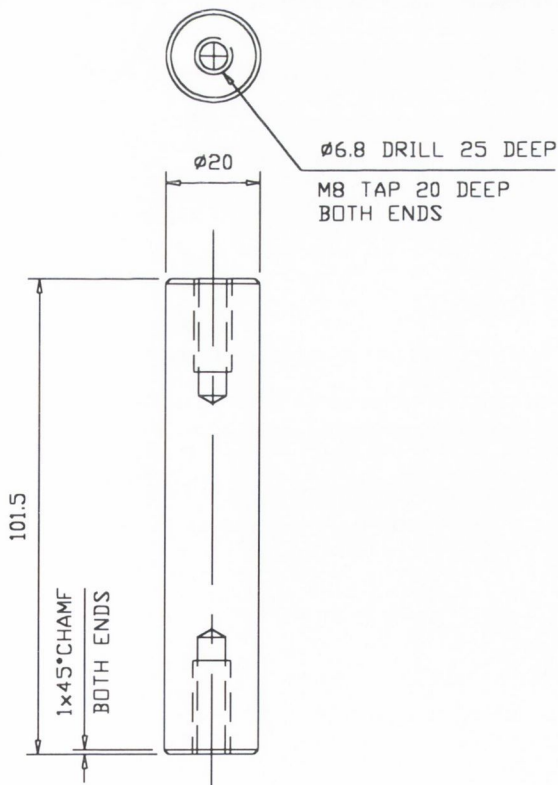
Spindle

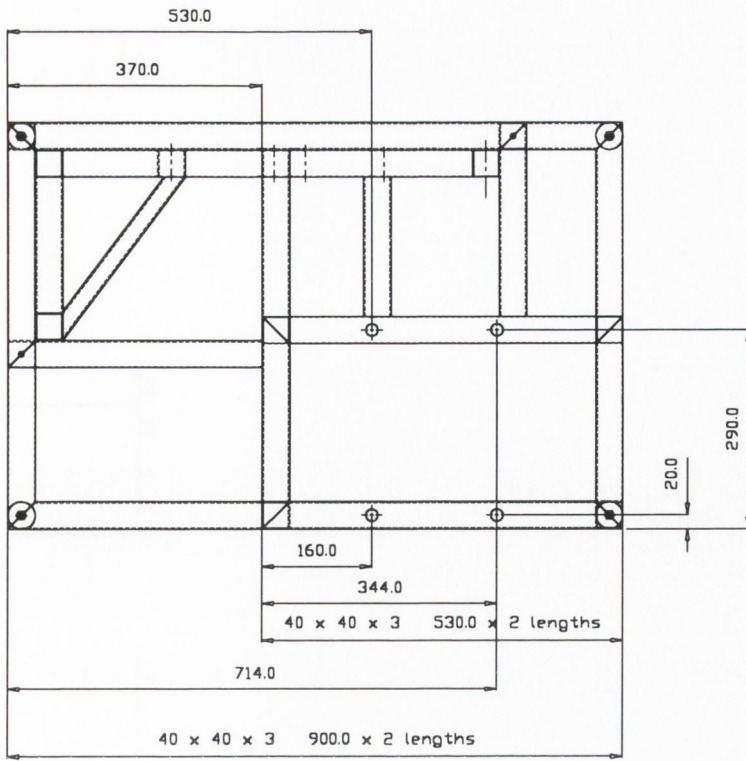
MATL. SILVER STEEL
1 NO REQD



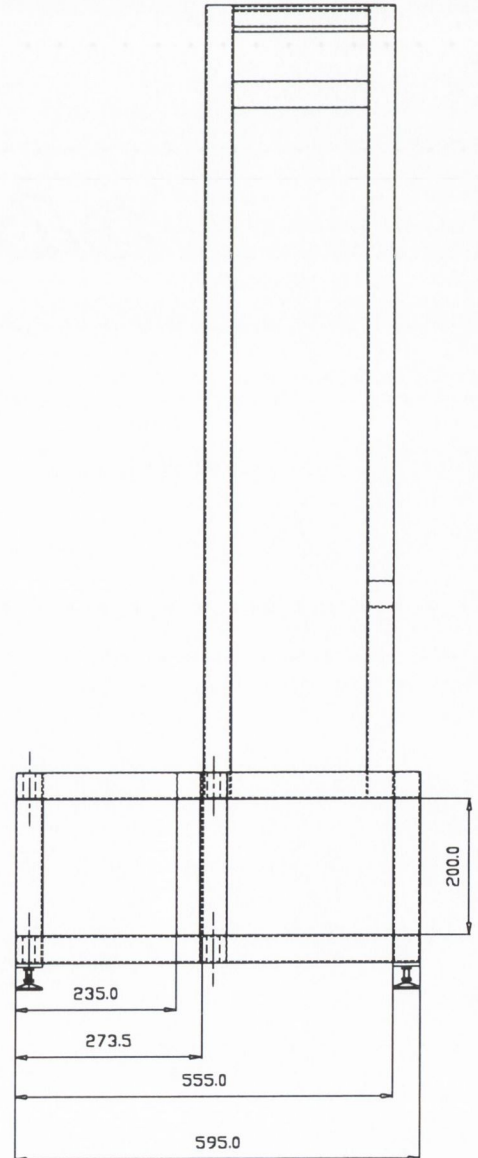
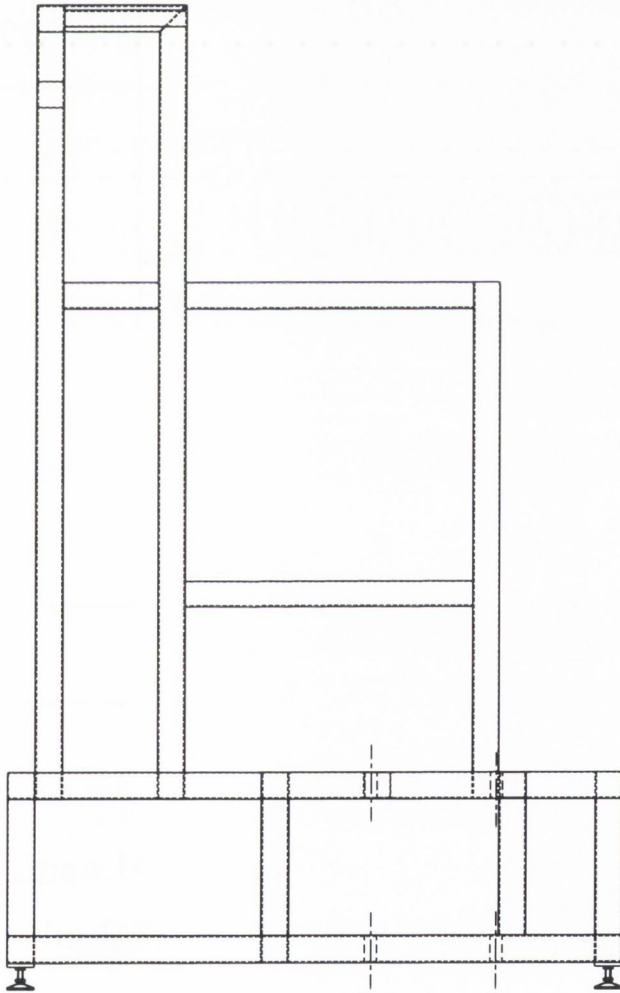
Spacing Pillar

MATL. MILD STEEL
6 NO REQD

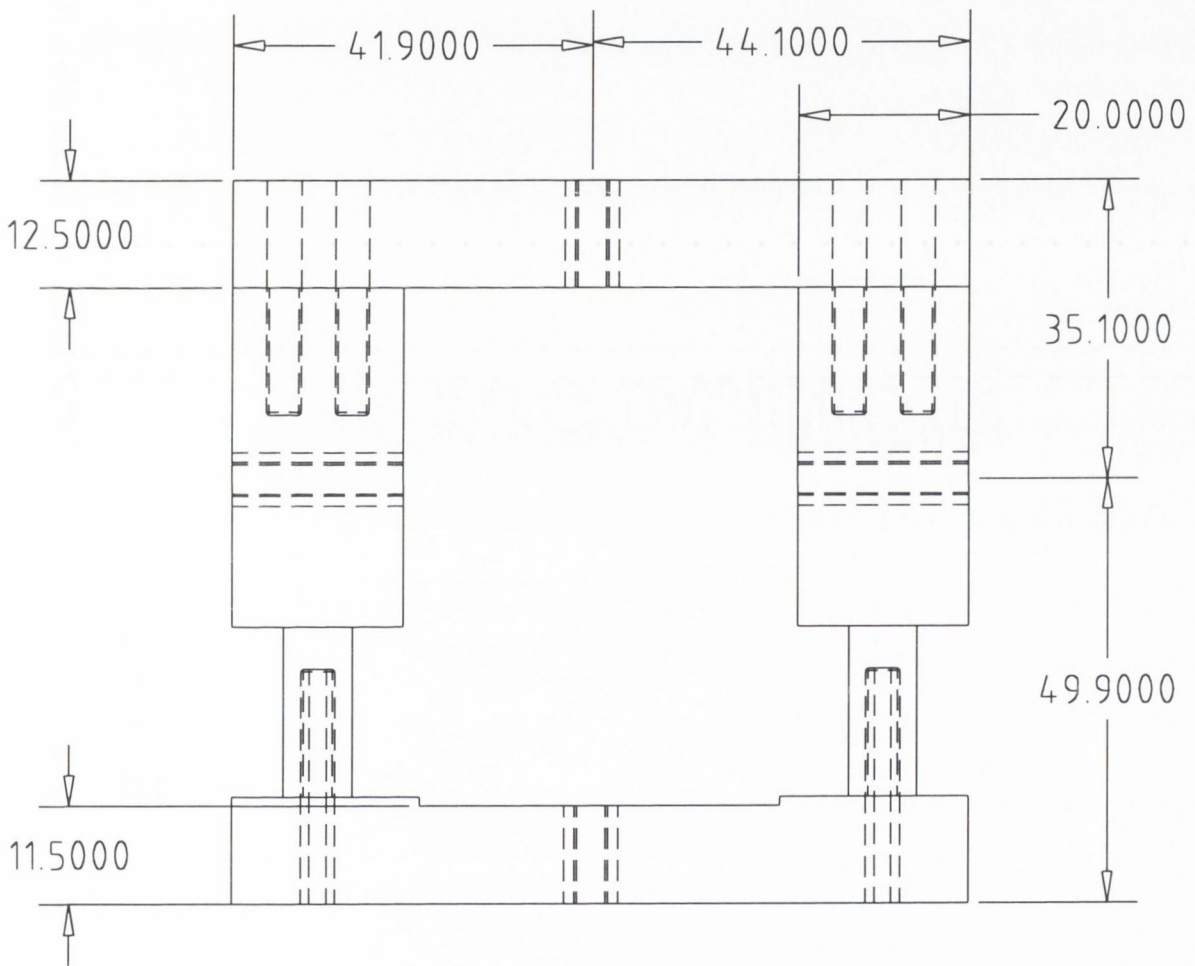
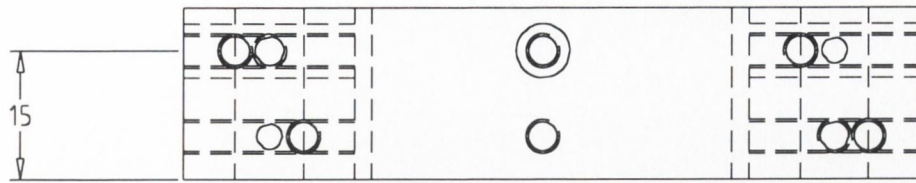




Modifications made to frame after initial validation



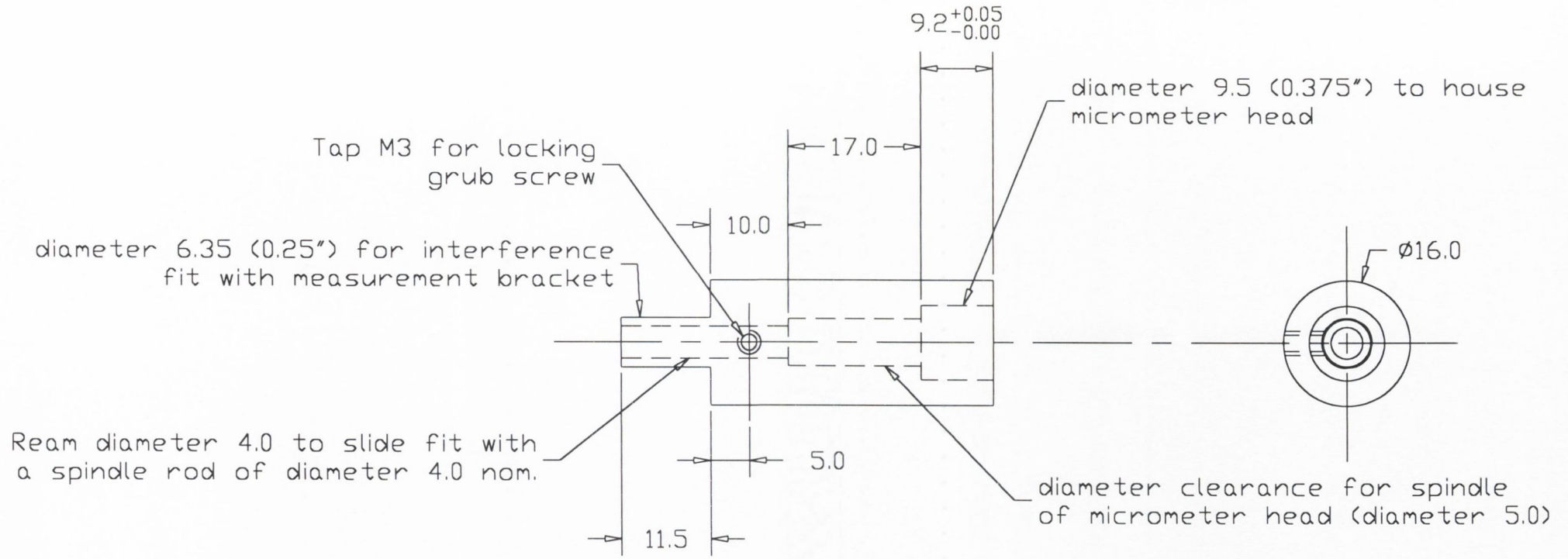
Holder for micrometer heads



Note: Open the holes as indicated by the red lines for an interference fit with the 6.35mm diameter of the shaft of the Micrometer Housings

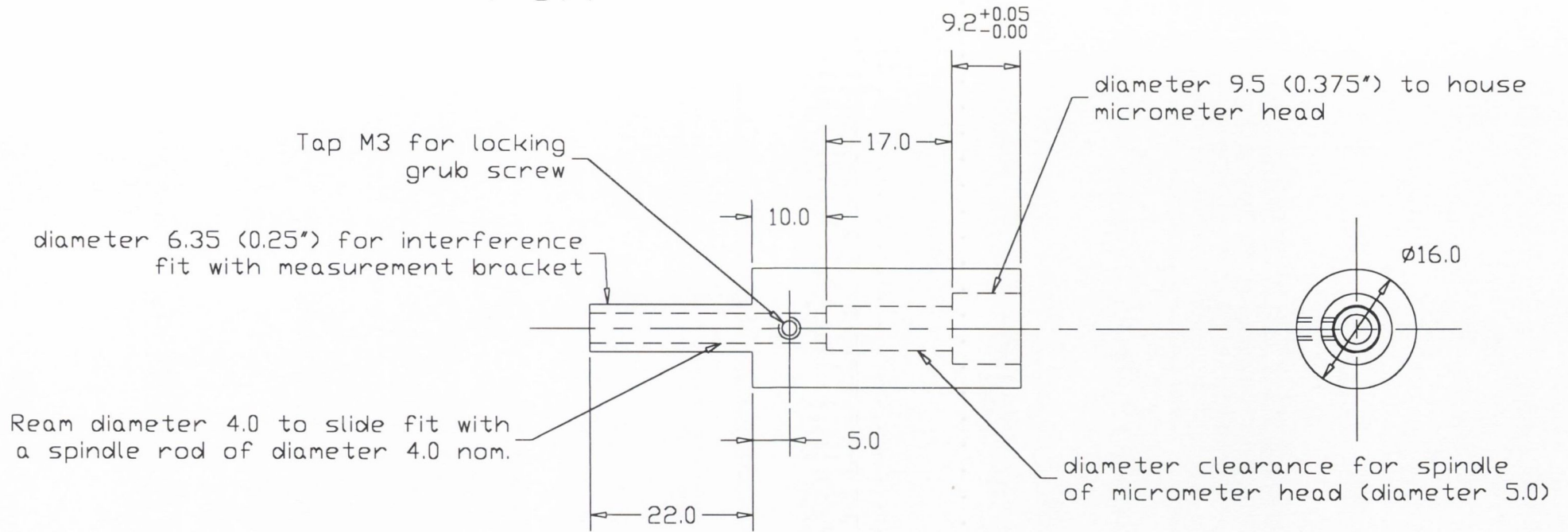
Micrometer housing - posterior

2 off

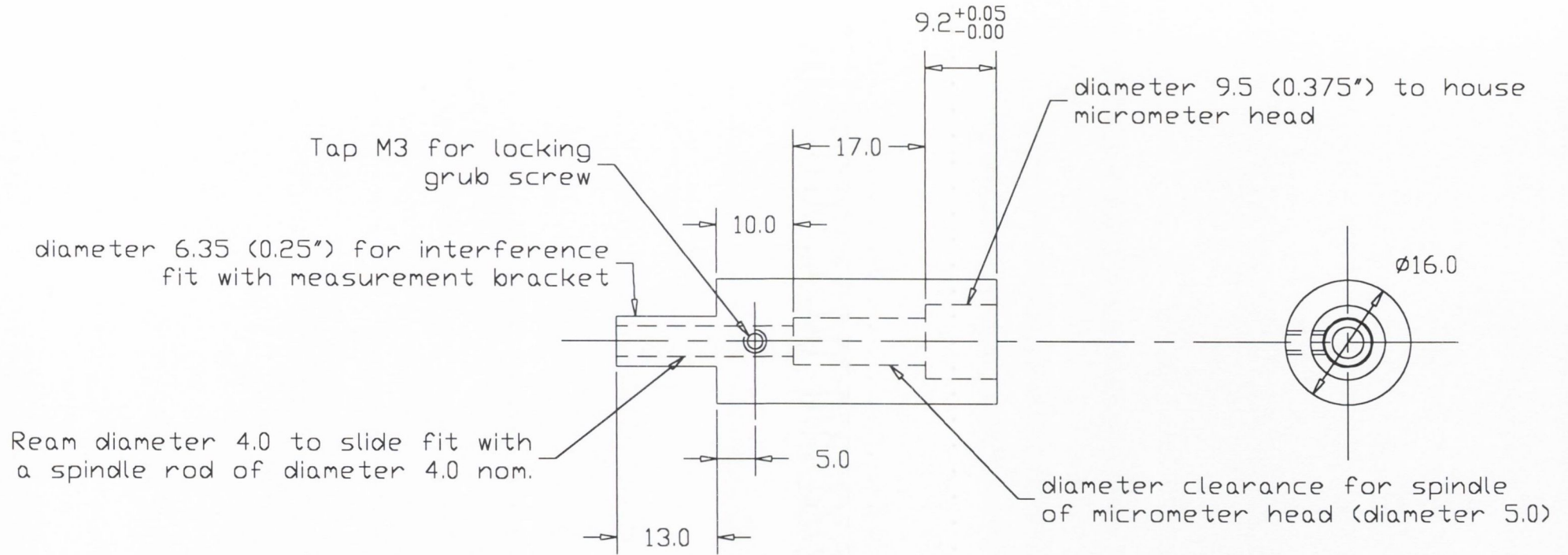


Micrometer housing: medial/lateral

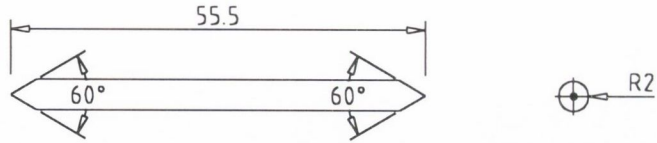
4 off



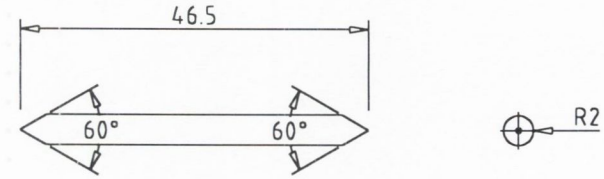
Micrometer housing: anterior
2 off



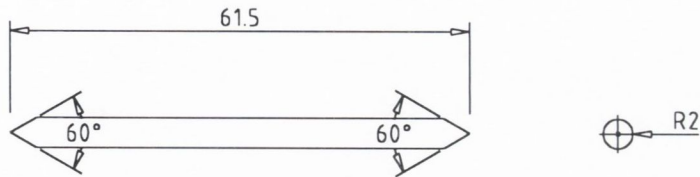
Pins to fit inside micrometer holders



Spindle rod to fit into 98-Microhouse-M/L
Material: Tool Steel
4 off

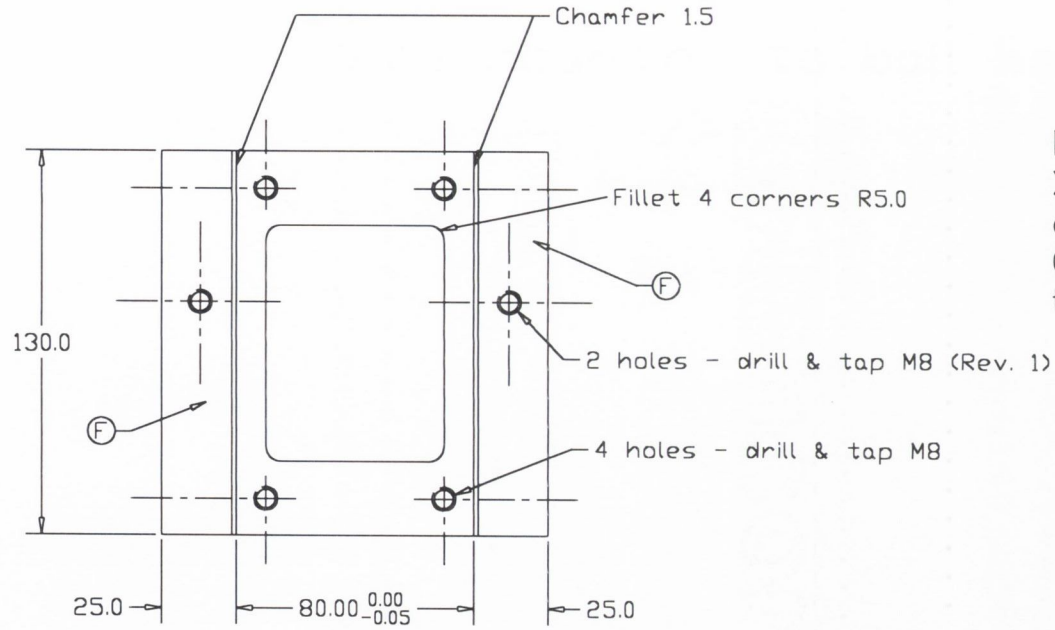


Spindle rod to fit into 98-Microhouse-A
Material: Tool Steel
2 off

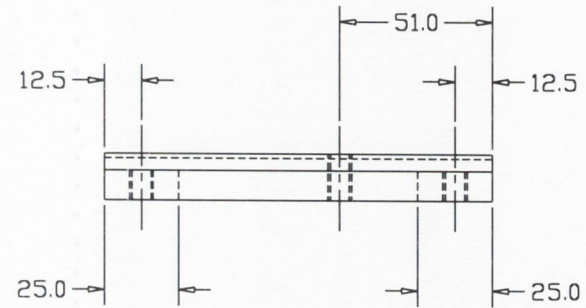
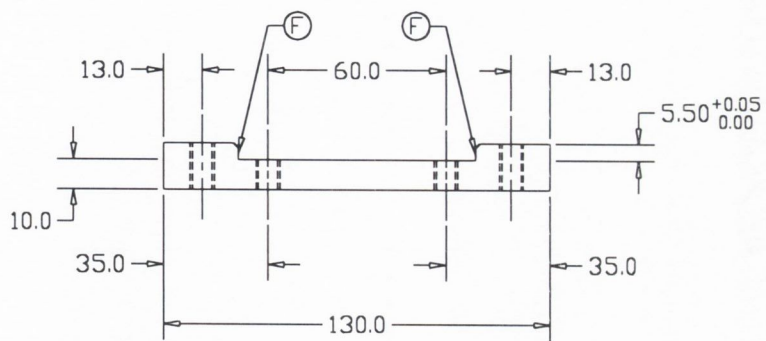


Spindle rod to fit into 98-Microhouse-P
Material: Tool Steel
2 off

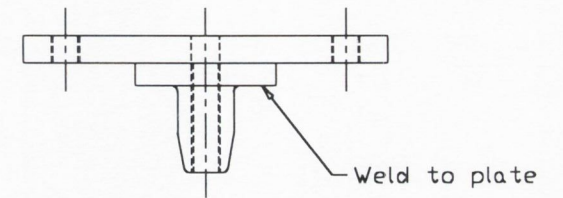
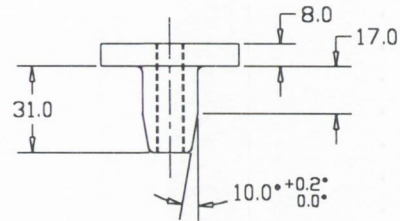
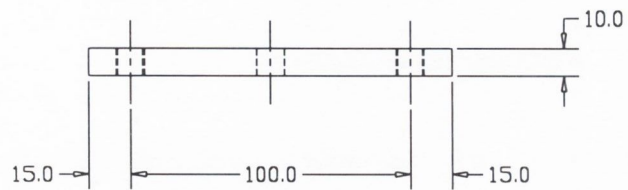
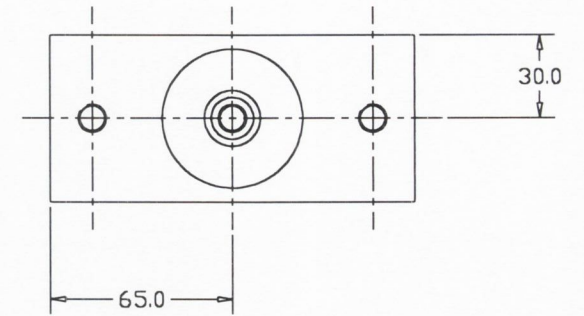
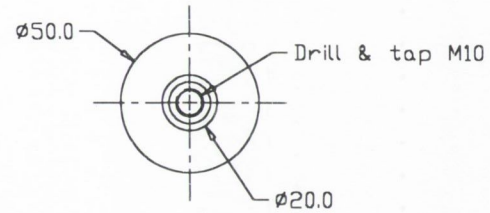
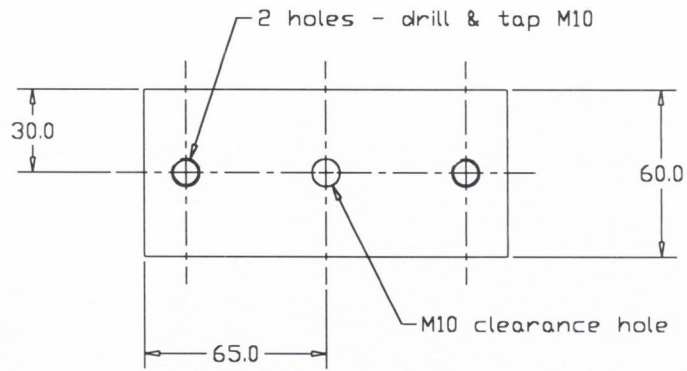
Mounting base for x-y table



Note:
 XY Table to slide fit
 onto machined recess.
 Grind contact faces ⓕ
 to 0.8



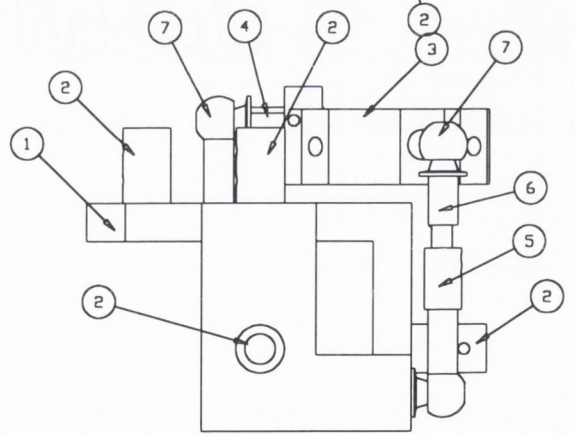
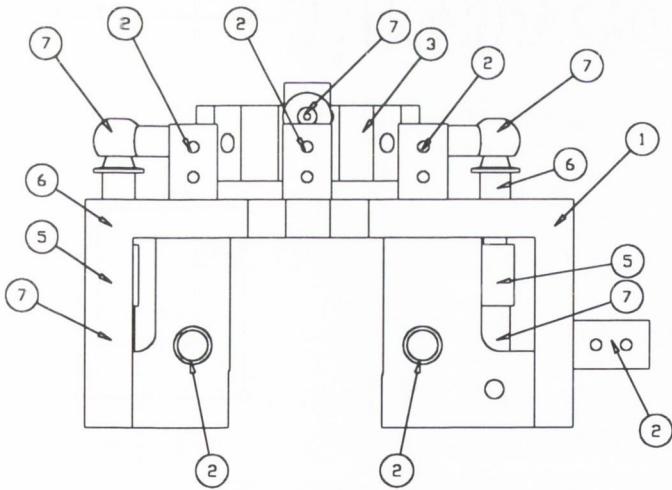
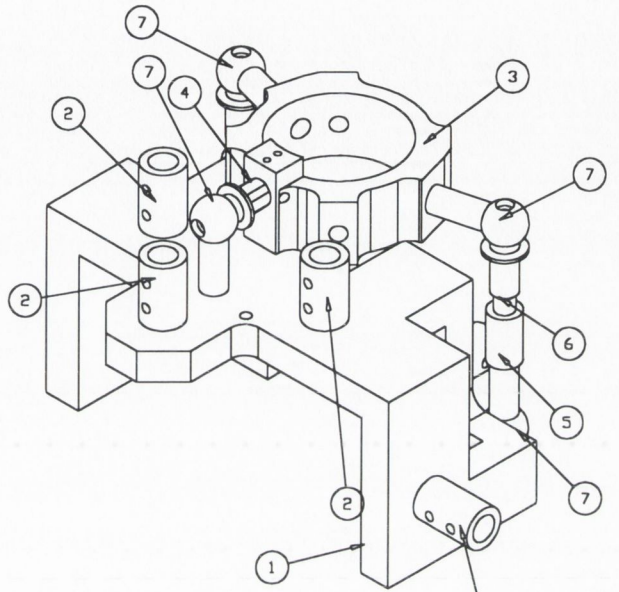
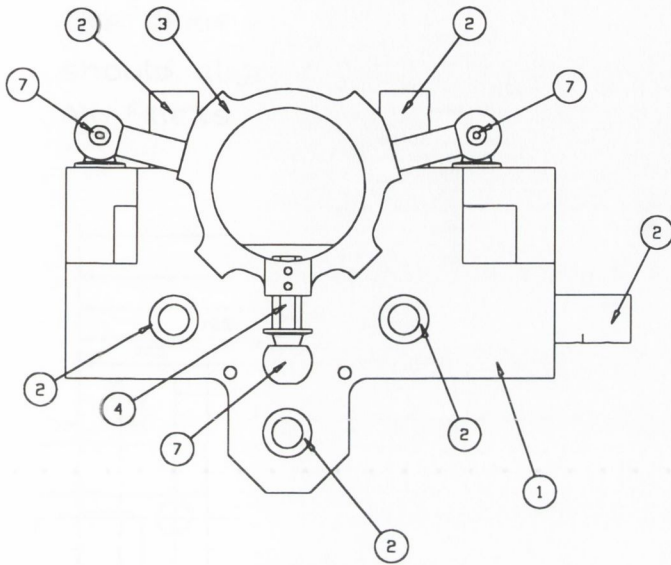
Vice mounting to ball head coupling



APPENDIX H

Note: These drawings have been produced by Suzanne Maher and Victor Waide.

Assembly drawing of migration measurement device

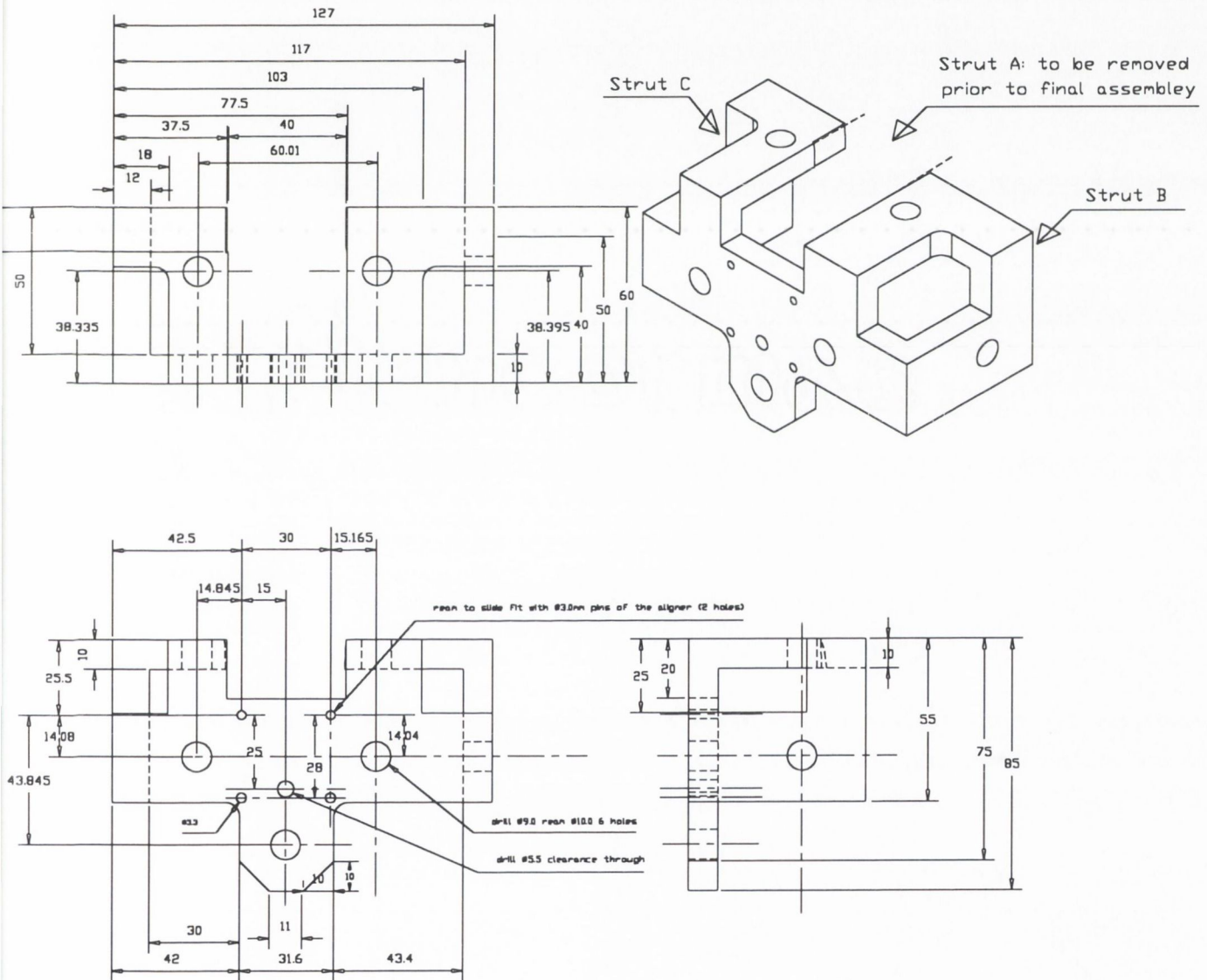


1 = LVDT Bracket
 2 = LVDT cylinder
 3 = Femoral ring

4 = Main tie
 5 = Side linker
 6 = Side Tie
 7 = Ball nad socket coupling

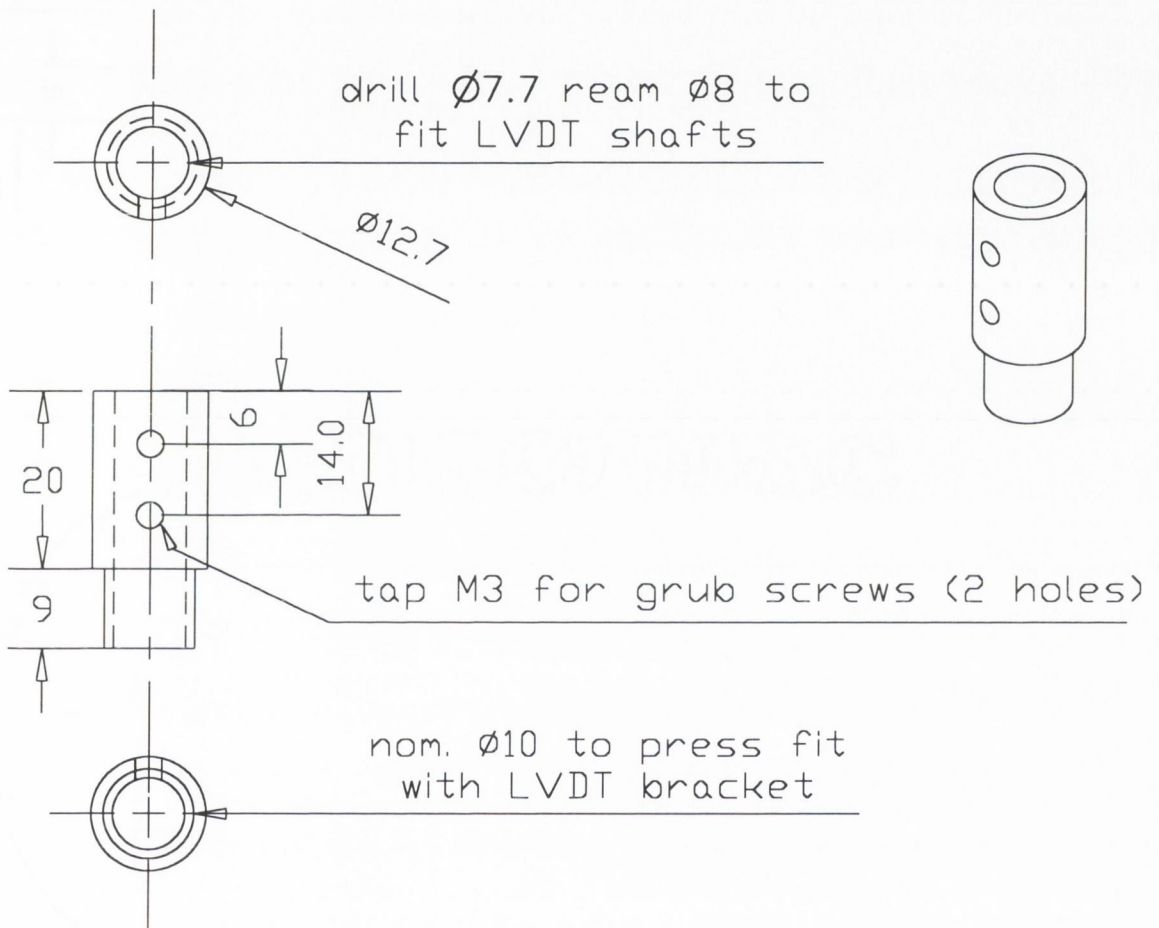
LVDT Bracket

The $\varnothing 3\text{mm}$ holes, must be aligned with the holes in the aligner
 The $\varnothing 10\text{mm}$ holes are drilled relative to the $\varnothing 3\text{mm}$ holes
 The $\varnothing 6\text{mm}$ holes should be mutually perpendicular, and
 should align with the subsidence measurement device
 All fillets of R5.0 unless otherwise stated



LVDT Cylinder

Quantity: 6 Material: Aluminium
Note: Press fit to LVDT Bracket



Femur Ring

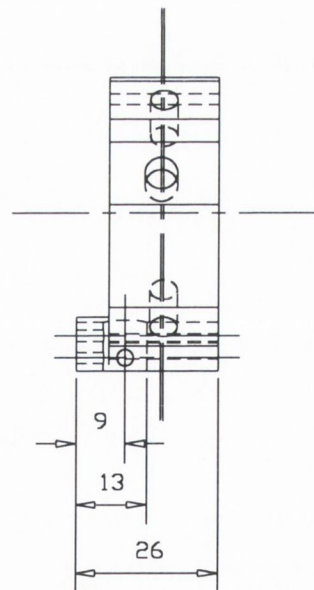
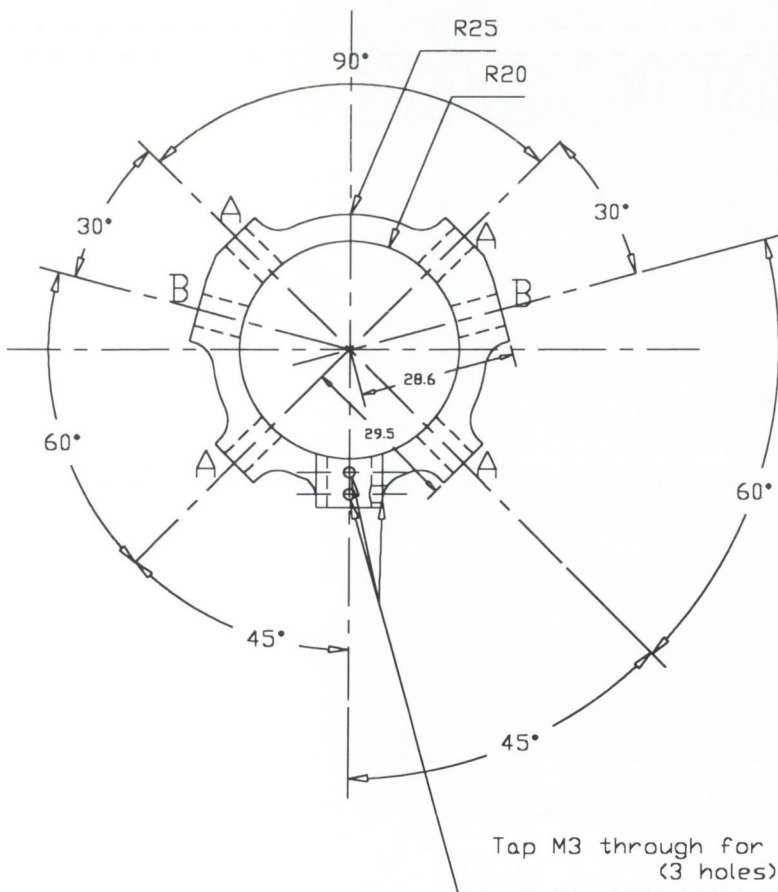
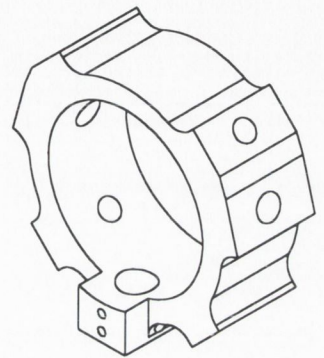
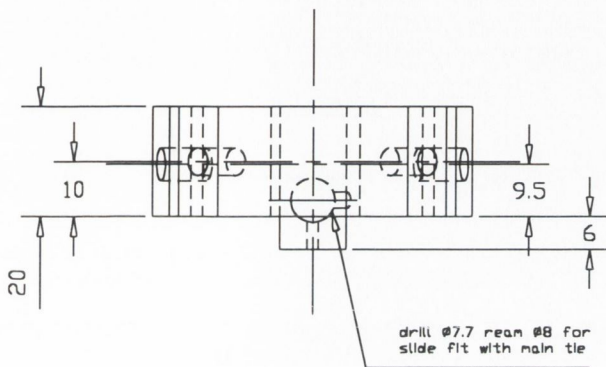
Quantity: 1 Material: Aluminium

All fillets are R5.0 unless otherwise stated

Holes marked A: tap M6 for pointed femur bolts

(4 holes equi-spaced around the femur ring)

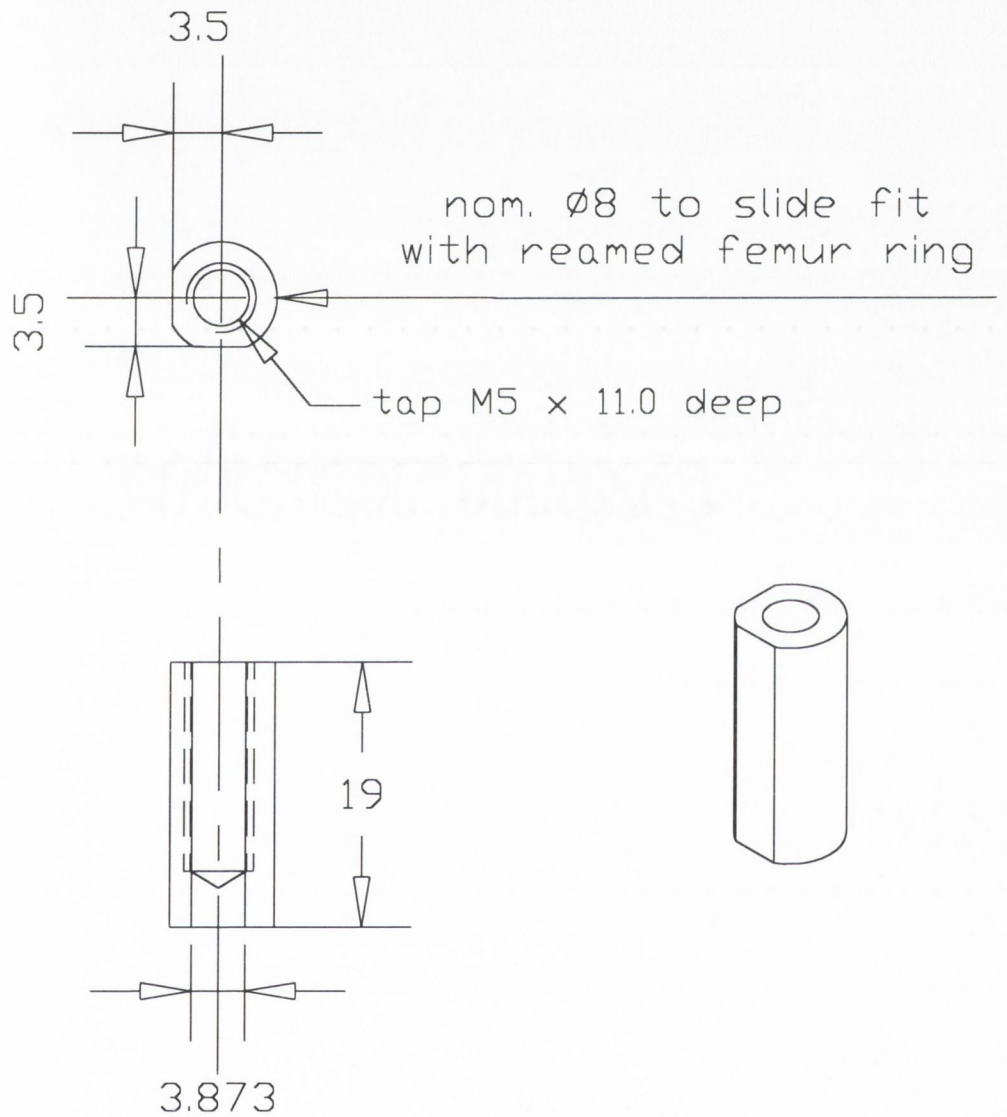
Holes marked B: drill $\varnothing 6\text{mm}$ clearance holes for ball and socket attachments



Main Tie

Note: To slide fit with Femur Ring

Quantity: 1 Material: Silver Steel

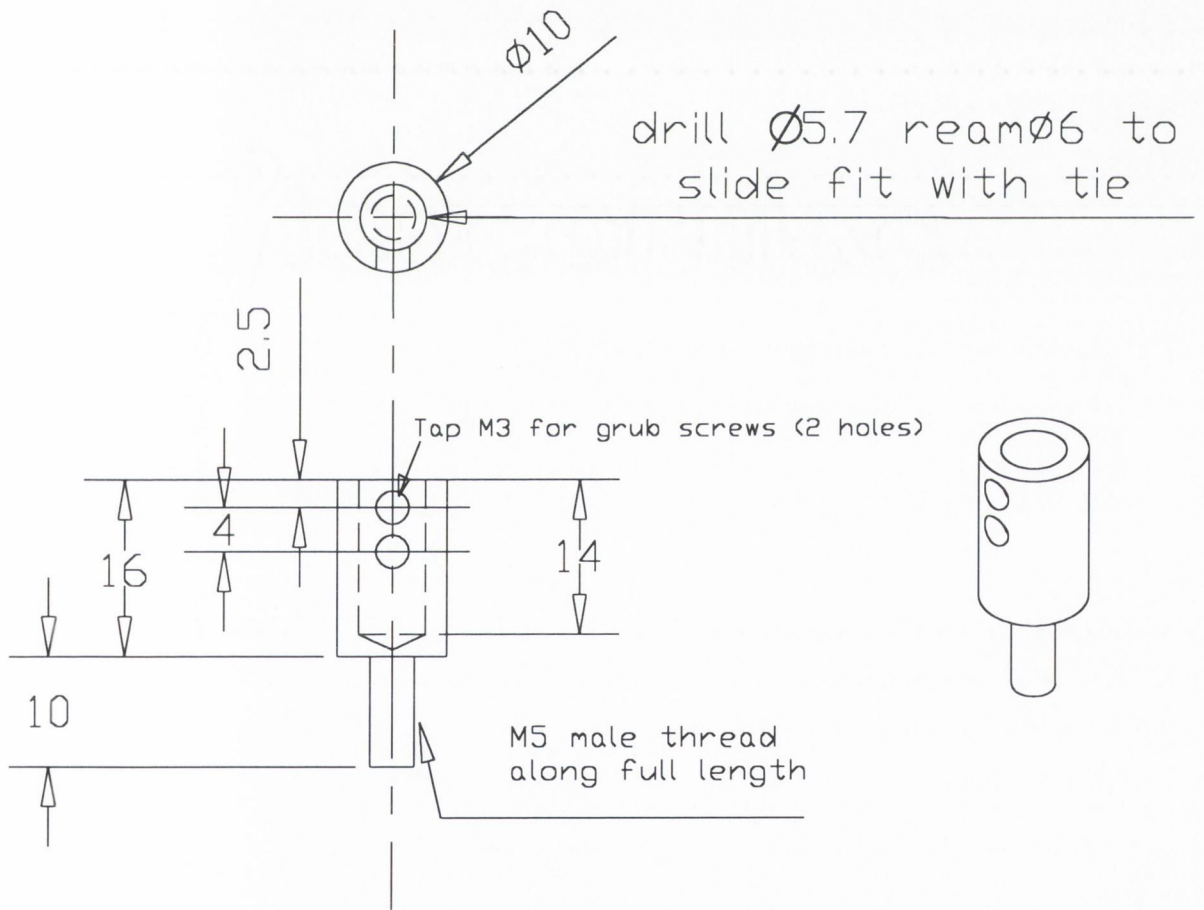


Side Linker

Note: grind down the drill bit to allow the blind hole to be drilled to a depth of 14mm and then reamed to its fullest depth possible

Note: To slide fit with Side Tie

Quantity :2 Material : Silver Steel



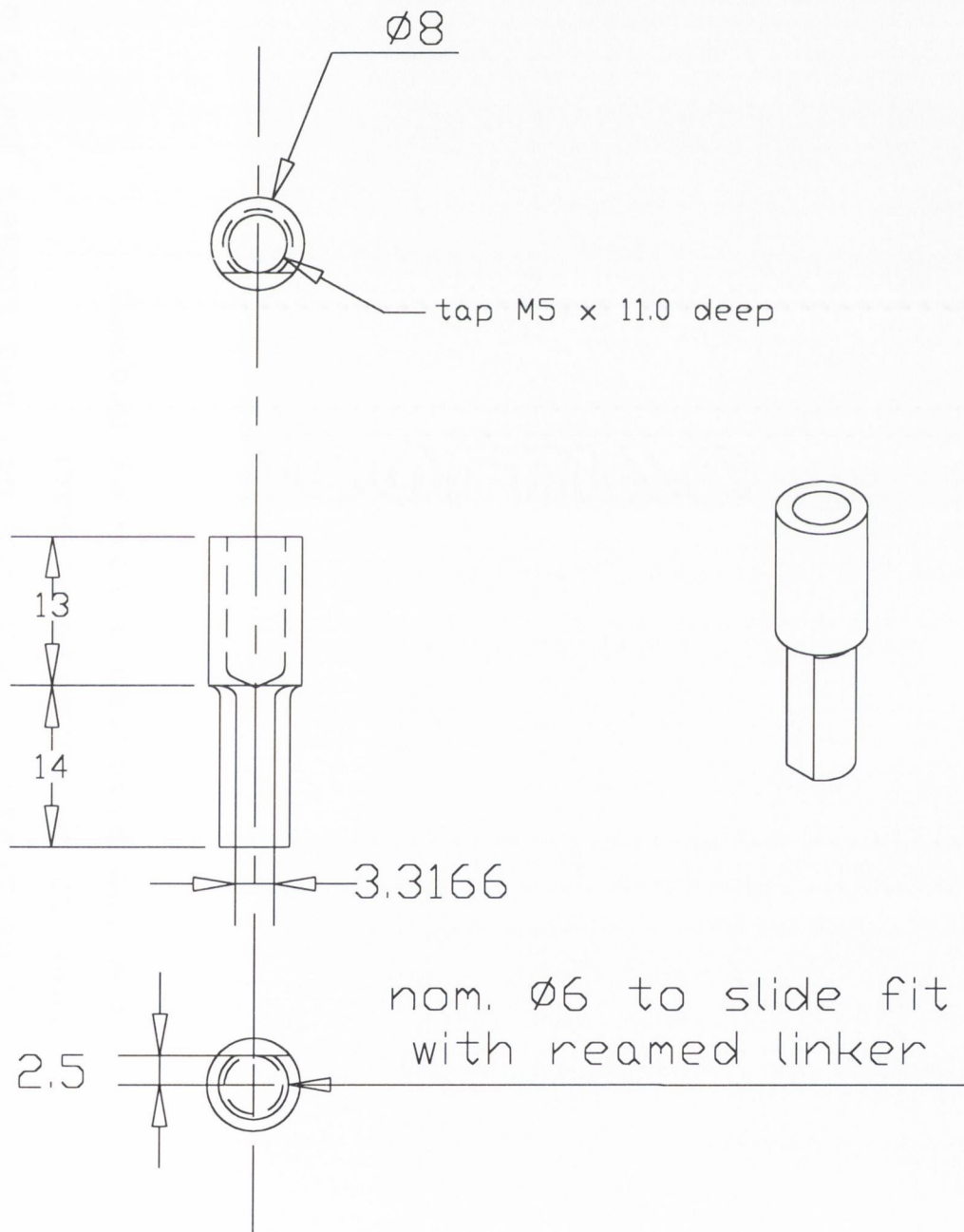
Side Tie

Note: grind down the drill bit to allow the blind hole to be drilled to a depth of 12mm

Note: To slide fit with Side Linker

Quantity: 2

Material: Silver Steel

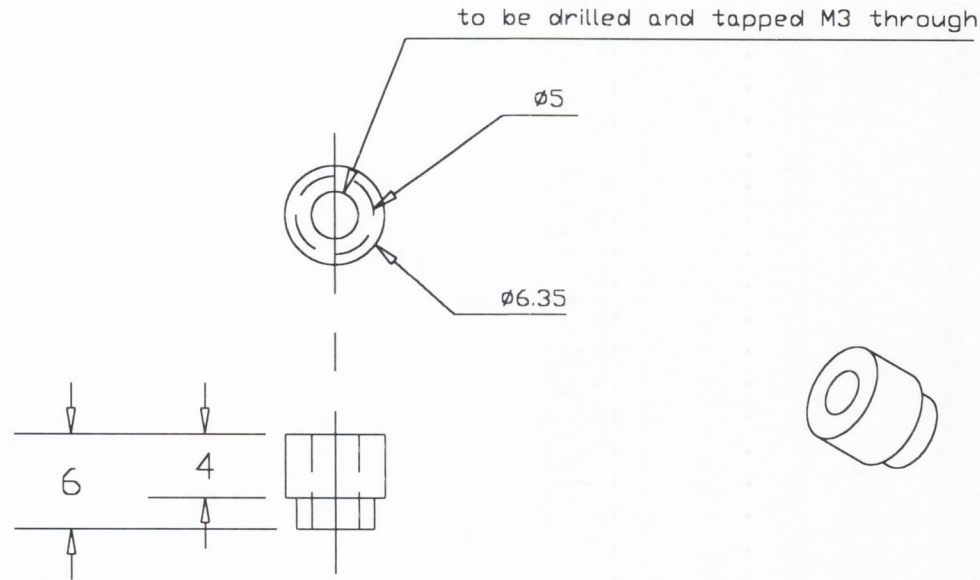


Risers for Ball and Socket Joints

Material: Stainless Steel 5 off

To be press fit into the ball and socket joints and
then to be soldered in place

See the attached assembly drawing



Glossary of Terms

The following medical and engineering terms are described with particular reference to the femur and hip replacements.

Distal	The part of the femur that is furthest from the body.
Proximal	The part of the femur that is closest to the body.
Medial	The central region of the femur.
Lateral	Parts of the femur that are furthest from the median plane - i.e. situated at the side of the organ.
Anterior	The front (ventral) portion of the femur.
Posterior	The back of the femur.
LVDT	Linear variable differential transformer: used to measure relative movement between two bodies. Consists of three coils, one for energisation, and two which pick up the change in induced current generated by a movable nickel core.
Migration	Permanent non-recoverable translation or rotation of a prosthesis relative to a femur in any direction.
Subsidence	Permanent non-recoverable translation of the prosthesis in the distal direction.
Inducible displacement	The amplitude of prosthesis translation or rotation in a particular direction.